

NASA TECHNICAL
MEMORANDUM



NASA TM X-3420

NASA TM X-3420

LONGITUDINAL AERODYNAMIC CHARACTERISTICS
OF A LOW-WING LIFT-FAN TRANSPORT
INCLUDING HOVER CHARACTERISTICS
IN AND OUT OF GROUND EFFECT

Danny R. Hoad and Garl L. Gentry, Jr.

Langley Research Center

Hampton, Va. 23665

NATIONAL AERONAUTICS AND SPACE ADMINISTRATION • WASHINGTON, D. C. • FEBRUARY 1977

1. Report No. NASA TM X-3420		2. Government Accession No.		3. Recipient's Catalog No.	
4. Title and Subtitle LONGITUDINAL AERODYNAMIC CHARACTERISTICS OF A LOW-WING LIFT-FAN TRANSPORT INCLUDING HOVER CHARACTERISTICS IN AND OUT OF GROUND EFFECT				5. Report Date February 1977	
				6. Performing Organization Code	
7. Author(s) Danny R. Hoad and Garl L. Gentry, Jr.				8. Performing Organization Report No. L-10942	
				10. Work Unit No. 505-11-21-09	
9. Performing Organization Name and Address NASA Langley Research Center and Langley Directorate, USAAMRDL Hampton, VA 23665				11. Contract or Grant No.	
				13. Type of Report and Period Covered Technical Memorandum	
12. Sponsoring Agency Name and Address National Aeronautics and Space Administration Washington, DC 20546 and U.S. Army Air Mobility R&D Laboratory Moffett Field, CA 94035				14. Army Project No. 1F161102AH45	
				15. Supplementary Notes Danny R. Hoad: Langley Directorate, U.S. Army Air Mobility R&D Laboratory.	
16. Abstract The longitudinal aerodynamic characteristics of a six-fan, tip-driven (remote) lift-fan VTOL transport through transition were determined by an investigation conducted in the Langley V/STOL tunnel. Tests were also made with the large midspan lift-fan pods and lift-cruise fans removed to determine their influence on the stability and control of the configuration. Data were obtained for a range of model height above ground. The data are presented without analysis or discussion.					
17. Key Words (Suggested by Author(s)) Remote lift fan VTOL aerodynamics Ground effect Low wing			18. Distribution Statement Unclassified - Unlimited Subject Category 02		
19. Security Classif. (of this report) Unclassified		20. Security Classif. (of this page) Unclassified		21. No. of Pages 148	22. Price* \$5.75

LONGITUDINAL AERODYNAMIC CHARACTERISTICS OF A LOW-WING
LIFT-FAN TRANSPORT INCLUDING HOVER CHARACTERISTICS
IN AND OUT OF GROUND EFFECT

Danny R. Hoad* and Carl L. Gentry, Jr.
Langley Research Center

SUMMARY

A wind-tunnel investigation has been conducted on the effects of ground proximity on the longitudinal forces and moments of a tip-driven (remote) lift-fan VTOL transport. Longitudinal aerodynamic data were obtained at various fan-exit deflection angles simulating aircraft configurations through transition. The large midspan lift-fan pods and lift-cruise fans were removed to determine their influence on the stability and control of the configuration. Data were also obtained at zero wind speed for a range of model height above ground. The data are presented without analysis or discussion.

INTRODUCTION

A viable VTOL transport using tip-driven lift fans providing vertical thrust is of considerable interest for future application. The design of VTOL aircraft requires a detailed knowledge of the propulsion-induced effects, in and out of ground effect, in hover and in transition flight. General research has been expended to date on basic VTOL concepts (refs. 1 to 4). Configuration-oriented investigations have been conducted with small-scale wind-tunnel models (including free-flight model tests) at the NASA Langley Research Center (refs. 5 to 8) and with large-scale wind-tunnel models at the NASA Ames Research Center (refs. 9 to 13). Flight tests have also been conducted on VTOL transport configurations (refs. 14 and 15).

Preliminary design work has been undertaken by several organizations for a lift-fan VTOL transport. Hawker Siddeley has conducted a preliminary design study on a 16-fan VTOL transport (ref. 16); McDonnell Douglas Corporation, on a 6-fan VTOL transport (ref. 17); and Dornier GMBH, on a 12-fan VTOL transport (ref. 18). The NASA Ames Research Center has sponsored a series of conceptual design studies (refs. 17, 19, and 20). For the present investigation, NASA Langley Research Center chose a preliminary

*Langley Directorate, U.S. Army Air Mobility R&D Laboratory.

version of one of the configurations in reference 20 to provide basic longitudinal aerodynamic characteristics of a representative configuration.

The configuration is a low-wing tip-driven lift-fan VTOL transport. Two lift fans were enclosed in each pod located approximately midspan on each wing and two lift-cruise fans were located on the aft portion of the fuselage. A turbojet engine is used to drive each tip-turbine fan.

The investigation was conducted in the Langley V/STOL tunnel. Three configurations of 8.6-percent scale model were tested at zero wind speed at various heights above the ground board. They were also tested through a range of angle of attack at speeds from hover through transition at two power conditions. The data from the investigation have been corrected for wall effects (ref. 21).

SYMBOLS

The aerodynamic data in this report are referred to the stability-axis system. (See fig. 1.) All of the moment data are referred to a moment center located on the fuselage reference line at the 32.17-percent point of the mean geometric chord, the center of thrust in the hover condition. (See fig. 2.)

A_j	fan-exit area (0.078 m ² total for six fans)
C_D	drag coefficient, $\frac{D}{q_\infty S}$
C_L	lift coefficient, $\frac{L}{q_\infty S}$
C_m	pitching-moment coefficient, $\frac{M_Y}{q_\infty S \bar{c}}$
C_μ	fan-thrust coefficient, $\frac{T}{q_\infty S}$
c	local wing chord, m
\bar{c}	mean geometric chord (M.G.C.), m
c_h	local chord, horizontal stabilizer, m
c_v	local chord, vertical stabilizer, m
D	drag, N

D_e	effective fan-exit diameter (0.314 m), $\sqrt{\frac{4A_j}{\pi}}$
h	height, orthogonally, from ground plane to moment reference center of model, m
i_t	horizontal-tail incidence angle (positive direction, trailing edge down), deg
L	lift, N
M_X	rolling moment, m-N
M_Y	pitching moment, m-N
M_Z	yawing moment, m-N
M_∞	free-stream Mach number
p_a	ambient pressure, Pa
p_{te}	exit local total pressure, Pa
q_∞	free-stream dynamic pressure, Pa
S	wing area, m ²
T	static thrust, N
V_e	effective velocity ratio, $\sqrt{\frac{q_\infty}{T/2A_j}}$
V_j	fan-exit velocity, m/sec
V_∞	free-stream velocity, m/sec
\dot{w}_p	fan-primary mass flow, kg/sec
\dot{w}_s	fan-inlet mass flow, kg/sec
X, Y, Z	axes and forces along axes, N

x	chordwise station measured from airfoil nose, m
z_l	lower-surface distance perpendicular to chord of airfoil, m
z_u	upper-surface distance perpendicular to chord of airfoil, m
α	angle of attack, deg
β	angle of sideslip, deg
δ_e	elevator deflection angle (positive direction, trailing edge down), deg
δ_f	wing trailing-edge flap deflection angle (positive direction, trailing edge down), deg
δ_L	lift-fan louver deflection angle (positive direction, rearward), deg
$\delta_{L,J}$	lift-fan exit-flow deflection angle (positive direction, rearward), deg
δ_{LC}	lift-cruise fan-exit deflection angle (positive direction, down), deg
$\delta_{LC,J}$	lift-cruise fan-exit-flow deflection angle (positive direction, down), deg
ρ_j	fluid density, fan-exit flow, kg/m ³
ρ_∞	fluid density, free-stream flow, kg/m ³
ϕ	angle of roll, deg

Abbreviations:

B.L.	buttock line, distance along Y-axis, m
Fus. Ref.	fuselage reference line, W.L. 0.2184 m
H-tail	horizontal tail
V-tail	vertical tail

Sta. station

W.L. water line, distance along Z-axis, m

MODEL AND APPARATUS

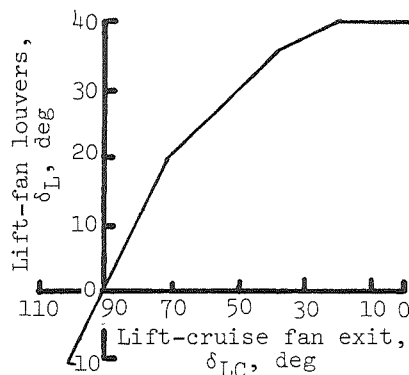
The model used in this investigation was a 8.6-percent-scale model of the tip-driven (remote) lift-fan VTOL transport described in reference 20. A three-view drawing of the base model used for model geometric references is presented in figure 2, and a three-view drawing of the VTOL transport model, in figure 3. The ordinates for the wing are given in table I at four spanwise locations. Figure 4 is a photograph of the model installed in the Langley V/STOL tunnel.

The 30-percent-chord translating wing flaps were single slotted. The flap slot was 1-percent local wing chord when deflected at 40° from the wing reference chord. Cross-sectional views of the flap and wing are presented in figure 5. The 30-percent-chord, simple-hinged ailerons (fig. 2) had a deflection range of $\pm 25^\circ$ in 5° increments.

The geometric characteristics of the horizontal tail are presented in figure 6. (See table II for ordinates.) It was pivoted about the 60.5-percent root chord with an incidence range of $\pm 180^\circ$ in 2.5° increments. The 25-percent-chord, simple-hinged elevator had a deflection range of $\pm 15^\circ$ in 5° increments. Ordinates for the vertical tail are given in table III. The 28-percent-chord, simple-hinged rudder had a deflection range of $\pm 25^\circ$ in 5° increments.

Six tip-turbine fan engine simulators, similar to the one shown in figure 7, were used to represent the four lift fans mounted in pods on the wing and the two lift-cruise fans mounted on the fuselage. Each fan simulator was instrumented with: (1) a magnetic fan-speed indicator; (2) bearing temperature measurement devices; (3) 20 total pressure probes in the exit; and (4) tip and hub static pressure taps in the exit. Each fan required an oil mist system for bearing lubrication.

A pod was located on each wing at the 52.8-percent semispan. In each pod, two lift fans were mounted with vertical fan axes. (See fig. 8.) These fans were mounted forward of the moment reference center to provide a thrust balance in hover with the aft lift-cruise fans. The transition from take-off to wingborne flight or wingborne flight to landing was accomplished by deflecting, from the fan axis, a set of louvers in the exit of the lift fans on a schedule with deflection of the lift-cruise fan exits as shown in the following sketch:



The louver deflections (see fig. 9) tested were -5° for landing, 0° for hover, 7.5° for take-off, 20° for speed in the middle of transition, 40° for the high-speed end of transition, and closed (90°) for wingborne flight.

The lift-cruise fans are located with axis horizontal on the aft portion of the fuselage. (See fig. 3.) Transition flight was simulated by deflecting the lift-cruise-fan exit, from the fan axis, in a lobster-tail fashion on a schedule with the lift-fan louvers. The deflected lift-cruise-fan exits were 94° for landing (fig. 10(a)), 90° for hover (fig. 10(b)), 82° for take-off (fig. 10(c)), 70° for midtransition (fig. 10(d)), and 0° for end of transition (fig. 10(e)). The 0° deflection of the lift-cruise fans was also used with lift-fan inlets and exits closed for wingborne flight.

The lift-fan pods and lift-cruise fans were separately removable such that a component breakdown could be performed to determine their effect on the aerodynamics and stability of the configuration.

The model was mounted in the Langley V/STOL tunnel on a sting-supported six-component strain-gage balance for measurement of the total forces and moments.

TEST AND CORRECTIONS

The free-stream dynamic pressure for the investigation varied from 0 to 2672 Pa $M_\infty = 0.240$. The Reynolds number (based on wing \bar{c} and free-stream velocity) ranged from 0 to 1.376×10^6 . The data presented in this report have been corrected for wind-tunnel wall effects using reference 21.

Calibrations were made to determine the individual thrust and the individual primary mass flow and fan-inlet mass flow of each fan simulator for each exit deflection angle. The data were obtained at zero airspeed and reflect static fan parameters only. Figure 11 presents the thrust as a function of fan speed and as a function of exit pressure ratio for a typical lift fan and a typical lift-cruise fan for each exit deflection angle. The

primary mass flow and fan-inlet mass flow for a typical lift fan and a typical lift-cruise fan at each deflection angle are presented in figure 12. The fan-exhaust deflection angles for a typical lift fan and a typical lift-cruise fan at each deflection angle are presented in figure 13. The fan-exhaust deflection for the 40° lift-fan louver was approximately 20°; therefore, it was used to simulate the 20° deflection lift-fan configuration. As a result, the fan-exhaust deflection of 40° required for the end-of-transition configuration was not available for the present investigation.

Thrust coefficient and effective-velocity ratio in this report were determined from the static-thrust calibration as a function of rpm (using the total of the individually measured thrusts) from the following equation:

$$C_{\mu} = \frac{T}{q_{\infty} S}$$

$$V_e = \sqrt{\frac{\rho_{\infty} V_{\infty}^2}{\rho_j V_j^2}} = \sqrt{\frac{q_{\infty}}{T/2A_j}}$$

The relationship between C_{μ} and V_e is presented in figure 14.

Ground-effect data were obtained at zero wind velocity for two angles of attack and two roll angles. The wind-tunnel walls were removed for all hovering tests to reduce circulation induced by them. The height of the model above the floor was measured orthogonally from the floor to the moment reference center of the model. Three configurations were tested in ground effect at zero wind speed: (1) landing configuration, $\delta_L = -5^\circ$, $\delta_{LC} = 94^\circ$; (2) take-off configuration, $\delta_L = 7.5^\circ$, $\delta_{LC} = 82^\circ$; and (3) hover configuration, $\delta_L = 0^\circ$, $\delta_{LC} = 90^\circ$. The longitudinal aerodynamic characteristics of the model were obtained such that the free-stream dynamic pressure over the model at a particular fan-exhaust deflection configuration matched that proposed for the corresponding airplane configuration in reference 20. The effective velocity ratios proposed in reference 20 were simulated by pairs of velocity ratios in the wind tunnel, one slightly lower and one slightly higher than the one given in the reference. Data were obtained through a range of angles of attack from approximately -6° to 20° . Data were obtained for all configurations at various tail incidences and various elevator deflections for selected configurations.

PRESENTATION OF RESULTS

The data are being presented without analysis or discussion. The ground-effect data at zero wind speed are shown in ratios of lift and drag to thrust and pitching moment

and rolling moment to the product of the thrust and effective exit diameter of the operating fans. These parameters are presented at various thrust settings as a function of the ratio of height above the floor to the effective exit diameter of the operating fans.

Data for power-on transition configurations ($\delta_L = -5^\circ$ and $\delta_{LC} = 94^\circ$; $\delta_L = 0^\circ$ and $\delta_{LC} = 90^\circ$; $\delta_L = 7.5^\circ$ and $\delta_{LC} = 82^\circ$; and $\delta_L = 40^\circ$ and $\delta_{LC} = 70^\circ$) are given as ratios of lift and drag to thrust and of pitching moment to the product of thrust and the effective exit diameter of the operating fans. Data for the wingborne flight configuration (δ_L closed and $\delta_{LC} = 0^\circ$) appear as lift, drag, and pitching-moment coefficients. All power-off data are presented in the latter format as well as the power-on data for the configuration of $\delta_L = 40^\circ$ and $\delta_{LC} = 70^\circ$.

Results of the investigation are presented in the following figures:

	Figure
Effect of ground proximity on induced loads of configurations at zero wind speed for -	
Hover with $\delta_L = 0^\circ$; $\delta_{LC} = 90^\circ$:	
Tail off; $\alpha = 0^\circ$; $\phi = 0^\circ$	15(a)
$i_t = 0^\circ$; $\alpha = 0^\circ$; $\phi = 0^\circ$	15(b)
Tail off; $\alpha = 10^\circ$; $\phi = 0^\circ$	15(c)
Tail off; $\alpha = 0^\circ$; $\phi = 10^\circ$	15(d)
$i_t = 0^\circ$; $\alpha = 0^\circ$; $\phi = 10^\circ$	15(e)
Landing configuration with $\delta_L = -5^\circ$; $\delta_{LC} = 94^\circ$:	
Tail off; $\alpha = 0^\circ$; $\phi = 0^\circ$	16(a)
$i_t = 0^\circ$; $\alpha = 0^\circ$; $\phi = 0^\circ$	16(b)
$i_t = 0^\circ$; $\alpha = 10^\circ$; $\phi = 0^\circ$	16(c)
$i_t = 0^\circ$; $\alpha = 0^\circ$; $\phi = 10^\circ$	16(d)
Take-off configuration with $\delta_L = 7.5^\circ$; $\delta_{LC} = 82^\circ$:	
Tail off; $\alpha = -4^\circ$; $\phi = 0^\circ$	17(a)
$i_t = 0^\circ$; $\alpha = -4^\circ$; $\phi = 0^\circ$	17(b)
$i_t = 0^\circ$; $\alpha = 0^\circ$; $\phi = 0^\circ$	17(c)
$i_t = 0^\circ$; $\alpha = 0^\circ$; $\phi = 10^\circ$	17(d)
$i_t = 0^\circ$; $\alpha = -4^\circ$; $\phi = 10^\circ$	17(e)
Longitudinal aerodynamic characteristics of the VTOL transition configuration with $\delta_L = 0^\circ$; $\delta_{LC} = 90^\circ$ -	
Effect of tail incidence for $q_\infty = 239$ Pa; $M_\infty = 0.058$:	
Power off	18
Power on:	
$V_e = 0.12$	19(a)
$V_e = 0.18$	19(b)

Effect of elevator deflection for $q_\infty = 239$ Pa; $M_\infty = 0.058$:	
Power off	20
Power on:	
$V_e = 0.12$	21(a)
$V_e = 0.18$	21(b)
Effect of effective velocity ratio	22
Effect of closed lift-fan inlets and exits for $q_\infty = 239$ Pa; $M_\infty = 0.058$	23
Longitudinal aerodynamic characteristics of the VTOL transition configuration with $\delta_L = -5^\circ$; $\delta_{LC} = 94^\circ$ -	
Effect of tail incidence for $q_\infty = 168$ Pa; $M_\infty = 0.048$:	
Power off	24
Power on:	
$V_e = 0.12$	25(a)
$V_e = 0.15$	25(b)
Effect of effective velocity ratio	26
Effect of closed lift-fan inlets and exits for $q_\infty = 168$ Pa; $M_\infty = 0.048$	27
Longitudinal aerodynamic characteristics of the VTOL transition configuration with $\delta_L = 7.5^\circ$; $\delta_{LC} = 82^\circ$ -	
Effect of tail incidence:	
Power off:	
$q_\infty = 187$ Pa; $M_\infty = 0.052$	28
$q_\infty = 455$ Pa; $M_\infty = 0.080$	29
Power on for $q_\infty = 177$ Pa; $M_\infty = 0.050$:	
$V_e = 0.12$	30(a)
$V_e = 0.15$	30(b)
Power on for $q_\infty = 440$ Pa; $M_\infty = 0.078$:	
$V_e = 0.20$	31(a)
$V_e = 0.24$	31(b)
Effect of elevator deflection:	
Power off for $q_\infty = 455$ Pa; $M_\infty = 0.080$	32
Power on for $q_\infty = 440$ Pa; $M_\infty = 0.078$:	
$V_e = 0.20$	33(a)
$V_e = 0.24$	33(b)
Effect of effective velocity ratio	34
Effect of closed lift-fan inlets and exits for $q_\infty = 455$ Pa; $M_\infty = 0.080$	35

Longitudinal aerodynamic characteristics of the VTOL transition

configuration with $\delta_L = 40^\circ$; $\delta_{LC} = 70^\circ -$

Effect of tail incidence:

Power off:

 $q_\infty = 728 \text{ Pa}$; $M_\infty = 0.102$ 36 $q_\infty = 1245 \text{ Pa}$; $M_\infty = 0.134$ 37

Power on:

 $q_\infty = 709 \text{ Pa}$; $M_\infty = 0.100$: $V_e = 0.24$ 38(a) $V_e = 0.29$ 38(b) $q_\infty = 1230 \text{ Pa}$; $M_\infty = 0.133$: $V_e = 0.31$ 39(a) $V_e = 0.38$ 39(b) $q_\infty = 1230 \text{ Pa}$; $M_\infty = 0.133$: $C_\mu = 2.0$ 40(a) $C_\mu = 2.9$ 40(b) $q_\infty = 709 \text{ Pa}$; $M_\infty = 0.100$: $C_\mu = 3.4$ 41(a) $C_\mu = 5.1$ 41(b)

Effect of elevator deflection:

Power off:

 $q_\infty = 728 \text{ Pa}$; $M_\infty = 0.102$ 42 $q_\infty = 1245 \text{ Pa}$; $M_\infty = 0.134$ 43

Power on:

 $q_\infty = 709 \text{ Pa}$; $M_\infty = 0.100$: $V_e = 0.24$ 44(a) $V_e = 0.29$ 44(b) $q_\infty = 1230 \text{ Pa}$; $M_\infty = 0.133$: $V_e = 0.31$ 45(a) $V_e = 0.38$ 45(b) $q_\infty = 1230 \text{ Pa}$; $M_\infty = 0.133$: $C_\mu = 2.0$ 46(a) $C_\mu = 2.9$ 46(b) $q_\infty = 709 \text{ Pa}$; $M_\infty = 0.100$: $C_\mu = 3.4$ 47(a) $C_\mu = 5.1$ 47(b)

	Figure
Effect of effective velocity ratio	48
Effect of closed lift-fan inlets and exits for $q_\infty = 1245$ Pa; $M_\infty = 0.134$	49
Longitudinal aerodynamic characteristics of the VTOL configuration	
with $\delta_L =$ closed; $\delta_{LC} = 0^0$; $q_\infty = 2672$ Pa; $M_\infty = 0.236$ -	
Effect of tail incidence:	
Power off for $\delta_f = 40^0$	50
Power on for $\delta_f = 40^0$:	
$C_\mu = 0.19$	51
$C_\mu = 0.37$	52
Power off for $\delta_f = 0^0$	53
Power on for $\delta_f = 0^0$:	
$C_\mu = 0.19$	54
$C_\mu = 0.37$	55
Effect of elevator deflection:	
Power off for $\delta_f = 40^0$	56
Power on for $\delta_f = 40^0$:	
$C_\mu = 0.19$	57
$C_\mu = 0.37$	58
Power off for $\delta_f = 0^0$	59
Power on for $\delta_f = 0^0$:	
$C_\mu = 0.19$	60
$C_\mu = 0.37$	61
Effect of closed lift-cruise fan inlets	62
Longitudinal aerodynamic characteristics of components of VTOL configuration for -	
Effect of tail incidence for $q_\infty = 2672$ Pa; $M_\infty = 0.236$:	
Lift-fan pods and lift-cruise fans removed:	
$\delta_f = 40^0$	63
$\delta_f = 0^0$	64
Lift-fan pods removed:	
$\delta_f = 40^0$	65
$\delta_f = 0^0$	66

CONCLUDING REMARKS

Presented are unanalyzed data from a wind-tunnel investigation to determine the effect of ground proximity on the longitudinal forces and moments of a low-wing lift-fan VTOL transport.

Langley Research Center
National Aeronautics and Space Administration
Hampton, VA 23665
October 28, 1976

REFERENCES

1. Gentry, Garl L.; and Margason, Richard J.: Jet-Induced Lift Losses on VTOL Configurations Hovering In and Out of Ground Effect. NASA TN D-3166, 1966.
2. Margason, Richard J.: The Path of a Jet Directed at Large Angles to a Subsonic Free Stream. NASA TN D-4919, 1968.
3. Carter, Arthur W.: Effects of Jet-Exhaust Location on the Longitudinal Aerodynamic Characteristics of a Jet V/STOL Model. NASA TN D-5333, 1969.
4. Margason, Richard J.: Review of Propulsion-Induced Effects on Aerodynamics of Jet V/STOL Aircraft. NASA TN D-5617, 1970.
5. Newsom, William A., Jr.; and Moore, Frederick L.: Wind-Tunnel Investigation of a V/STOL Transport Model With Six Wing-Mounted Lift Fans. NASA TN D-5695, 1970.
6. Newsom, William A., Jr.: Wind-Tunnel Investigation of a V/STOL Transport Model With Four Pod-Mounted Lift Fans. NASA TN D-5942, 1970.
7. Newsom, William A., Jr.; and Grafton, Sue B.: Flight Investigation of a V/STOL Transport Model With Four Pod-Mounted Lift Fans. NASA TN D-6129, 1971.
8. Newsom, William A., Jr.; and Grafton, Sue B.: Flight Investigation of a V/STOL Transport Model Having Six Wing-Mounted Lift Fans. NASA TN D-6198, 1971.
9. Kirk, Jerry V.; Hickey, David H.; and Hall, Leo P.: Aerodynamic Characteristics of a Full-Scale Fan-In-Wing Model Including Results in Ground Effect With Nose-Fan Pitch Control. NASA TN D-2368, 1964.
10. Kirk, Jerry V.; Hodder, Brent K.; and Hall, Leo P.: Large-Scale Wind-Tunnel Investigation of a V/STOL Transport Model With Wing-Mounted Lift Fans and Fuselage-Mounted Lift-Cruise Engines for Propulsion. NASA TN D-4233, 1967.
11. Hall, Leo P.; and Kirk, Jerry V.: Large-Scale Wind-Tunnel Investigation of a V/STOL Transport Model With Podded Lift Fans Forward and Aft of a Low Mounted Wing. NASA TM X-62,102, 1971.
12. Dickinson, Stanley O.; Hall, Leo P.; and Hodder, Brent K.: Aerodynamic Characteristics of a Large-Scale V/STOL Transport Model With Tandem Lift Fans Mounted at Mid-Semispan of the Wing. NASA TN D-6234, 1971.
13. Kirk, Jerry V.; Dickinson, Stanley O.; Hall, Leo P.; and Coffman, Mary G.: Aerodynamic Characteristics of a Large Scale Lift Fan Transport Model With Podded Fans Forward and Lift Cruise Fans Mounted Above the Wing. NASA TM X-62,151, 1972.

14. Holzhauser, Curt A.; Morello, Samuel A.; Innis, Robert C.; and Patton, James M., Jr.:
A Flight Evaluation of a VTOL Jet Transport Under Visual and Simulated Instrument
Conditions. NASA TN D-6754, 1972.
15. XV-5A Lift Fan Flight Research Aircraft. Phase I Flight Test Results – Vol. I.
Rep. No. 166 (Contract DA 44-177-TC-715), Gen. Elec. Co., Mar. 1966.
16. Szlenkier, T. K.: Latest Civil V/STOL Aircraft Projects of Hawker Siddeley Aviation.
NASA TT F-14629, 1972.
17. V/STOL Aircraft Advanced Eng., McDonnell Aircraft Co.: Conceptual Design Studies
of a V/STOL Civil Lift Fan Transport Including Effect of Size and Fan Pressure
Ratio. NASA CR-2426, 1974.
18. Betrachtungen zum Entwurf des V/STOL-Projekts – Dornier Do 231. LRT, bd. 16,
nr. 1, Jan. 1970, pp. 15-20.
19. Eldridge, W. M.; Ferrell, J. A.; McKee, J. W.; Wayne, J. F., Jr.; and Zabinsky, J. M.:
Conceptual Design Studies of Candidate V/STOL Lift Fan Commercial Short
Haul Transport for 1980-85 V/STOL Lift Fan Study. NASA CR-2183, 1973.
20. Knight, Ronald G.; Powell, William V., Jr.; and Prizlow, Jerome A.: Conceptual
Design Study of a V/STOL Lift Fan Commercial Short Haul Transport. NASA
CR-2185, 1973.
21. Heyson, Harry H.: Linearized Theory of Wind-Tunnel Jet-Boundary Corrections and
Ground Effect for VTOL-STOL Aircraft. NASA TR R-124, 1962.

TABLE I - WING AIRFOIL ORDINATES

Spanwise location: Root
c: 43.688 cm

x/c	z_u/c	z_l/c
0	0.0496	0.0465
.005	.0597	.0345
.010	.0648	.0287
.015	.0686	.0242
.020	.0719	.0205
.025	.0746	.0172
.035	.0792	.0117
.050	.0842	-.0048
.075	.0895	-.0042
.100	.0925	-.0113
.125	.0937	-.0173
.150	.0941	-.0224
.200	.0931	-.0305
.250	.0911	-.0366
.300	.0884	-.0406
.350	.0845	-.0427
.400	.0801	-.0436
.450	.0752	-.0436
.500	.0701	-.0428
.550	.0647	-.0414
.600	.0589	-.0394
.650	.0528	-.0371
.700	.0462	-.0343
.750	.0384	-.0311
.800	.0303	-.0271
.850	.0221	-.0222
.900	.0140	-.0166
.950	.0058	-.0102
1.000	-.0024	-.0028

Spanwise location: 17.26 cm
c: 38.52 cm

x/c	z_u/c	z_l/c
0	0.0495	0.0471
.0071	.0604	.0348
.0127	.0647	.0302
.0184	.0682	.0267
.0241	.0711	.0238
.0297	.0737	.0213
.0354	.0760	.0191
.0468	.0799	.0152
.0694	.0857	.0092
.0978	.0908	.0035
.1262	.0943	-.0010
.1545	.0967	-.0045
.2112	.0990	-.0099
.2679	.0991	-.0139
.3246	.0975	-.0165
.3813	.0946	-.0177
.4381	.0906	-.0177
.4948	.0858	-.0166
.5515	.0801	-.0148
.6082	.0736	-.0122
.6649	.0662	-.0089
.7216	.0580	-.0050
.7783	.0495	-.0003
.8350	.0417	.0050
.8917	.0347	.0105
.9484	.0283	.0163
1.000	.0224	.0219

Spanwise location: 31.67 cm
c: 34.20 cm

x/c	z_u/c	z_l/c
0	0.0493	0.0477
.0034	.0552	.0418
.0097	.0604	.0381
.0161	.0641	.0360
.0225	.0673	.0345
.0289	.0700	.0332
.0353	.0724	.0321
.0417	.0746	.0312
.0481	.0767	.0303
.0545	.0786	.0296
.0608	.0803	.0288
.0736	.0834	.0274
.1055	.0896	.0243
.1375	.0943	.0214
.1694	.0978	.0188
.2014	.1004	.0165
.2652	.1037	.0128
.3291	.1048	.0105
.3930	.1043	.0098
.4568	.1019	.0105
.5207	.0980	.0124
.5846	.0931	.0155
.6484	.0871	.0197
.7123	.0803	.0247
.7762	.0733	.0299
.8400	.0663	.0352
.9039	.0593	.0404
.9678	.0523	.0457
1.0000	.0487	.0483

Spanwise location: 84.54 cm
c: 18.37 cm

x/c	z_u/c	z_l/c
0	0.2195	0.2136
.0066	.2315	.1986
.0185	.2395	.1922
.0304	.2446	.1931
.0423	.2487	.1938
.0542	.2520	.1942
.0661	.2550	.1945
.0780	.2577	.1946
.0899	.2602	.1947
.1017	.2624	.1947
.1255	.2664	.1947
.1493	.2699	.1947
.1733	.2729	.1947
.1969	.2755	.1947
.2444	.2797	.1950
.3039	.2833	.1958
.3634	.2854	.1973
.4228	.2859	.1994
.4823	.2851	.2023
.5417	.2834	.2059
.6012	.2809	.2103
.6606	.2775	.2156
.7201	.2734	.2216
.7796	.2691	.2279
.8390	.2645	.2342
.8985	.2598	.2405
.9579	.2550	.2468
1.000	.2516	.2512

TABLE II. - HORIZONTAL TAIL AIRFOIL ORDINATES

x/c	z_u/c	z_l/c
0	0	0
.0050	.0073	-.0073
.0075	.0088	-.0088
.0125	.0111	-.0111
.0250	.0152	-.0152
.0500	.0210	-.0210
.0750	.0253	-.0253
.1000	.0288	-.0288
.1500	.0342	-.0342
.2000	.0384	-.0384
.2500	.0414	-.0414
.3000	.0434	-.0434
.3500	.0446	-.0446
.4000	.0450	-.0450
.4500	.0442	-.0442
.5000	.0424	-.0424
.5500	.0398	-.0398
.6000	.0366	-.0366
.6500	.0328	-.0328
.7000	.0286	-.0286
.7500	.0240	-.0240
.8000	.0193	-.0193
.8500	.0145	-.0145
.9000	.0097	-.0097
.9500	.0050	-.0050
1.0000	.0002	-.0002

TABLE III. - VERTICAL TAIL AIRFOIL ORDINATES

Location: W.L. 24.68 cm
c: 39.97 cm

x/c	z_u/c	z_l/c
0	0	0
.0050	.0085	-.0085
.0075	.0102	-.0102
.0125	.0129	-.0129
.0250	.0178	-.0178
.0500	.0245	-.0245
.0750	.0295	-.0295
.1000	.0336	-.0336
.1500	.0400	-.0400
.2000	.0447	-.0447
.2500	.0482	-.0482
.3000	.0507	-.0507
.3500	.0521	-.0521
.4000	.0525	-.0525
.4500	.0515	-.0515
.5000	.0494	-.0494
.5500	.0464	-.0464
.6000	.0427	-.0427
.6500	.0383	-.0383
.7000	.0334	-.0334
.7500	.0280	-.0280
.8000	.0225	-.0225
.8500	.0169	-.0169
.9000	.0114	-.0114
.9500	.0058	-.0058
1.0000	.0002	-.0002

Location: W.L. 57.01 cm
c: 26.00 cm

x/c	z_u/c	z_l/c
0	0	0
.0050	.0073	-.0073
.0075	.0088	-.0088
.0125	.0111	-.0111
.0250	.0152	-.0152
.0500	.0210	-.0210
.0750	.0253	-.0253
.1000	.0288	-.0288
.1500	.0342	-.0342
.2000	.0384	-.0384
.2500	.0414	-.0414
.3000	.0434	-.0434
.3500	.0446	-.0446
.4000	.0450	-.0450
.4500	.0442	-.0442
.5000	.0424	-.0424
.5500	.0398	-.0398
.6000	.0366	-.0366
.6500	.0328	-.0328
.7000	.0286	-.0286
.7500	.0240	-.0240
.8000	.0193	-.0193
.8500	.0145	-.0145
.9000	.0097	-.0097
.9500	.0050	-.0050
1.0000	.0002	-.0002

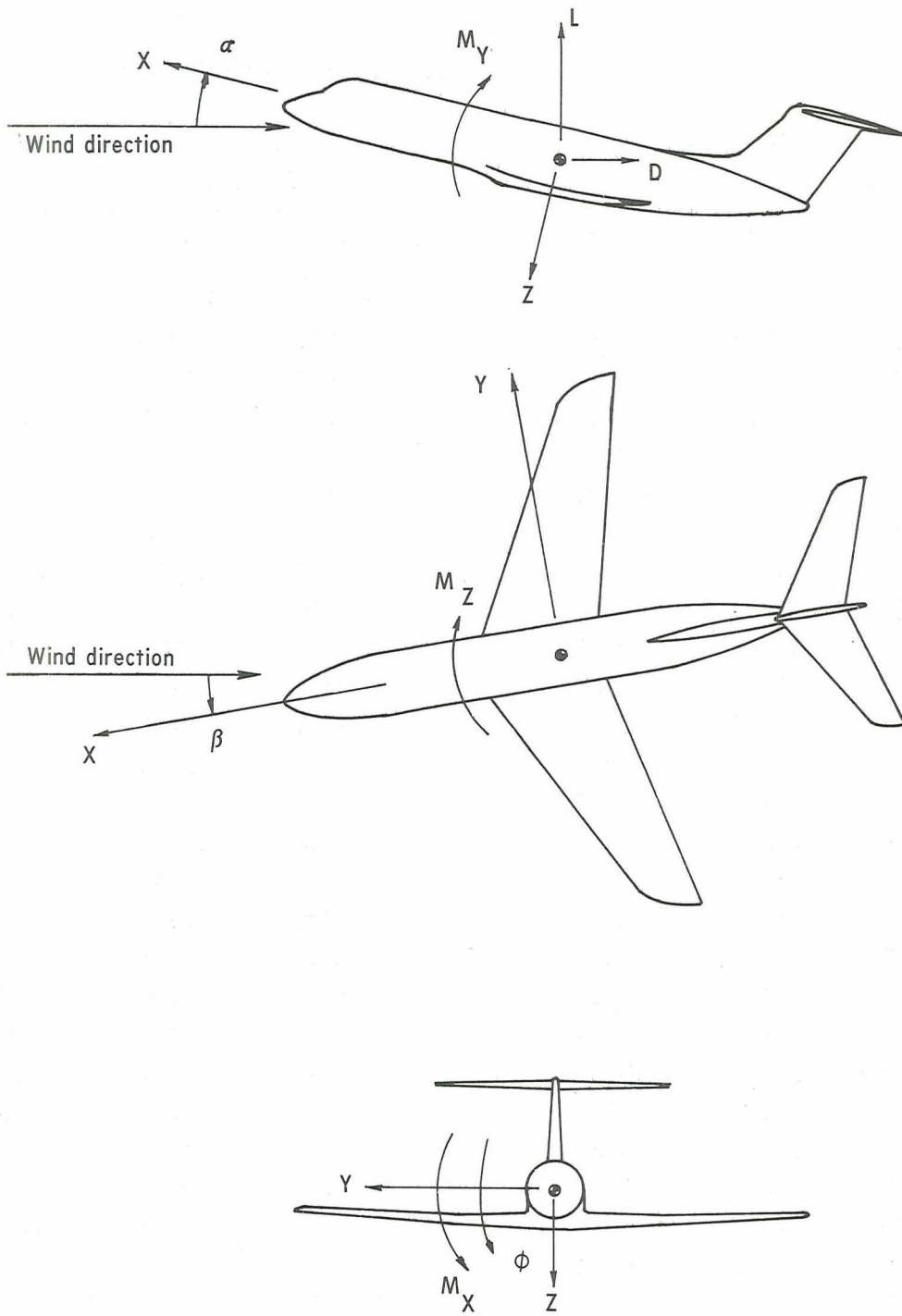


Figure 1.- Axis system used in presentation of data. Arrows indicate positive direction of forces and moments.

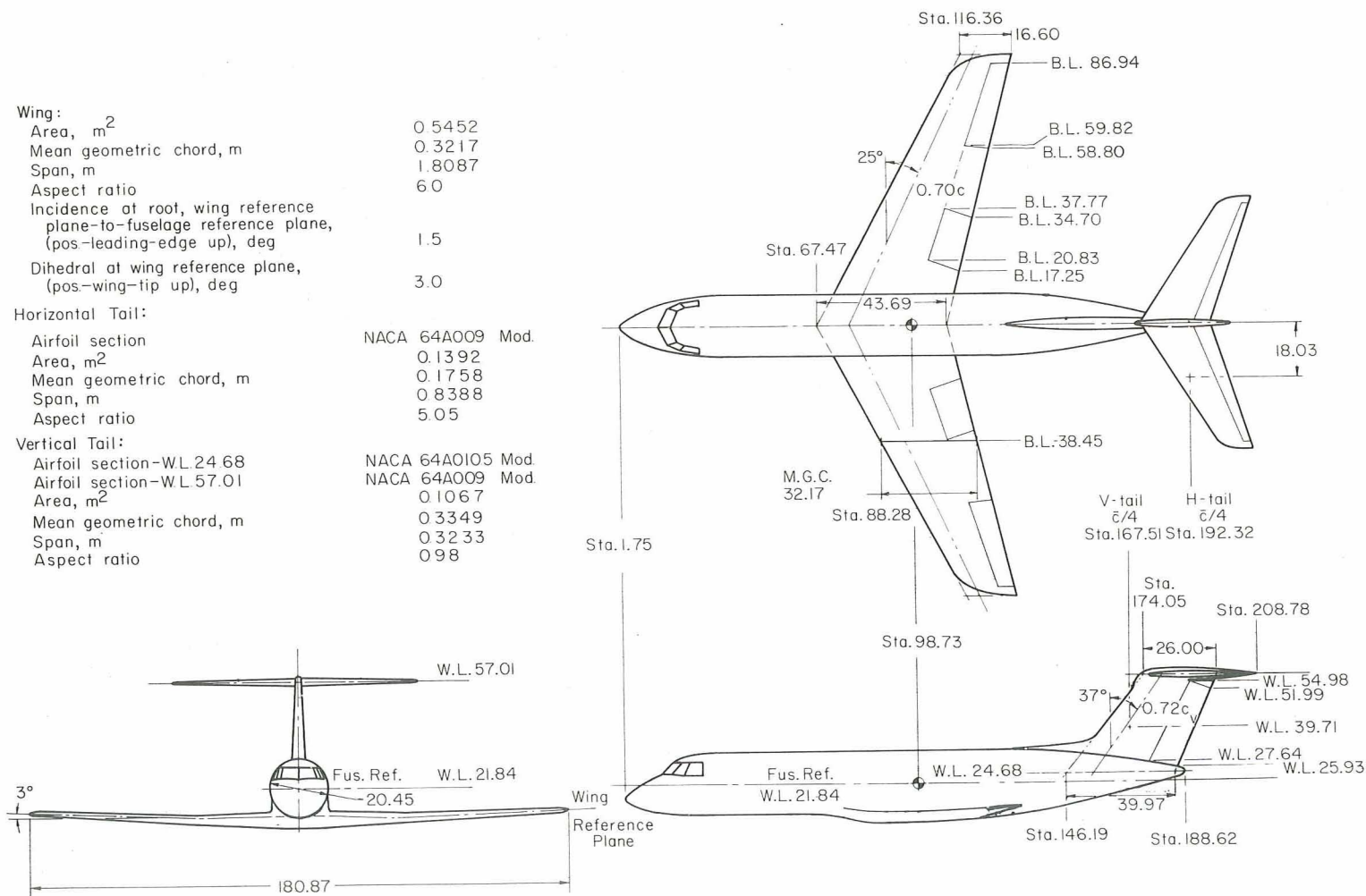


Figure 2.- Dimensional characteristics of the base model. Dimensions are in centimeters unless otherwise noted.

Wing:	
Area, m ²	0.5452
Mean geometric chord, m	0.3217
Span, m	1.8087
Aspect ratio	6.0
Incidence at root, wing reference plane-to-fuselage reference plane, (pos.-leading-edge up), deg	1.5
Dihedral at wing reference plane, (pos.-wing-tip up), deg	3.0
Horizontal Tail:	
Airfoil section	NACA 64A009 Mod.
Area, m ²	0.1392
Mean geometric chord, m	0.1758
Span, m	0.8388
Aspect ratio	5.05
Vertical Tail:	
Airfoil section-W.L. 24.68	NACA 64A010.5 Mod.
Airfoil section-W.L. 57.01	NACA 64A009 Mod.
Area, m ²	0.1067
Mean geometric chord, m	0.3349
Span, m	0.3233
Aspect ratio	0.98

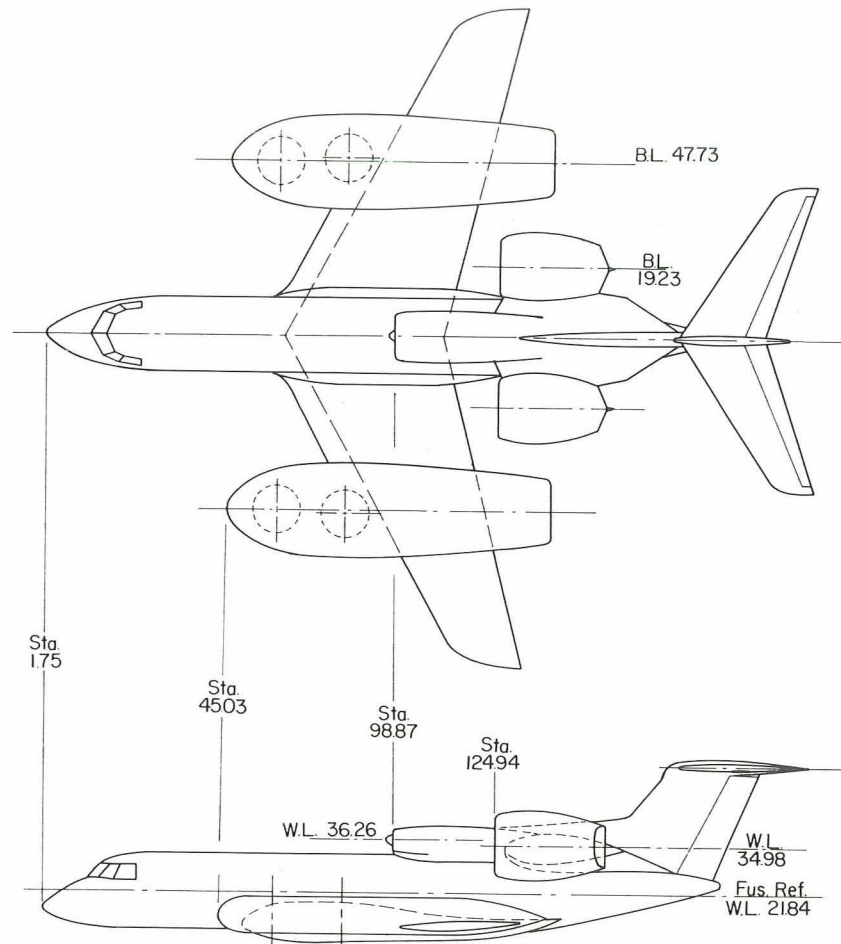
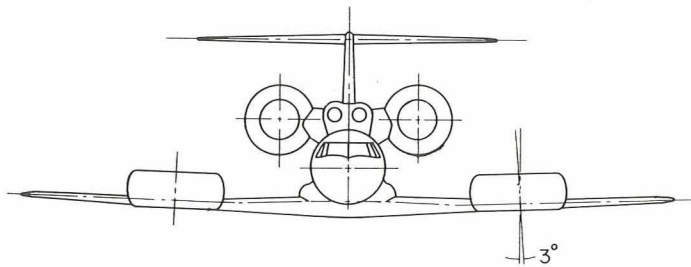
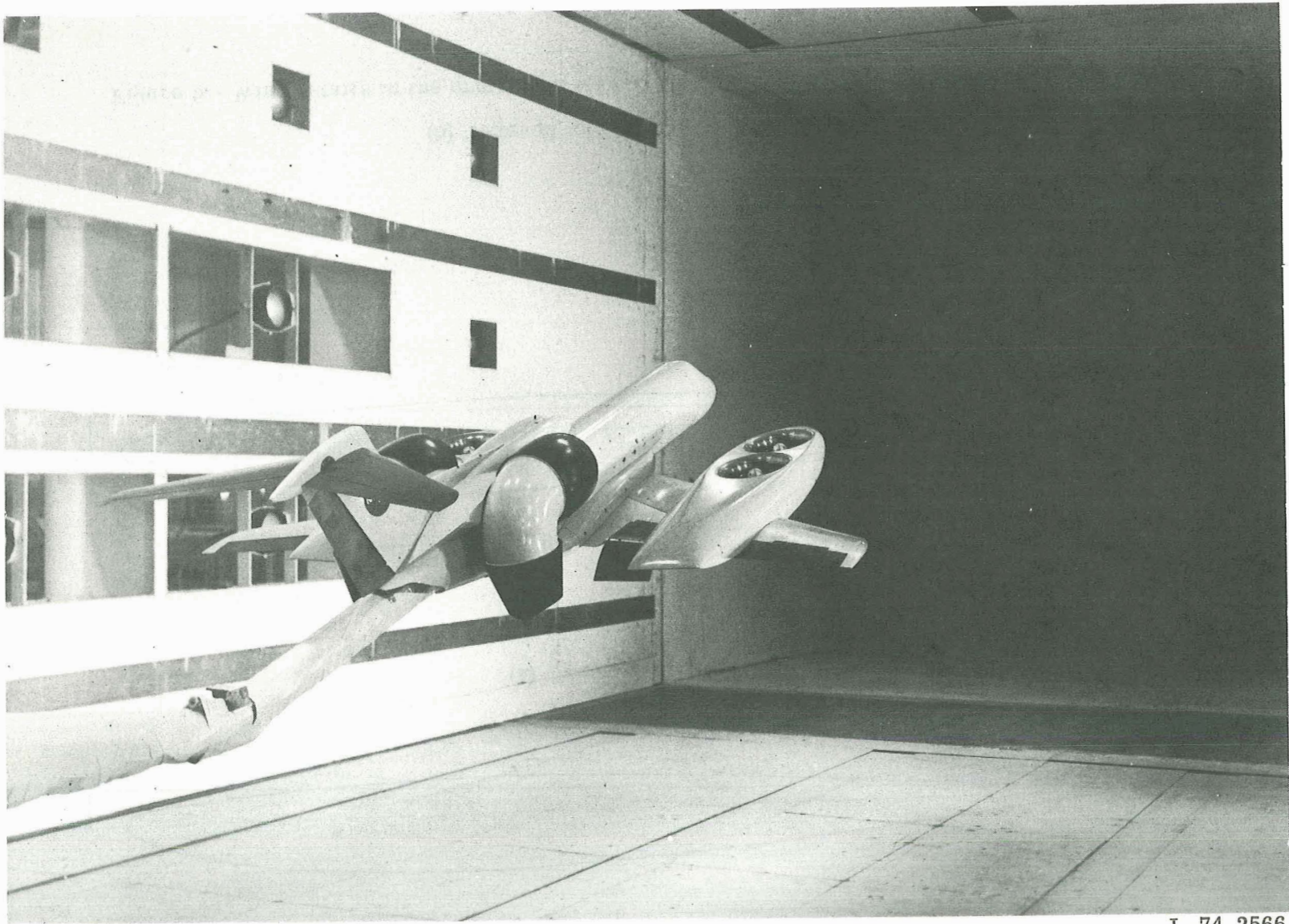
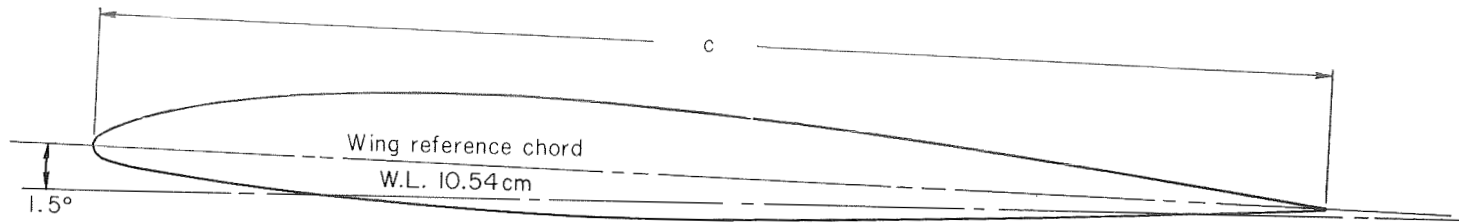


Figure 3.- Dimensional characteristics of the low-wing VTOL transport model.
Dimensions are in centimeters unless otherwise noted.

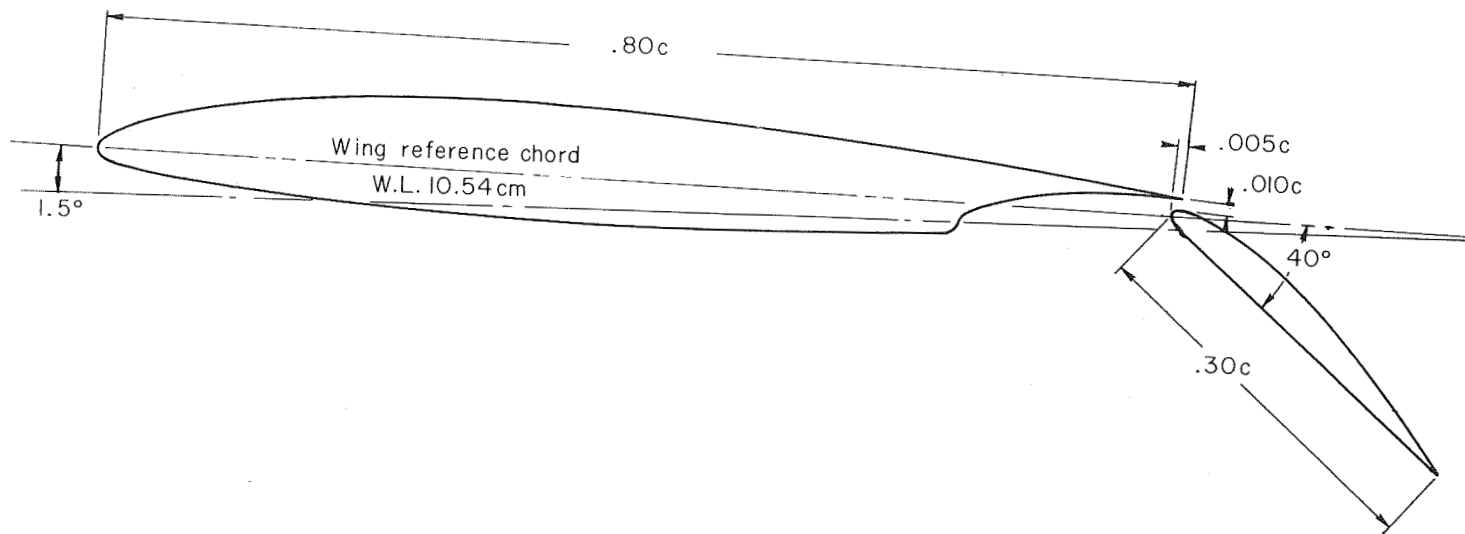


L-74-2566

Figure 4.- Three-quarter rear view of the low-wing VTOL transport mounted in the Langley V/STOL tunnel.



(a) Cruise configuration.



(b) Take-off and landing configuration.

Figure 5.- Wing details in the cruise and take-off and landing configurations. B.L. 31.62 cm.

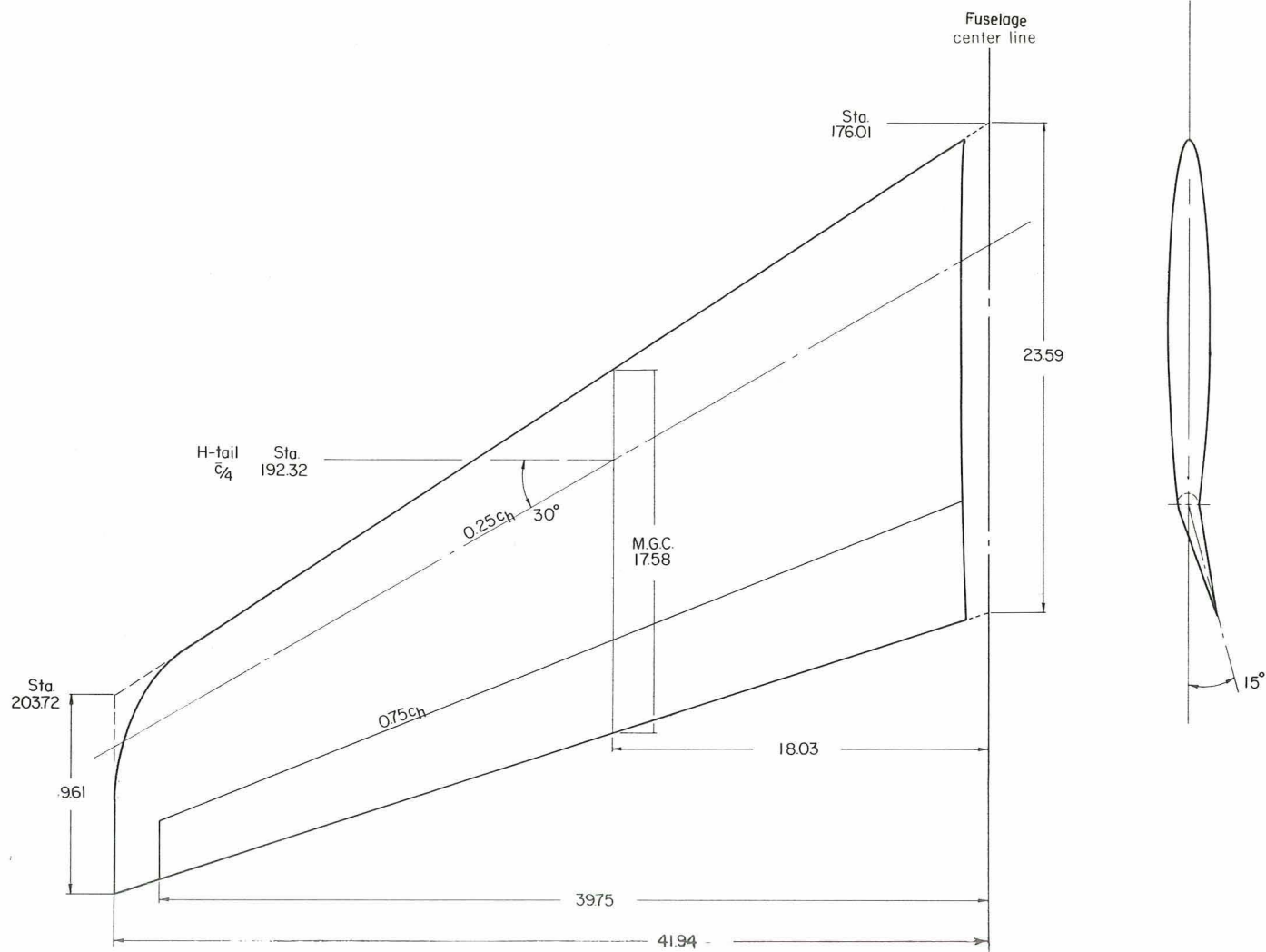


Figure 6.- Details of the horizontal tail used in the wind-tunnel investigation.
 Linear dimensions are in centimeters or fraction of local chord.

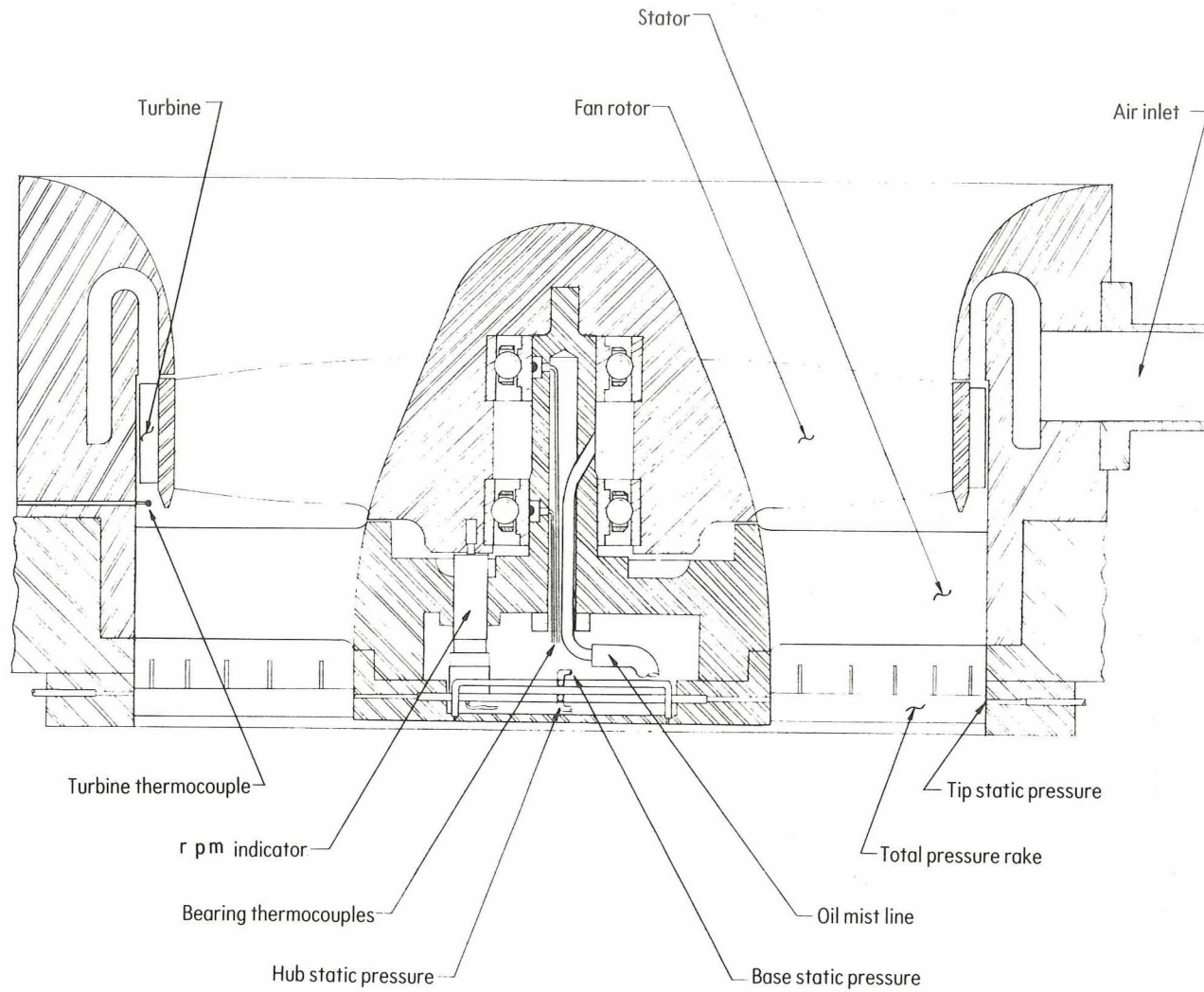


Figure 7.- Details of basic fan assembly with instrumentation.

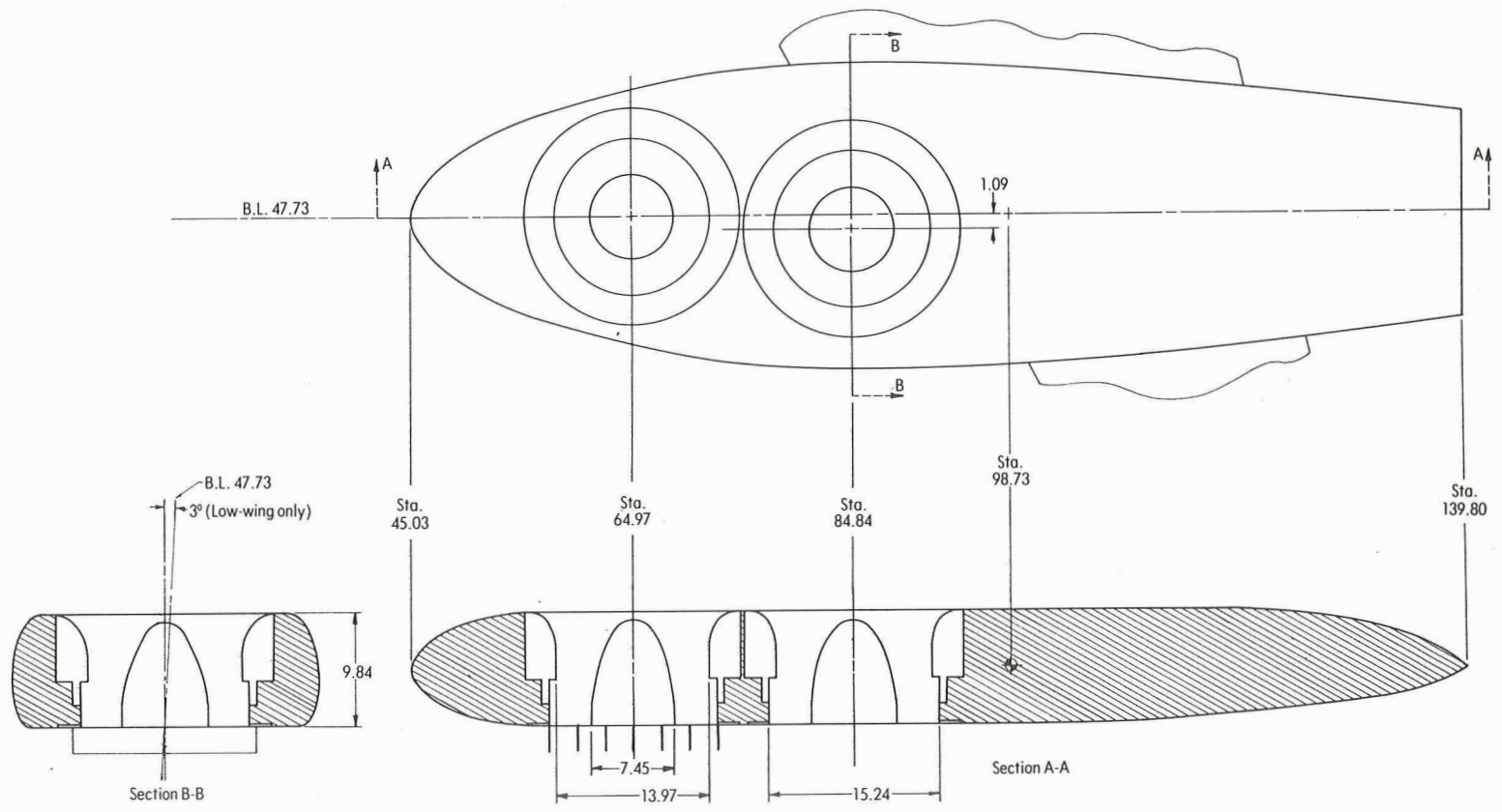


Figure 8.- Details of lift-fan pod and fan location. Linear dimensions are in centimeters.

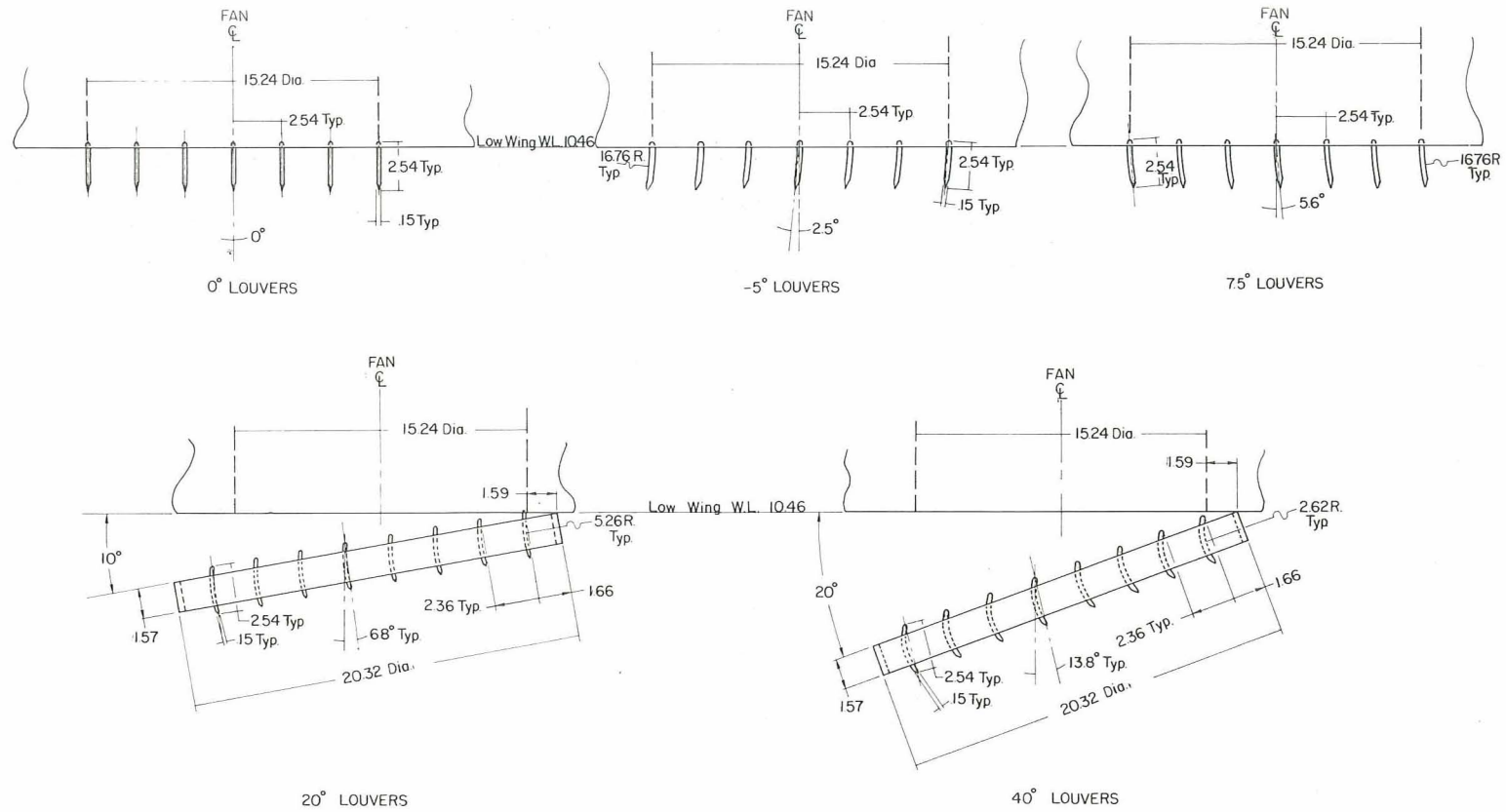


Figure 9.- Details of louver assemblies on each lift-fan exit. Linear dimensions are in centimeters.

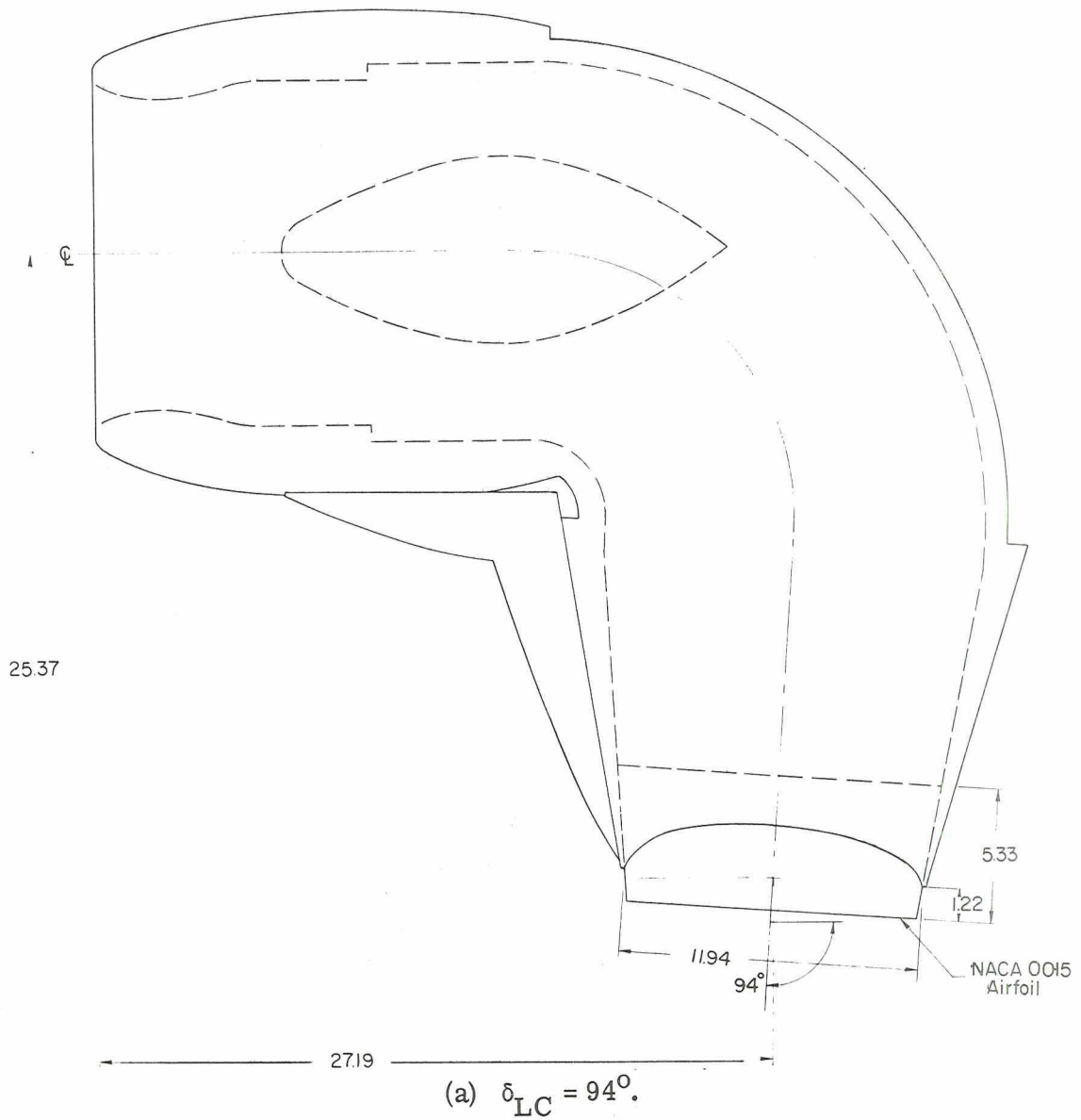


Figure 10.- Details of lift-cruise deflector assemblies.
 Linear dimensions are in centimeters.

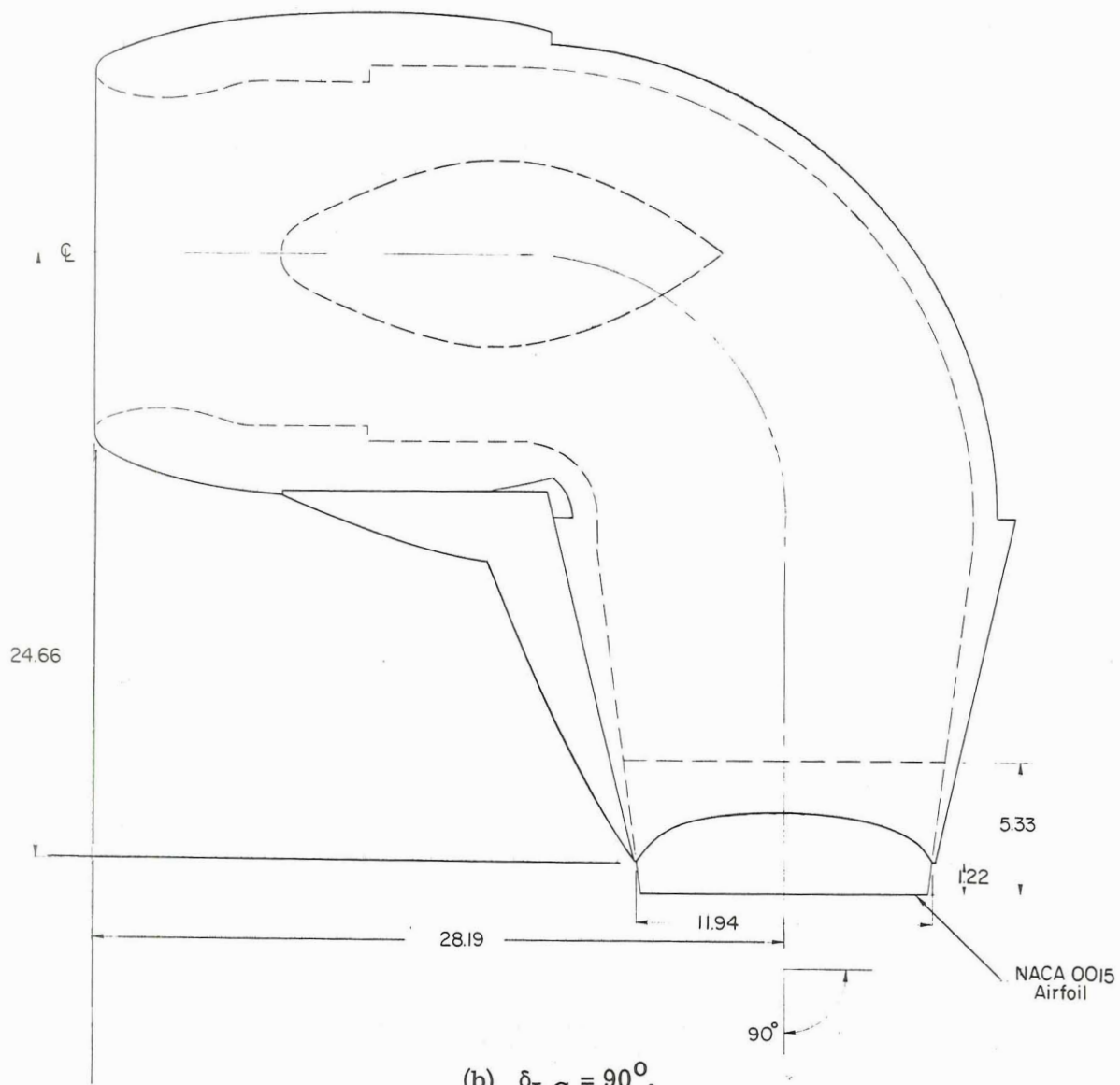
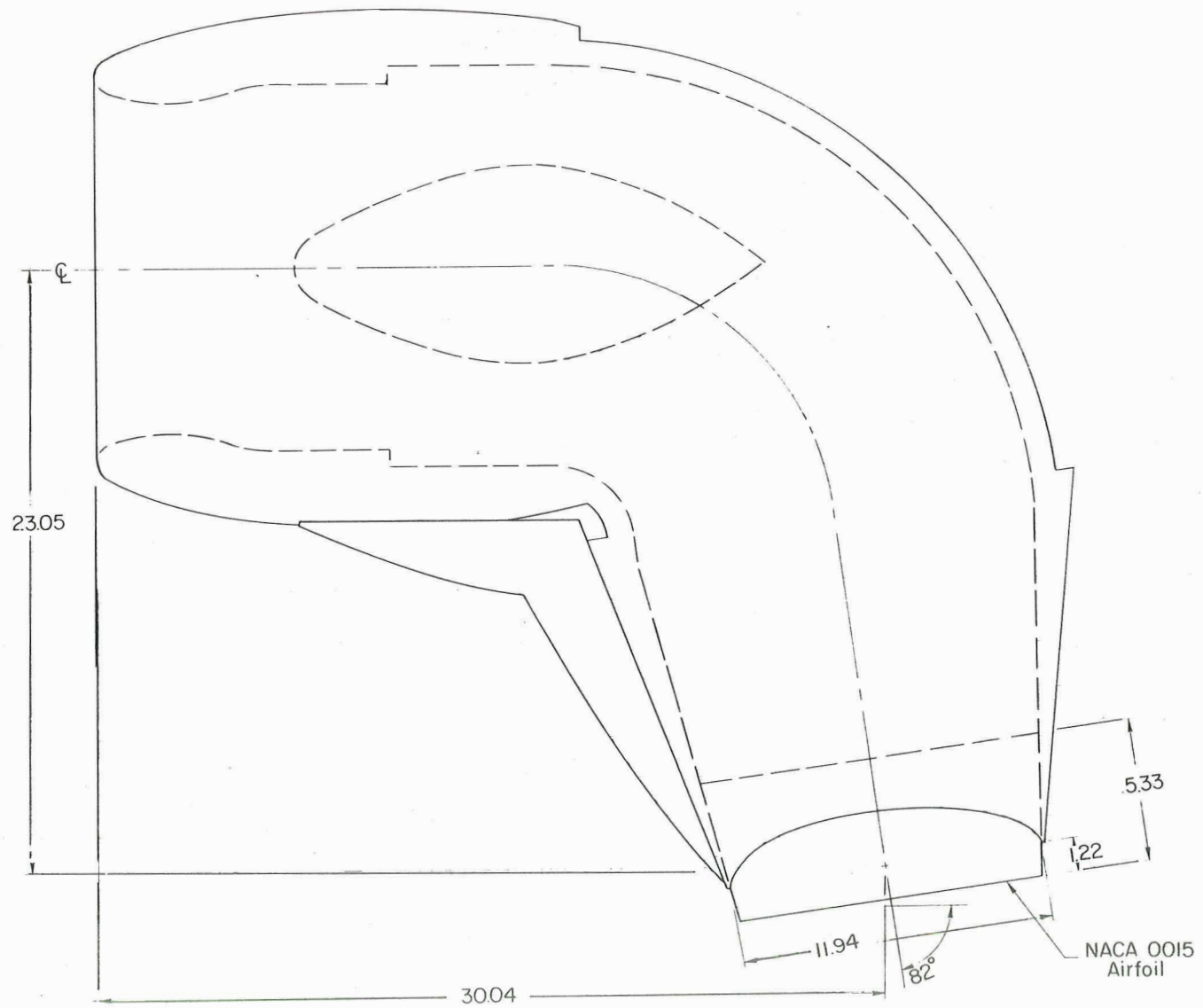
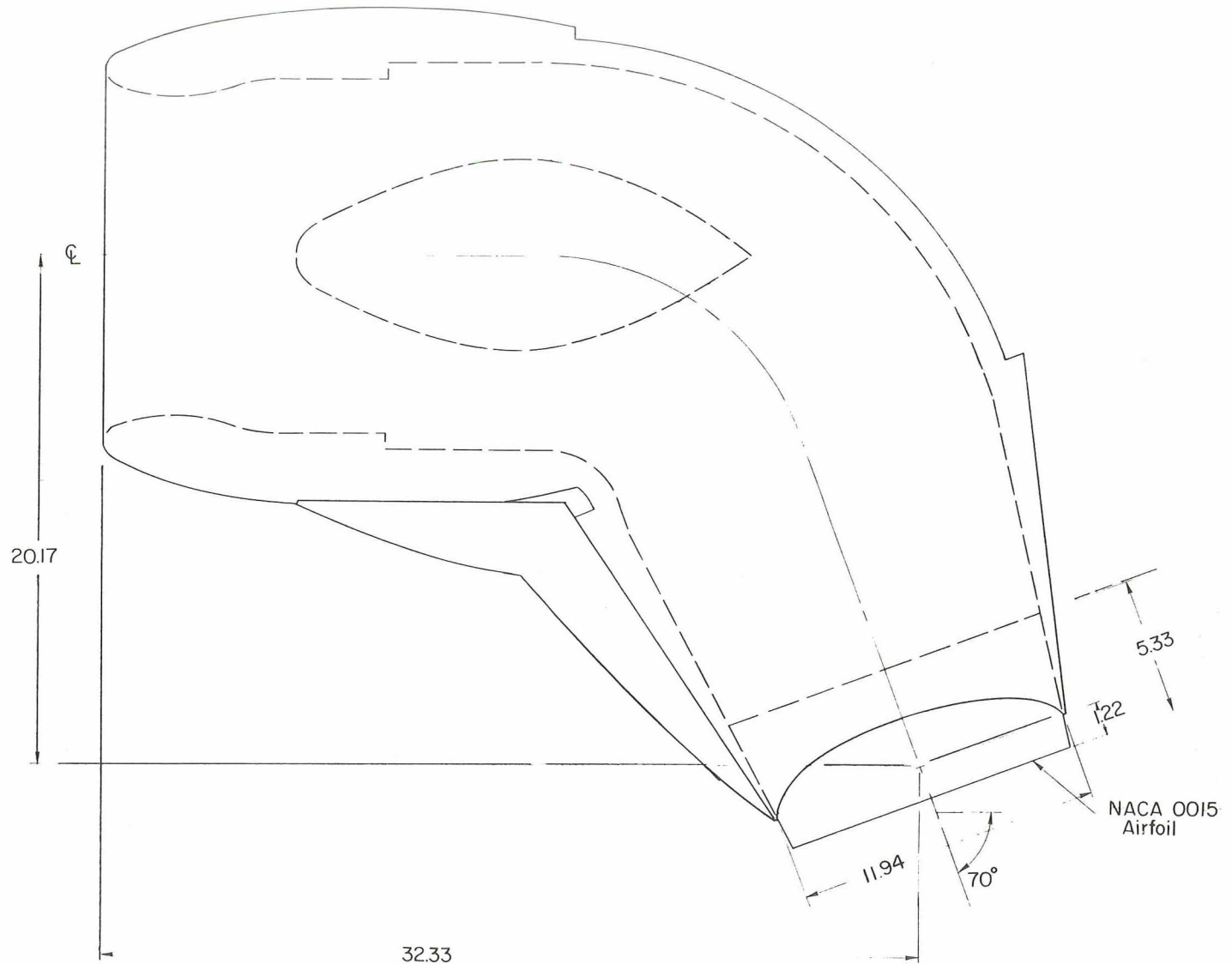


Figure 10.- Continued.



(c) $\delta_{LC} = 82^\circ$.

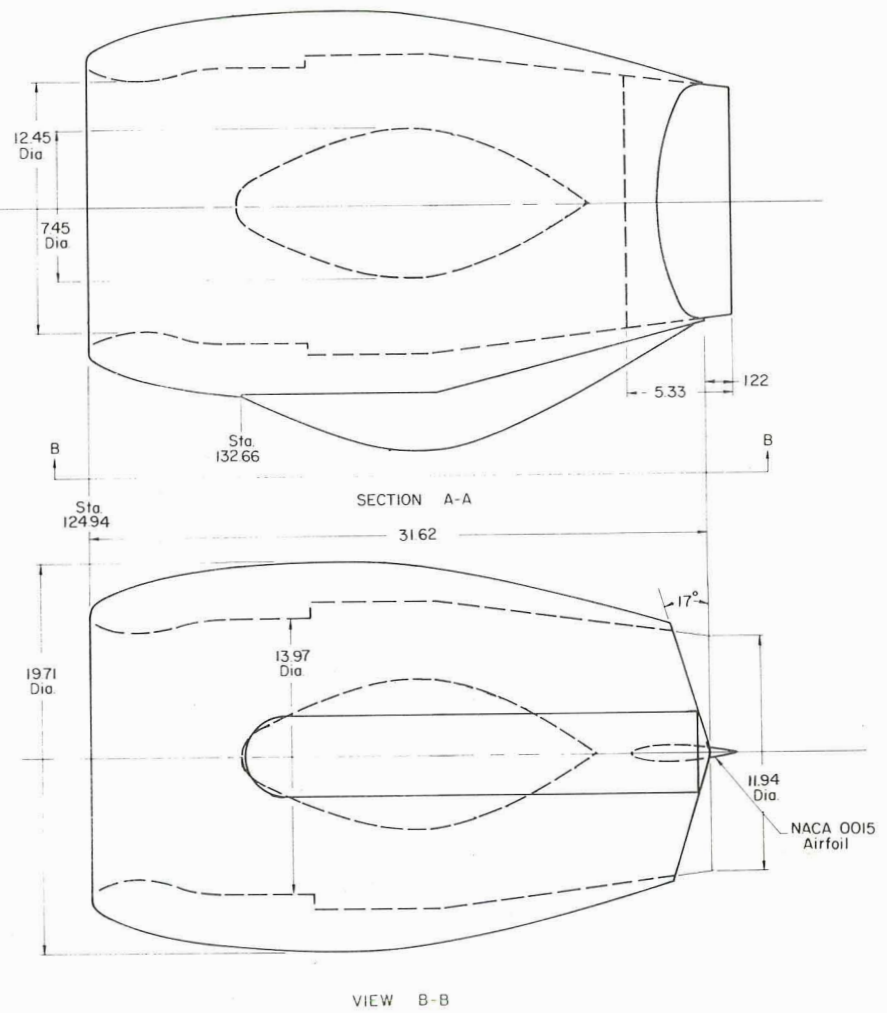
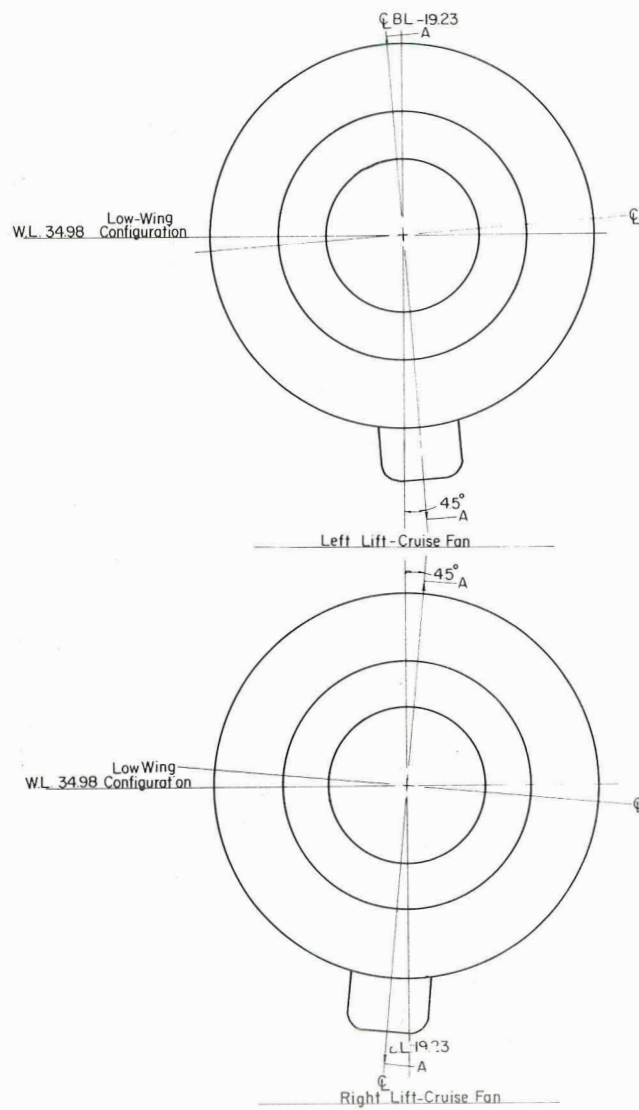
Figure 10.- Continued.



32.33

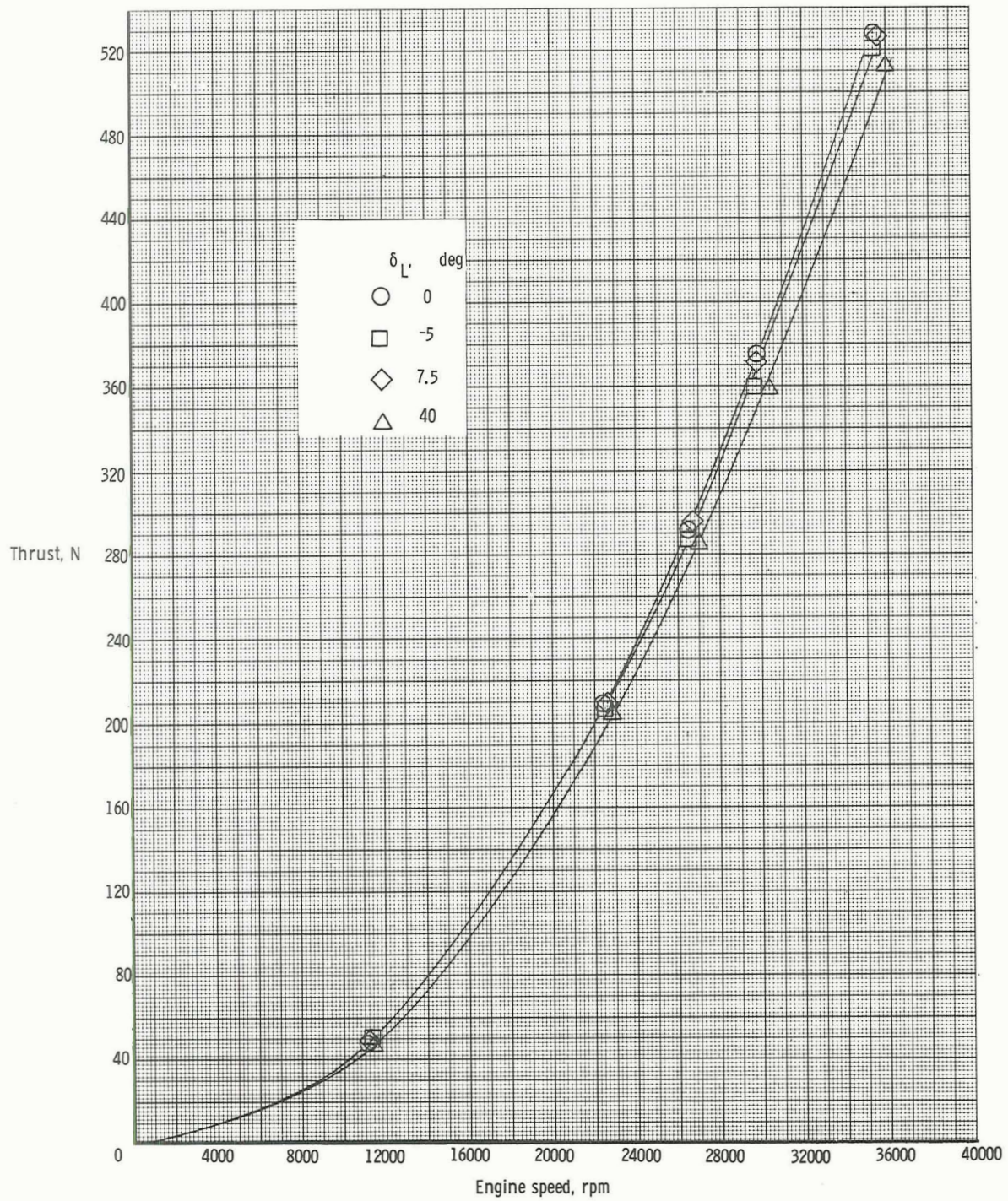
(d) $\delta_{LC} = 70^\circ$.

Figure 10.- Continued.



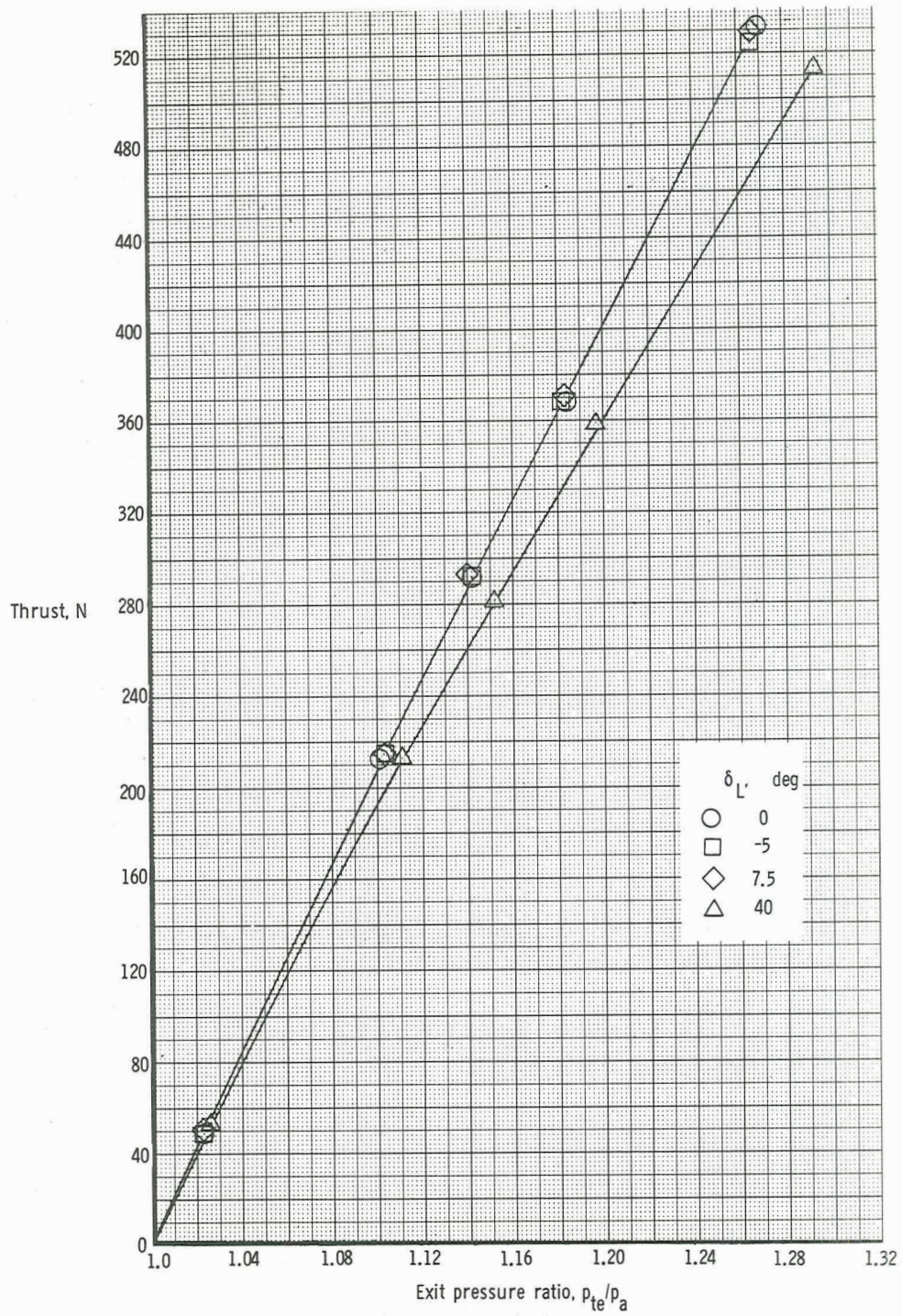
(e) $\delta_{LC} = 0^\circ$.

Figure 10.- Concluded.



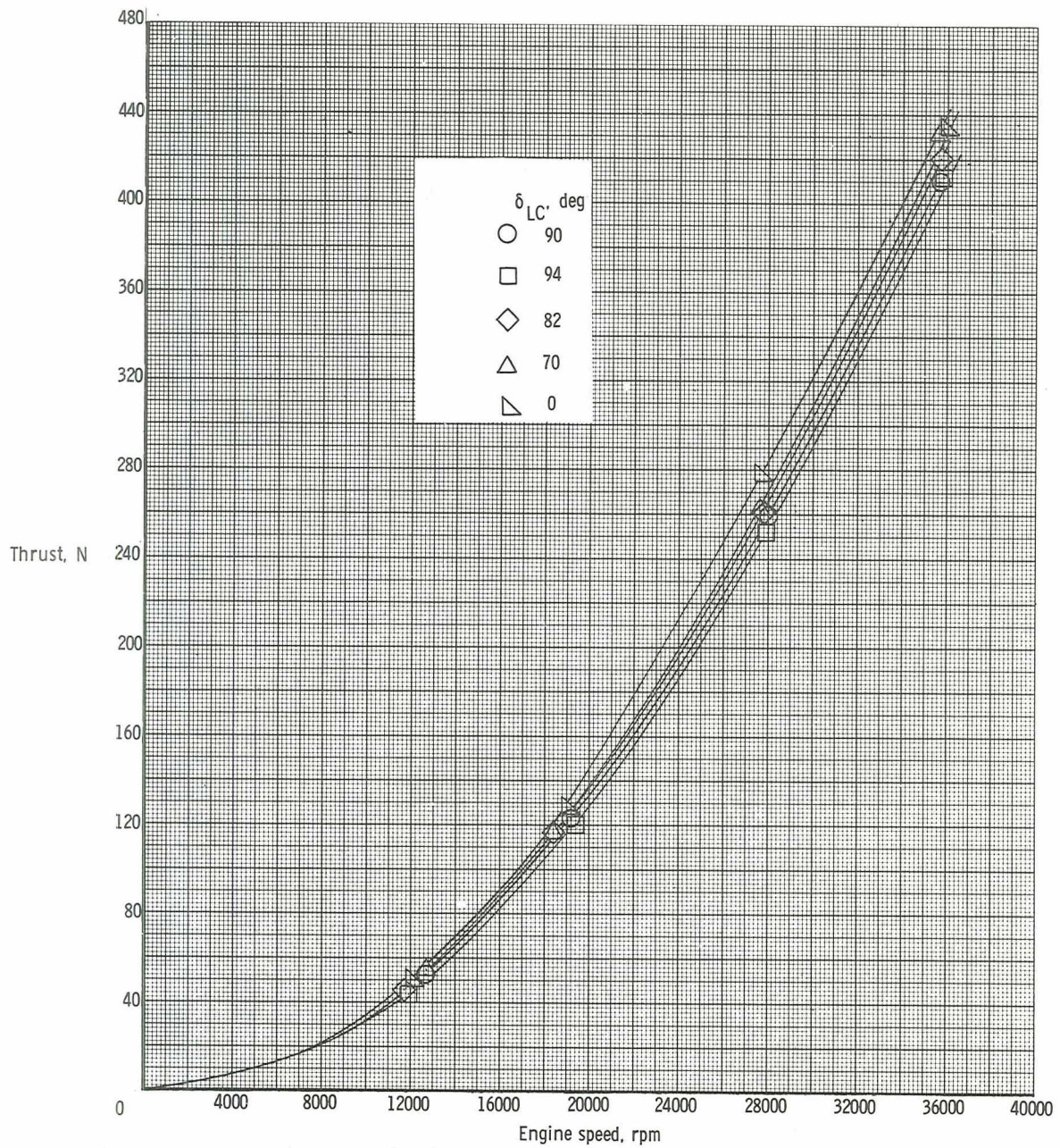
(a) Typical lift fan.

Figure 11.- Thrust calibration as a function of engine speed and exit pressure ratio.



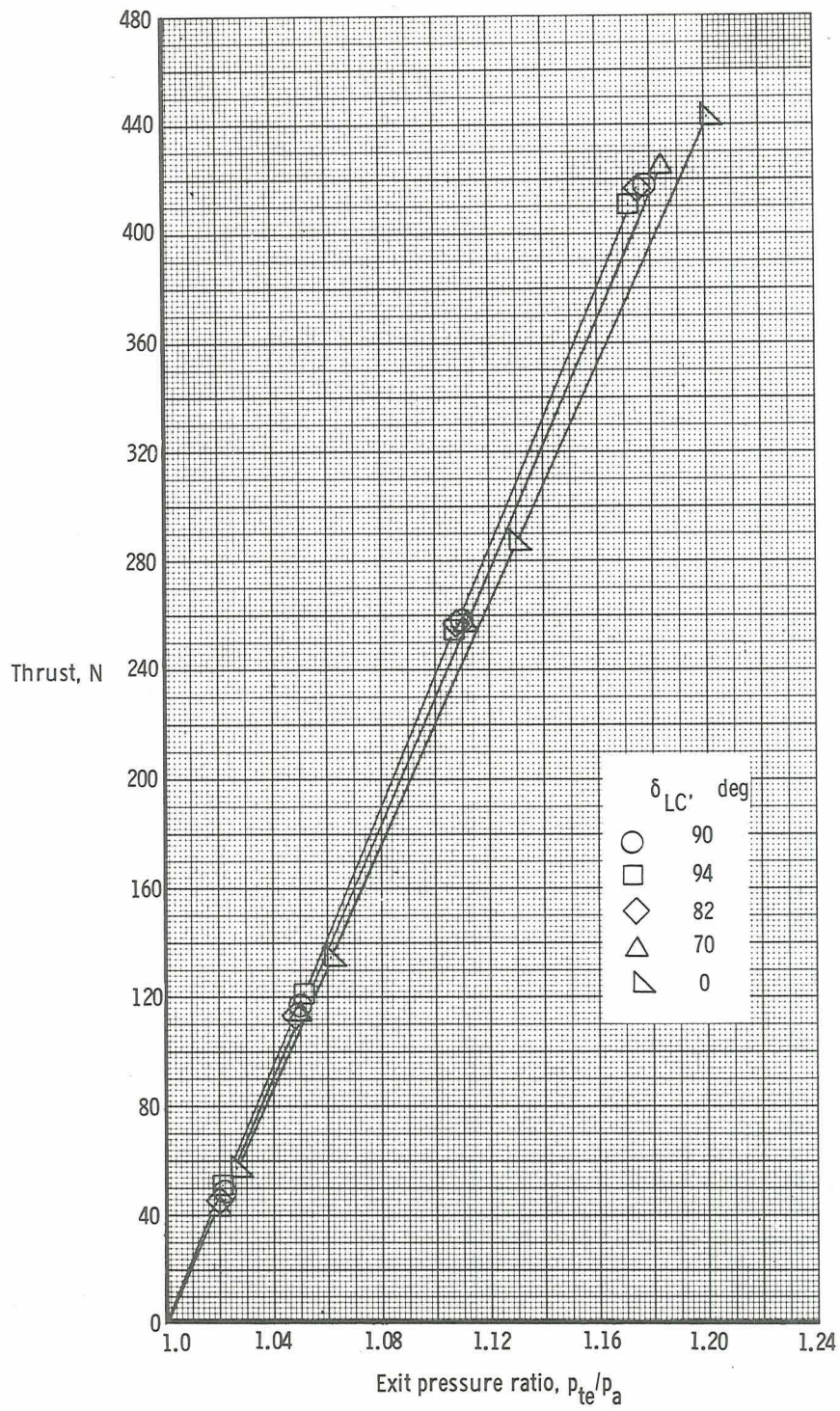
(a) Concluded.

Figure 11. - Continued.



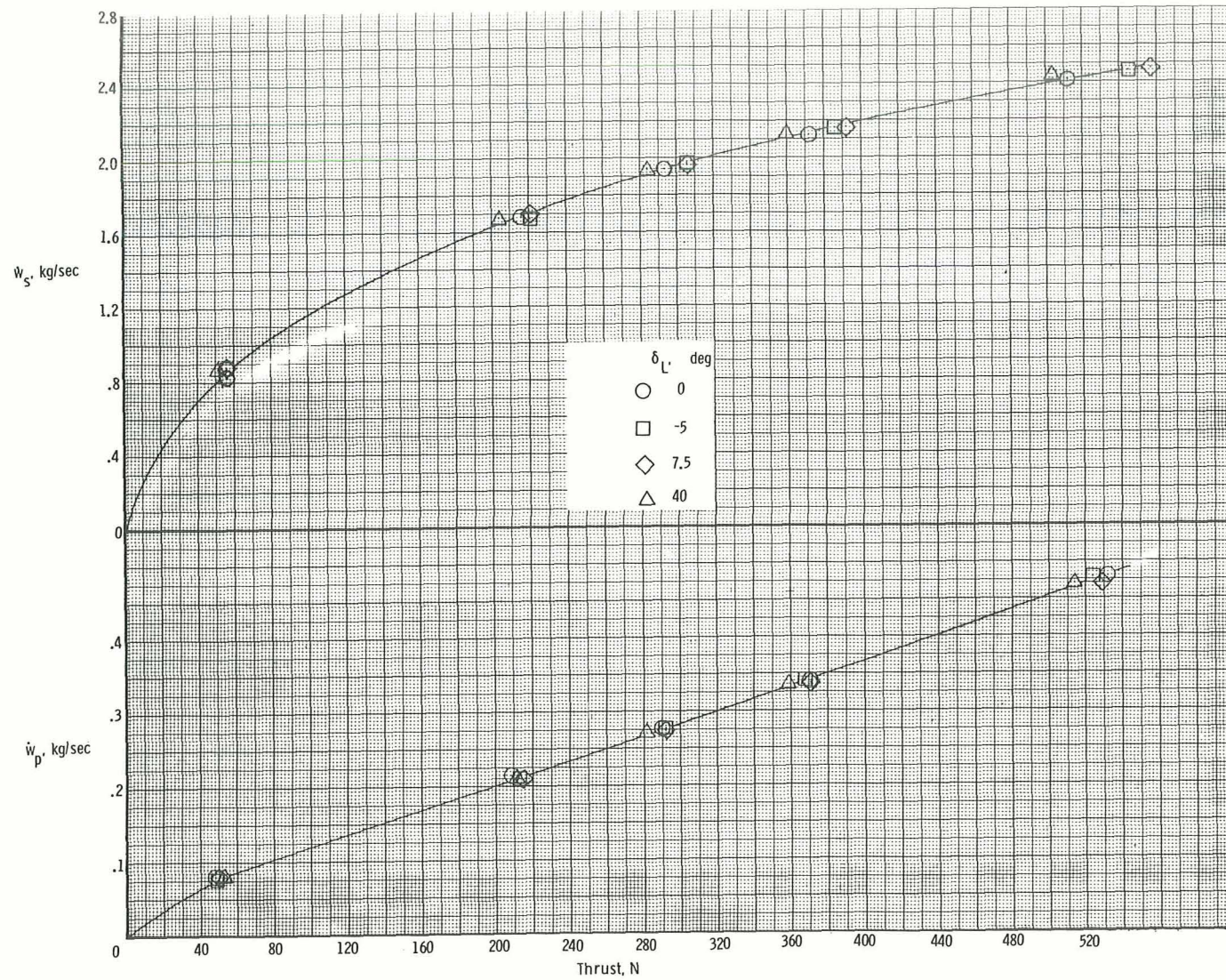
(b) Typical lift-cruise fan.

Figure 11.- Continued.



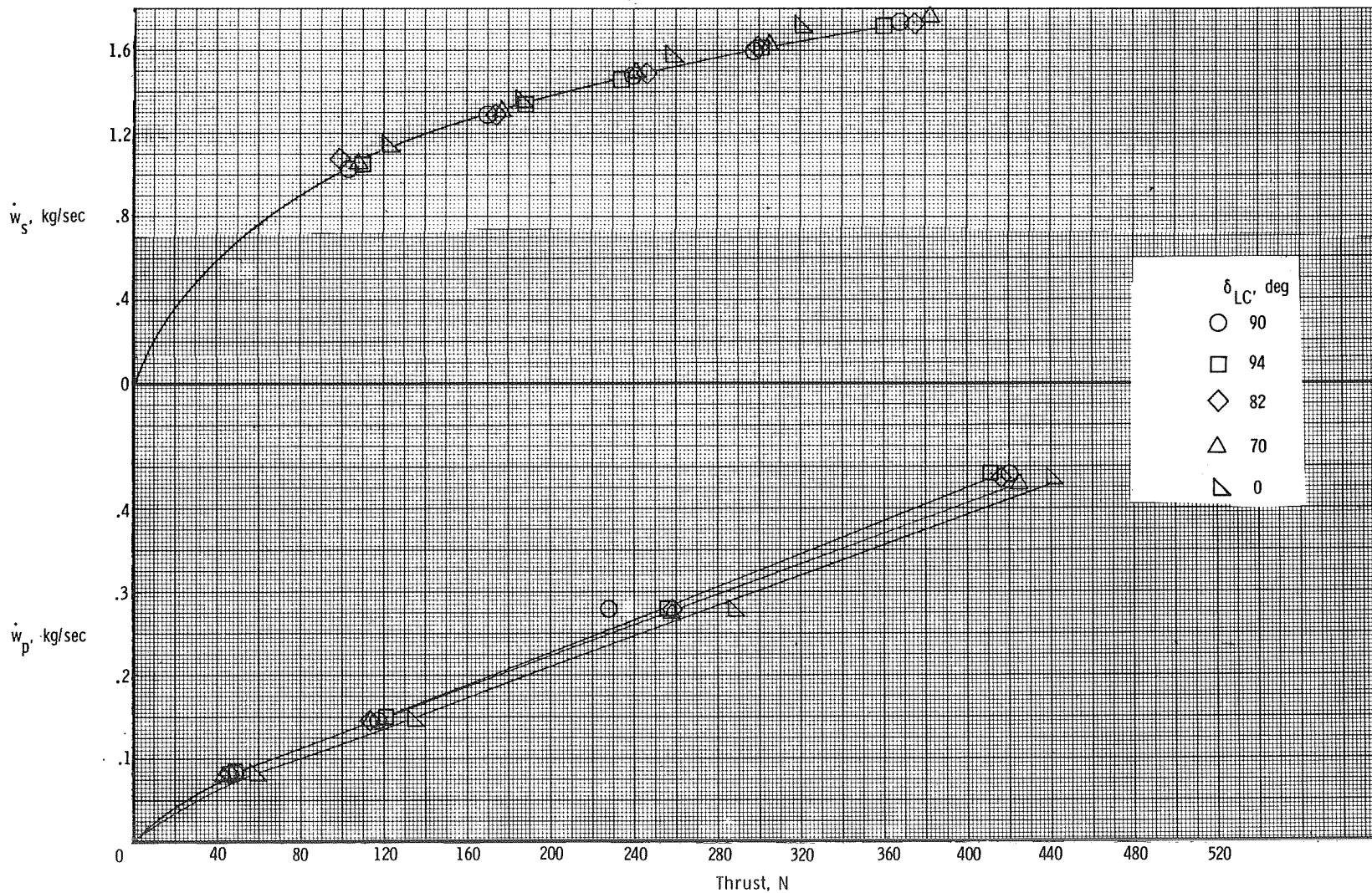
(b) Concluded.

Figure 11. - Concluded.



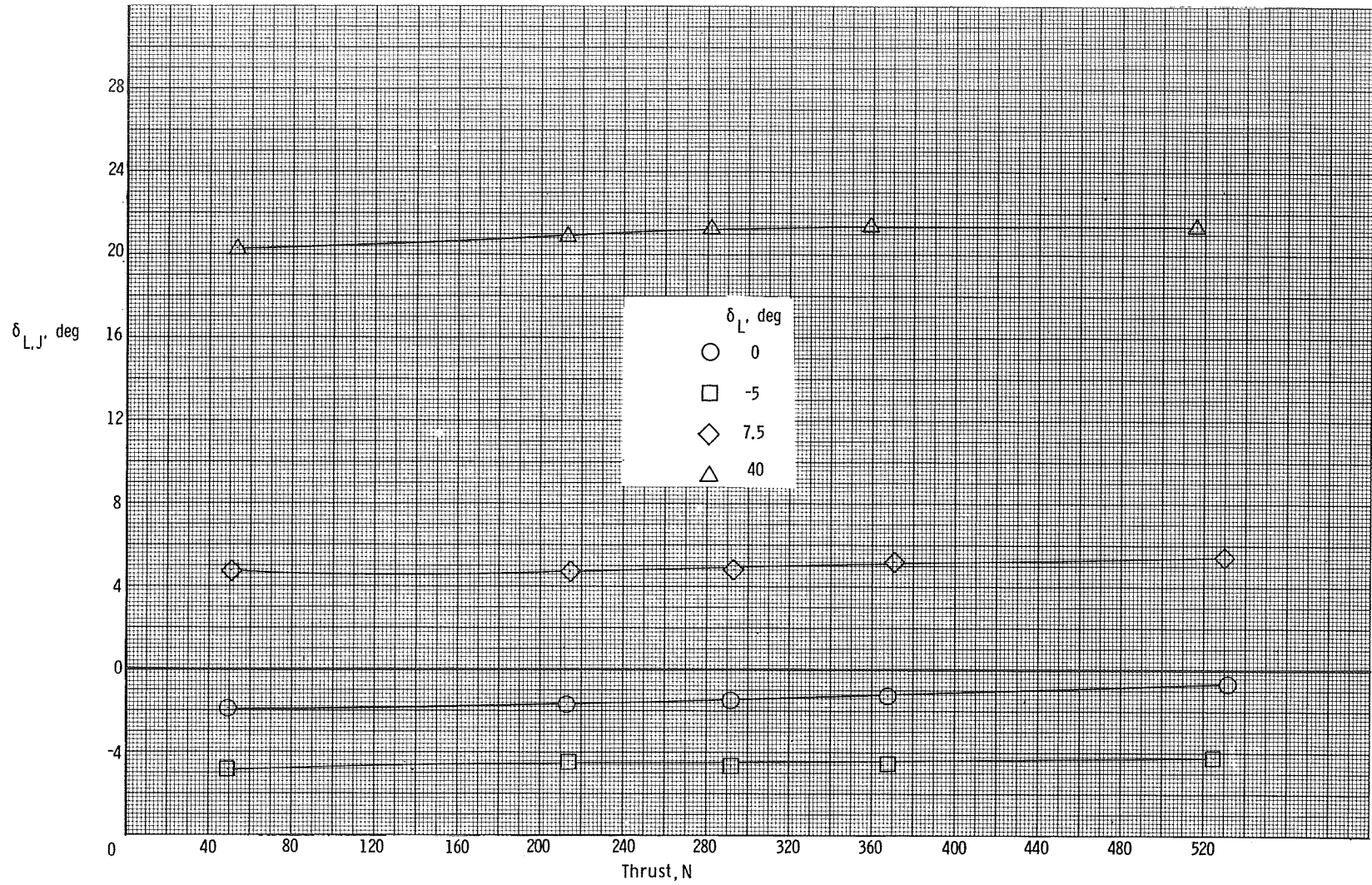
(a) Typical lift fan.

Figure 12.- Primary mass flow and fan-inlet mass flow rates.



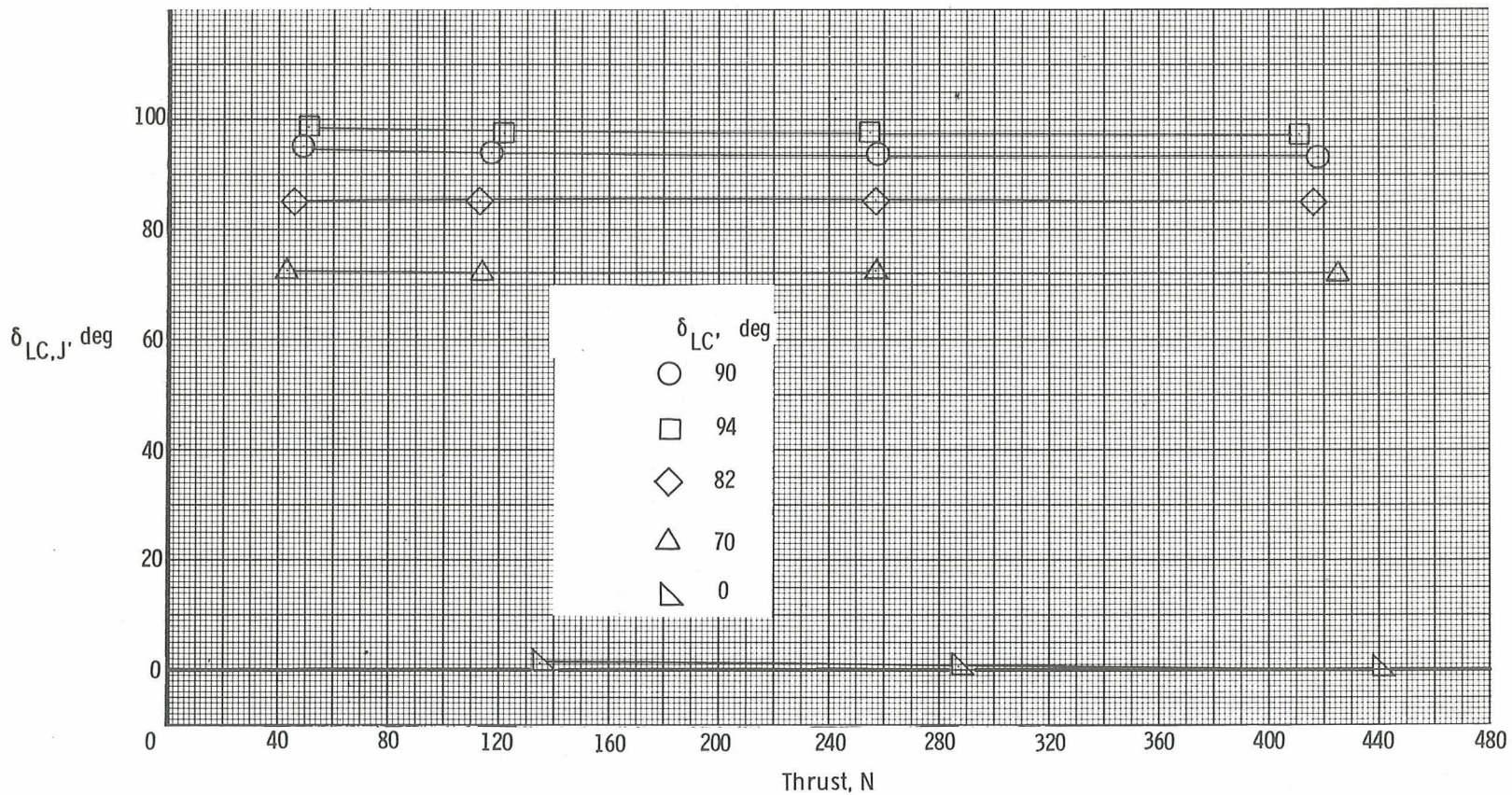
(b) Typical lift-cruise fan.

Figure 12. - Concluded.



(a) Typical lift fan.

Figure 13.- Fan-exhaust deflection angle.



(b) Typical lift-cruise fan.

Figure 13.- Concluded.

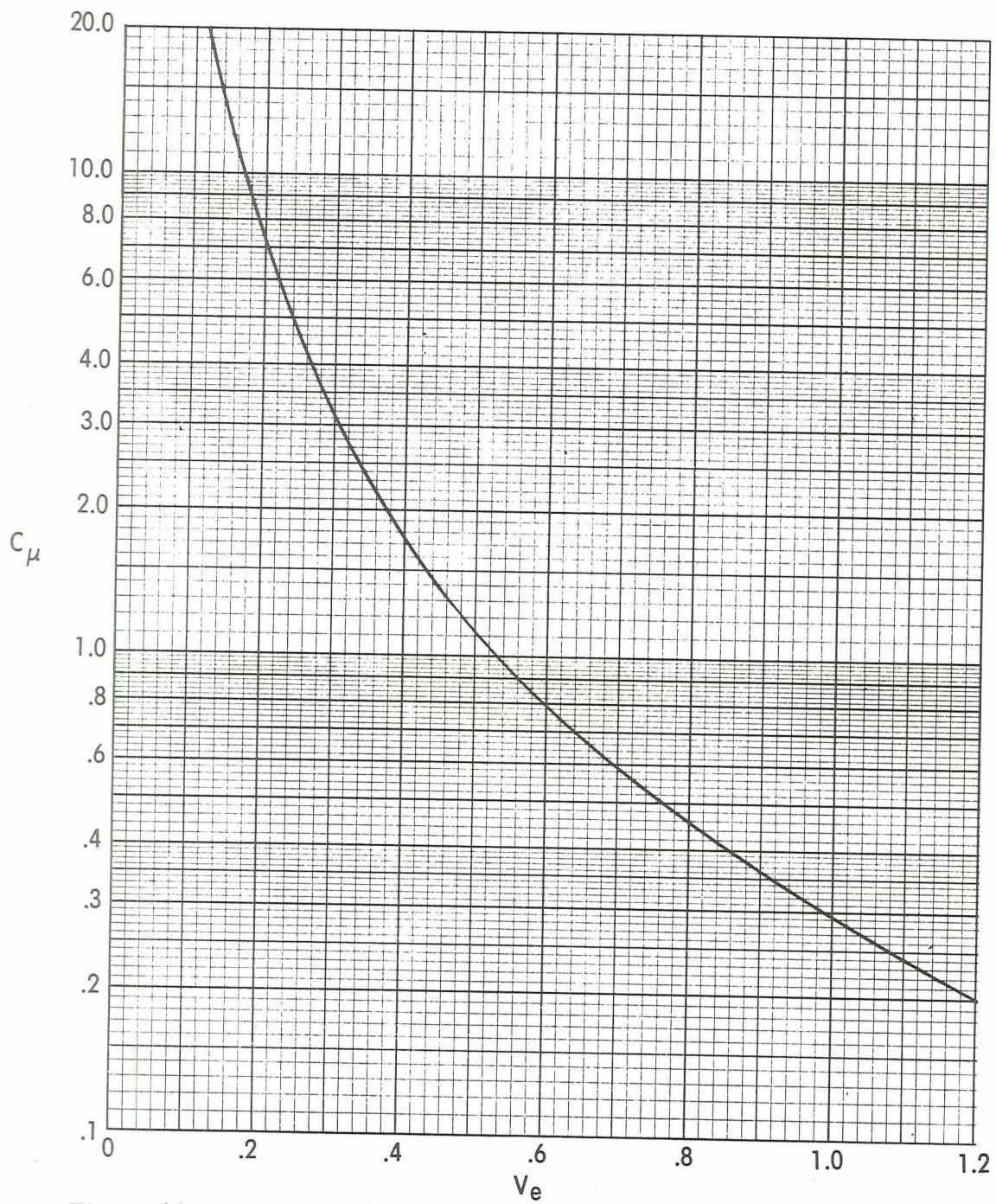
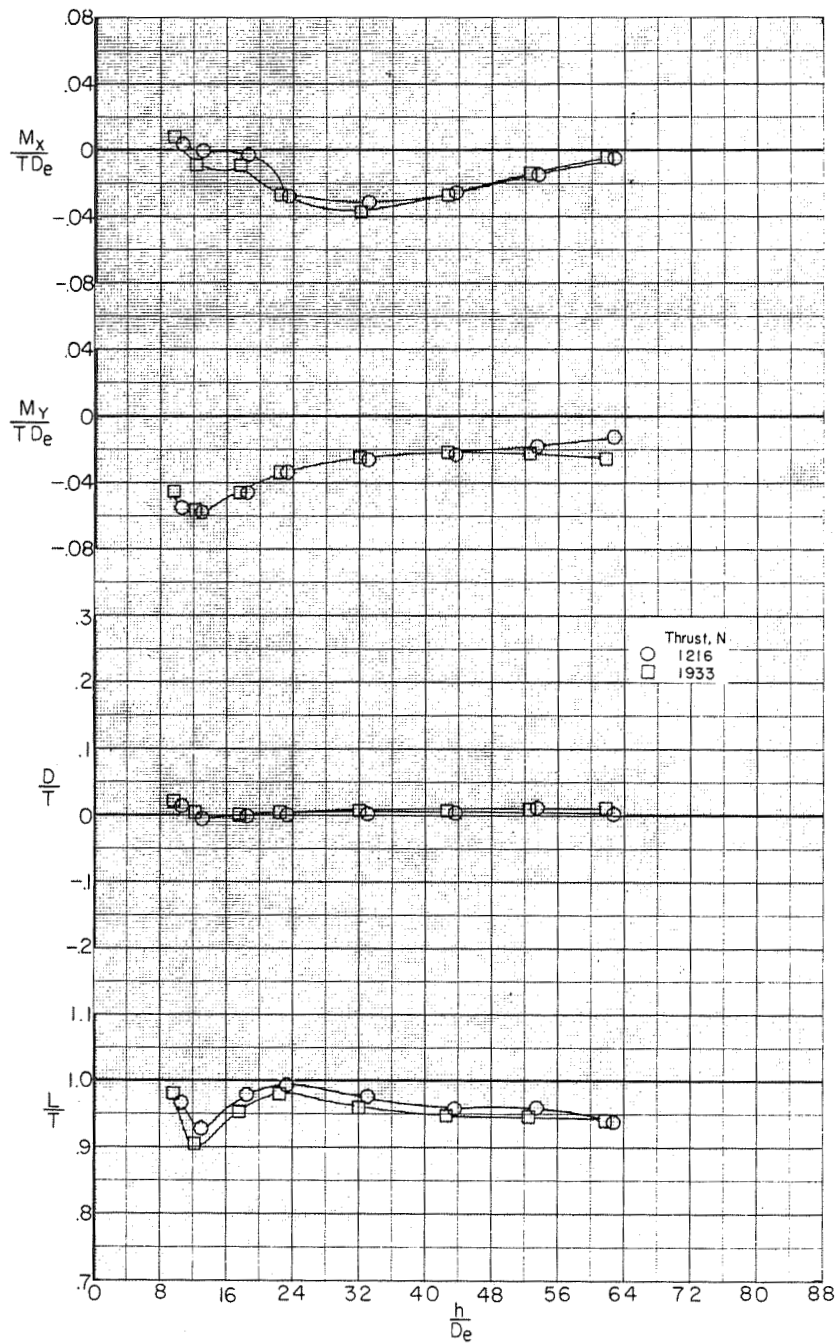
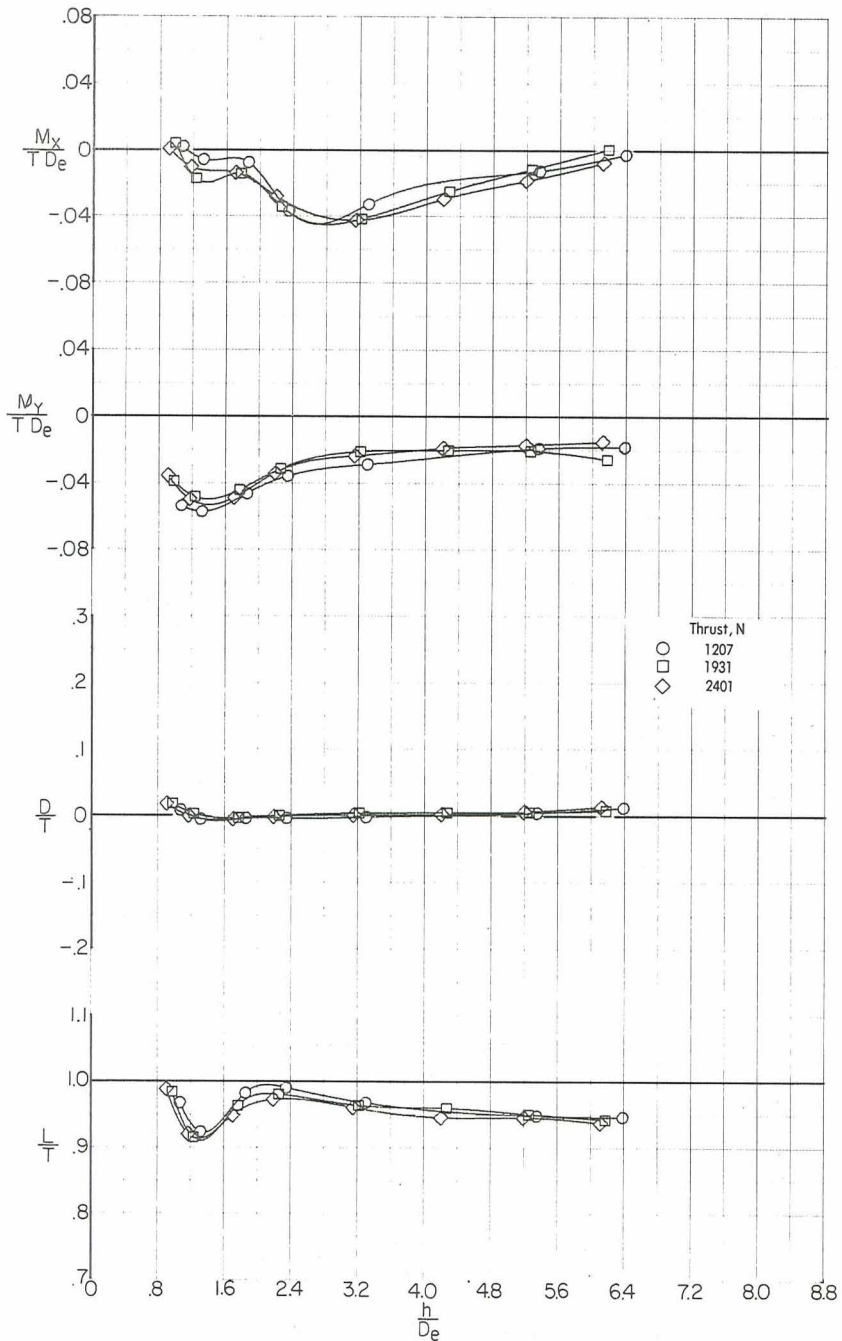


Figure 14.- Variation of thrust coefficient with effective velocity ratio.
All six fans operating.



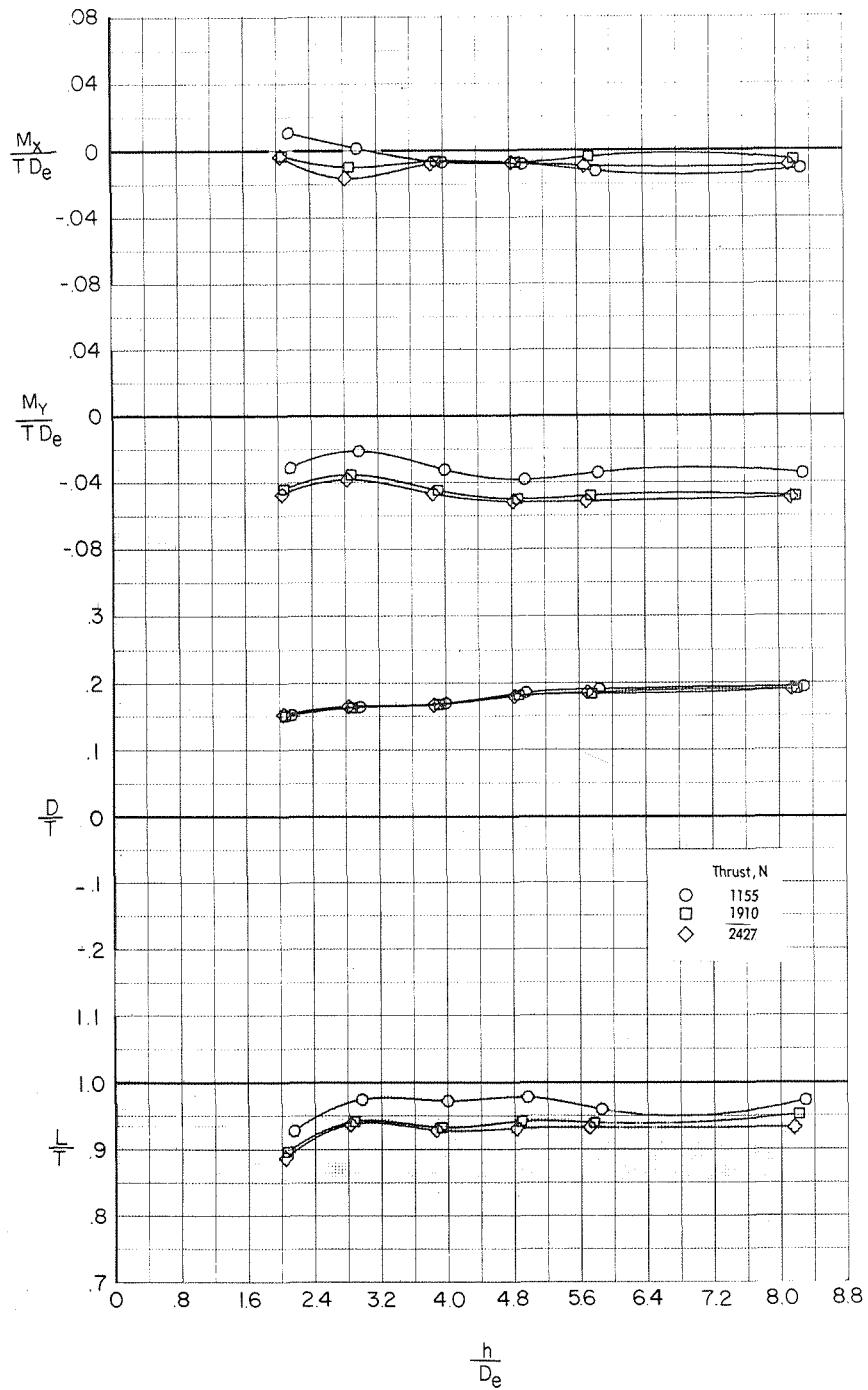
(a) Tail off; $\alpha = 0^\circ$; $\phi = 0^\circ$.

Figure 15.- Effect of ground proximity on induced loads of hover configuration at zero wind speed. ($\delta_L = 0^\circ$; $\delta_{LC} = 90^\circ$; $\delta_f = 40^\circ$.)



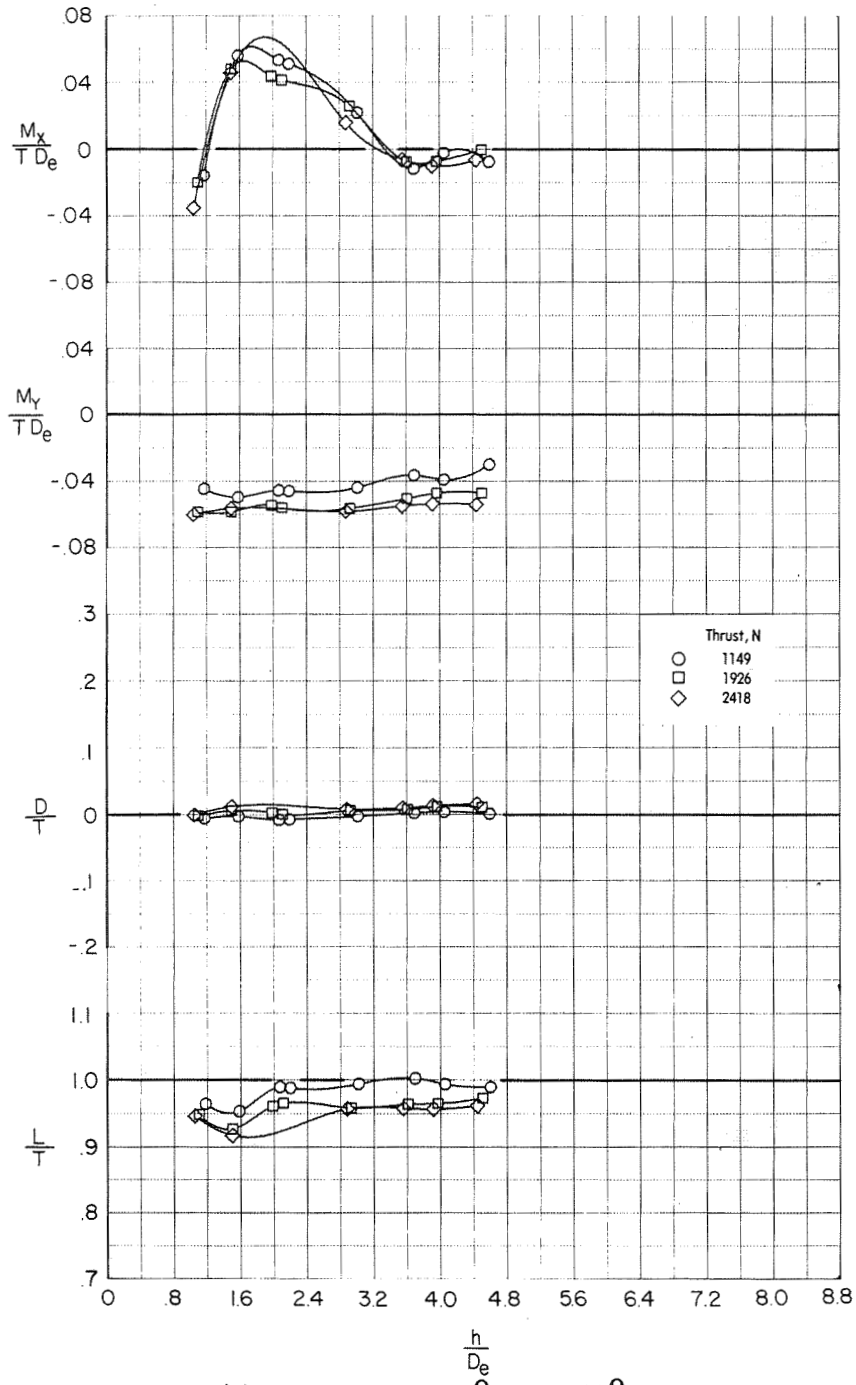
(b) $i_t = 0^\circ$; $\delta_e = 0^\circ$; $\alpha = 0^\circ$; $\phi = 0^\circ$.

Figure 15.- Continued.



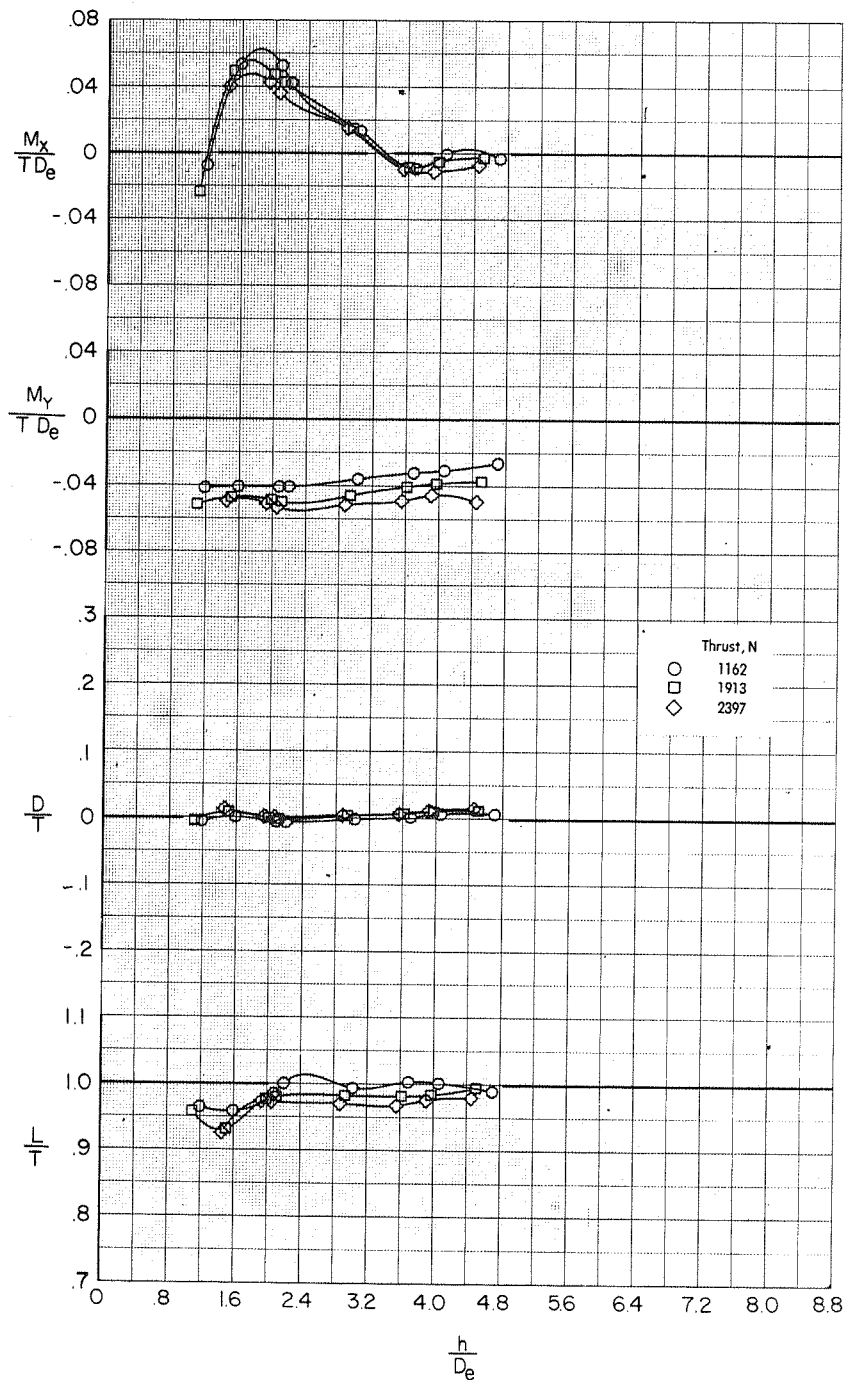
(c) Tail off; $\alpha = 10^\circ$; $\phi = 0^\circ$.

Figure 15.- Continued.



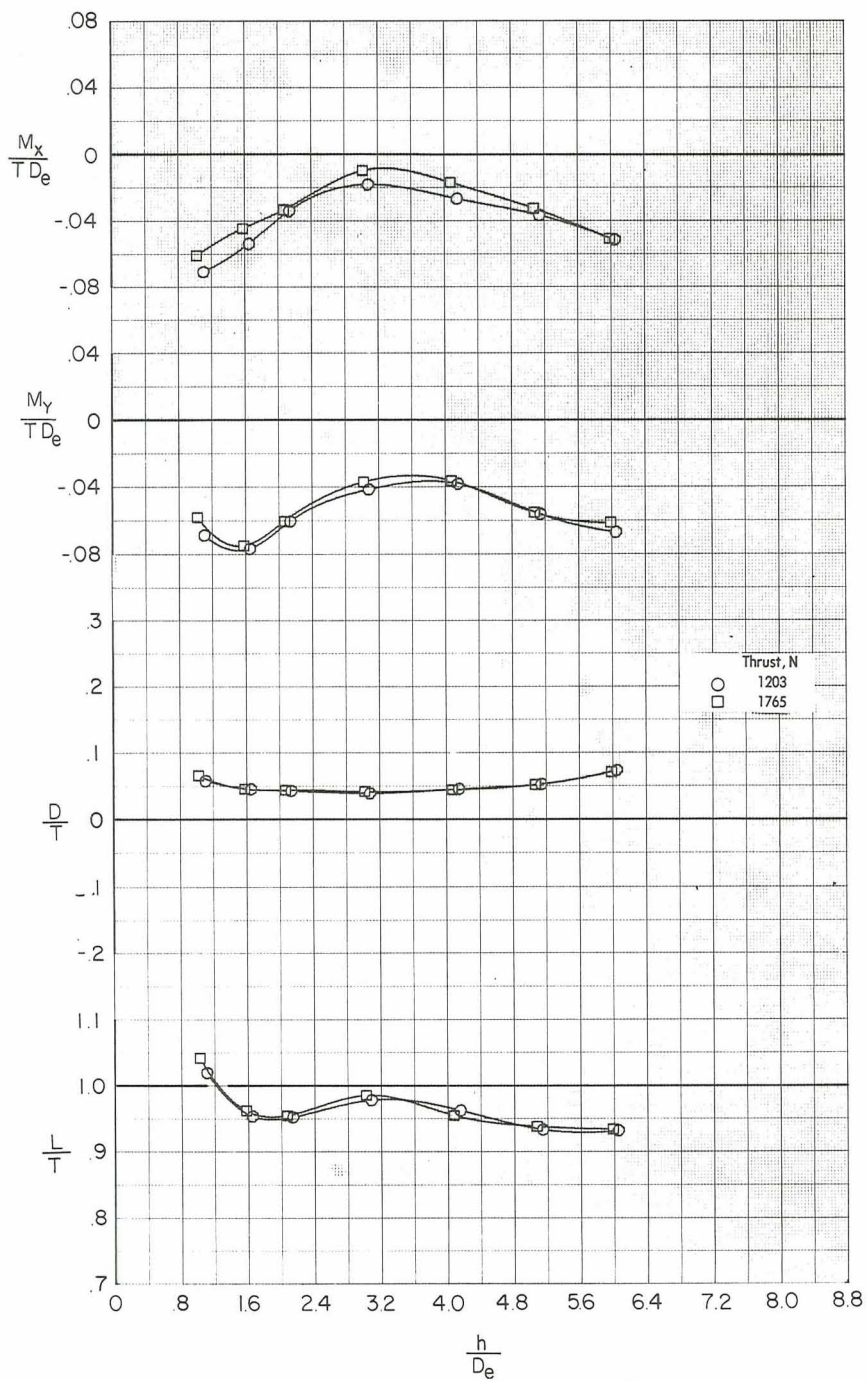
(d) Tail off; $\alpha = 0^\circ$; $\phi = 10^\circ$.

Figure 15.- Continued.



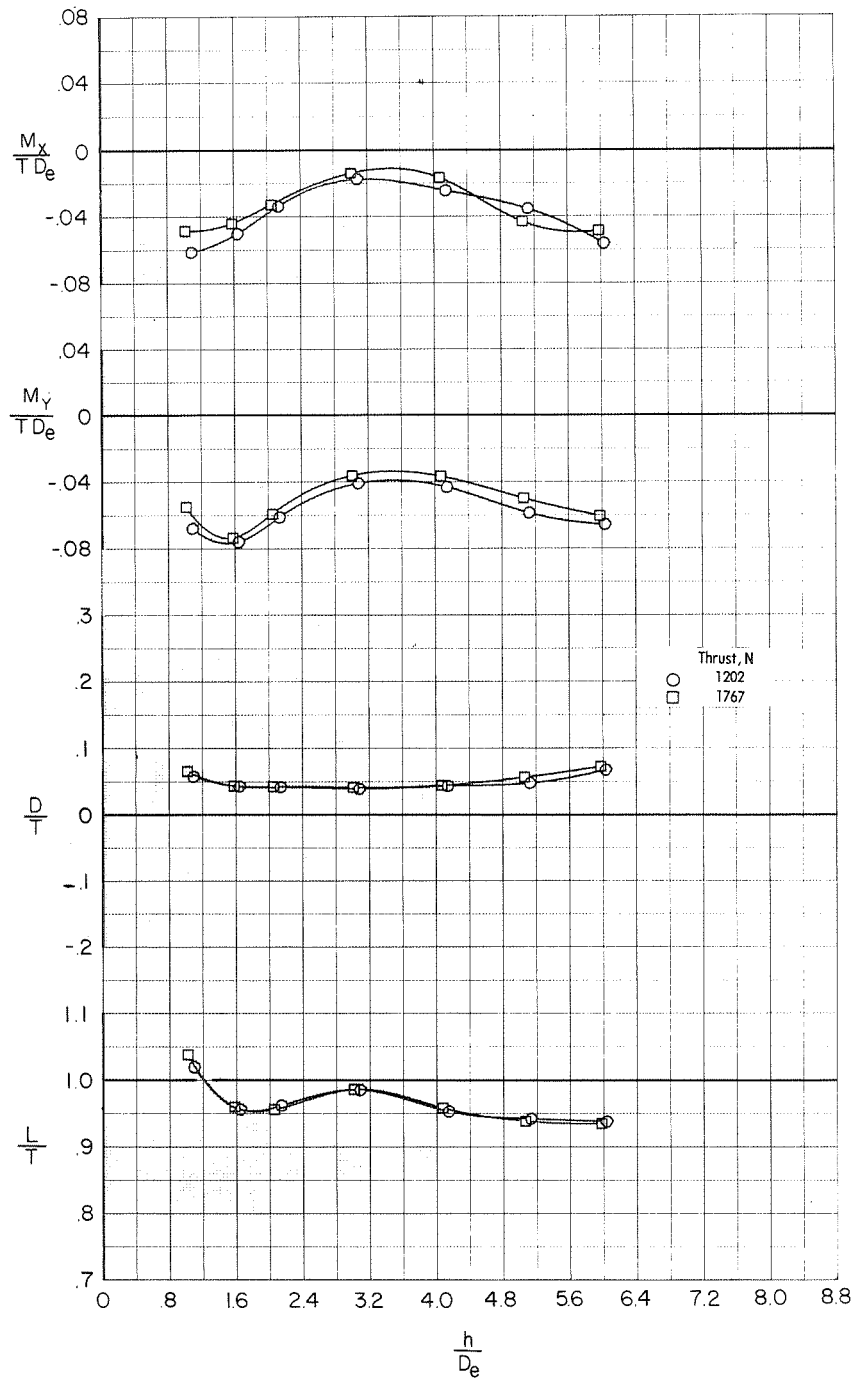
(e) $i_t = 0^{\circ}$; $\delta_e = 0^{\circ}$; $\alpha = 0^{\circ}$; $\phi = 10^{\circ}$.

Figure 15.- Concluded.



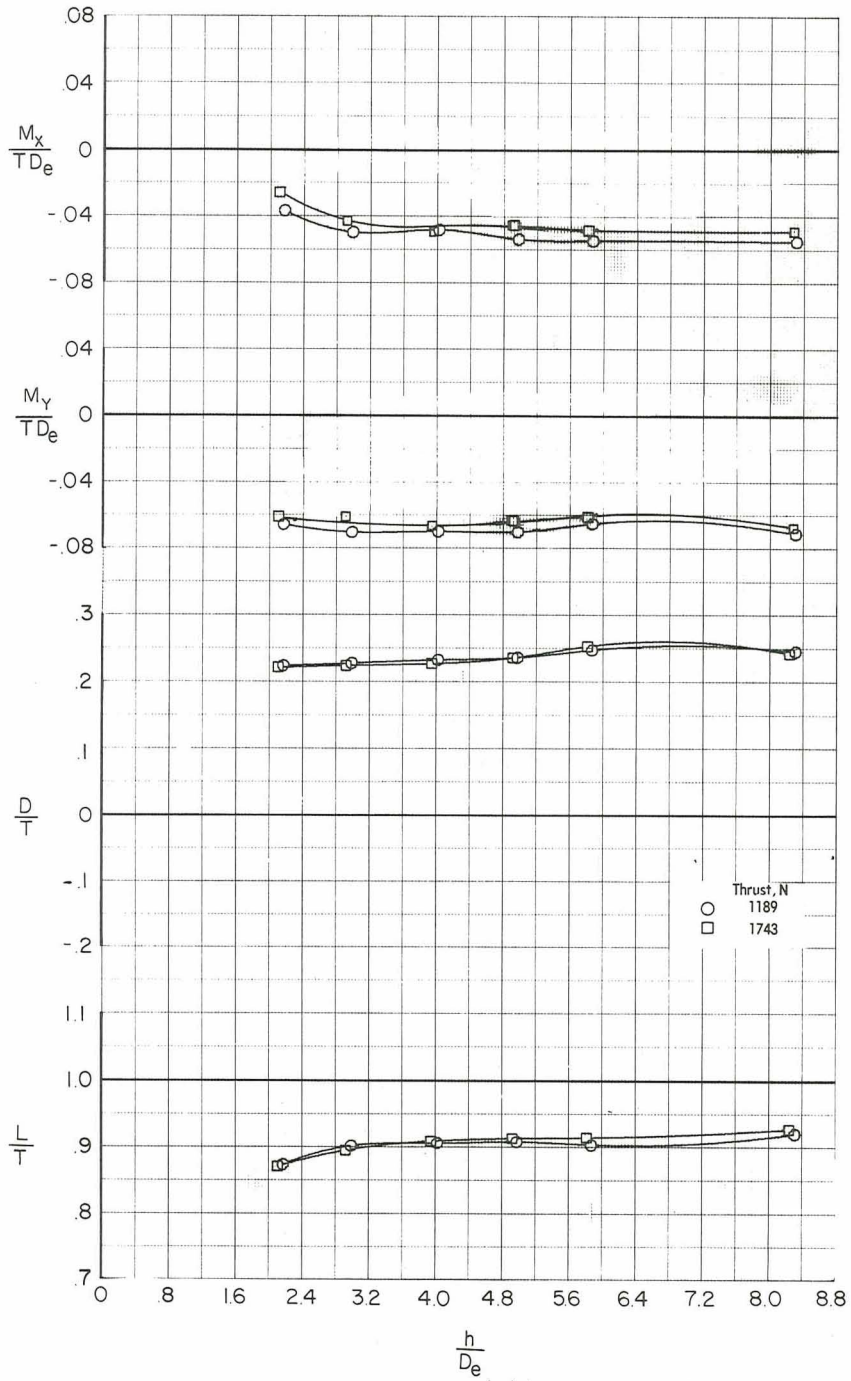
(a) Tail off; $\alpha = 0^\circ$; $\phi = 0^\circ$.

Figure 16.- Effect of ground proximity on induced loads of landing configuration at zero wind speed. ($\delta_L = -5^\circ$; $\delta_{LC} = 94^\circ$; $\delta_f = 40^\circ$.)



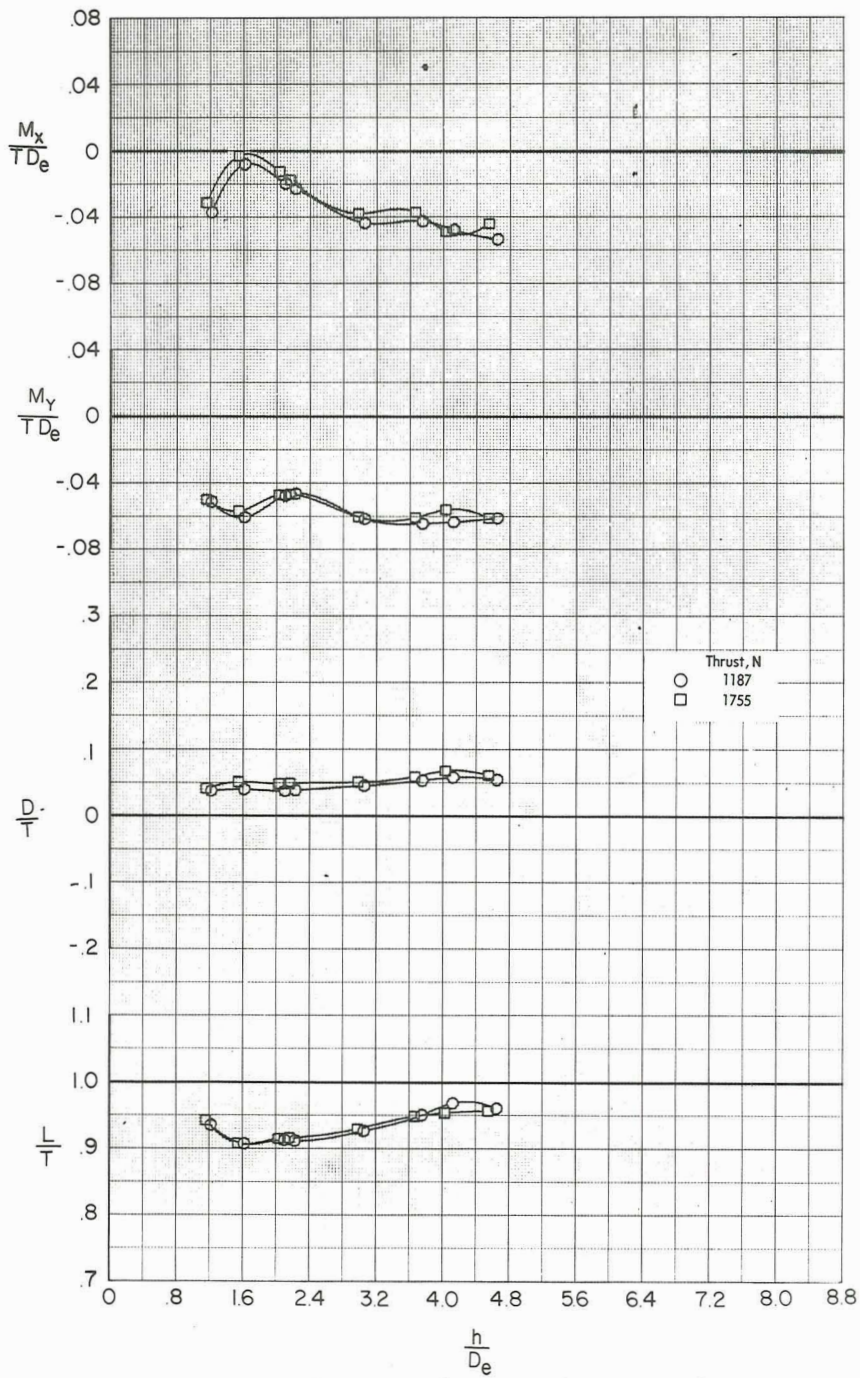
(b) $i_t = 0^\circ$; $\delta_e = 0^\circ$; $\alpha = 0^\circ$; $\phi = 0^\circ$.

Figure 16.- Continued.



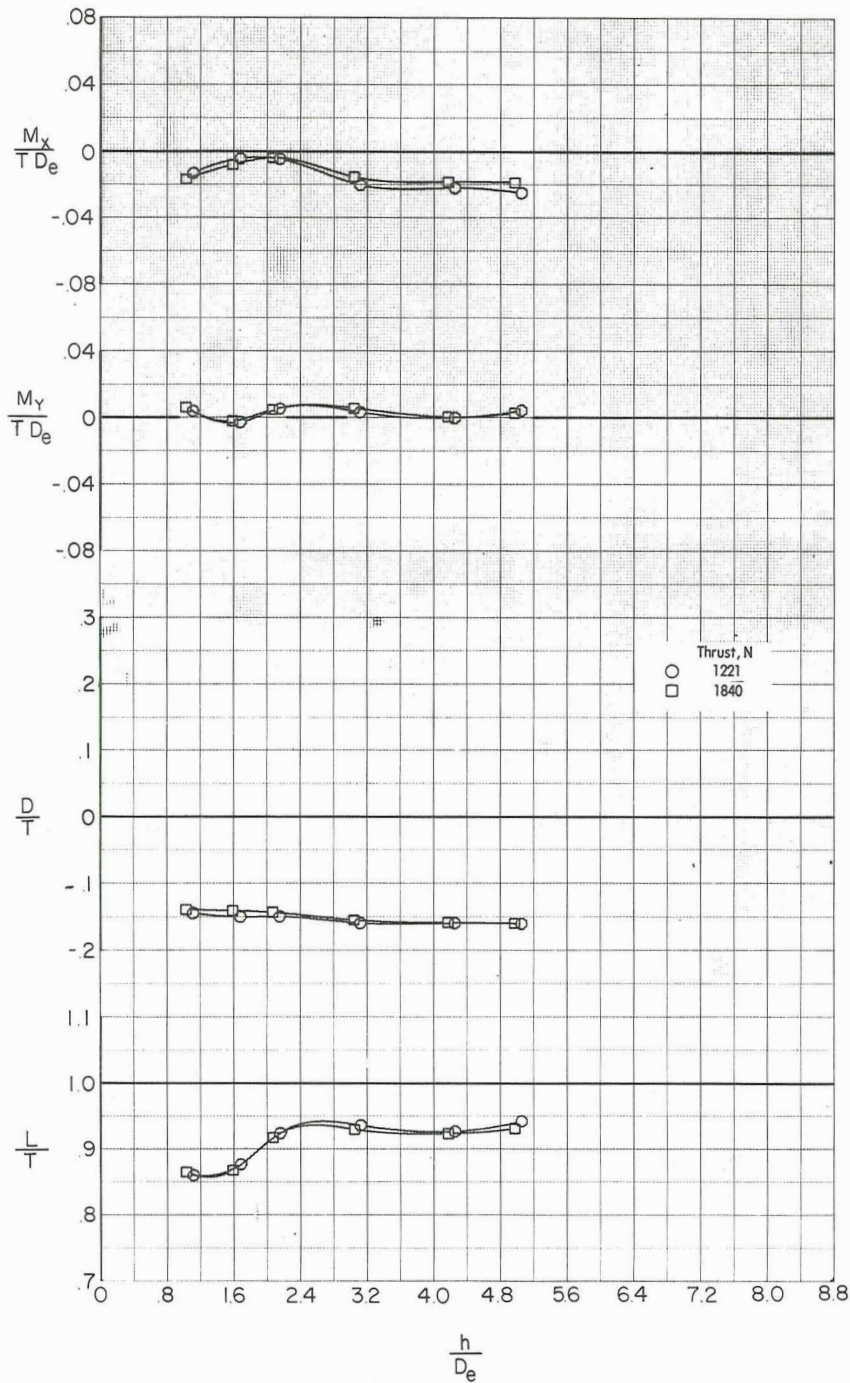
(c) $i_t = 0^\circ$; $\delta_e = 0^\circ$; $\alpha = 10^\circ$; $\phi = 0^\circ$.

Figure 16.- Continued.



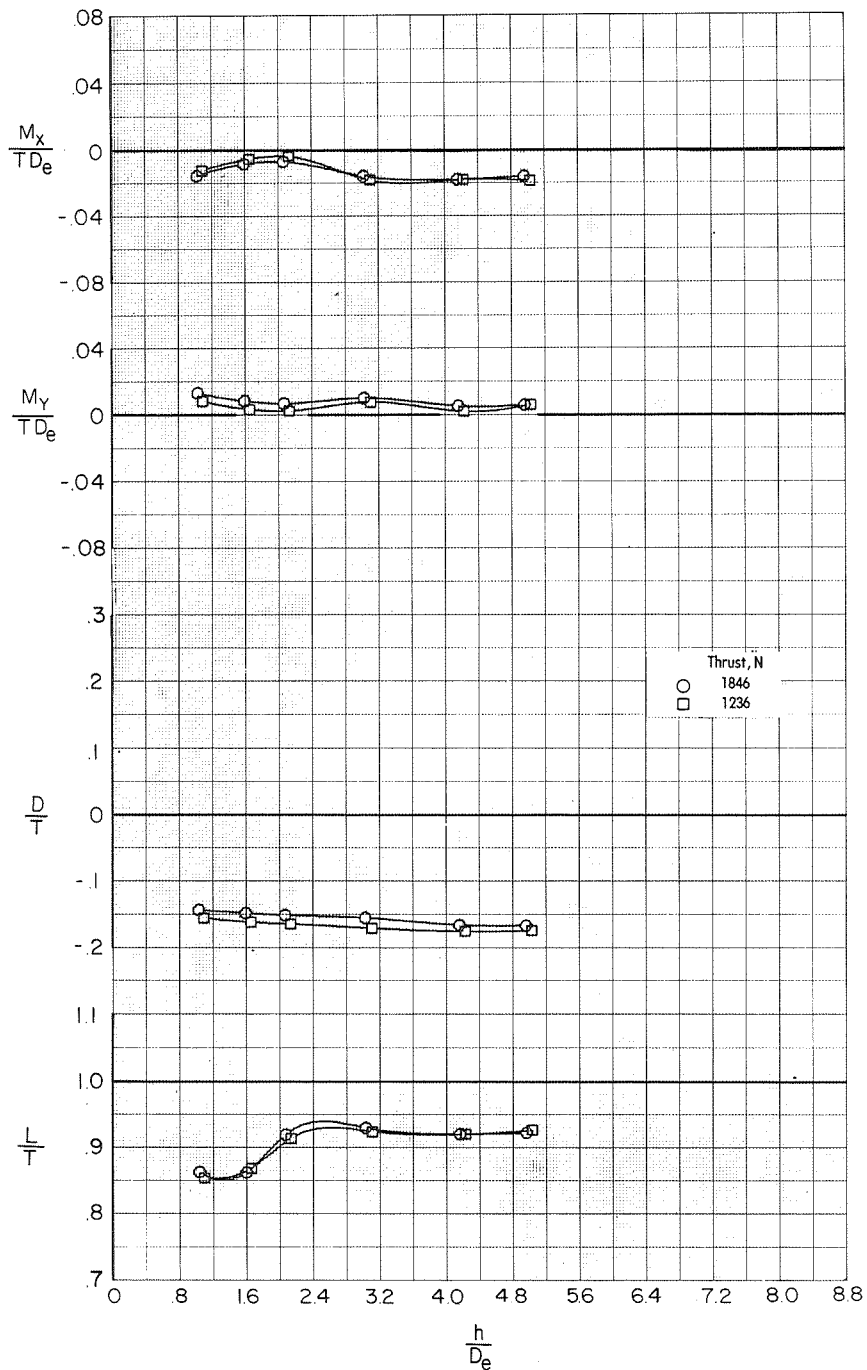
(d) $i_t = 0^{\circ}$; $\delta_e = 0^{\circ}$; $\alpha = 0^{\circ}$; $\phi = 10^{\circ}$.

Figure 16.- Concluded.



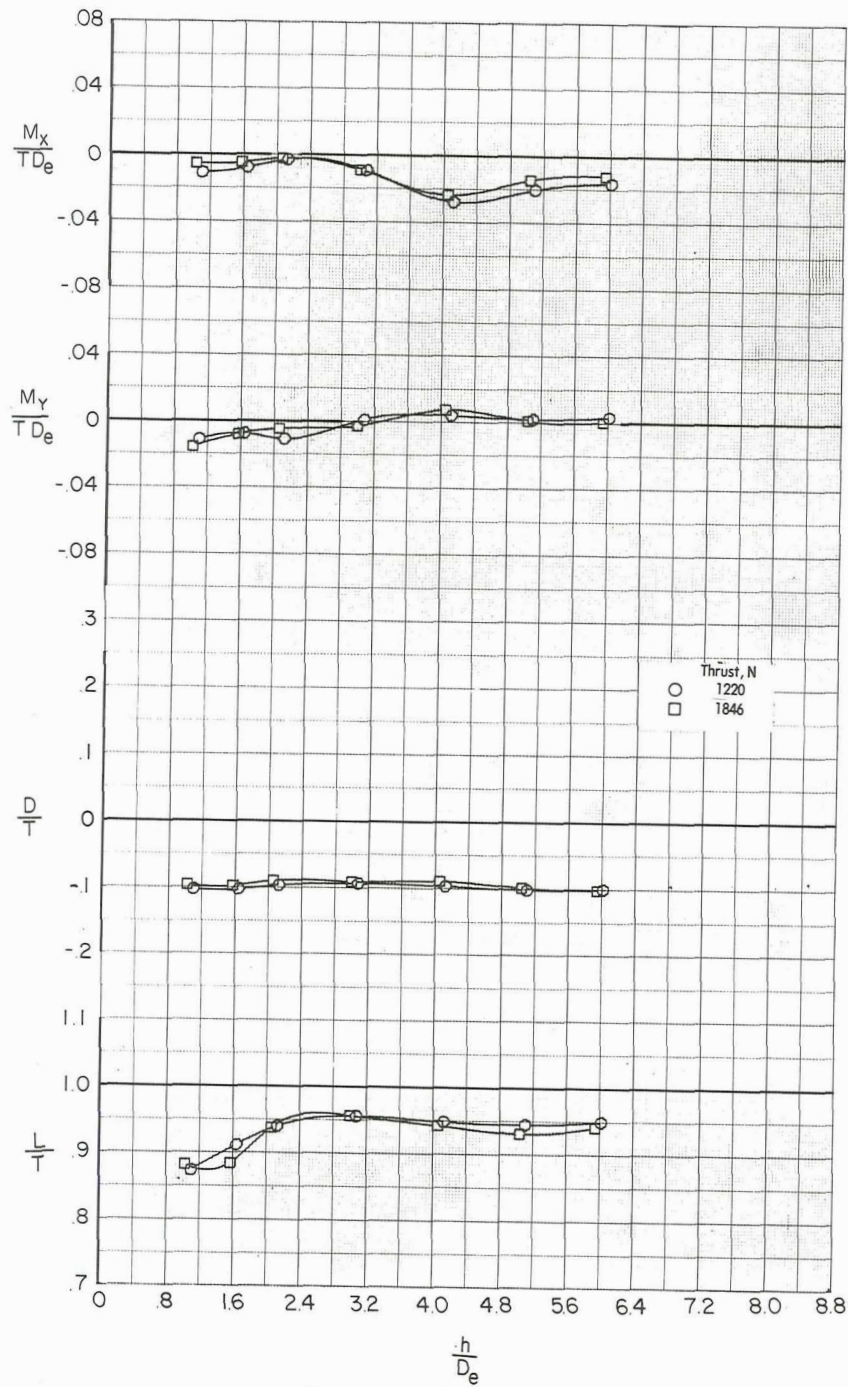
(a) Tail off; $\alpha = -4^\circ$; $\phi = 0^\circ$.

Figure 17.- Effect of ground proximity on induced loads of take-off configuration at zero wind speed. ($\delta_L = 7.5^\circ$; $\delta_{LC} = 82^\circ$; $\delta_f = 40^\circ$.)



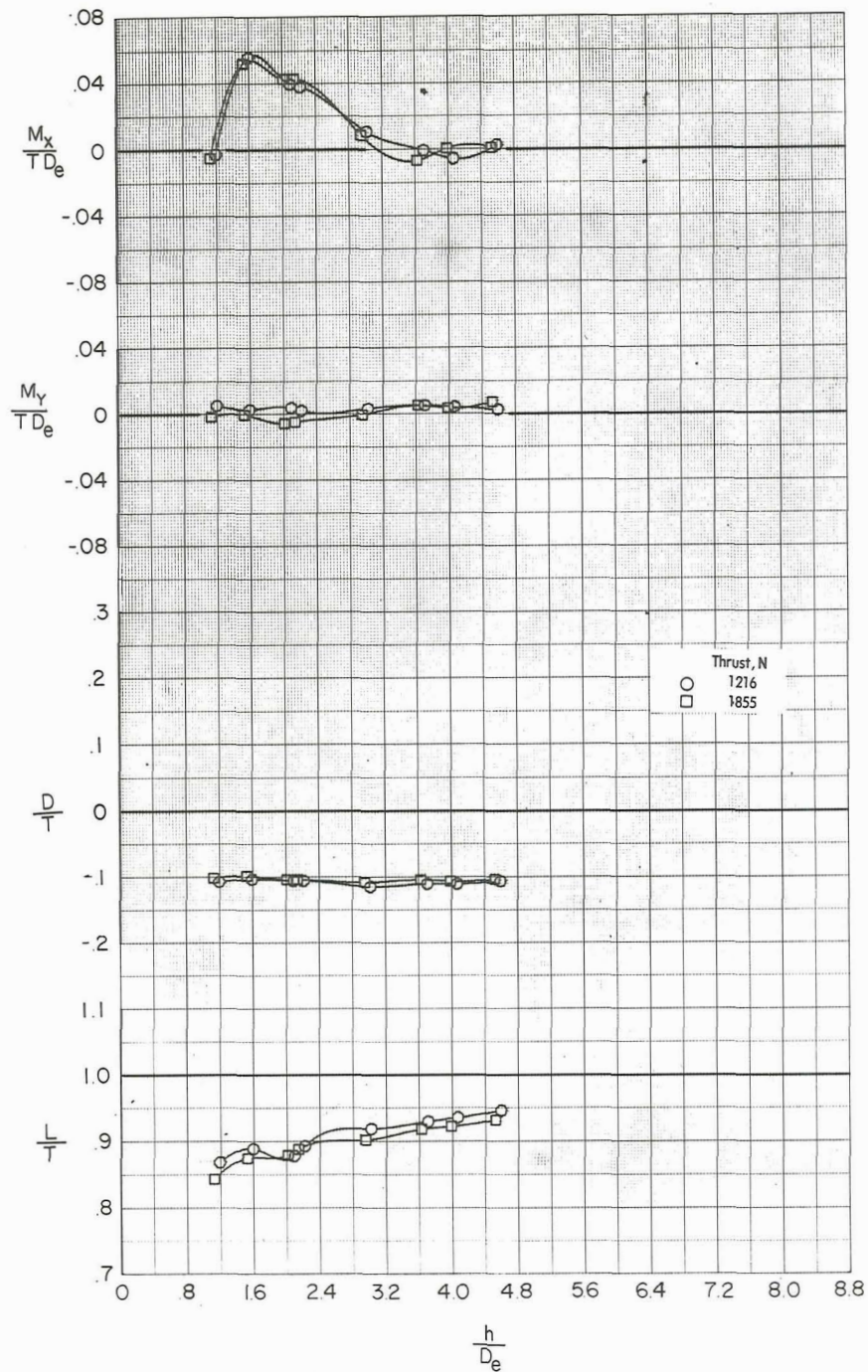
(b) $i_t = 0^{\circ}$; $\delta_e = 0^{\circ}$; $\alpha = -4^{\circ}$; $\phi = 0^{\circ}$.

Figure 17.- Continued.



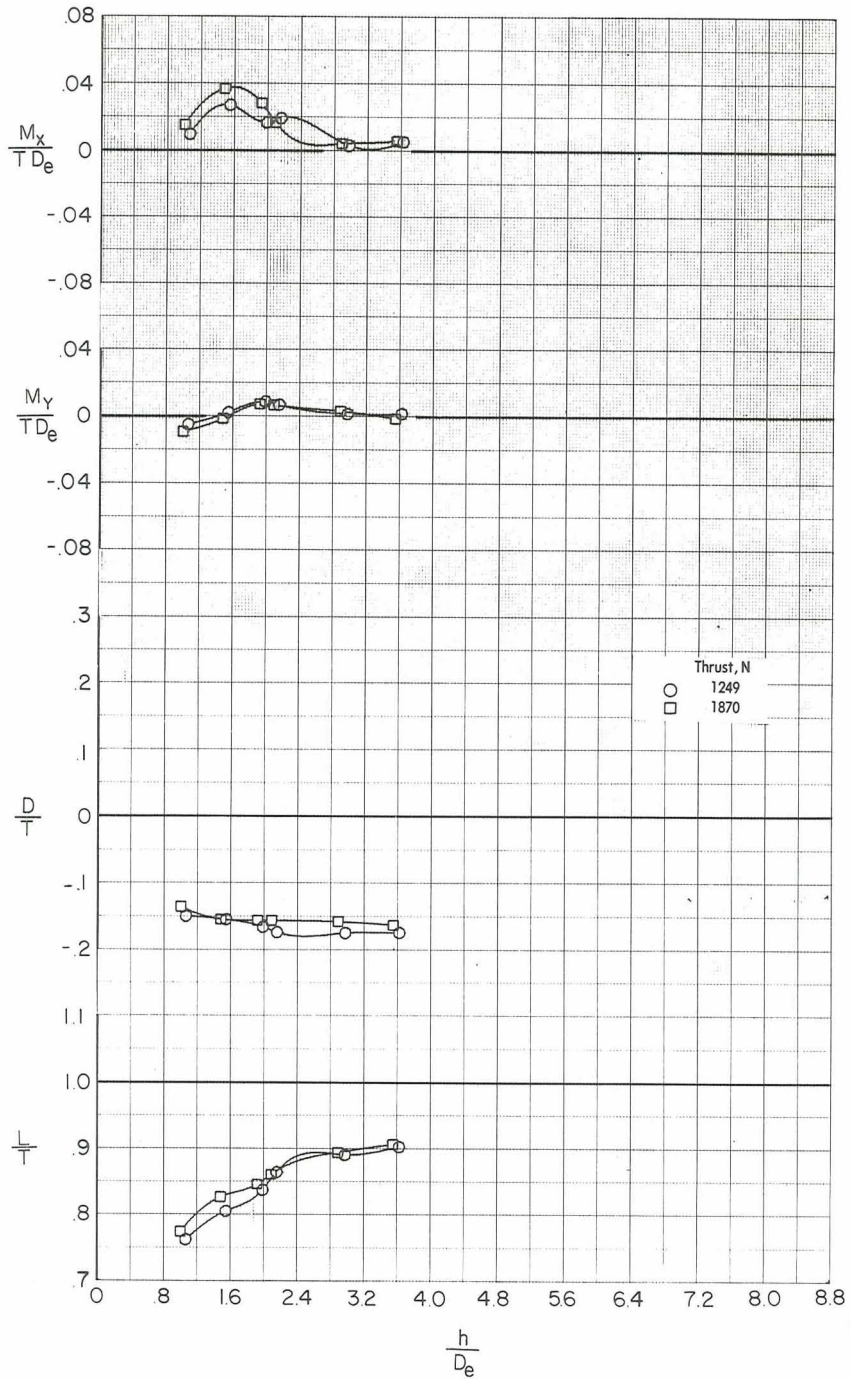
(c) $i_t = 0^\circ$; $\delta_e = 0^\circ$; $\alpha = 0^\circ$; $\phi = 0^\circ$.

Figure 17.- Continued.



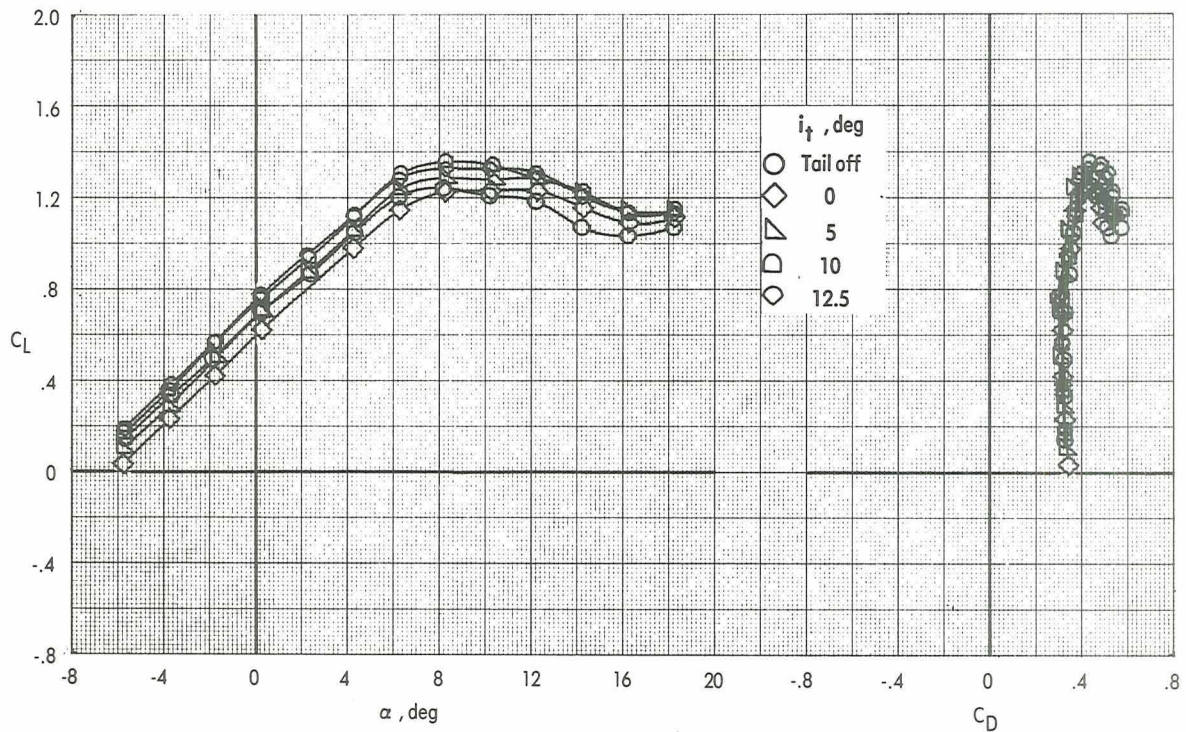
(d) $i_t = 0^\circ$; $\delta_e = 0^\circ$; $\alpha = 0^\circ$; $\phi = 10^\circ$.

Figure 17.- Continued.



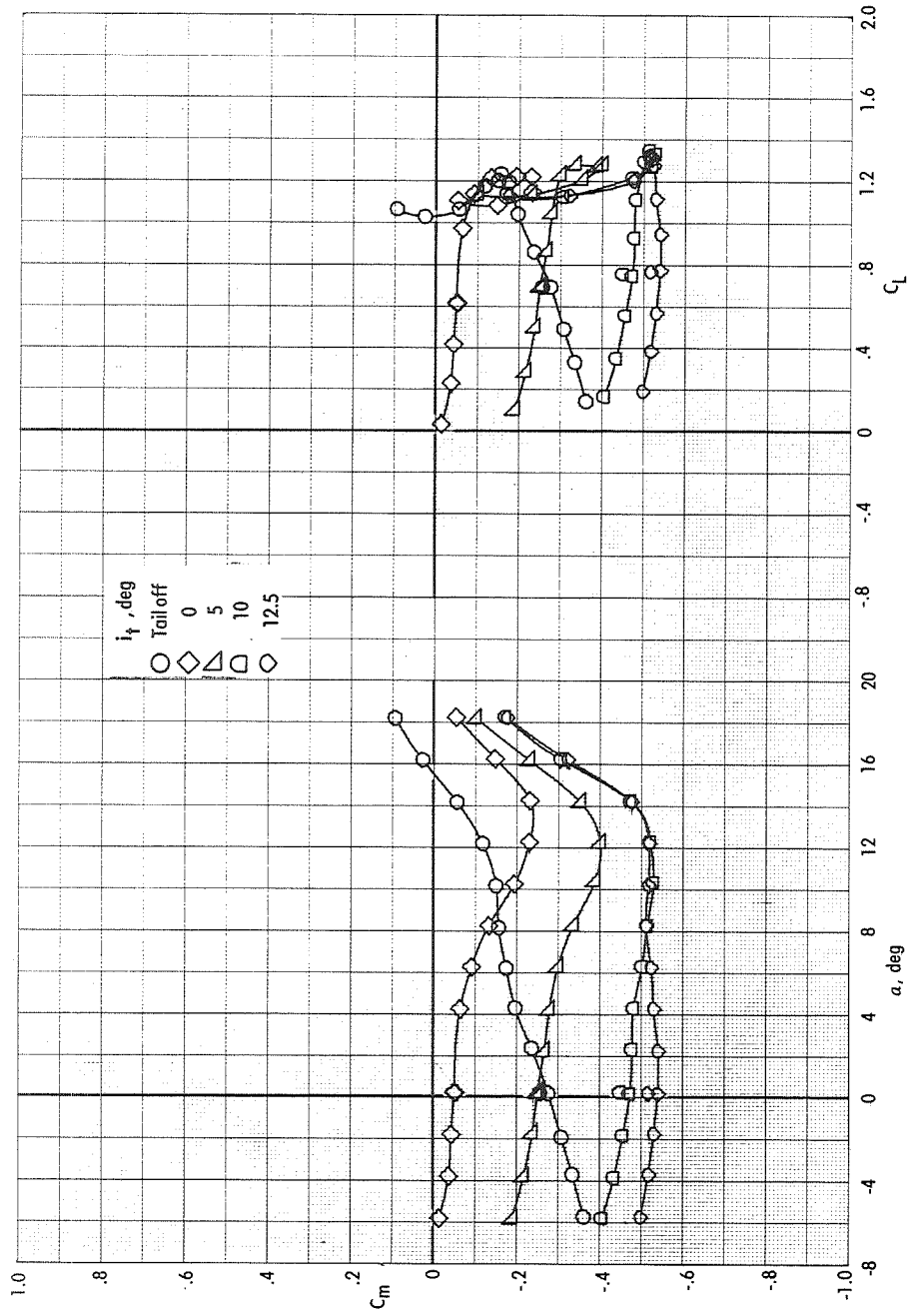
(e) $i_t = 0^{\circ}$; $\delta_e = 0^{\circ}$; $\alpha = -4^{\circ}$; $\phi = 10^{\circ}$.

Figure 17.- Concluded.



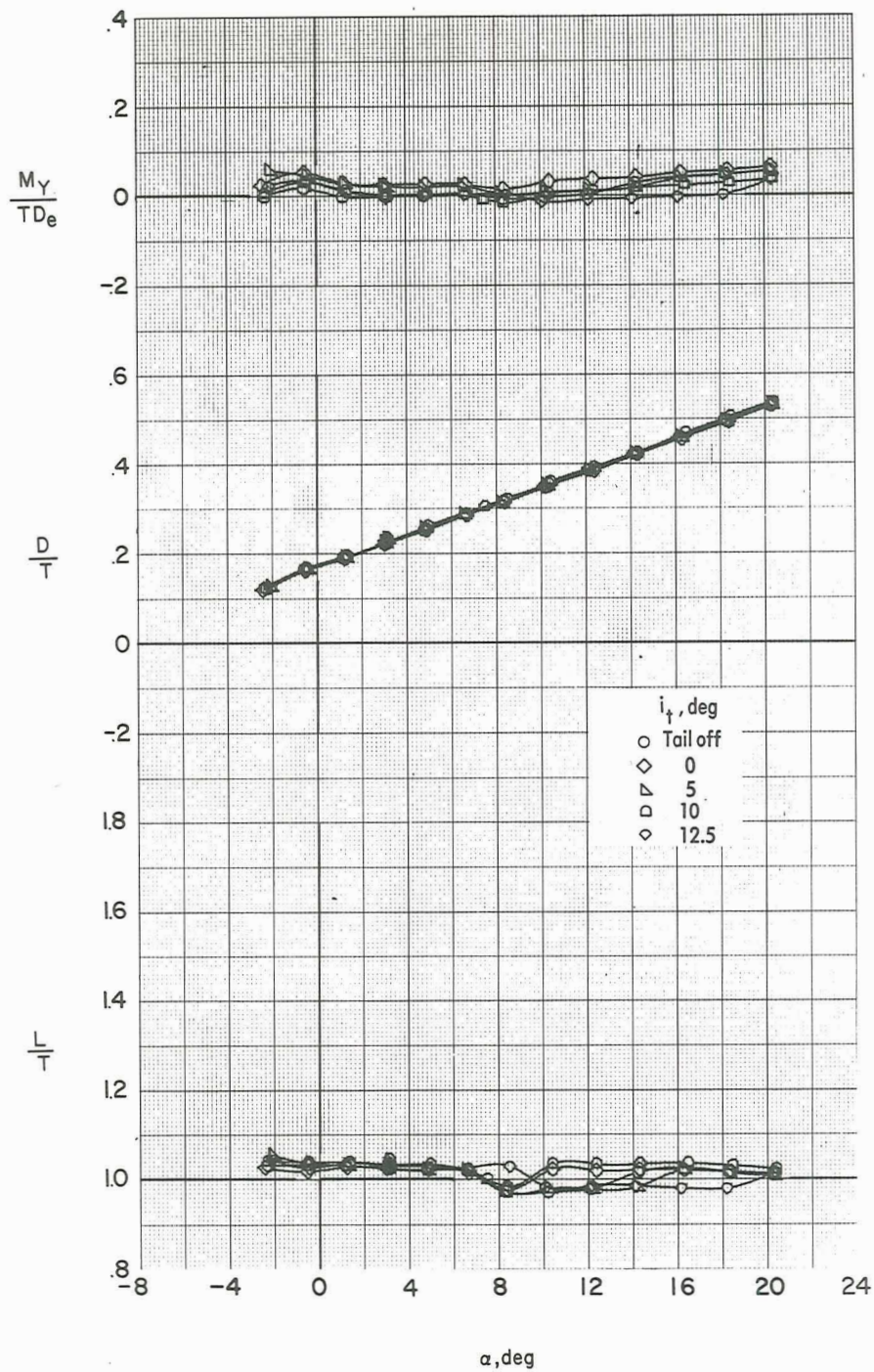
(a) Lift characteristics.

Figure 18.- Effect of tail incidence on longitudinal aerodynamic characteristics of the VTOL transition configuration ($\delta_L = 0^\circ$; $\delta_{LC} = 90^\circ$; $\delta_f = 40^\circ$; $\delta_e = 0^\circ$) with power off. $q_\infty = 239$ Pa; $M_\infty = 0.058$.



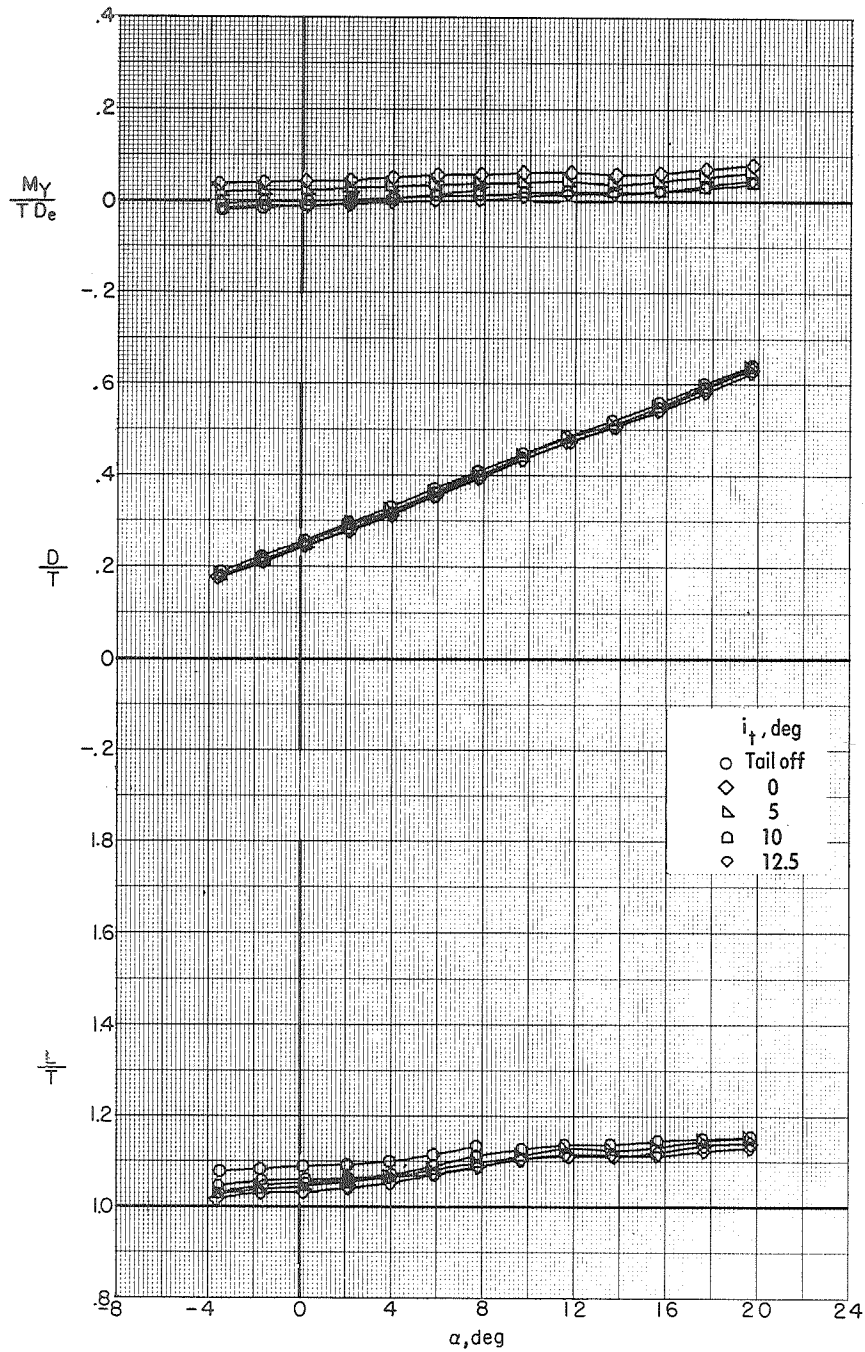
(b) Pitching-moment characteristics.

Figure 18.- Concluded.



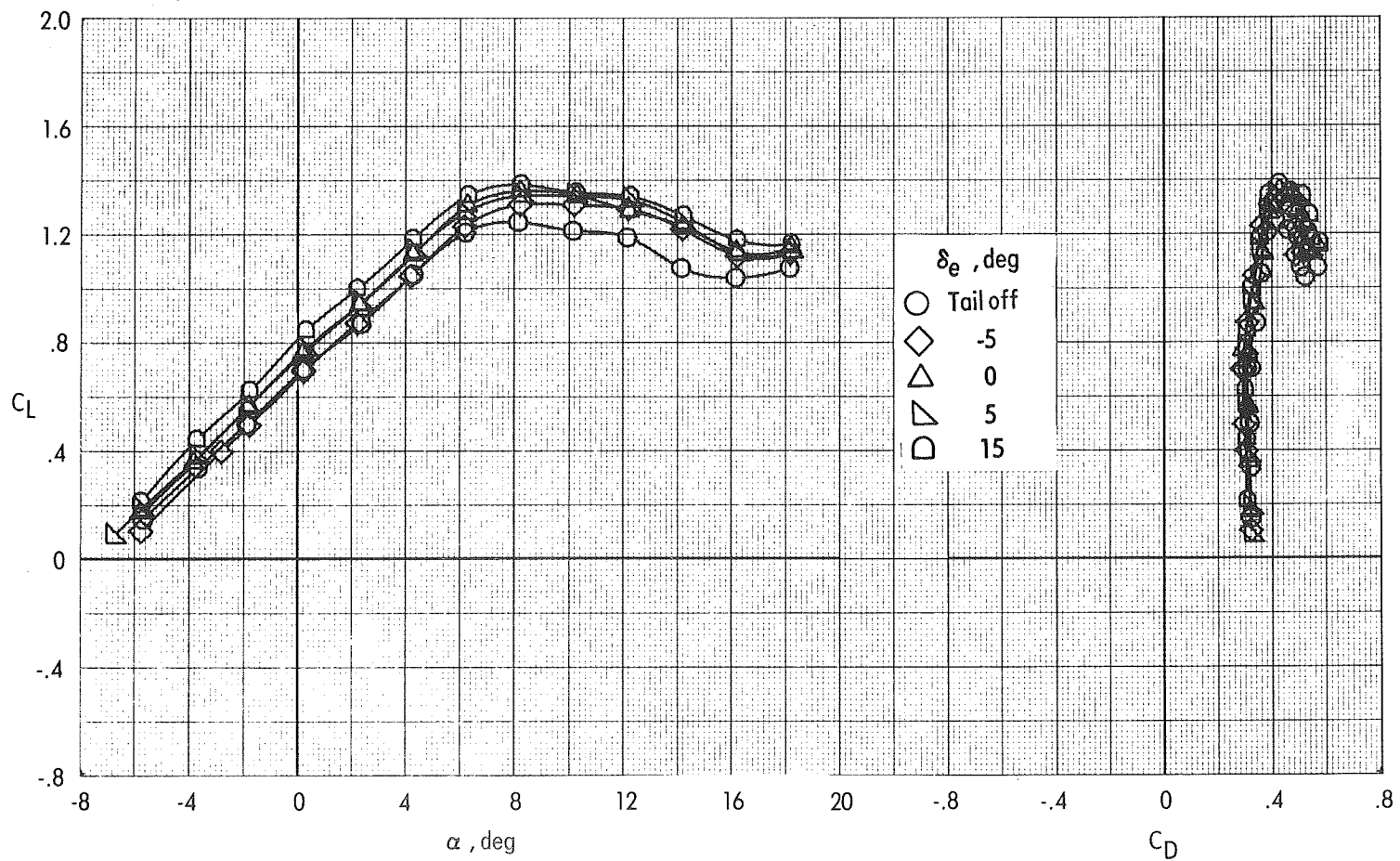
(a) $V_e = 0.12$.

Figure 19.- Effect of tail incidence on longitudinal aerodynamic characteristics of the VTOL transition configuration ($\delta_L = 0^\circ$; $\delta_{LC} = 90^\circ$; $\delta_f = 40^\circ$; $\delta_e = 0^\circ$) with power on. $q_\infty = 239$ Pa; $M_\infty = 0.058$.



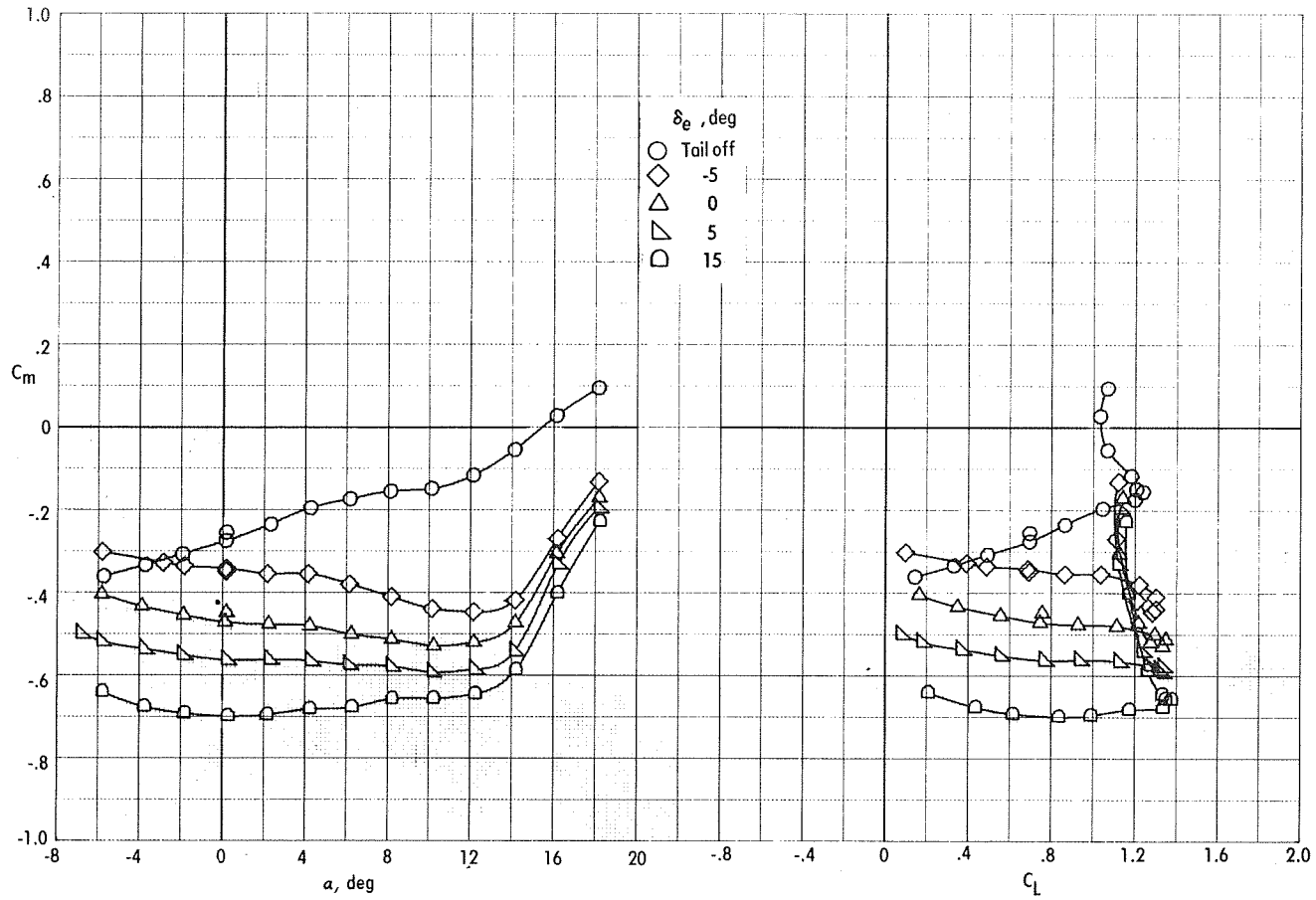
(b) $V_e = 0.18$.

Figure 19.- Concluded.



(a) Lift characteristics.

Figure 20.- Effect of elevator deflection on longitudinal aerodynamic characteristics of the VTOL transition configuration ($\delta_L = 0^\circ$; $\delta_{LC} = 90^\circ$; $\delta_f = 40^\circ$; $i_t = 10^\circ$) with power off. $q_\infty = 239$ Pa; $M_\infty = 0.058$.



(b) Pitching-moment characteristics.

Figure 20.- Concluded.

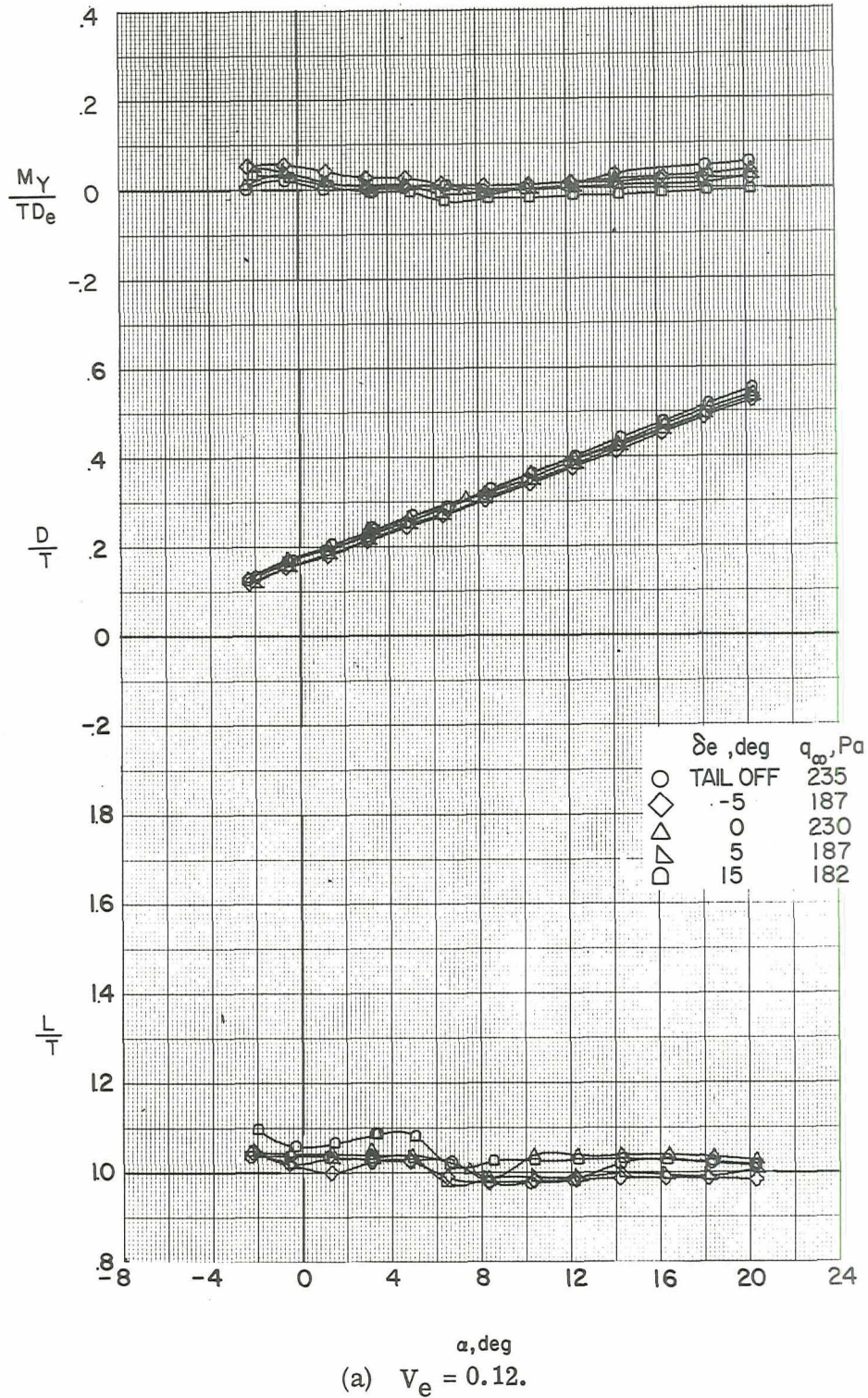
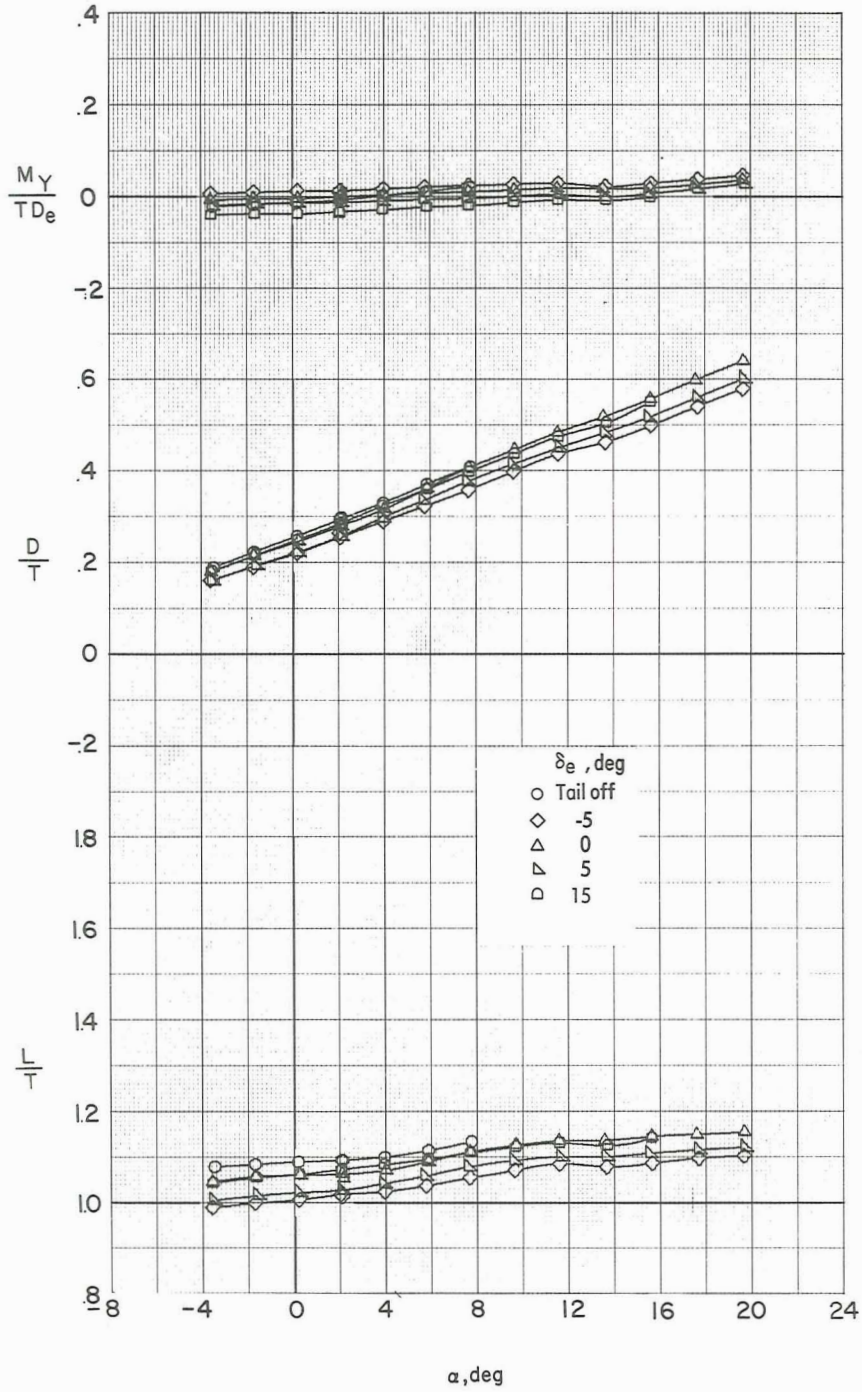


Figure 21.- Effect of elevator deflection on longitudinal aerodynamic characteristics of the VTOL transition configuration ($\delta_L = 0^\circ$; $\delta_{LC} = 90^\circ$; $\delta_f = 40^\circ$; $i_t = 10^\circ$) with power on.



(b) $V_e = 0.18$.

Figure 21. - Concluded.

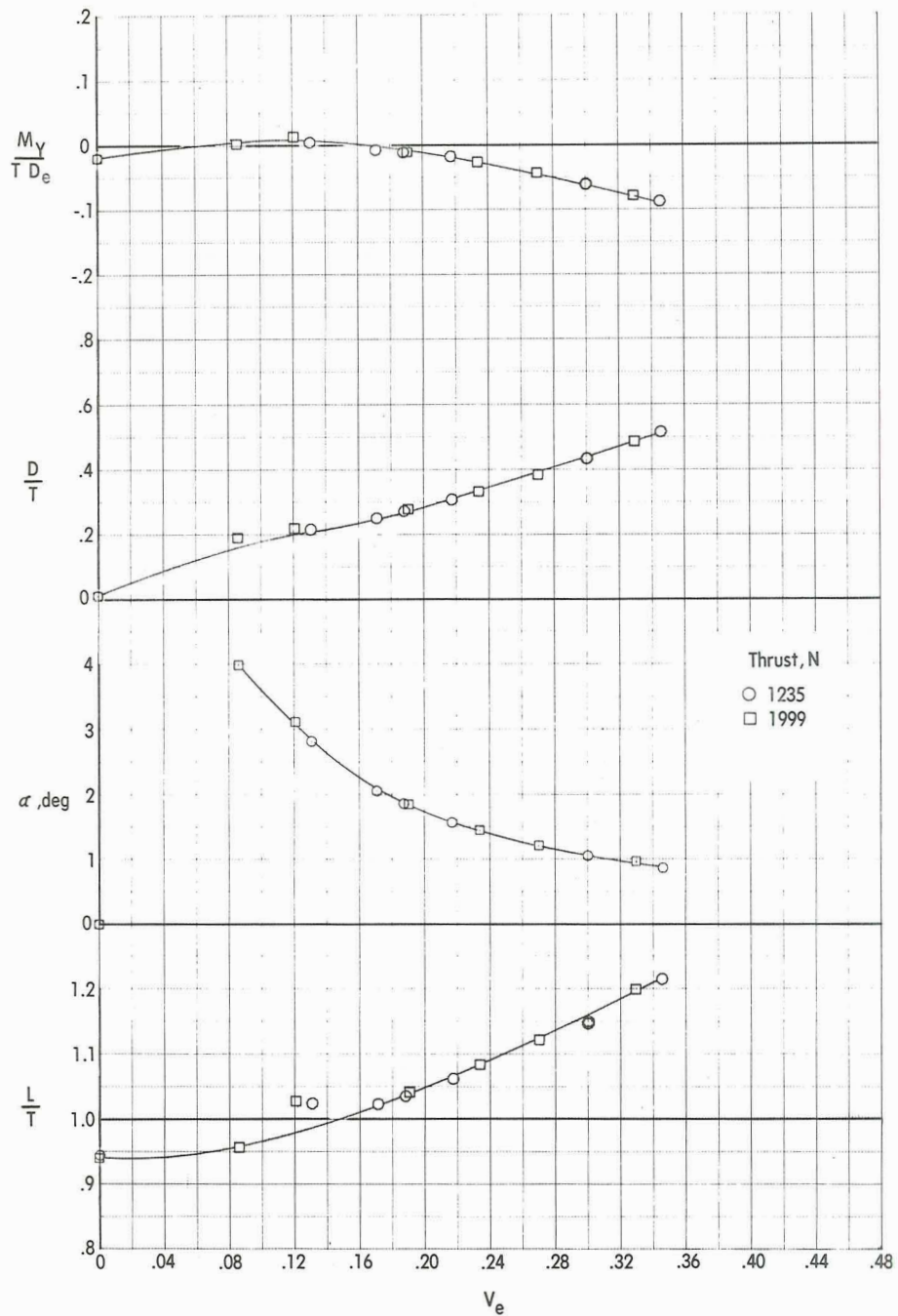
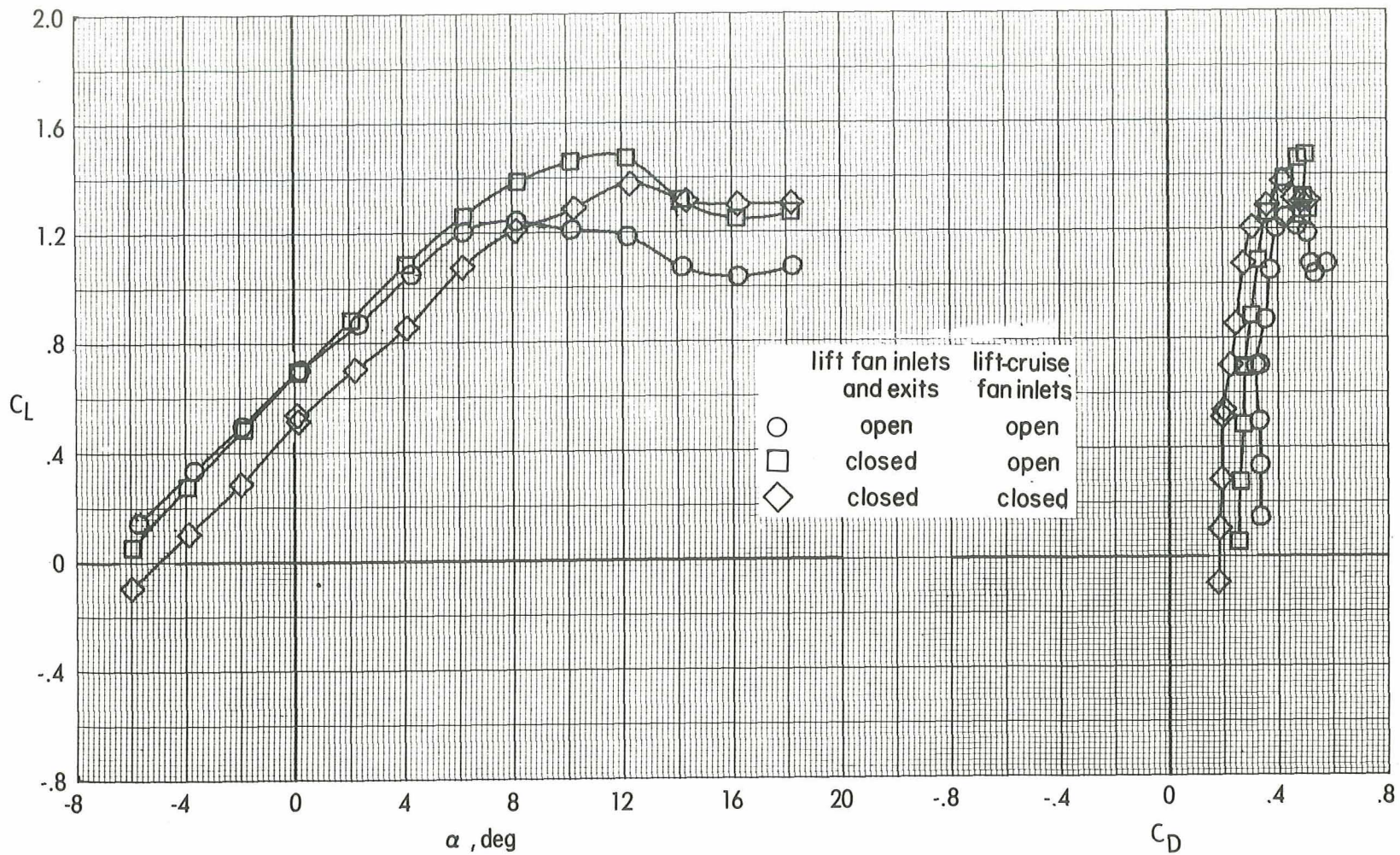
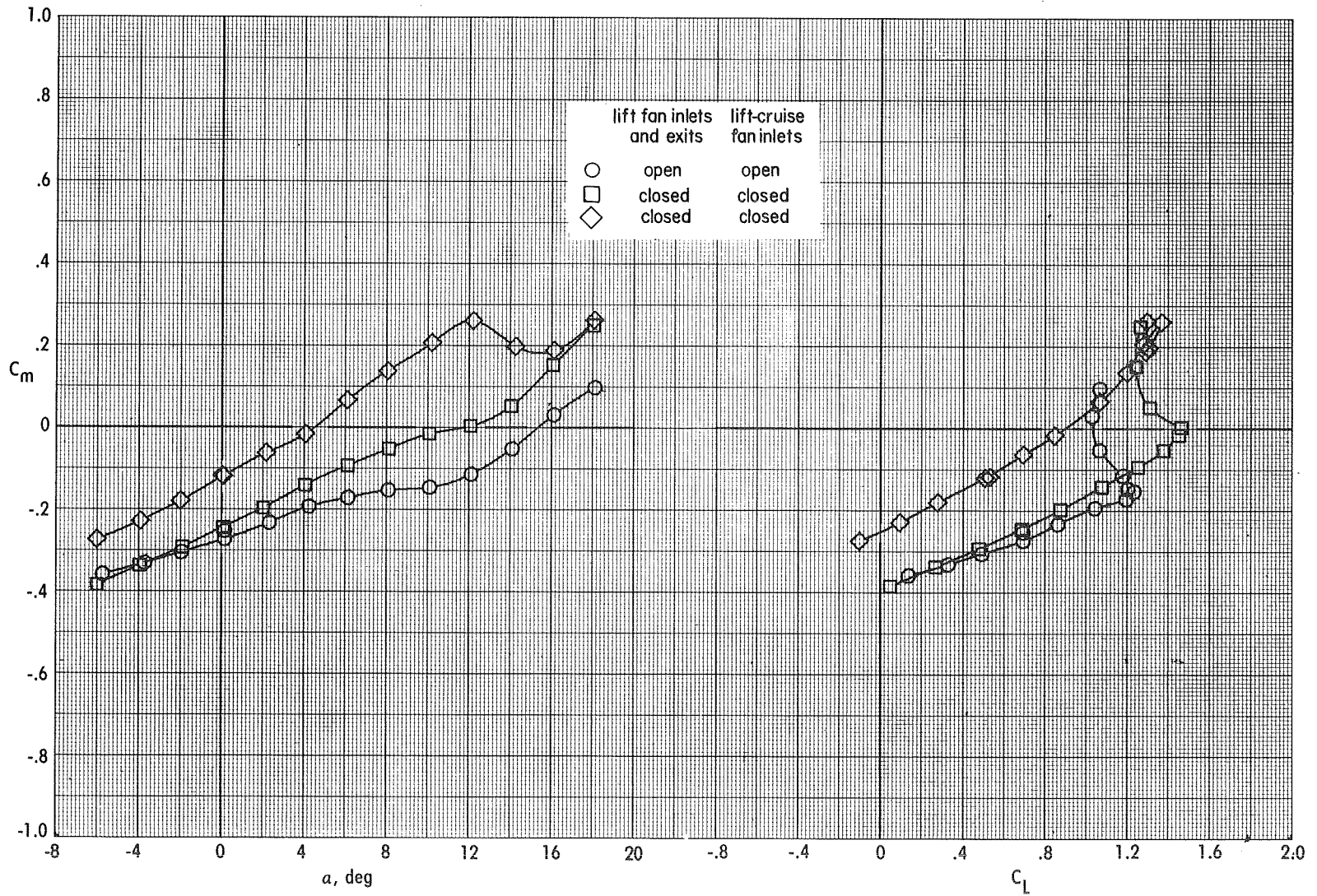


Figure 22.- Effect of velocity ratio on longitudinal aerodynamic characteristics of the VTOL transition configuration ($\delta_L = 0^\circ$; $\delta_{LC} = 90^\circ$; $\delta_f = 40^\circ$; $i_t = 10^\circ$; $\delta_e = 0^\circ$).



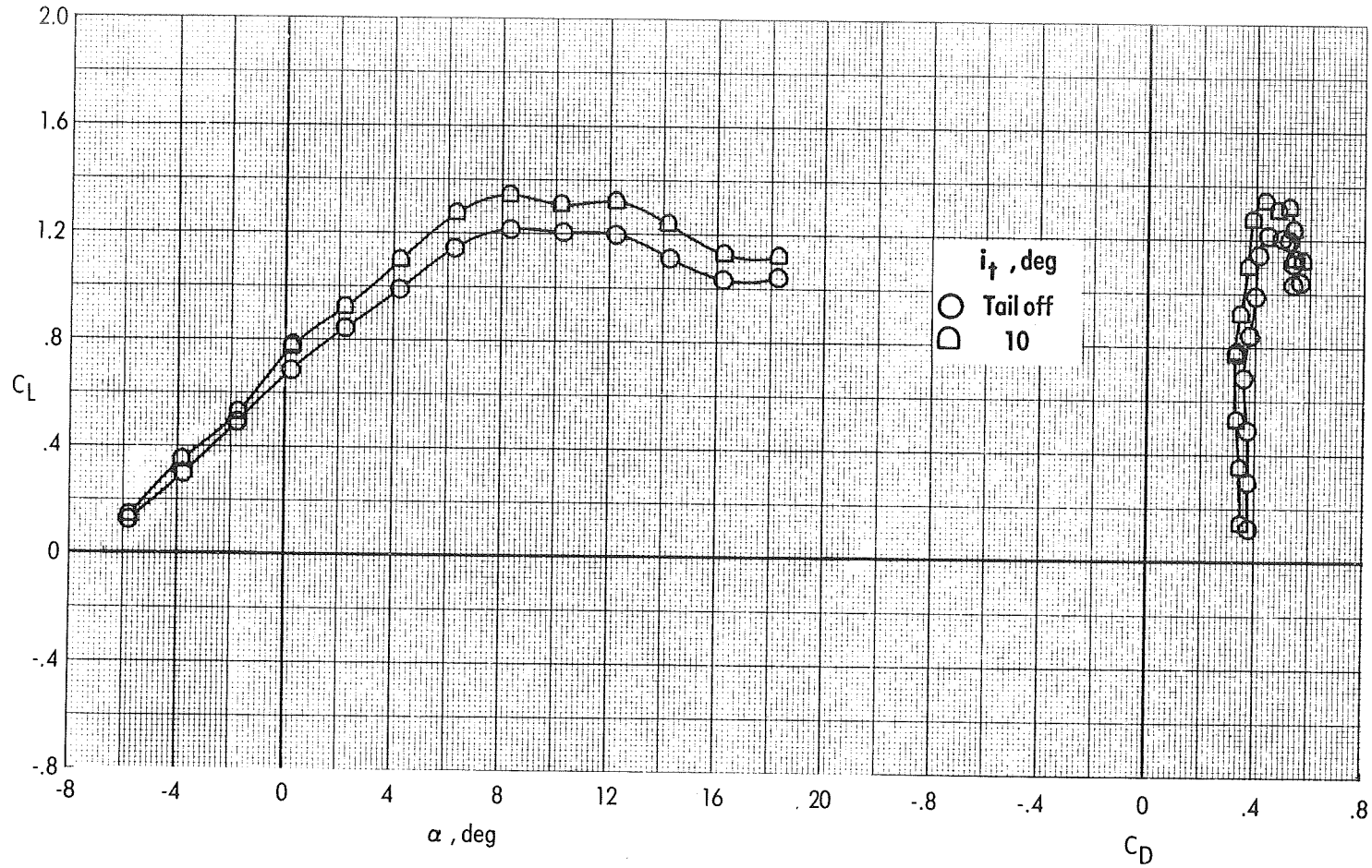
(a) Lift characteristics.

Figure 23.- Effect of closed lift-fan inlets and exits on longitudinal aerodynamics of the VTOL transition configuration ($\delta_L = 0^\circ$; $\delta_{LC} = 90^\circ$; $\delta_f = 40^\circ$; tail off) with power off. $q_\infty = 239$ Pa; $M_\infty = 0.058$.



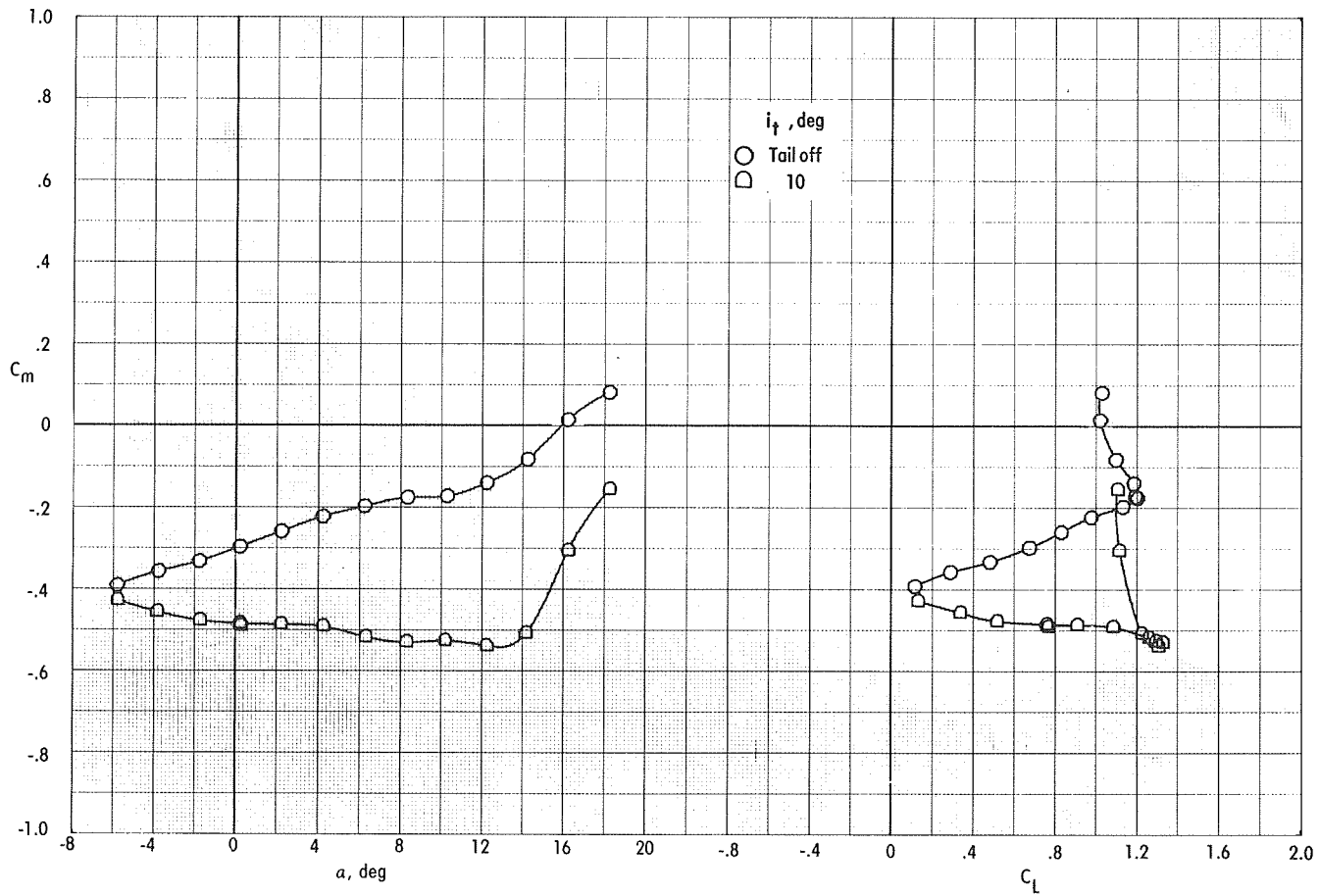
(b) Pitching-moment characteristics.

Figure 23.- Concluded.



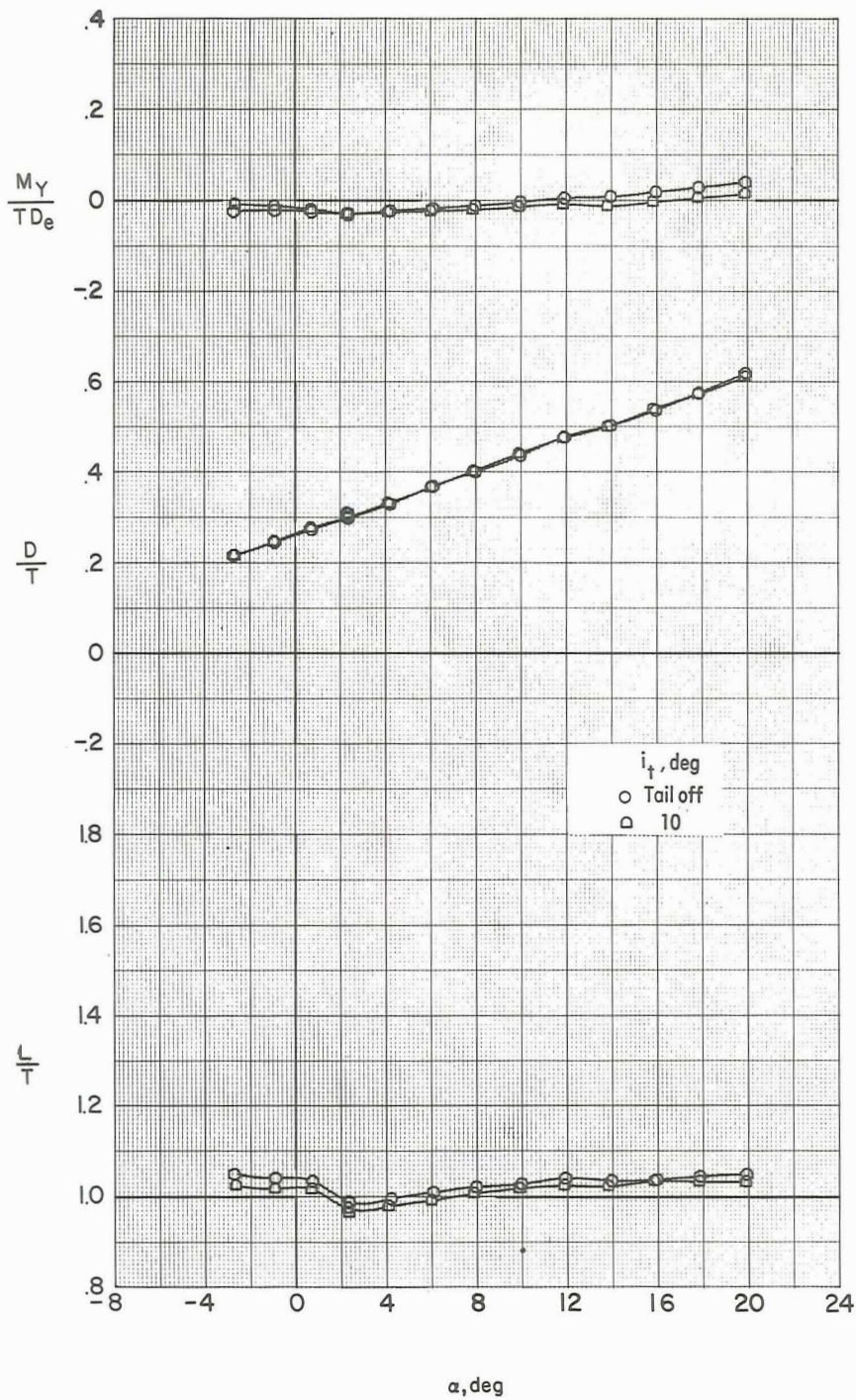
(a) Lift characteristics.

Figure 24.- Effect of tail incidence on longitudinal aerodynamic characteristics of the VTOL transition configuration ($\delta_L = -5^\circ$; $\delta_{LC} = 94^\circ$; $\delta_f = 40^\circ$; $\delta_e = 0^\circ$) with power off. $q_\infty = 168$ Pa; $M_\infty = 0.048$.



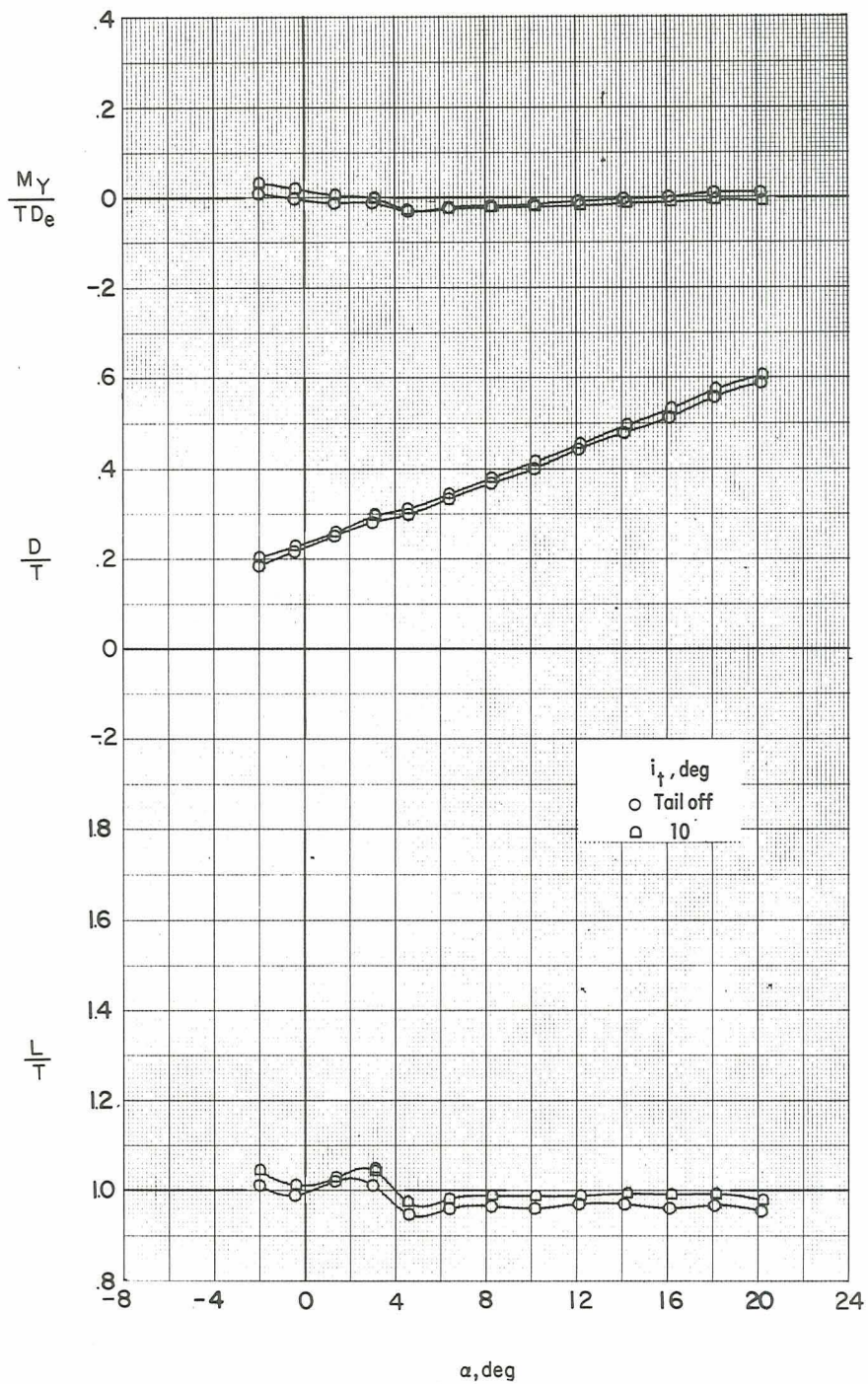
(b) Pitching-moment characteristics.

Figure 24.- Concluded.



(a) $V_e = 0.12$.

Figure 25.- Effect of tail incidence on longitudinal aerodynamic characteristics of the VTOL transition configuration ($\delta_L = -5^\circ$; $\delta_{LC} = 94^\circ$; $\delta_f = 40^\circ$; $\delta_e = 0^\circ$) with power on. $q_\infty = 168$ Pa; $M_\infty = 0.048$.



α , deg
 (b) $V_e = 0.15$.

Figure 25.- Concluded.

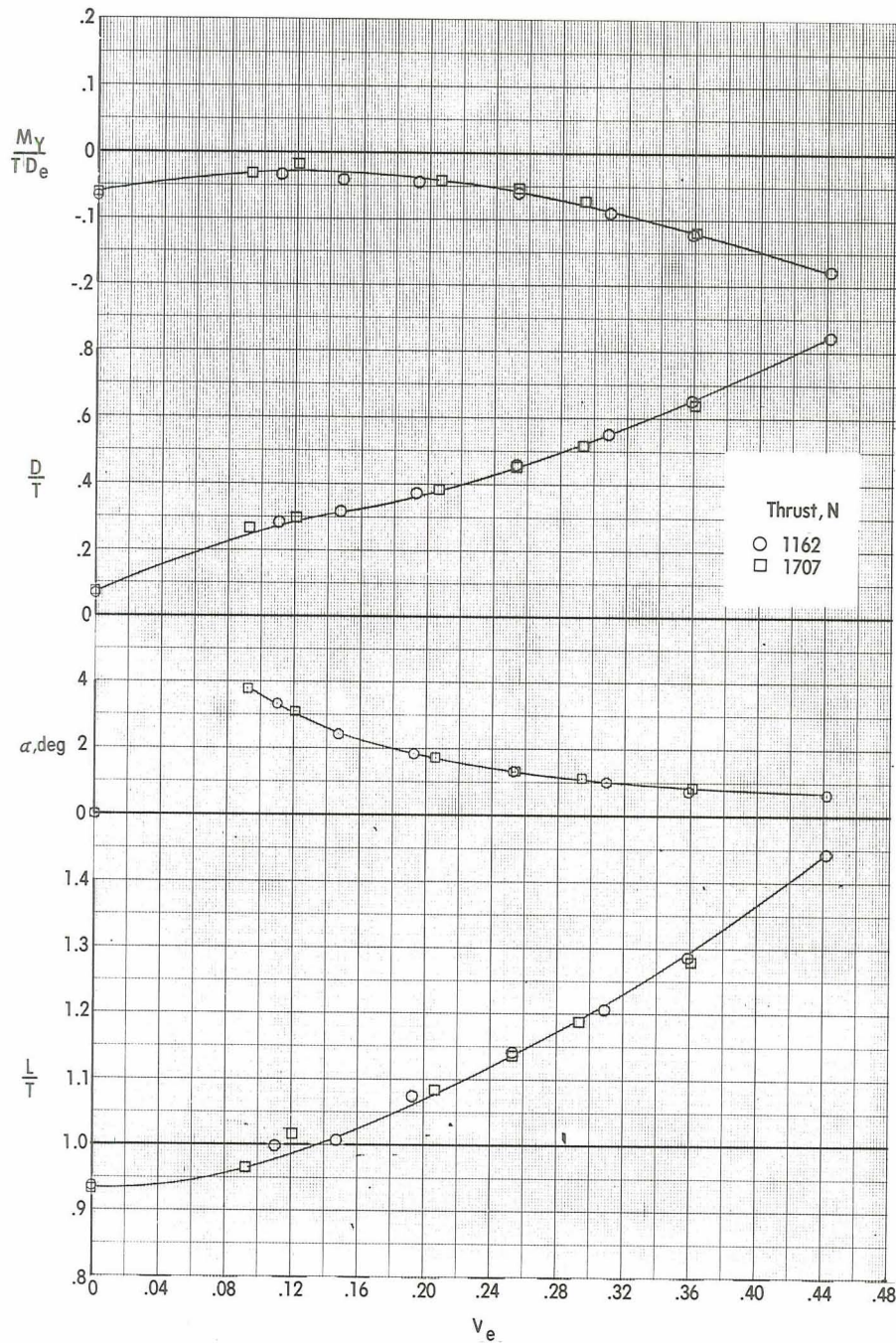
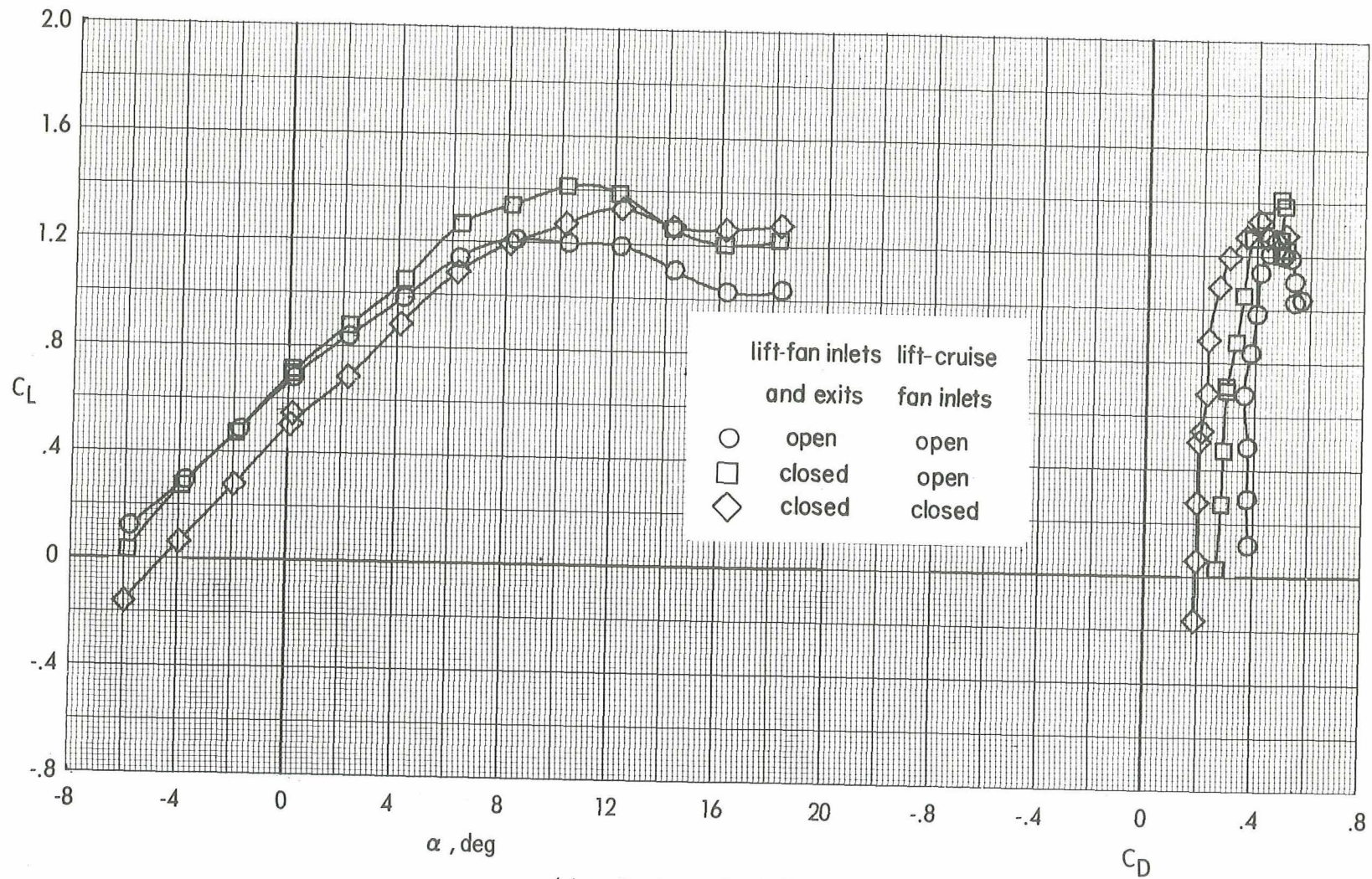
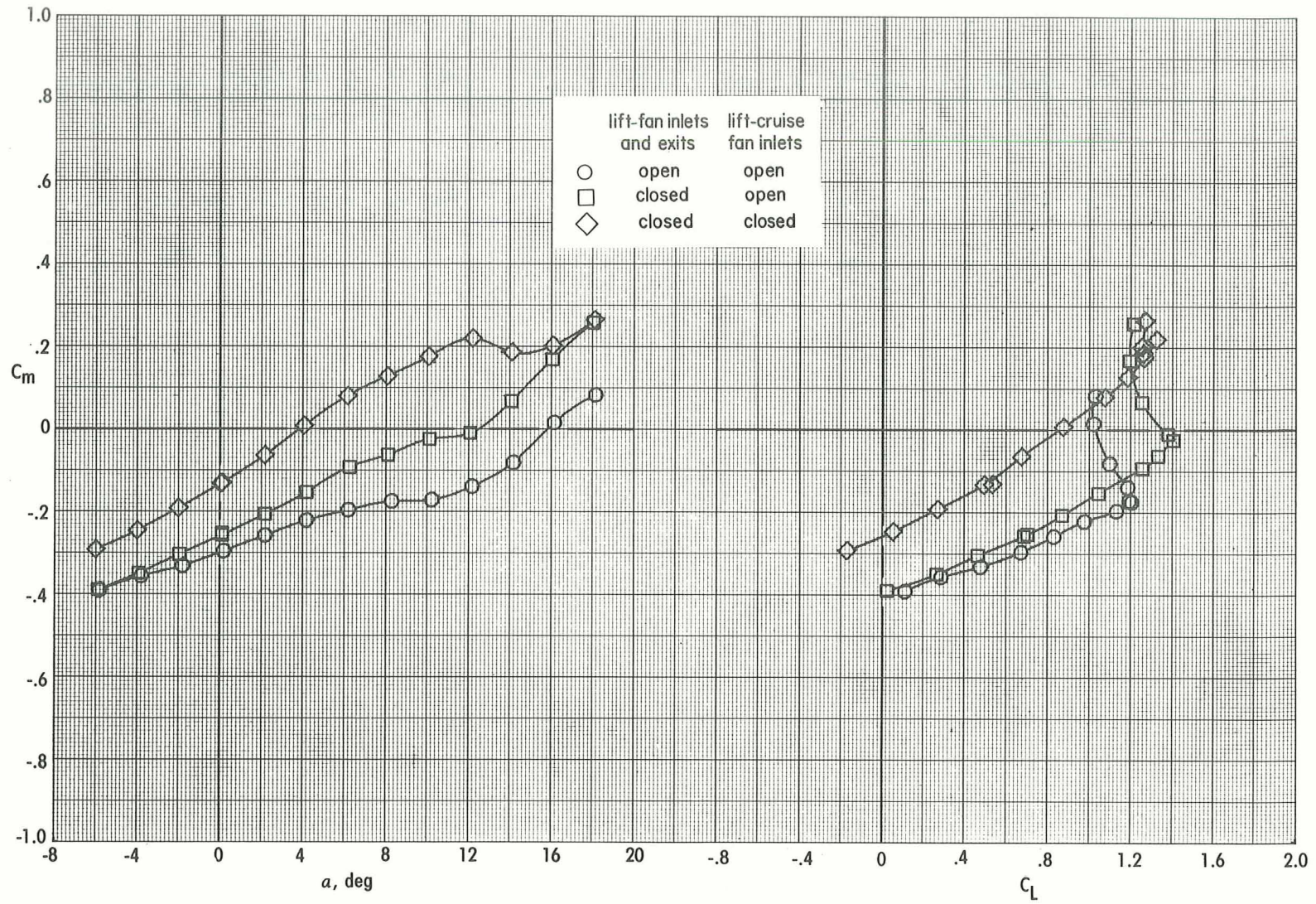


Figure 26.- Effect of effective velocity ratio on longitudinal aerodynamic characteristics of the VTOL transition configuration ($\delta_L = -5^\circ$; $\delta_{LC} = 94^\circ$; $\delta_f = 40^\circ$; $i_t = 10^\circ$; $\delta_e = 0^\circ$).



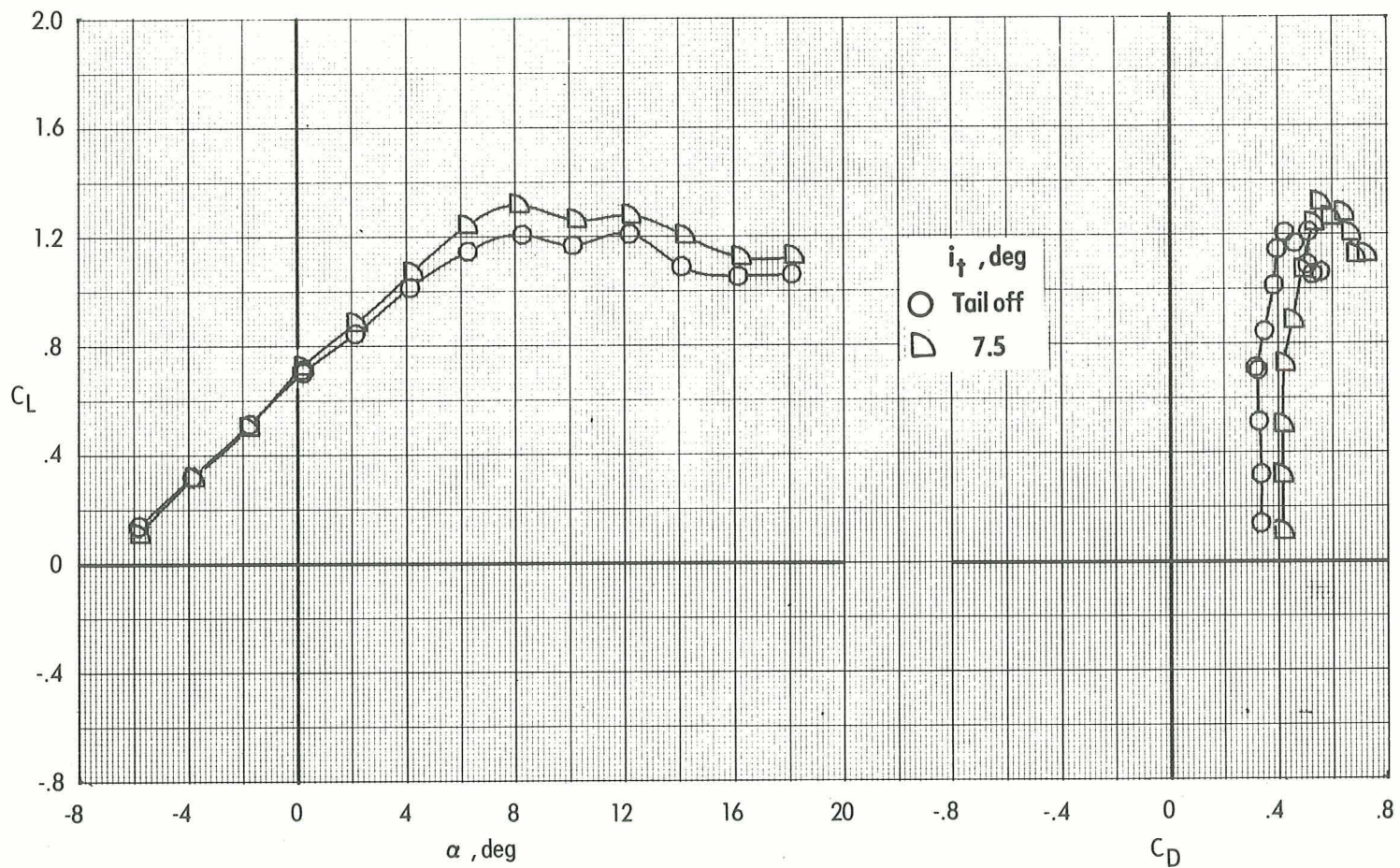
(a) Lift characteristics.

Figure 27.- Effect of closed lift-fan inlets and exits on longitudinal aerodynamics of the VTOL transition configuration ($\delta_L = -5^\circ$; $\delta_{LC} = 94^\circ$; $\delta_f = 40^\circ$; tail off) with power off. $q_\infty = 168$ Pa; $M_\infty = 0.048$.



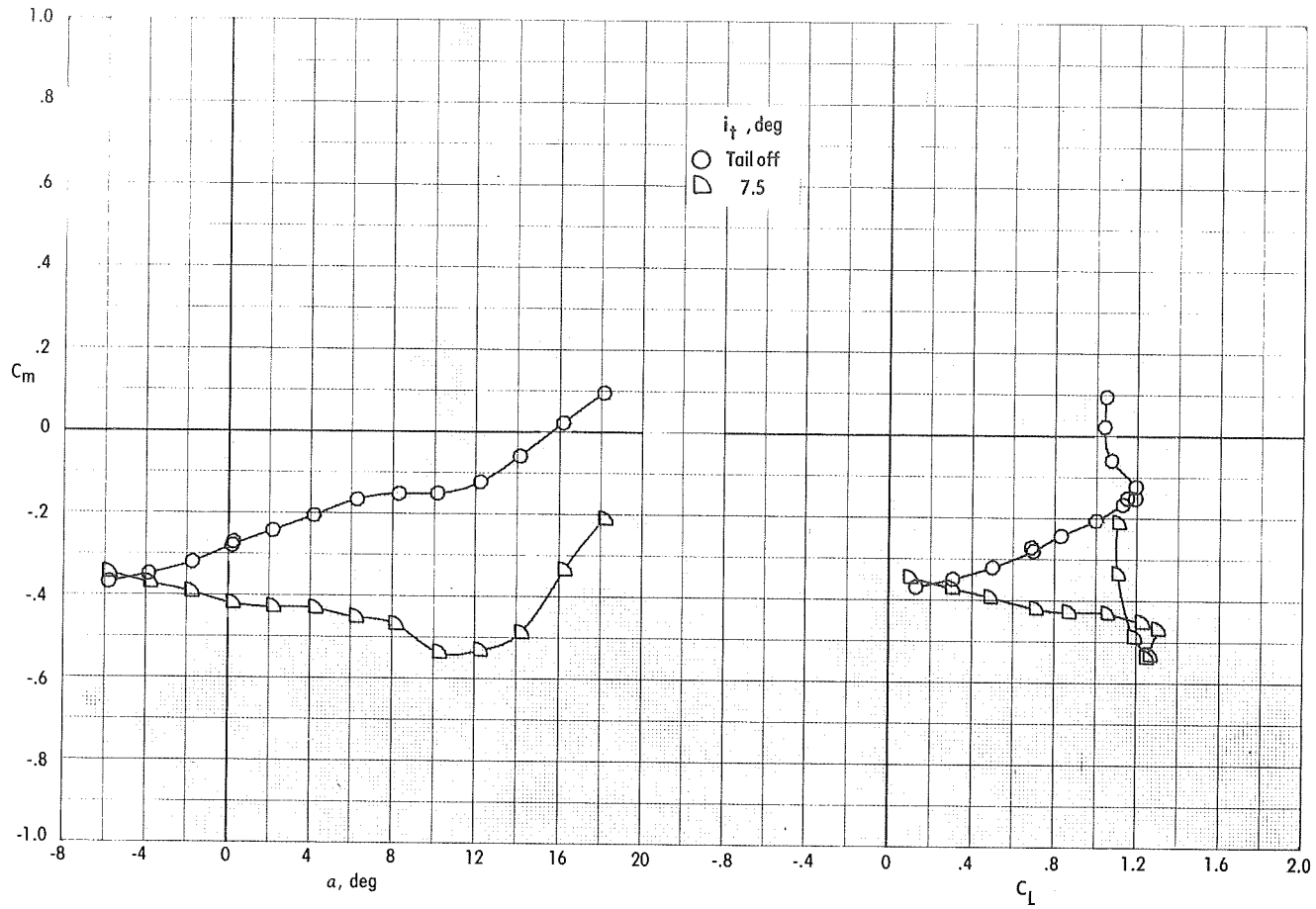
(b) Pitching-moment characteristics.

Figure 27.- Concluded.



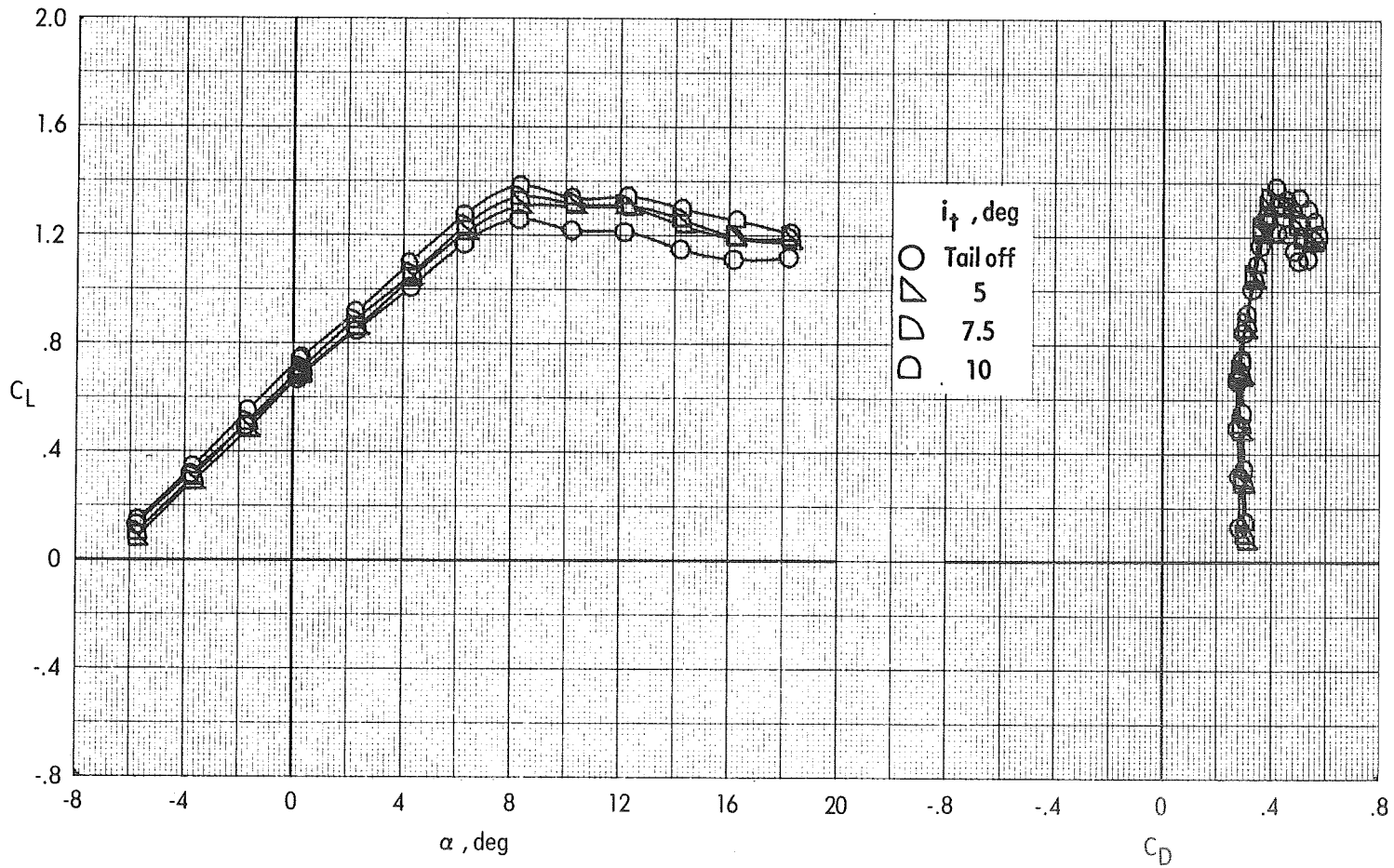
(a) Lift characteristics.

Figure 28.- Effect of tail incidence on longitudinal aerodynamic characteristics of the VTOL transition configuration ($\delta_L = 7.5^\circ$; $\delta_{LC} = 82^\circ$; $\delta_f = 40^\circ$; $\delta_e = 0^\circ$) with power off. $q_\infty = 187$ Pa; $M_\infty = 0.052$.



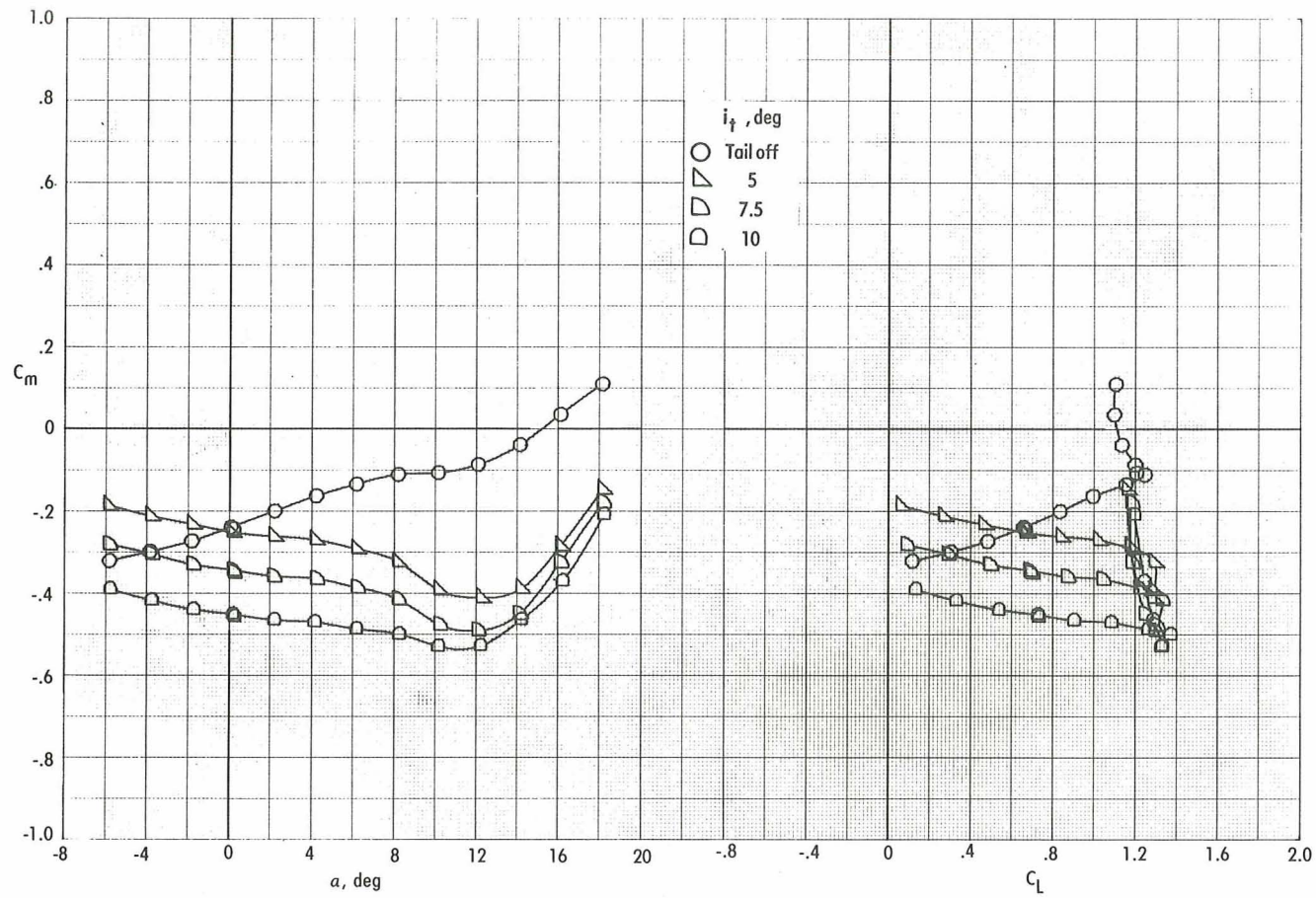
(b) Pitching-moment characteristics.

Figure 28.- Concluded.



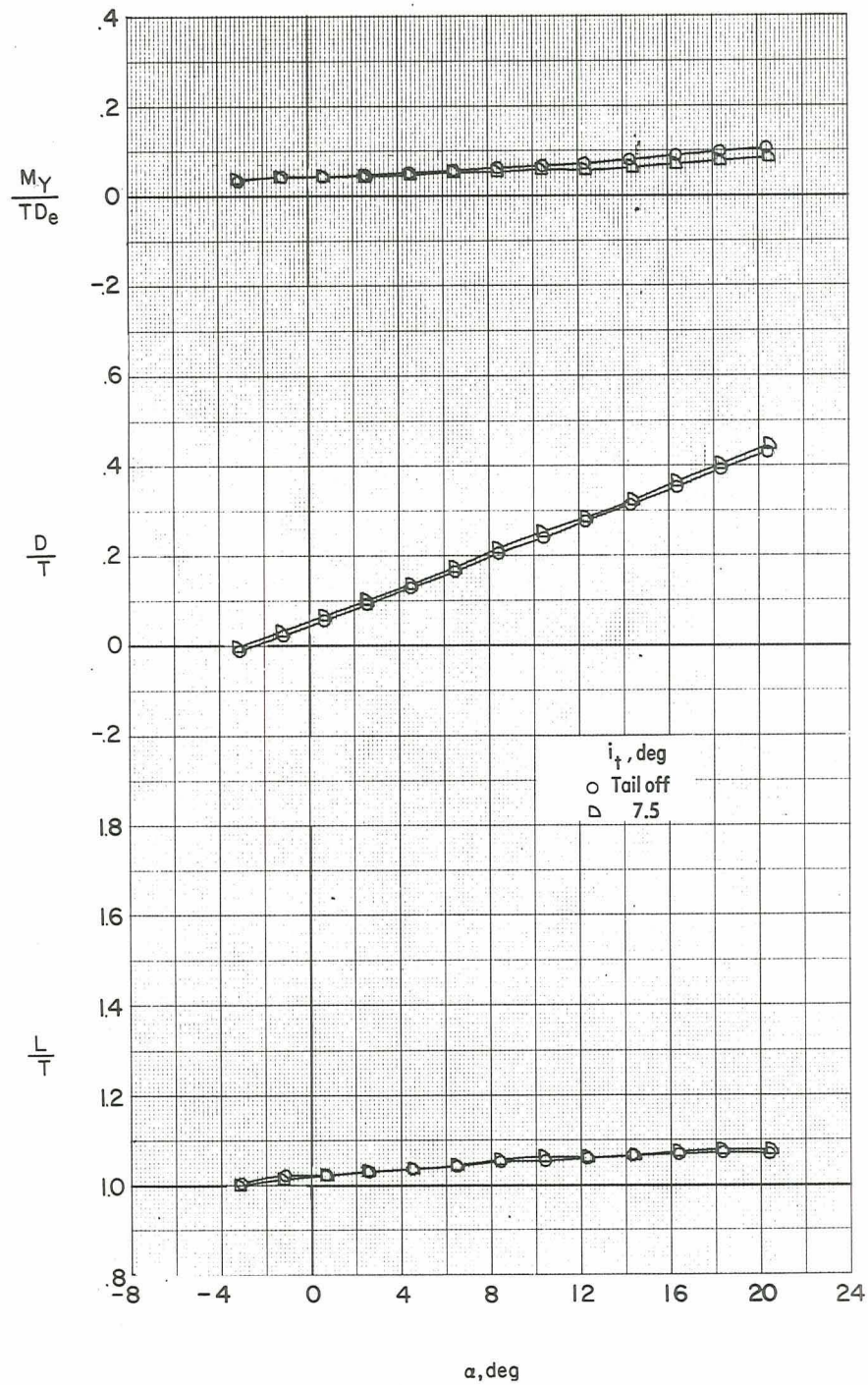
(a) Lift characteristics.

Figure 29.- Effect of tail incidence on longitudinal aerodynamic characteristics of the VTOL transition configuration ($\delta_L = 7.5^\circ$; $\delta_{LC} = 82^\circ$; $\delta_f = 40^\circ$; $\delta_e = 0^\circ$) with power off. $q_\infty = 455$ Pa; $M_\infty = 0.080$.



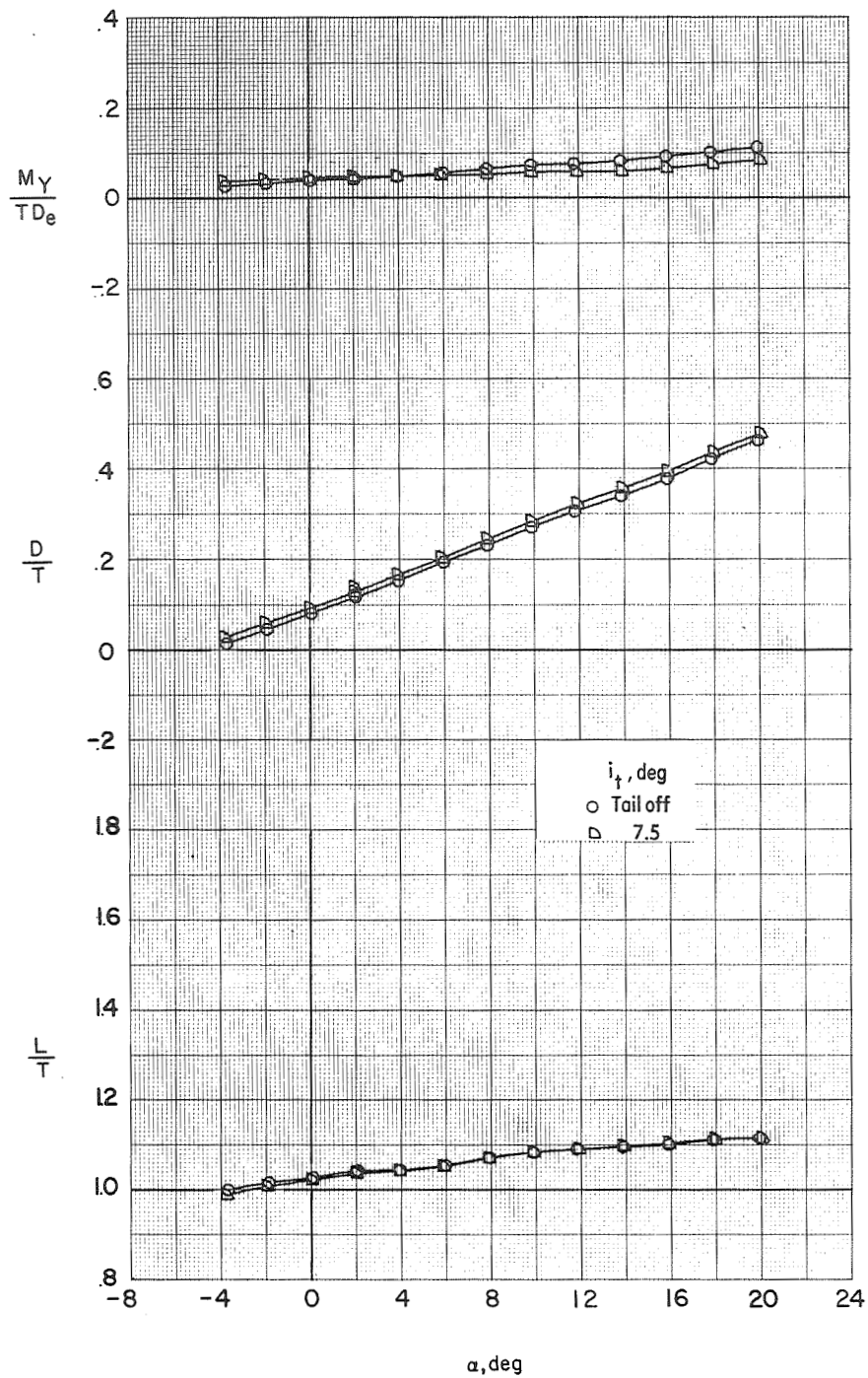
(b) Pitching-moment characteristics.

Figure 29.- Concluded.



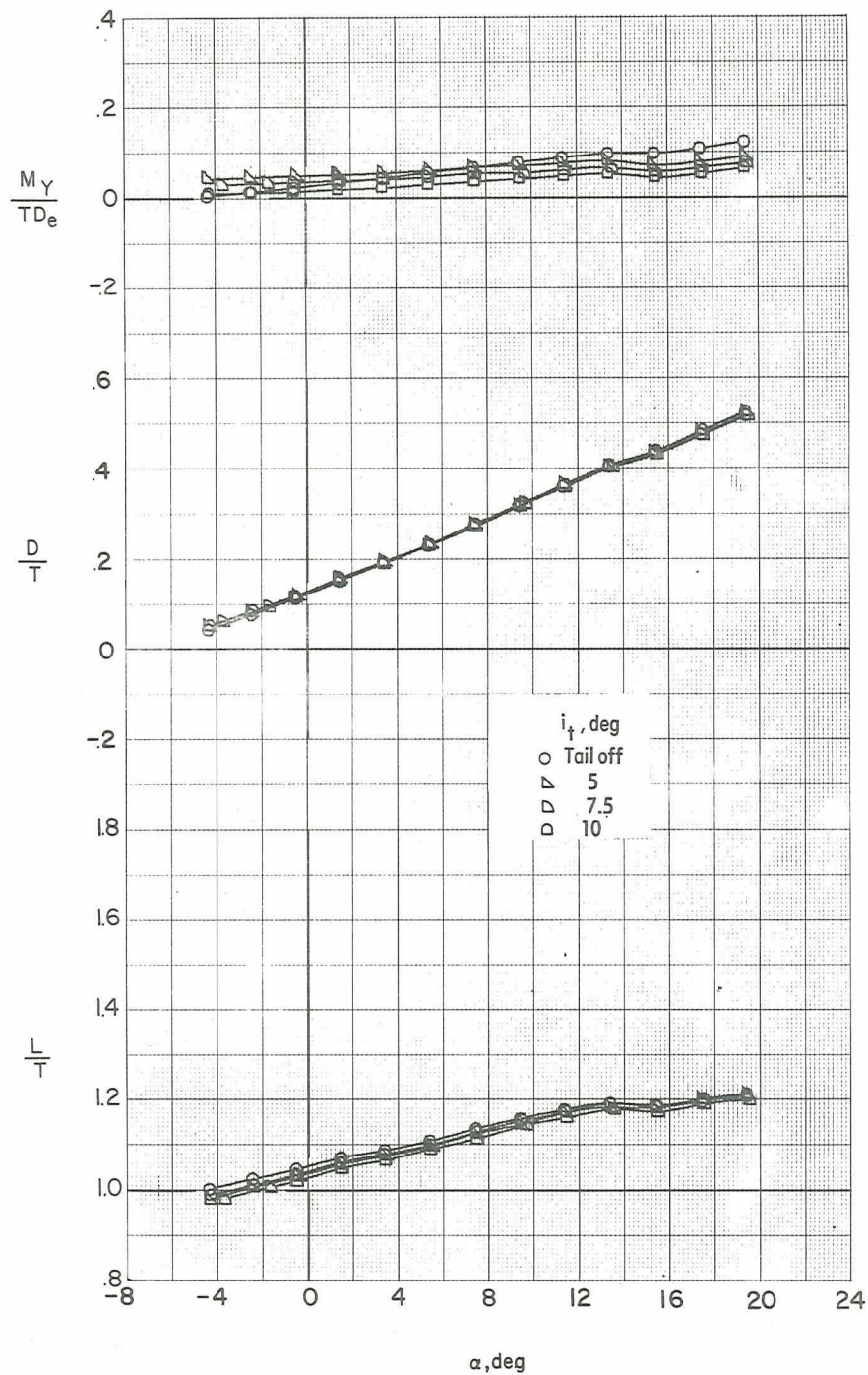
(a) $V_e = 0.12$.

Figure 30.- Effect of tail incidence on longitudinal aerodynamic characteristics of the VTOL transition configuration ($\delta_L = 7.5^\circ$; $\delta_{LC} = 82^\circ$; $\delta_f = 40^\circ$; $\delta_e = 0^\circ$) with power on. $q_\infty = 177$ Pa; $M_\infty = 0.050$.



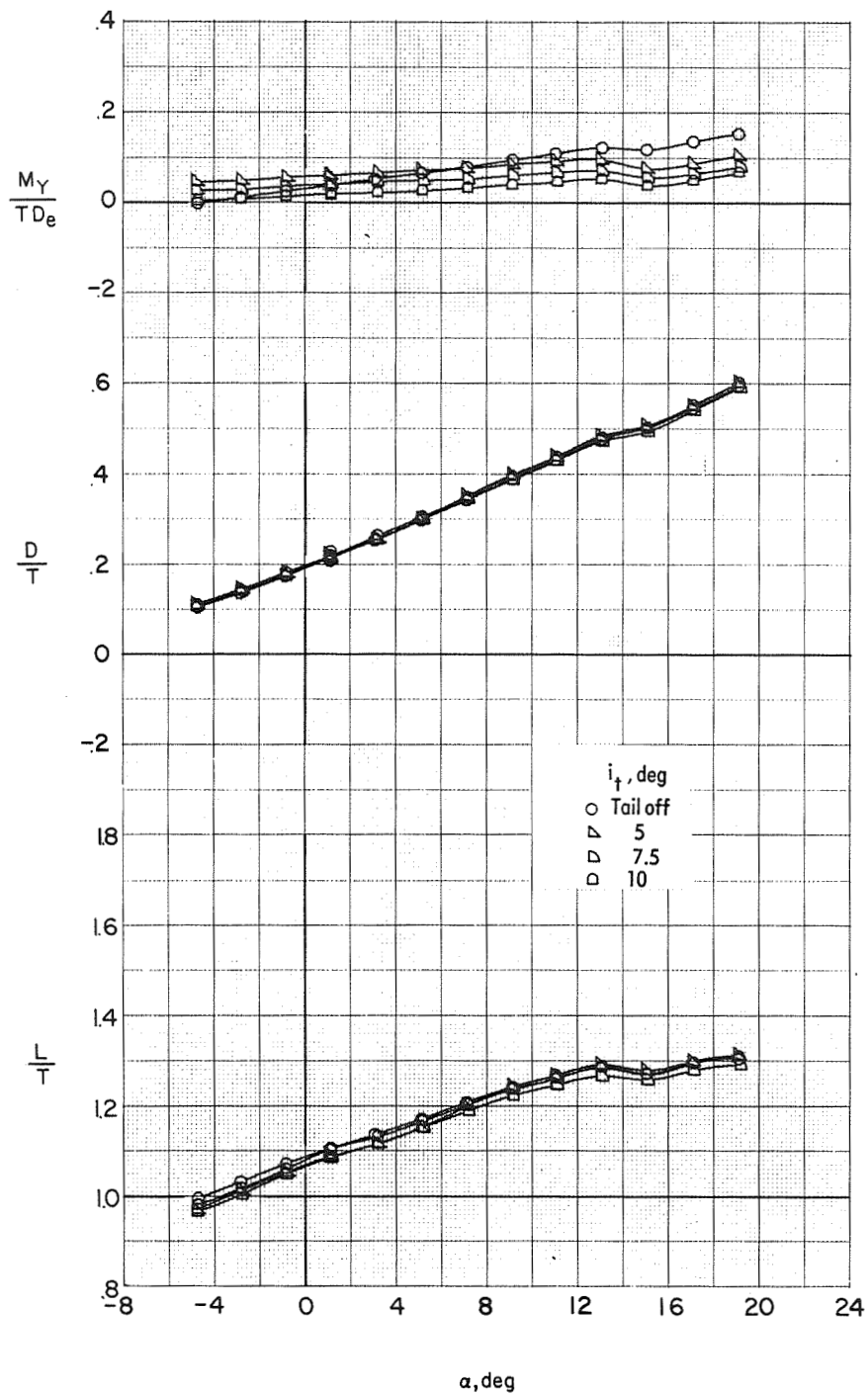
(b) $V_e = 0.15$.

Figure 30.- Concluded.



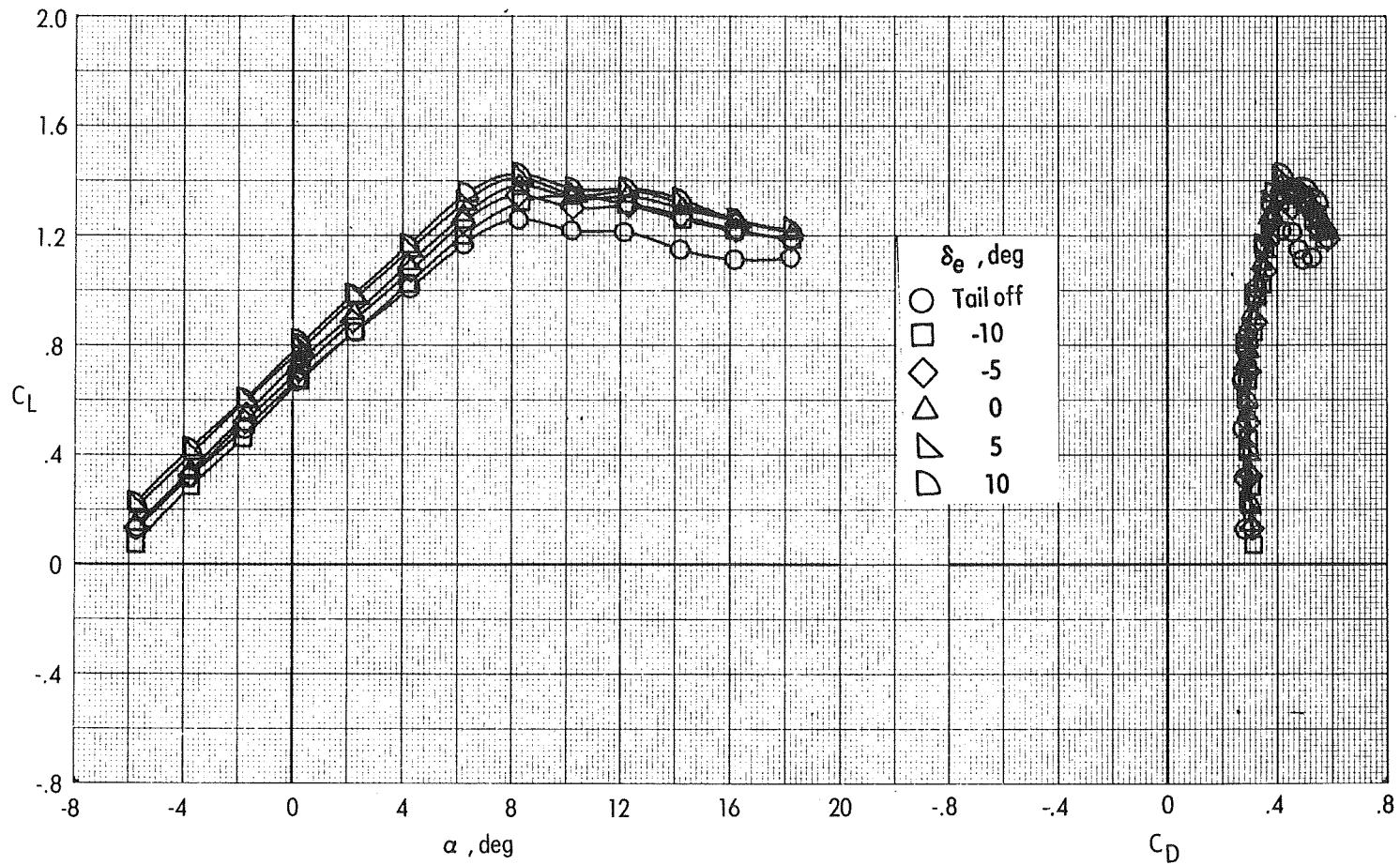
(a) $V_e = 0.20$.

Figure 31.- Effect of tail incidence on longitudinal aerodynamic characteristics of the VTOL transition configuration ($\delta_L = 7.5^\circ$; $\delta_{LC} = 82^\circ$; $\delta_f = 40^\circ$; $\delta_e = 0^\circ$) with power on. $q_\infty = 440$ Pa; $M_\infty = 0.078$.



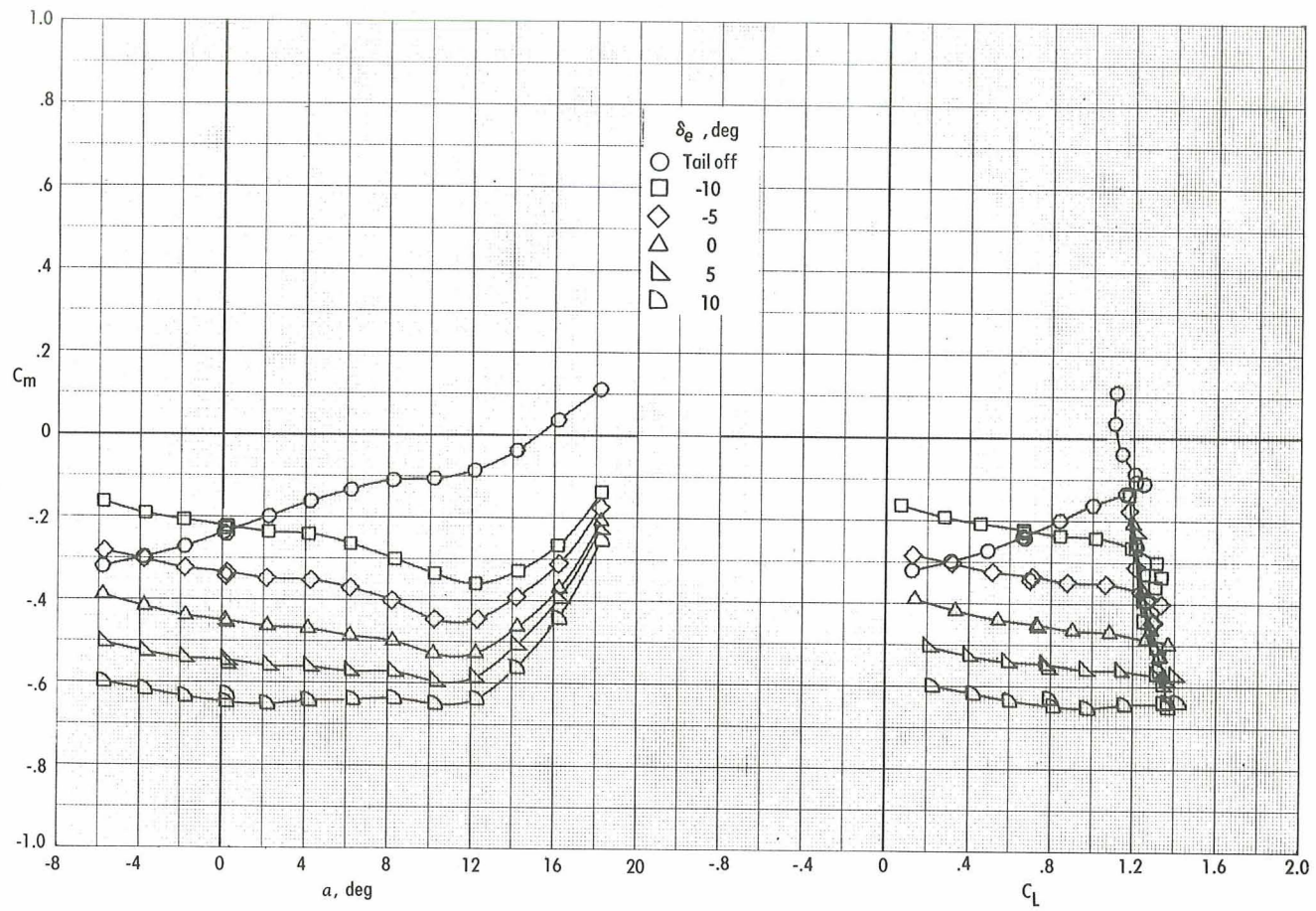
(b) $V_e = 0.24$.

Figure 31.- Concluded.



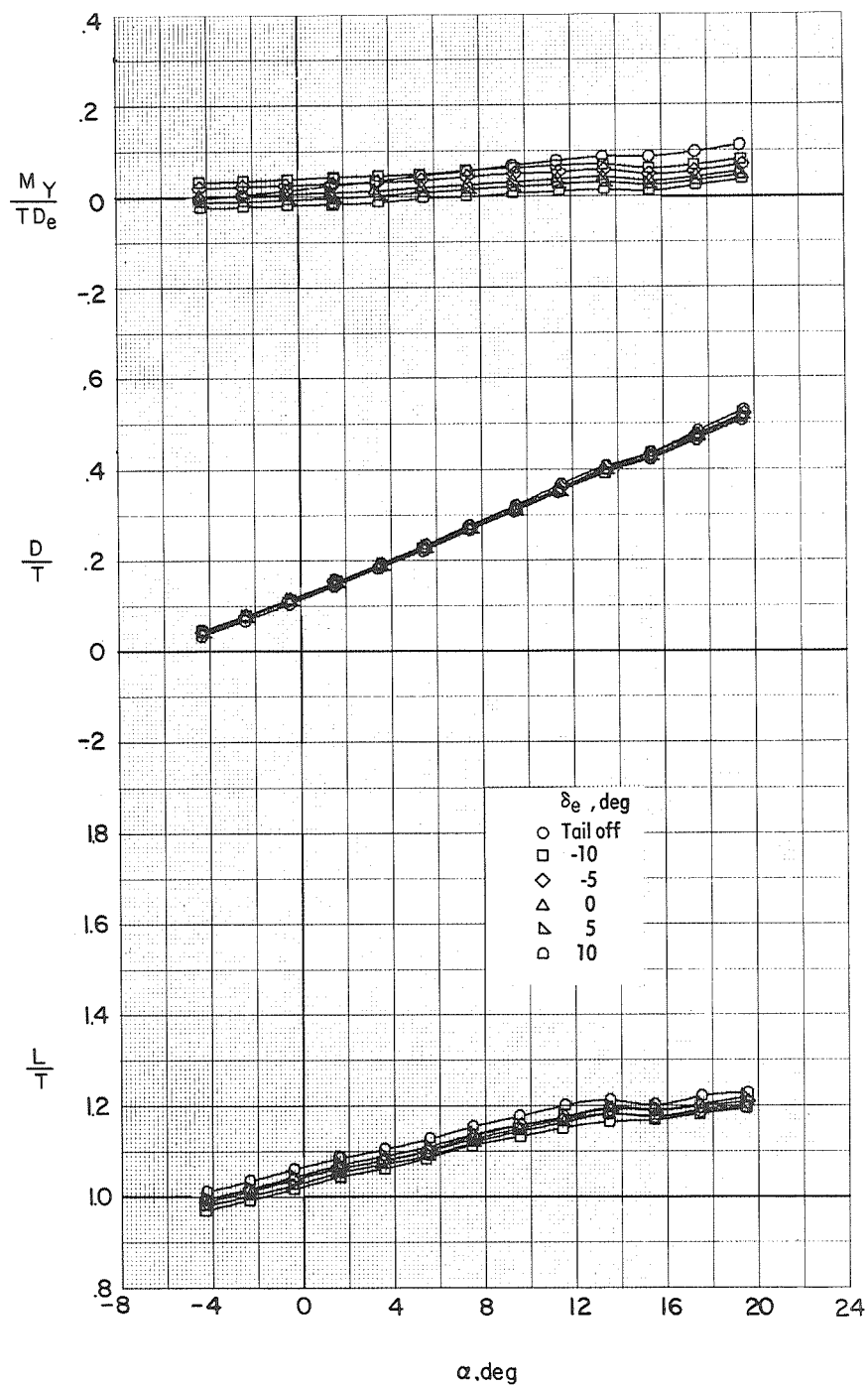
(a) Lift characteristics.

Figure 32.- Effect of elevator deflection on longitudinal aerodynamic characteristics of the VTOL transition configuration ($\delta_L = 7.5^\circ$; $\delta_{LC} = 82^\circ$; $\delta_f = 40^\circ$; $i_t = 10^\circ$) with power off. $q_\infty = 455 \text{ Pa}$; $M_\infty = 0.080$.



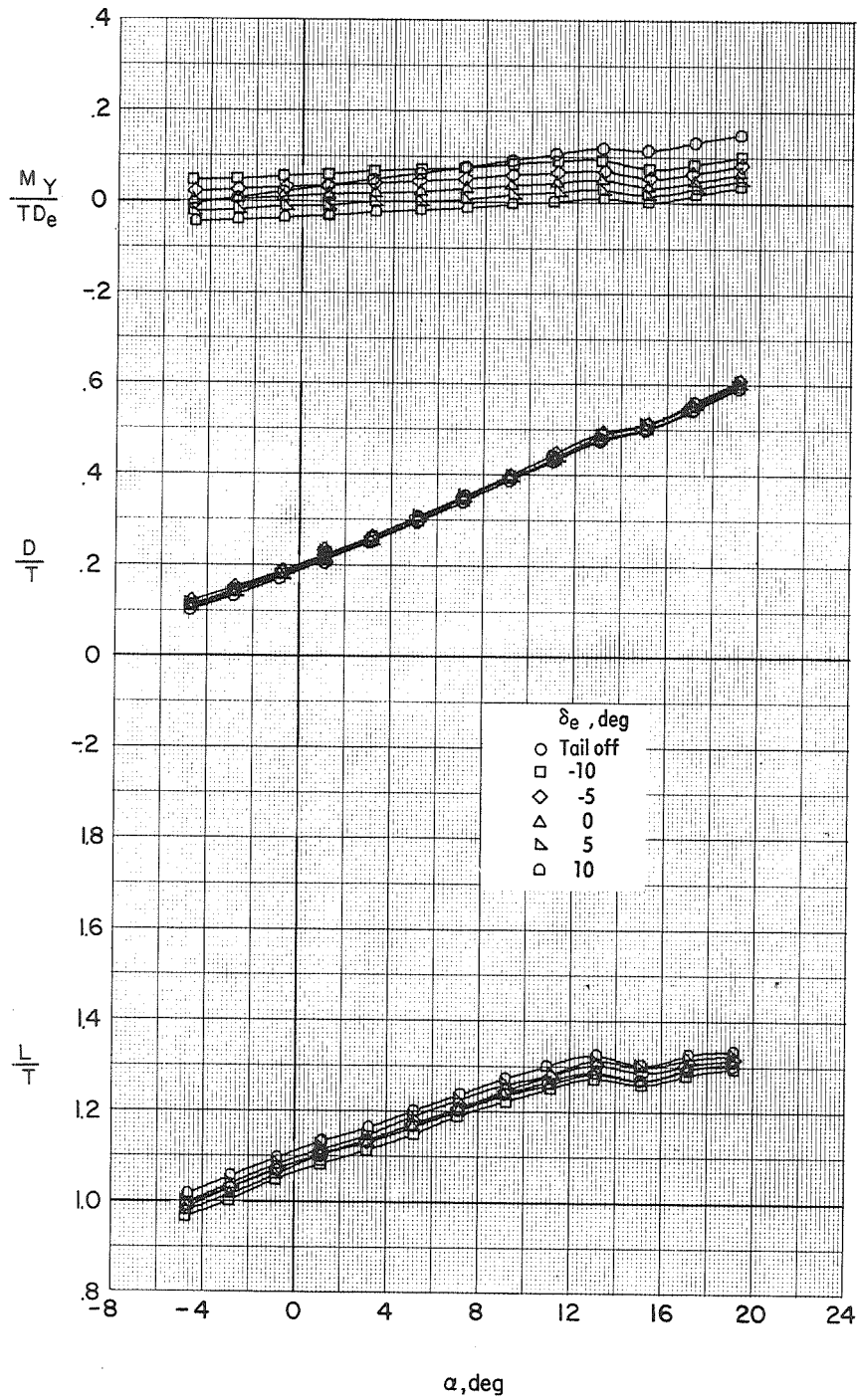
(b) Pitching-moment characteristics.

Figure 32.- Concluded.



(a) $V_e = 0.20$.

Figure 33.- Effect of elevator deflection on longitudinal aerodynamic characteristics of the VTOL transition configuration ($\delta_L = 7.5^0$; $\delta_{LC} = 82^0$; $\delta_f = 40^0$; $i_t = 10^0$) with power on. $q_\infty = 440$ Pa; $M_\infty = 0.078$.



(b) $V_e = 0.24.$

Figure 33.- Concluded.

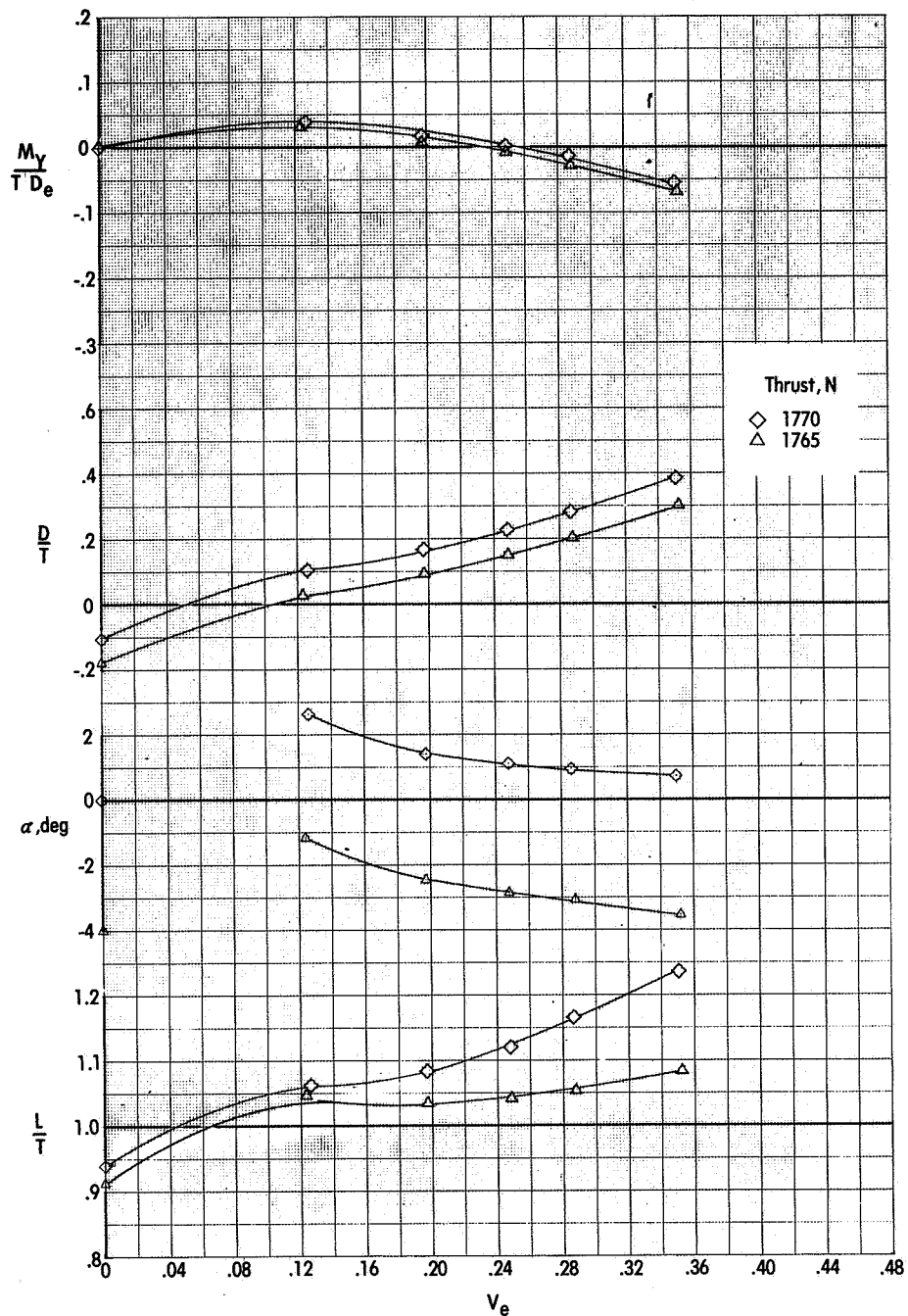
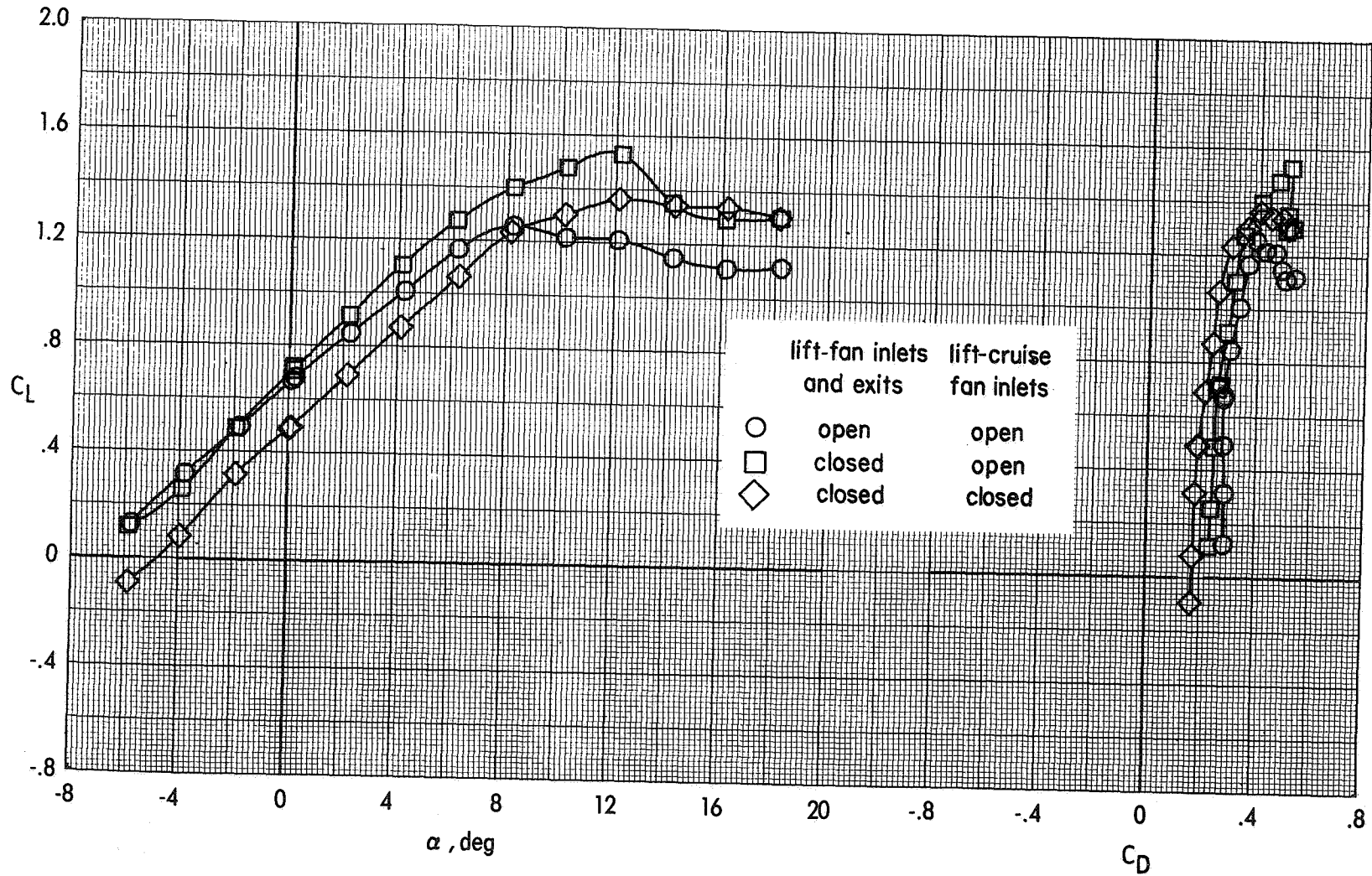
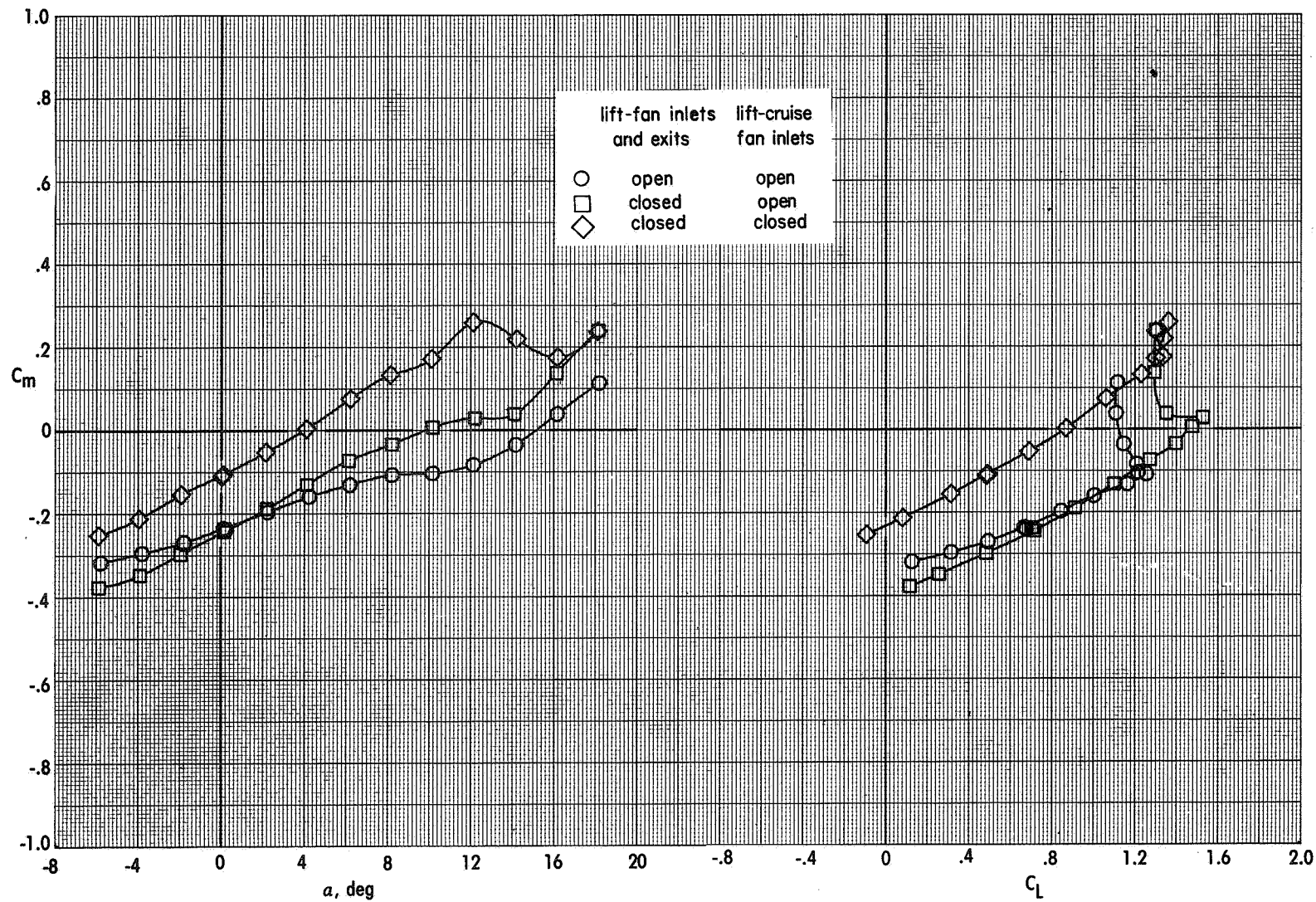


Figure 34.- Effect of effective velocity ratio on longitudinal aerodynamic characteristics of the VTOL transition configuration ($\delta_L = 7.5^\circ$; $\delta_{LC} = 82^\circ$; $\delta_f = 40^\circ$; $i_t = 10^\circ$; $\delta_e = 0^\circ$).



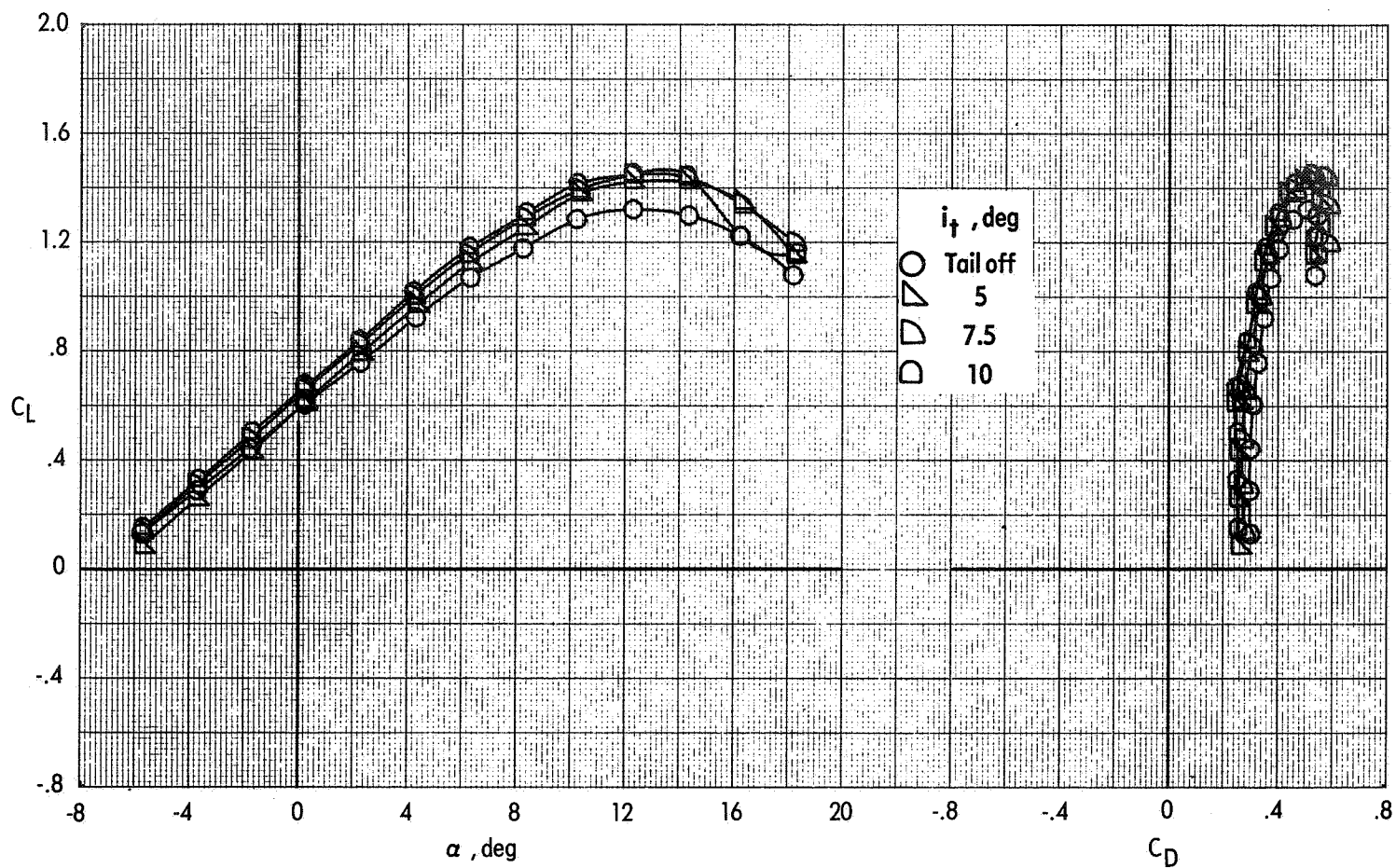
(a) Lift characteristics.

Figure 35.- Effect of closed lift-fan inlets and exits on longitudinal aerodynamics of the VTOL transition configuration ($\delta_L = 7.5^\circ$; $\delta_{LC} = 82^\circ$; $\delta_f = 40^\circ$; tail off) with power off. $q_\infty = 455 \text{ Pa}$; $M_\infty = 0.080$.



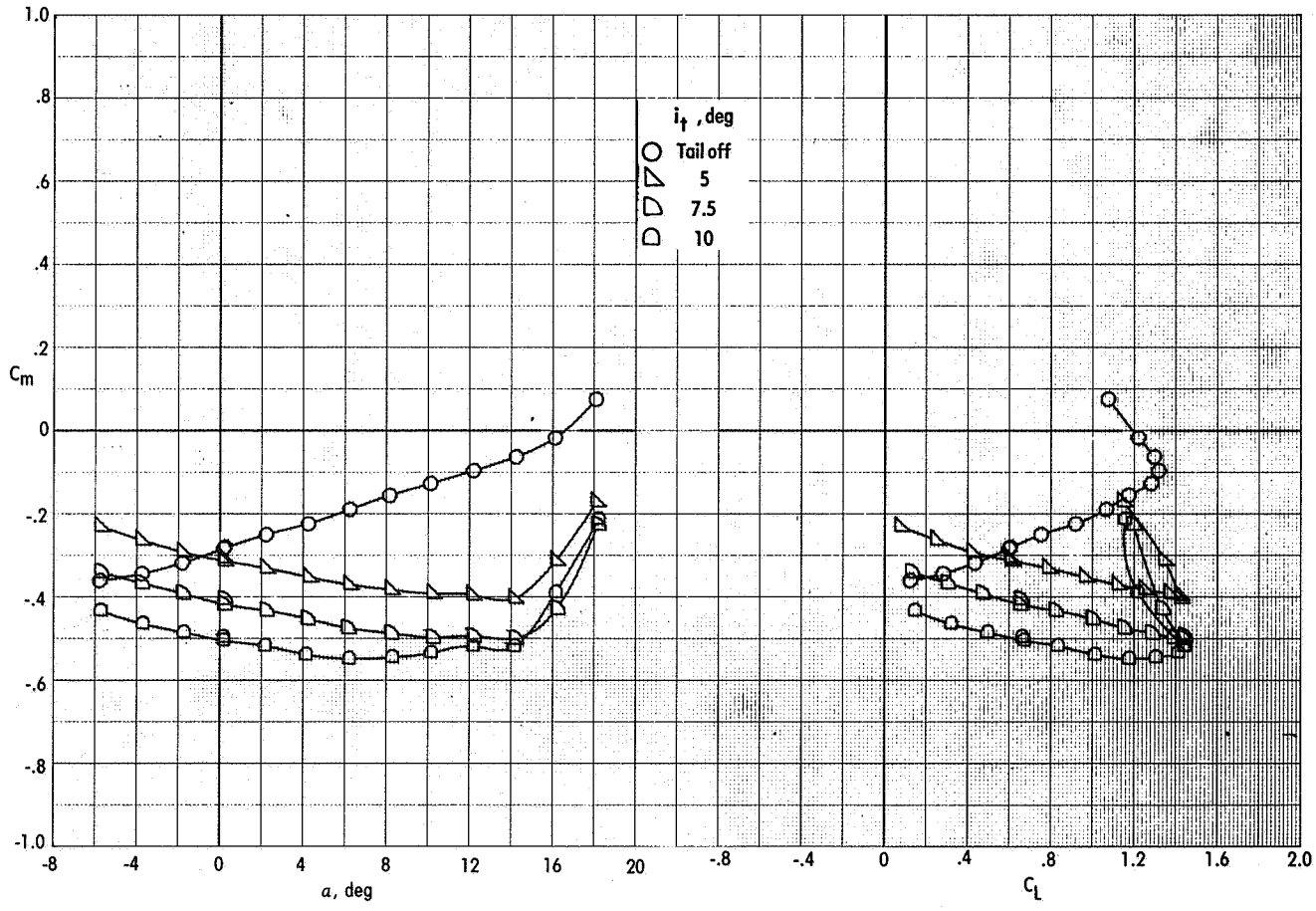
(b) Pitching-moment characteristics.

Figure 35.- Concluded.



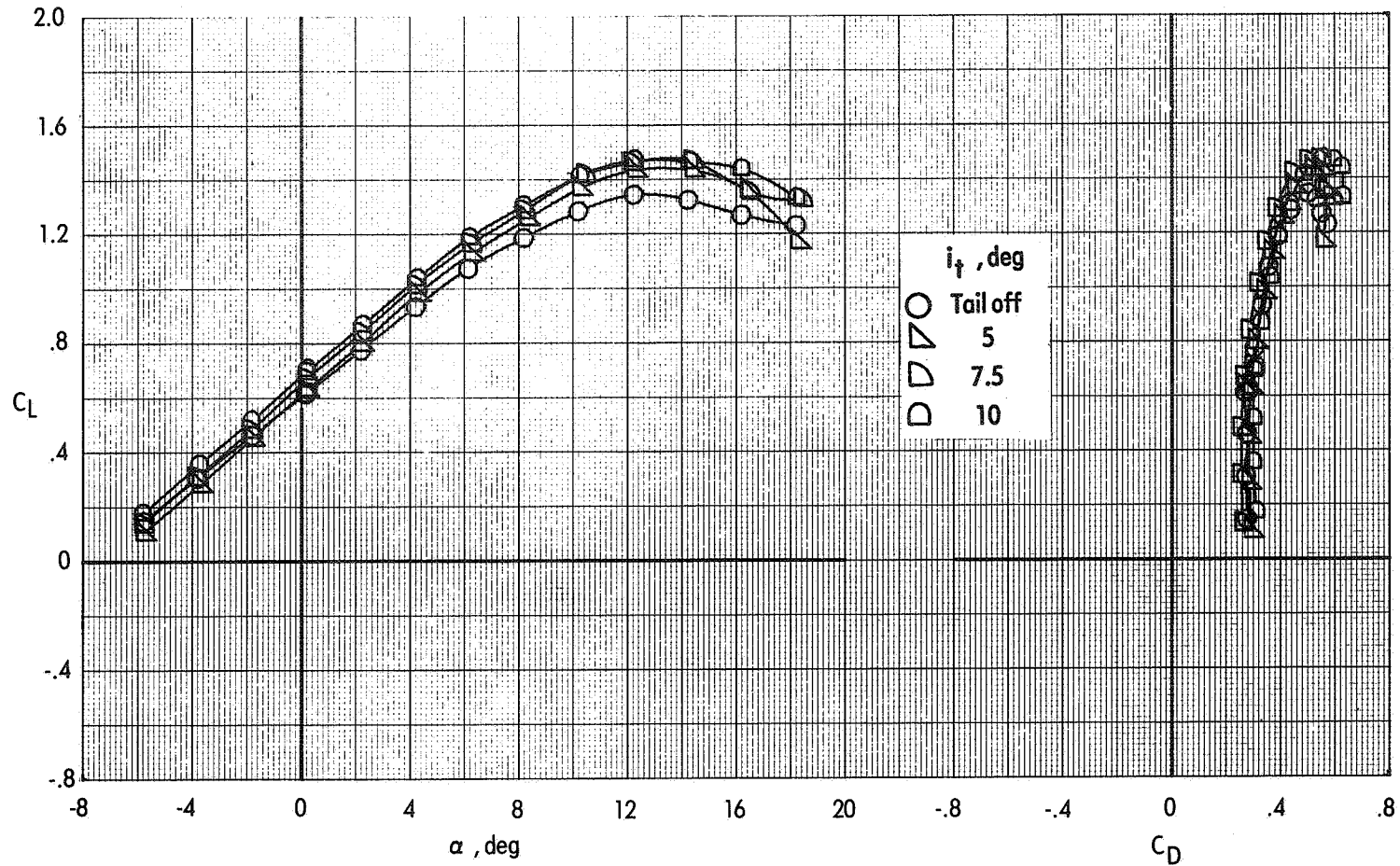
(a) Lift characteristics.

Figure 36.- Effect of tail incidence on longitudinal aerodynamic characteristics of the VTOL transition configuration ($\delta_L = 40^\circ$; $\delta_{LC} = 70^\circ$; $\delta_f = 40^\circ$; $\delta_e = 0^\circ$) with power off. $q_\infty = 728$ Pa; $M_\infty = 0.102$.



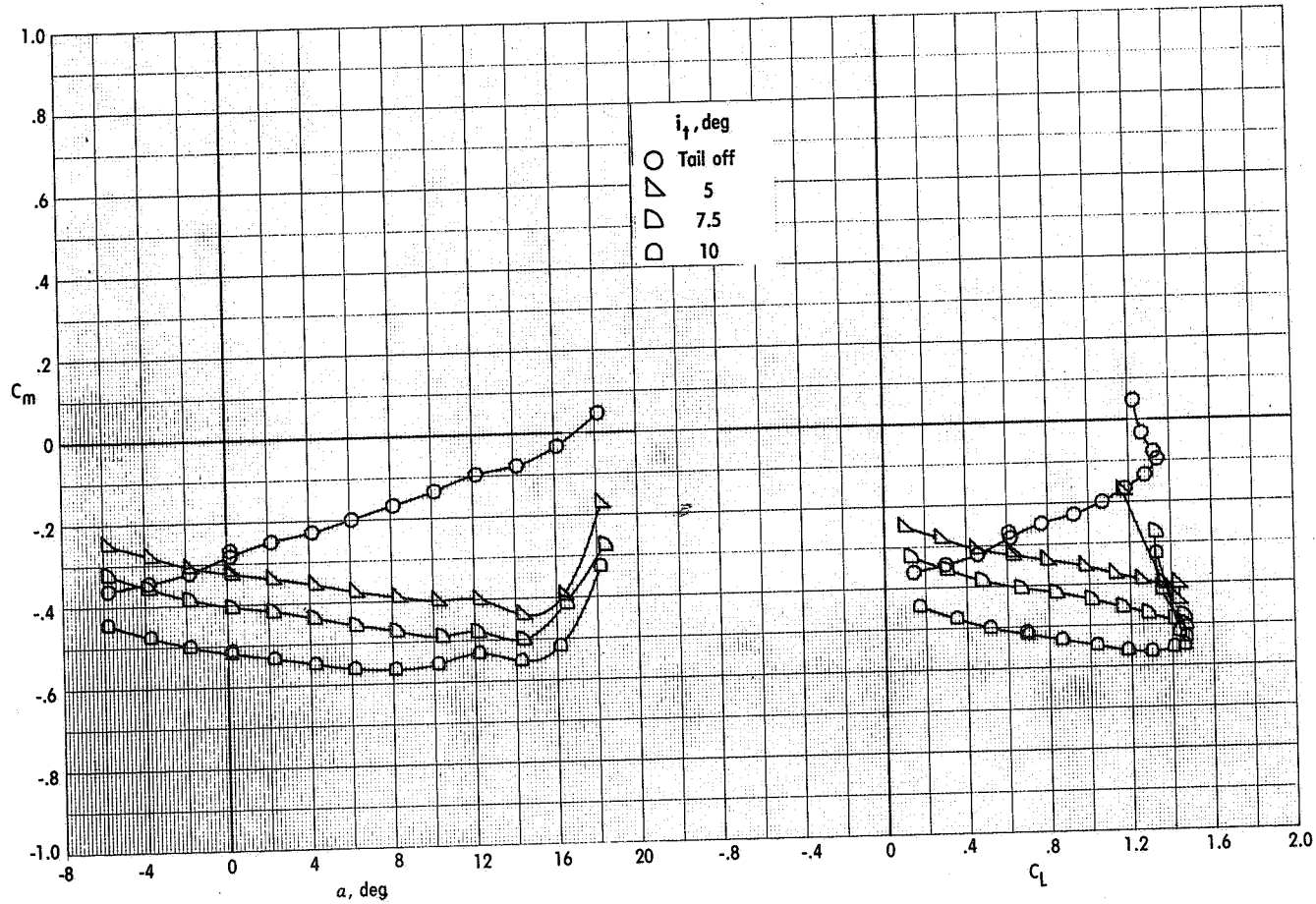
(b) Pitching-moment characteristics.

Figure 36.- Concluded.



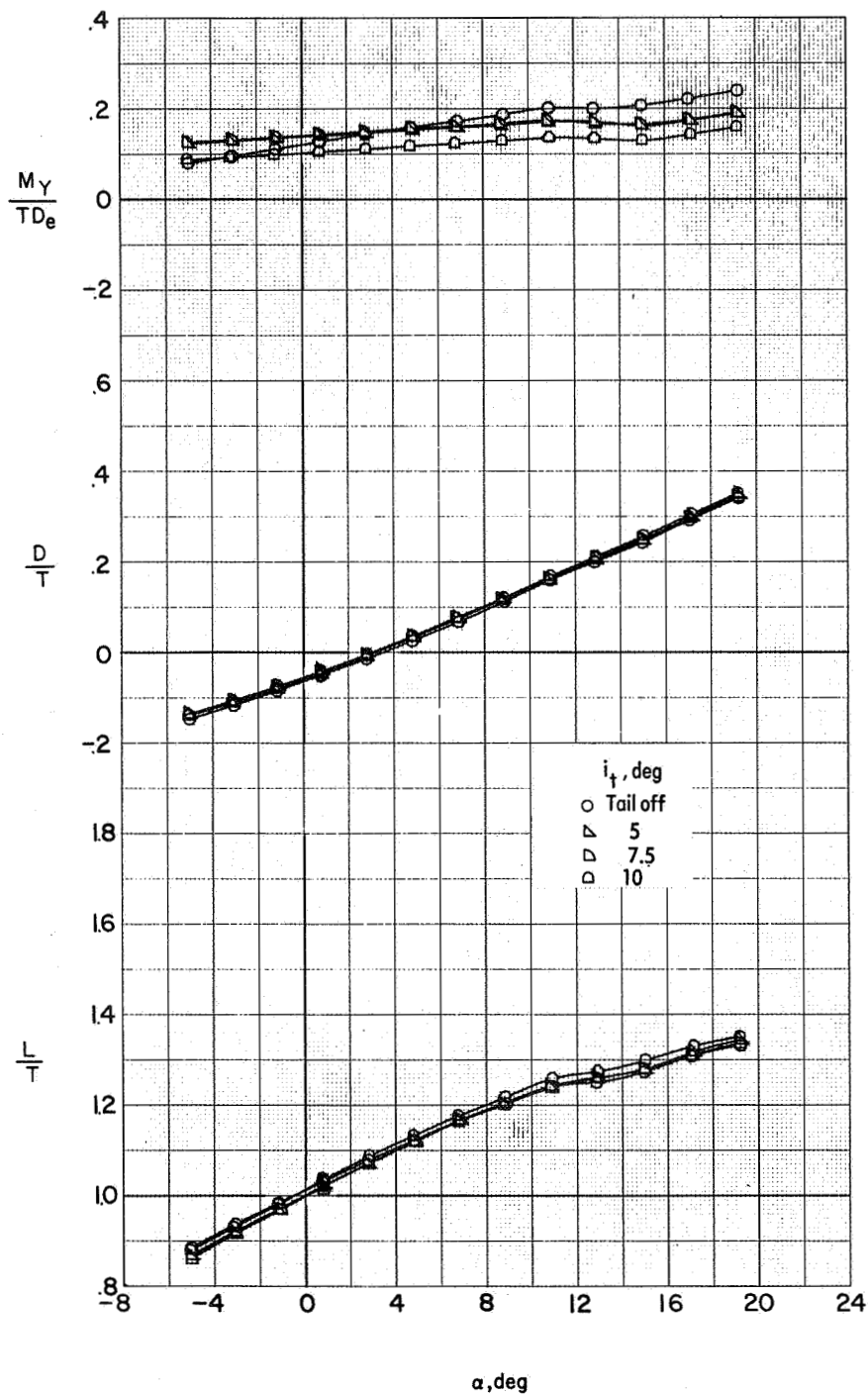
(a) Lift characteristics.

Figure 37.- Effect of tail incidence on longitudinal aerodynamic characteristics of the VTOL transition configuration ($\delta_L = 40^\circ$; $\delta_{LC} = 70^\circ$; $\delta_f = 40^\circ$; $\delta_e = 0^\circ$) with power off. $q_\infty = 1245$ Pa; $M_\infty = 0.134$.



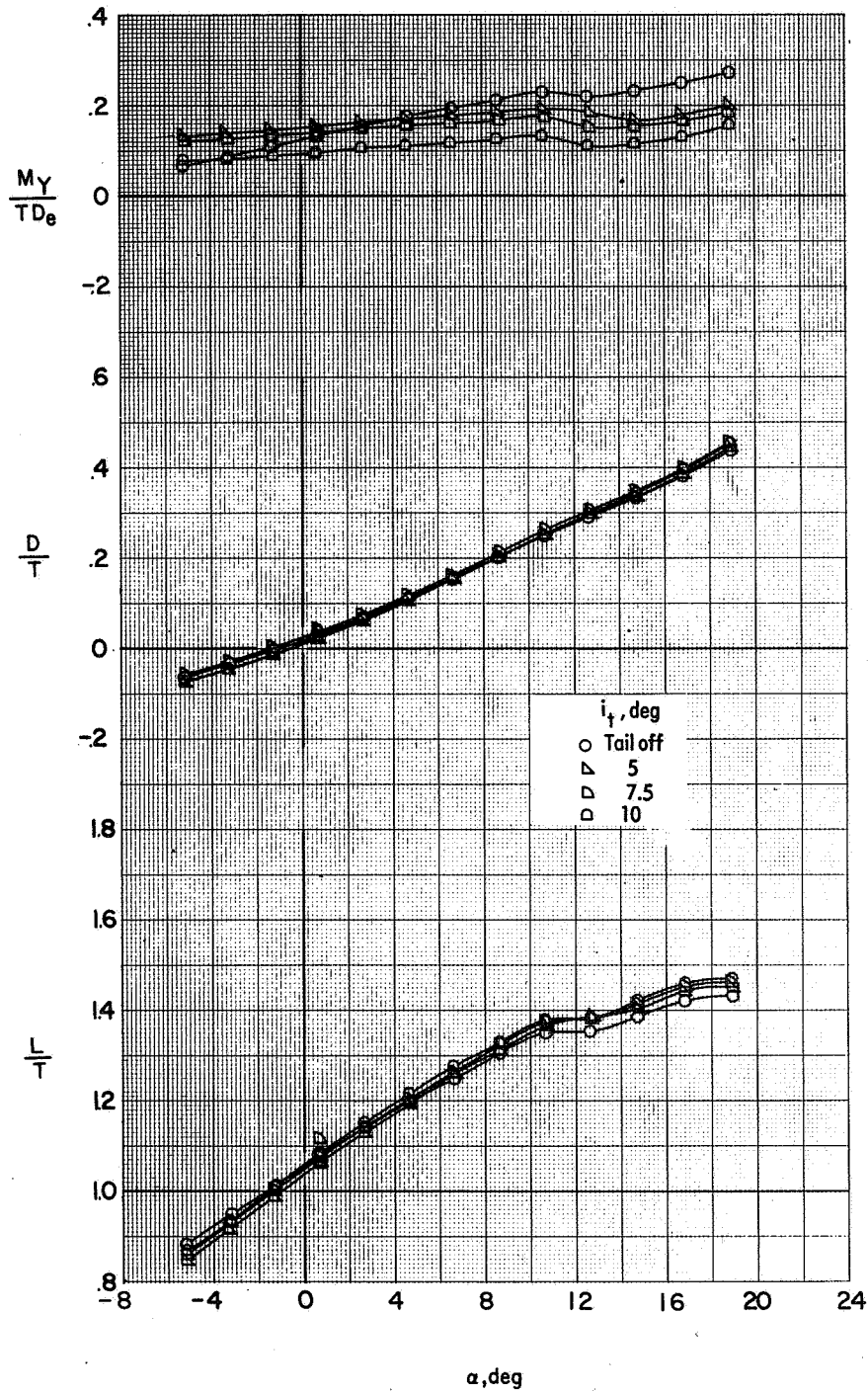
(b) Pitching-moment characteristics.

Figure 37.- Concluded.



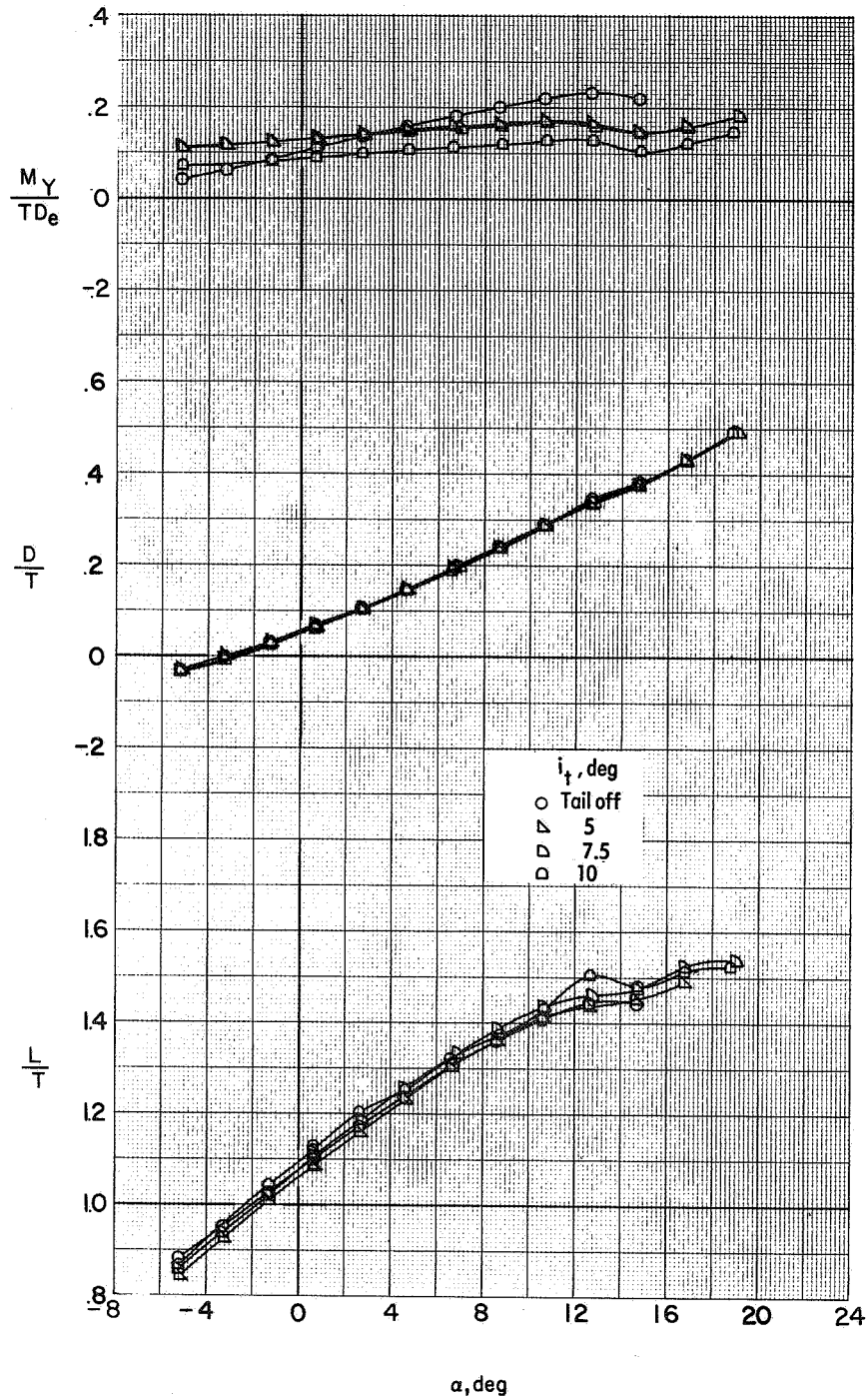
(a) $V_e = 0.24$.

Figure 38.- Effect of tail incidence on longitudinal aerodynamic characteristics of the VTOL transition configuration ($\delta_L = 40^\circ$; $\delta_{LC} = 70^\circ$; $\delta_f = 40^\circ$; $\delta_e = 0^\circ$) with power on. $q_\infty = 709$ Pa; $M_\infty = 0.100$.



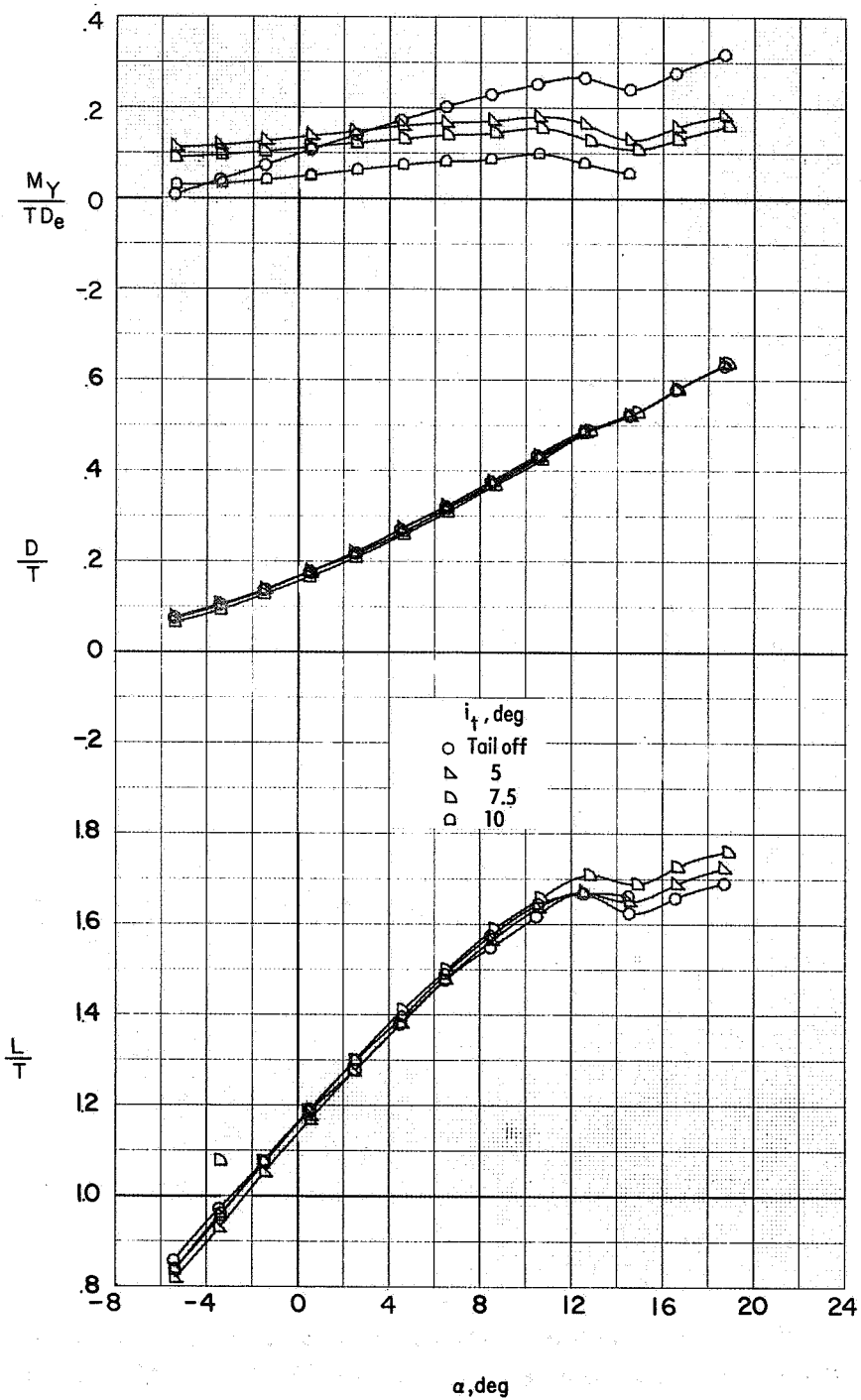
(b) $V_e = 0.29$.

Figure 38.- Concluded.



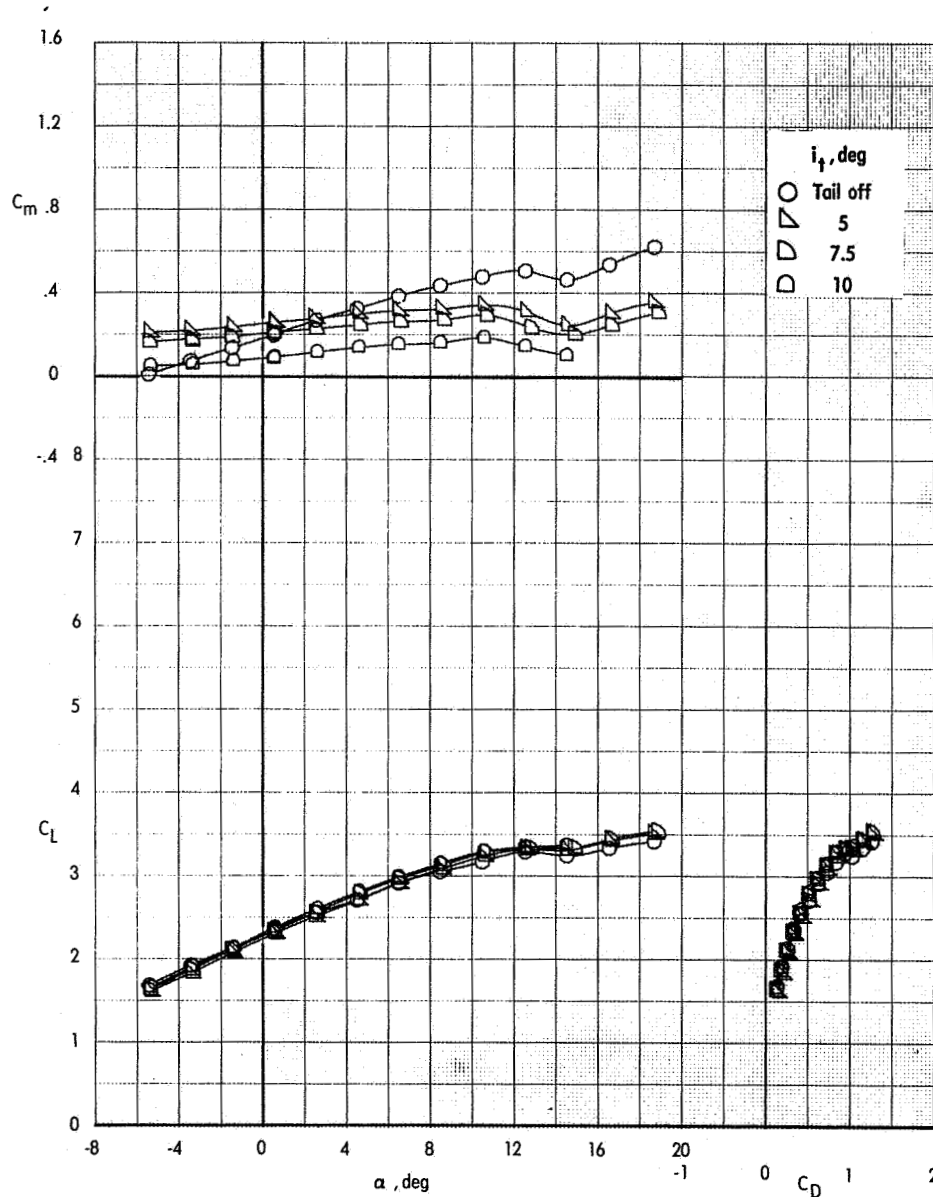
(a) $V_e = 0.31$.

Figure 39.- Effect of tail incidence on longitudinal aerodynamic characteristics of the VTOL transition configuration ($\delta_L = 40^\circ$; $\delta_{LC} = 70^\circ$; $\delta_f = 40^\circ$; $\delta_e = 0^\circ$) with power on. $q_\infty = 1230 \text{ Pa}$; $M_\infty = 0.133$.



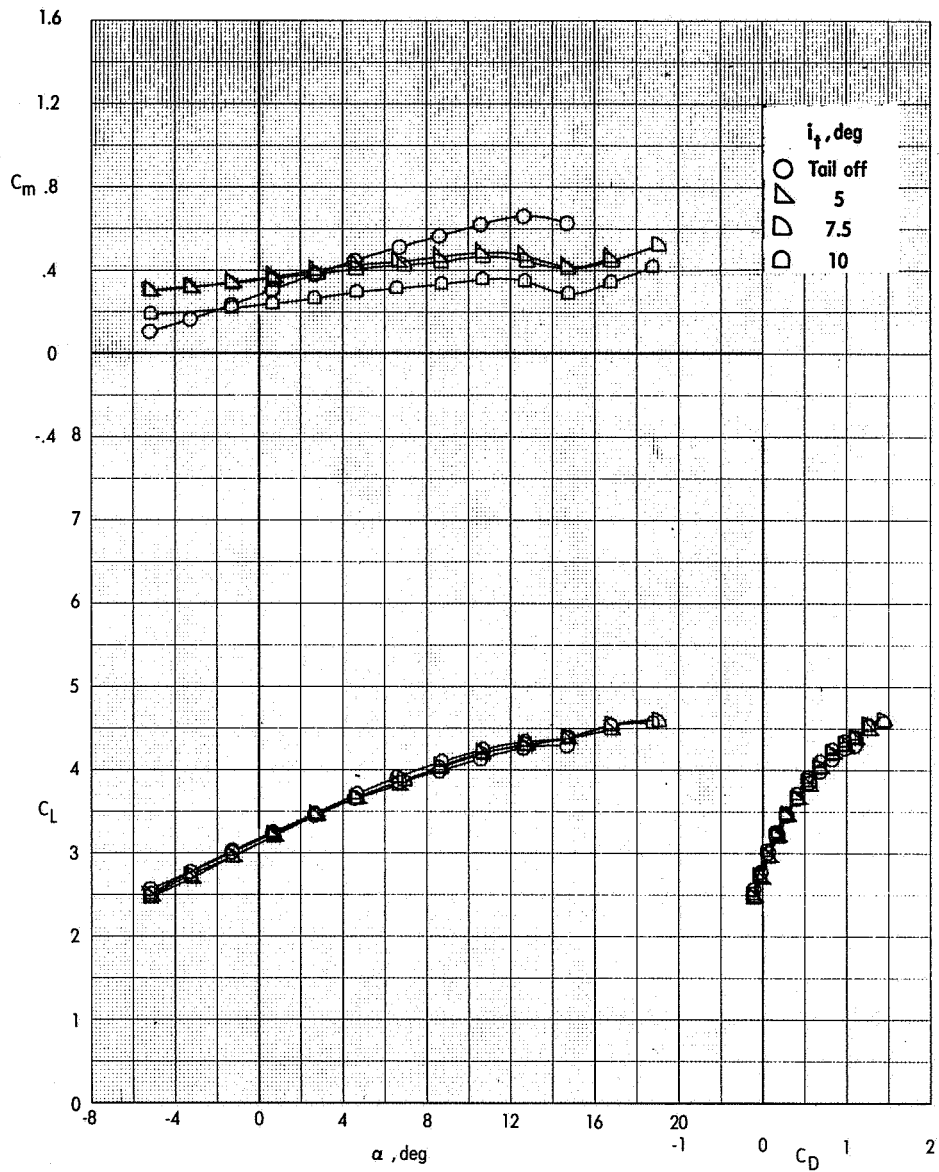
(b) $V_e = 0.38$.

Figure 39.- Concluded.



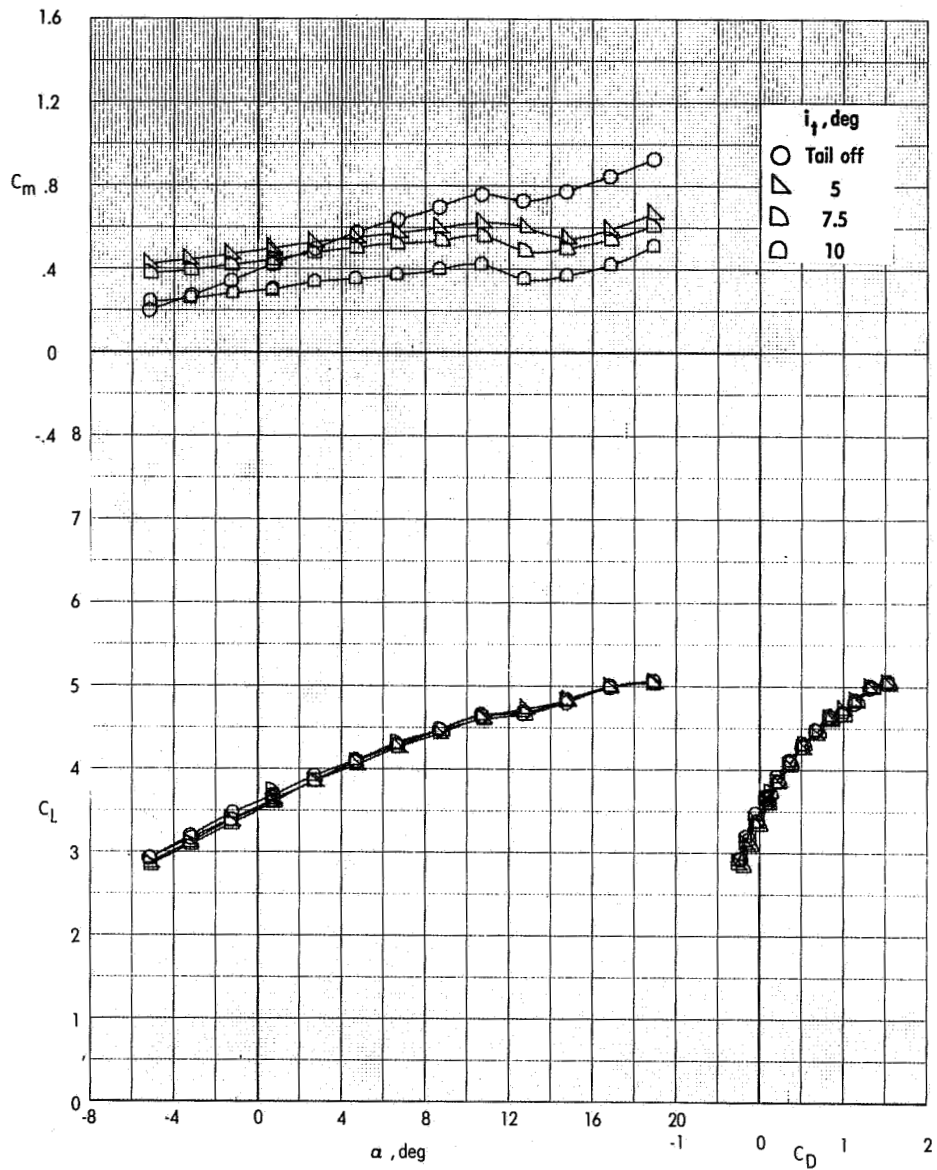
(a) $C_{\mu} = 2.0$.

Figure 40.- Effect of tail incidence on longitudinal aerodynamic characteristics of the VTOL transition configuration ($\delta_L = 40^\circ$; $\delta_{LC} = 70^\circ$; $\delta_f = 40^\circ$; $\delta_e = 0^\circ$) with power on. $q_\infty = 1230$ Pa; $M_\infty = 0.133$.



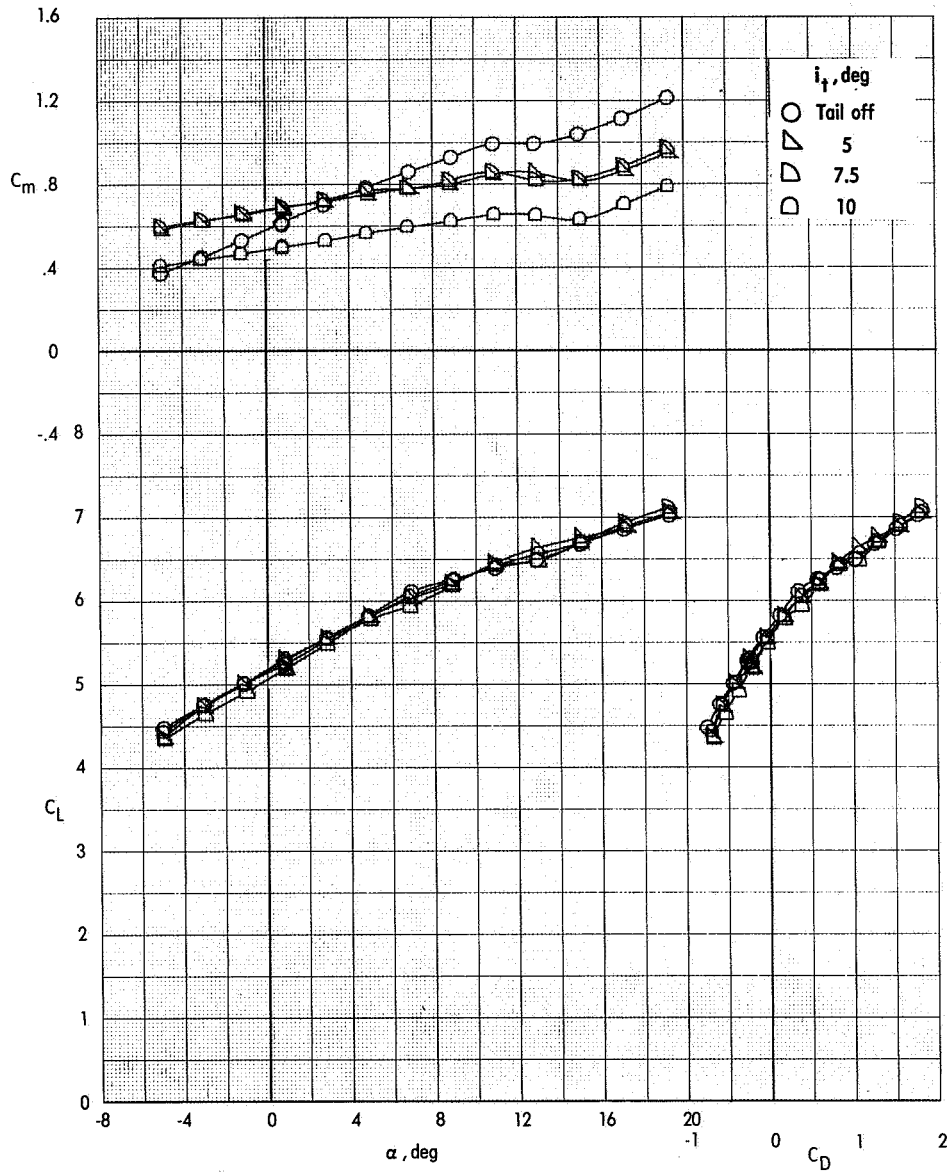
(b) $C_{\mu} = 2.9$.

Figure 40.- Concluded.



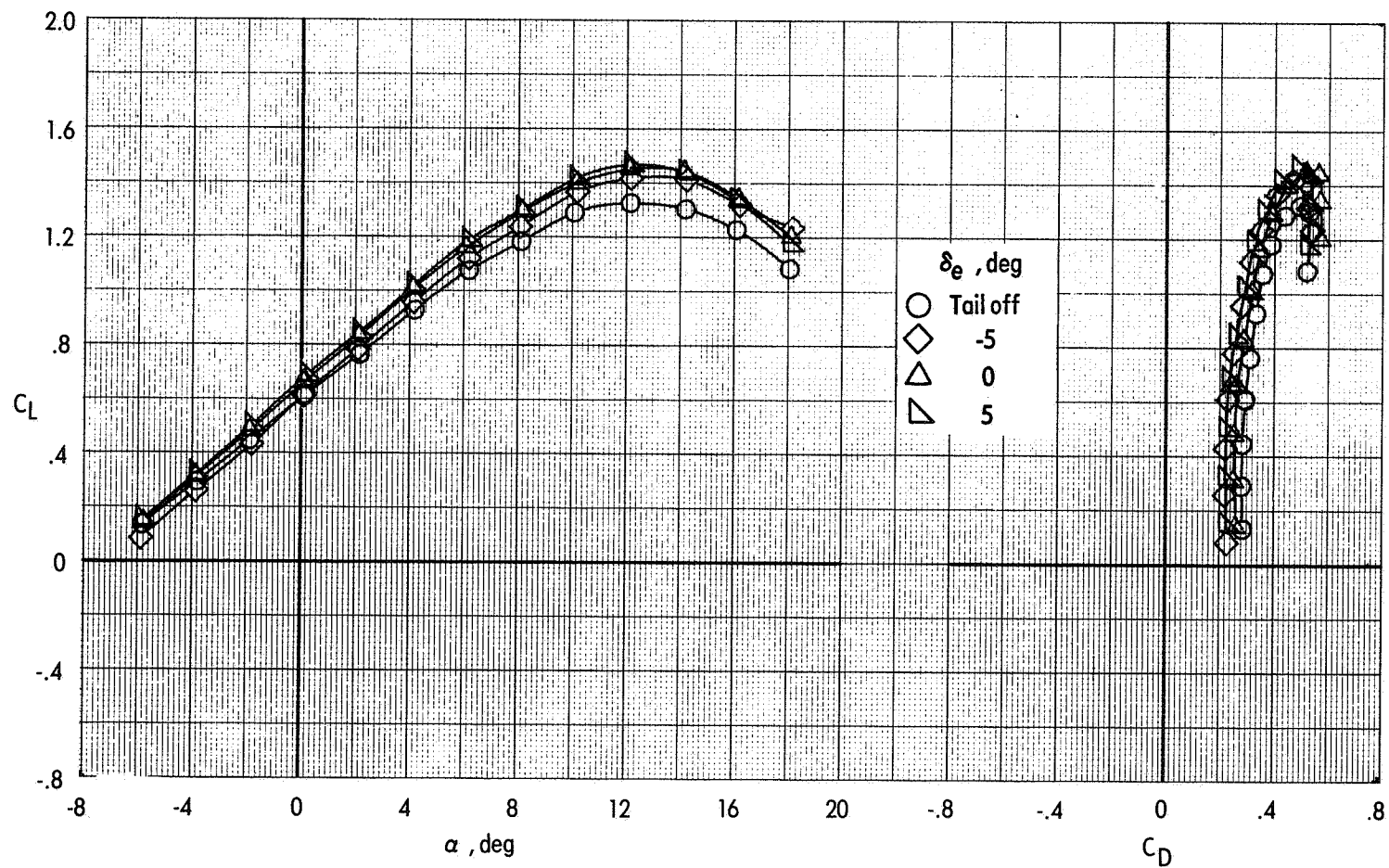
(a) $C_{\mu} = 3.4$.

Figure 41.- Effect of tail incidence on longitudinal aerodynamic characteristics of the VTOL transition configuration ($\delta_L = 40^\circ$; $\delta_{LC} = 70^\circ$; $\delta_f = 40^\circ$; $\delta_e = 0^\circ$) with power on. $q_\infty = 709$ Pa; $M_\infty = 0.100$.



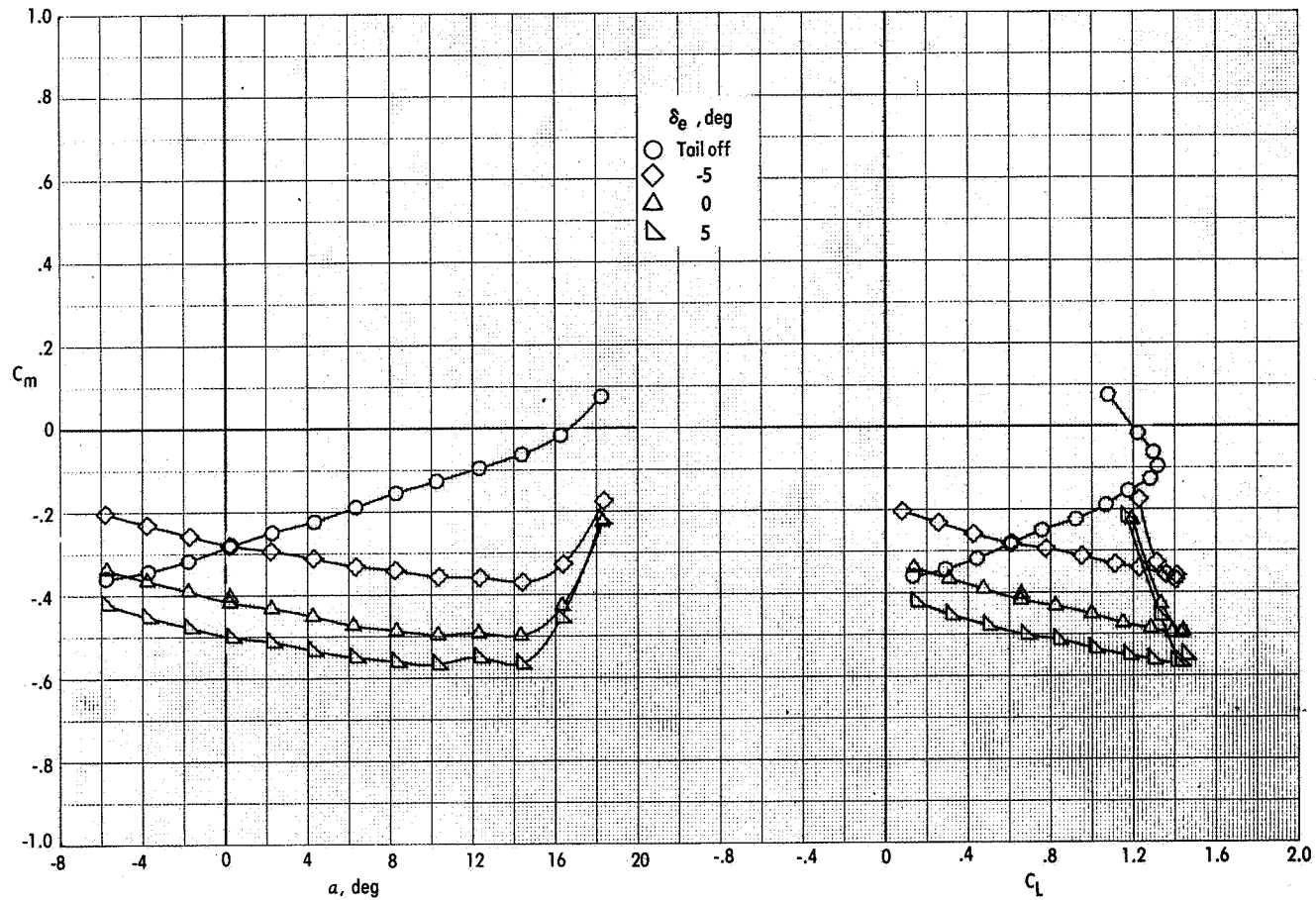
(b) $C_{\mu} = 5.1$.

Figure 41.- Concluded.



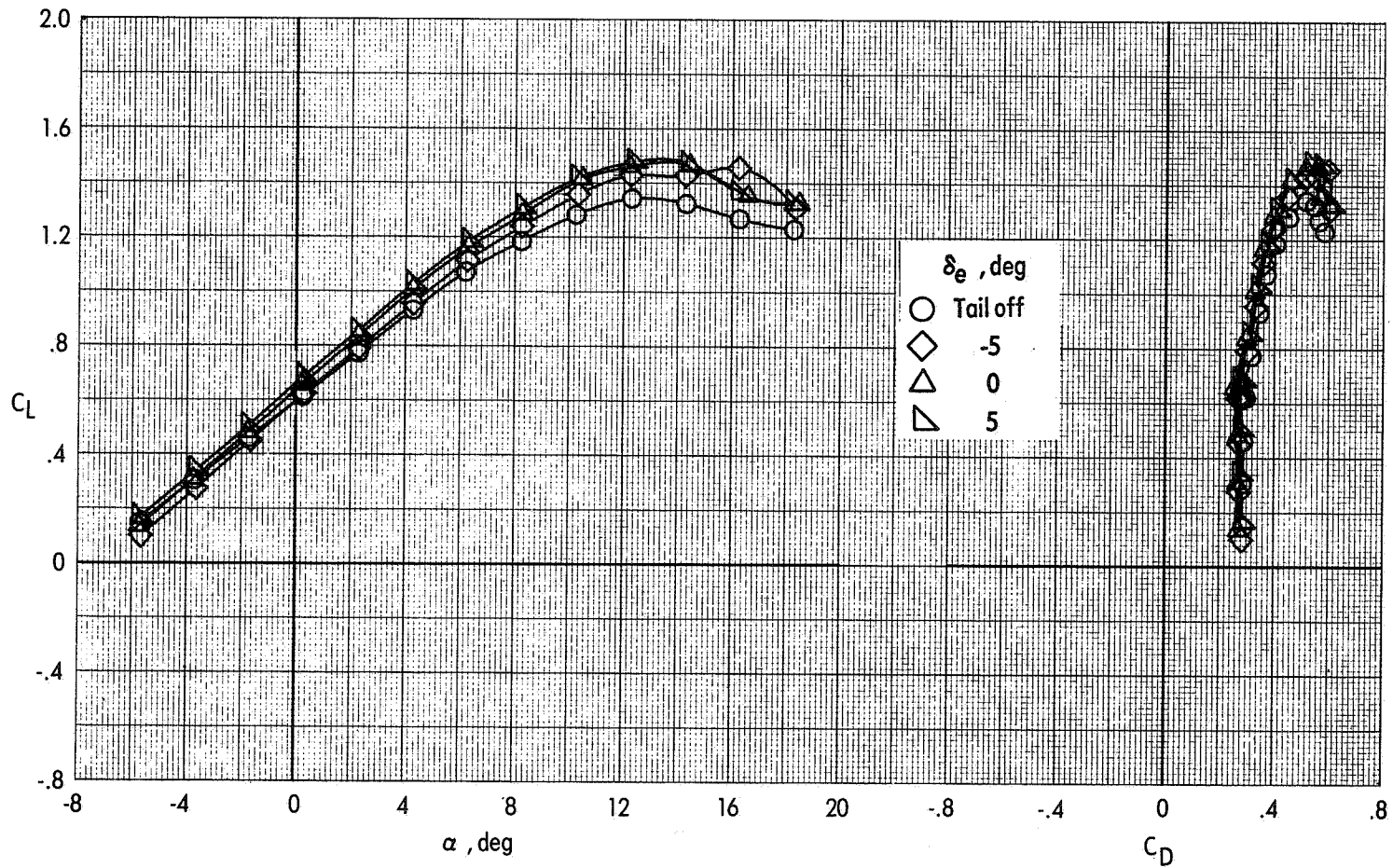
(a) Lift characteristics.

Figure 42.- Effect of elevator deflection on longitudinal aerodynamic characteristics of the VTOL transition configuration ($\delta_L = 40^\circ$; $\delta_{LC} = 70^\circ$; $\delta_f = 40^\circ$; $i_t = 7.5^\circ$) with power off. $q_\infty = 728$ Pa; $M_\infty = 0.102$.



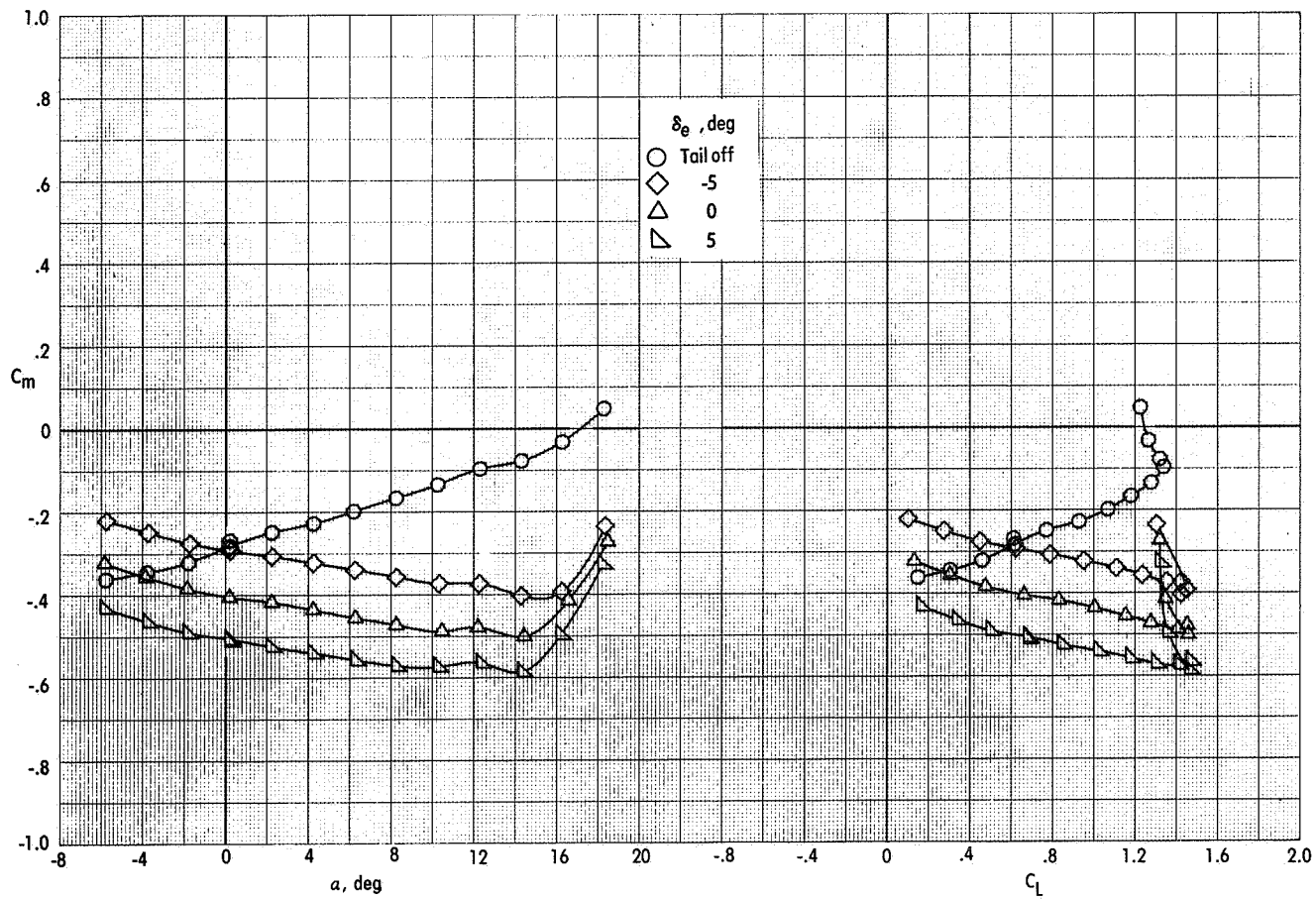
(b) Pitching-moment characteristics.

Figure 42. - Concluded.



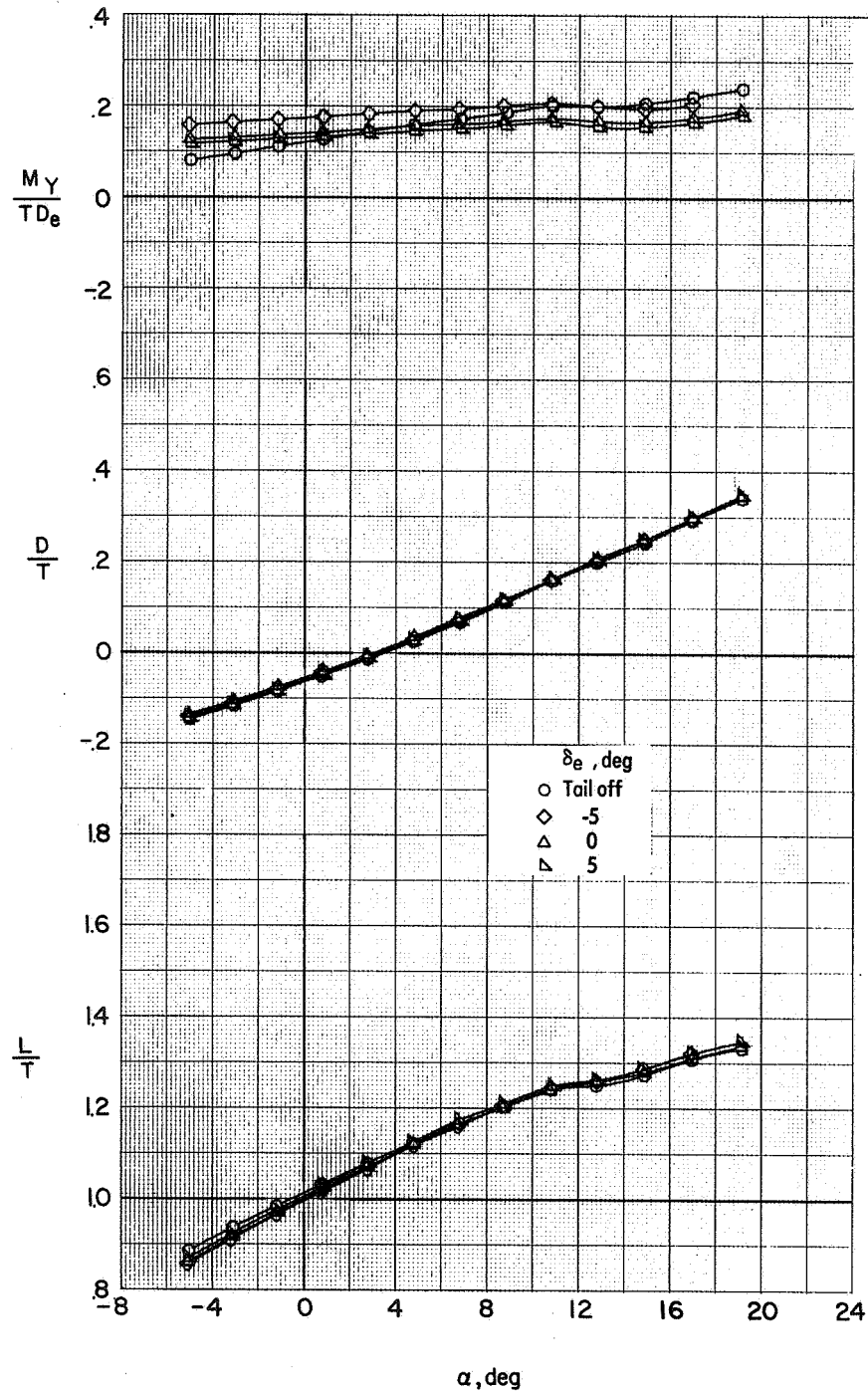
(a) Lift characteristics.

Figure 43.- Effect of elevator deflection on longitudinal aerodynamic characteristics of the VTOL transition configuration ($\delta_L = 40^\circ$; $\delta_{LC} = 70^\circ$; $\delta_f = 40^\circ$; $i_t = 7.5^\circ$) with power off. $q_\infty = 1245$ Pa; $M_\infty = 0.134$.



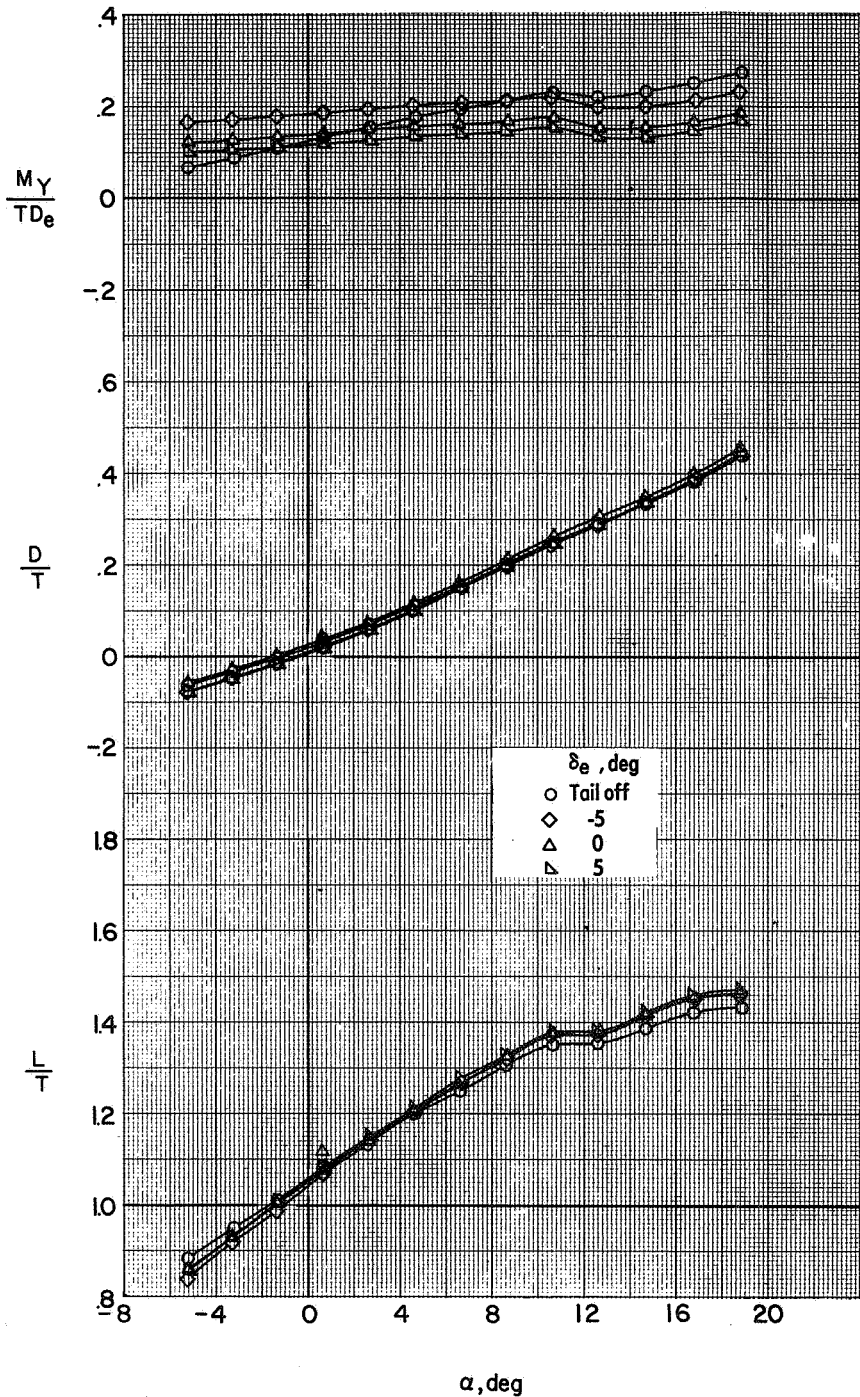
(b) Pitching-moment characteristics.

Figure 43. - Concluded.



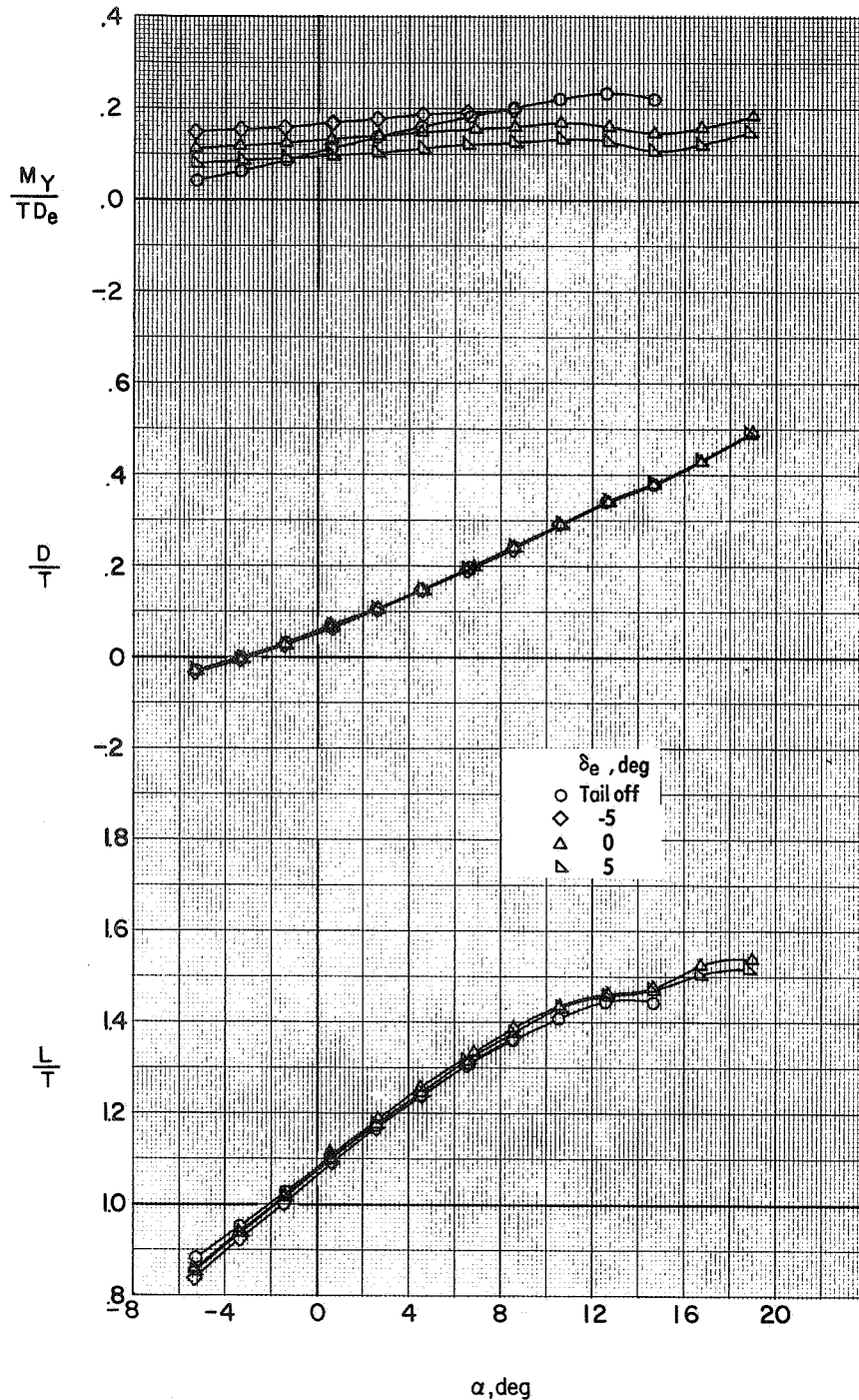
(a) $V_e = 0.24$.

Figure 44.- Effect of elevator deflection on longitudinal aerodynamic characteristics of the VTOL transition configuration ($\delta_L = 40^\circ$; $\delta_{LC} = 70^\circ$; $\delta_f = 40^\circ$; $i_t = 7.5^\circ$), with power on. $q_\infty = 709 \text{ Pa}$; $M_\infty = 0.100$.



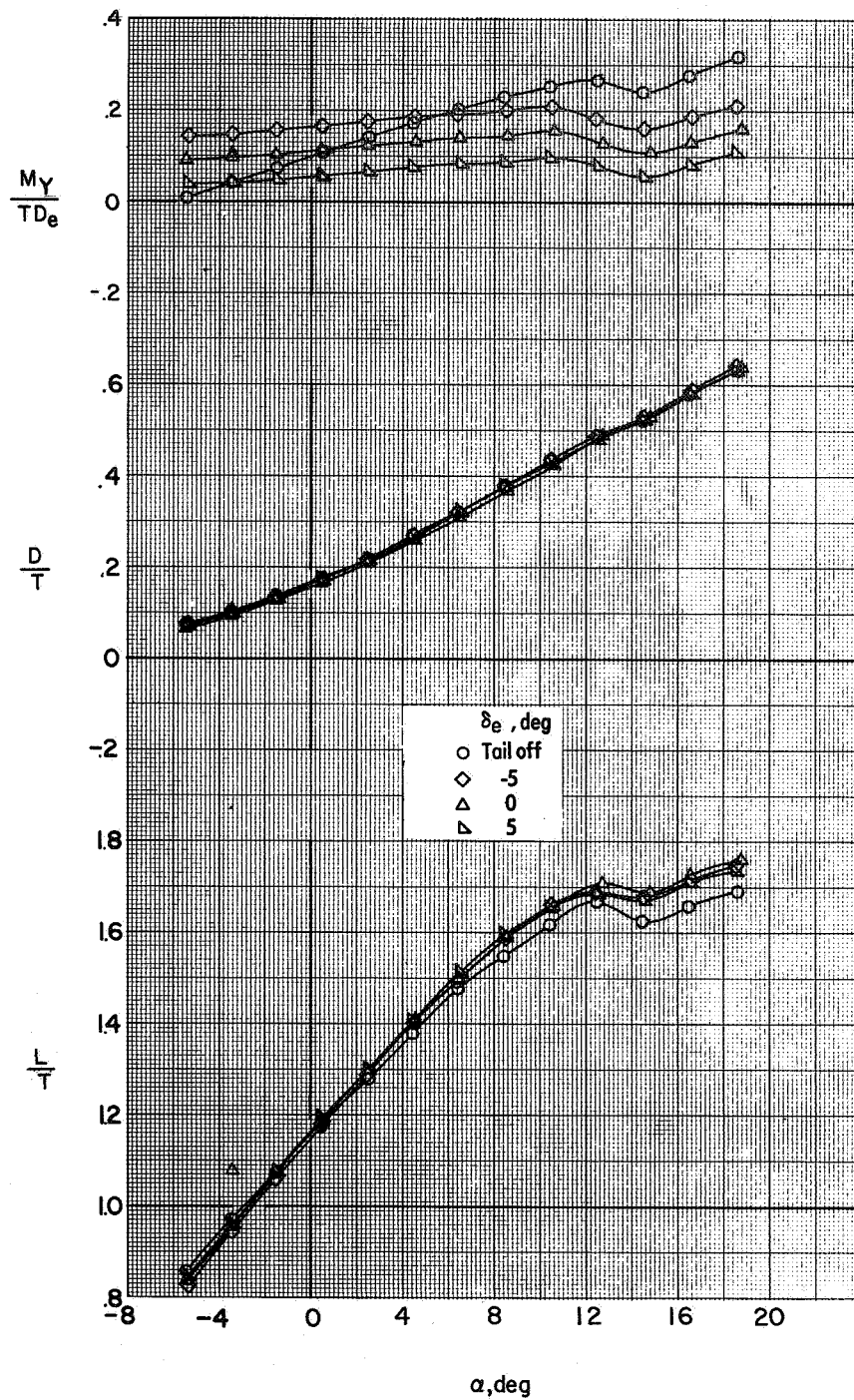
α, deg
 (b) $V_e = 0.29$.

Figure 44.- Concluded.



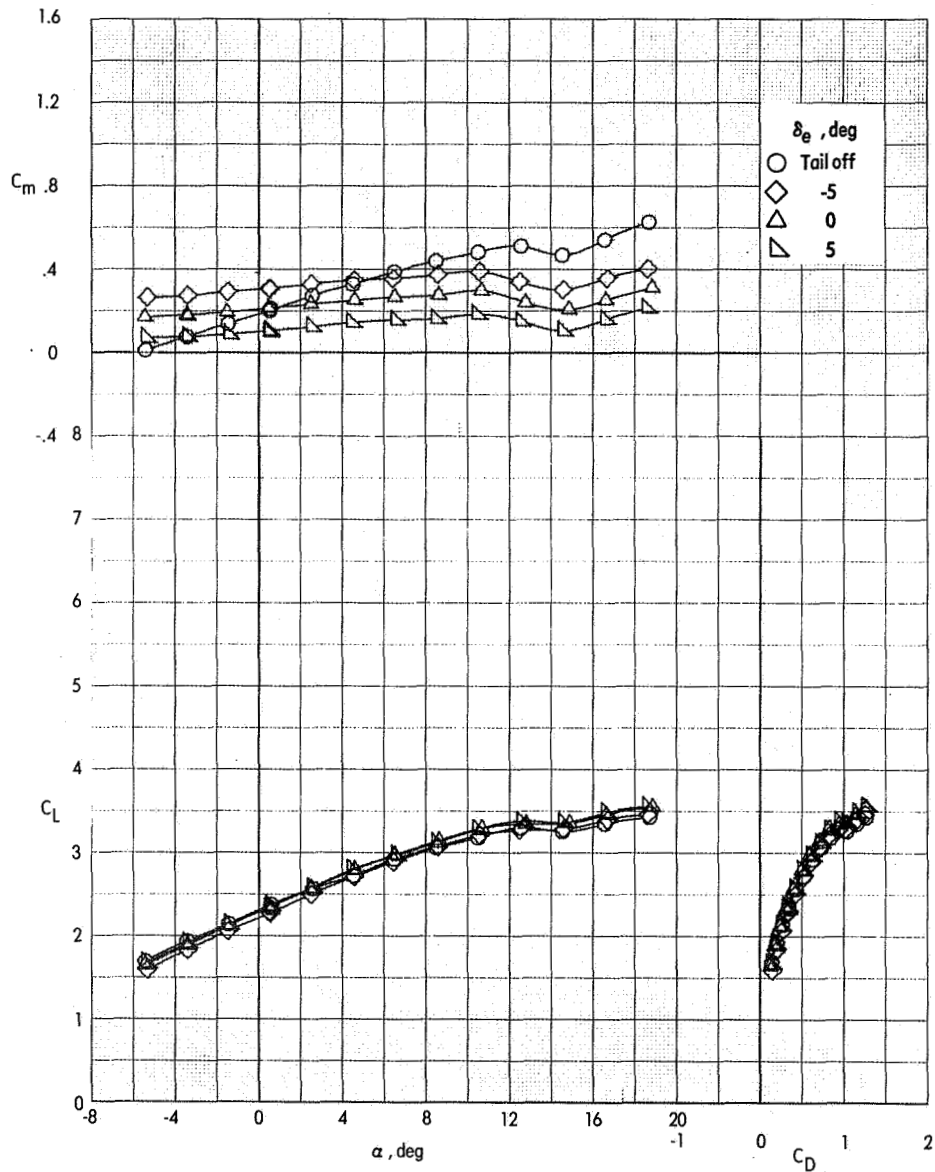
(a) $V_e = 0.31$.

Figure 45.- Effect of elevator deflection on longitudinal aerodynamic characteristics of the VTOL transition configuration ($\delta_L = 40^\circ$; $\delta_{LC} = 70^\circ$; $\delta_f = 40^\circ$; $i_t = 7.5^\circ$) with power on. $q_\infty = 1230 \text{ Pa}$; $M_\infty = 0.133$.



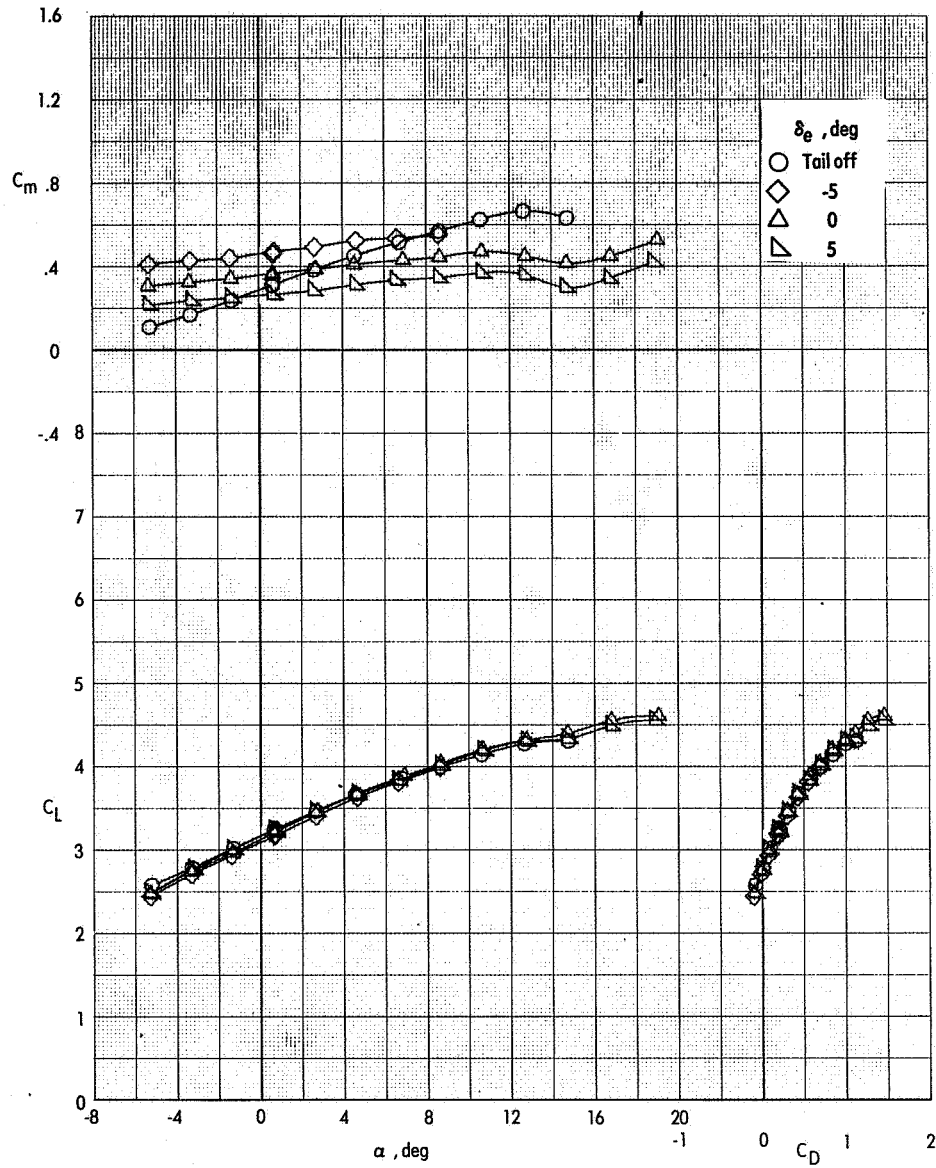
(b) $V_e = 0.38$.

Figure 45.- Concluded.



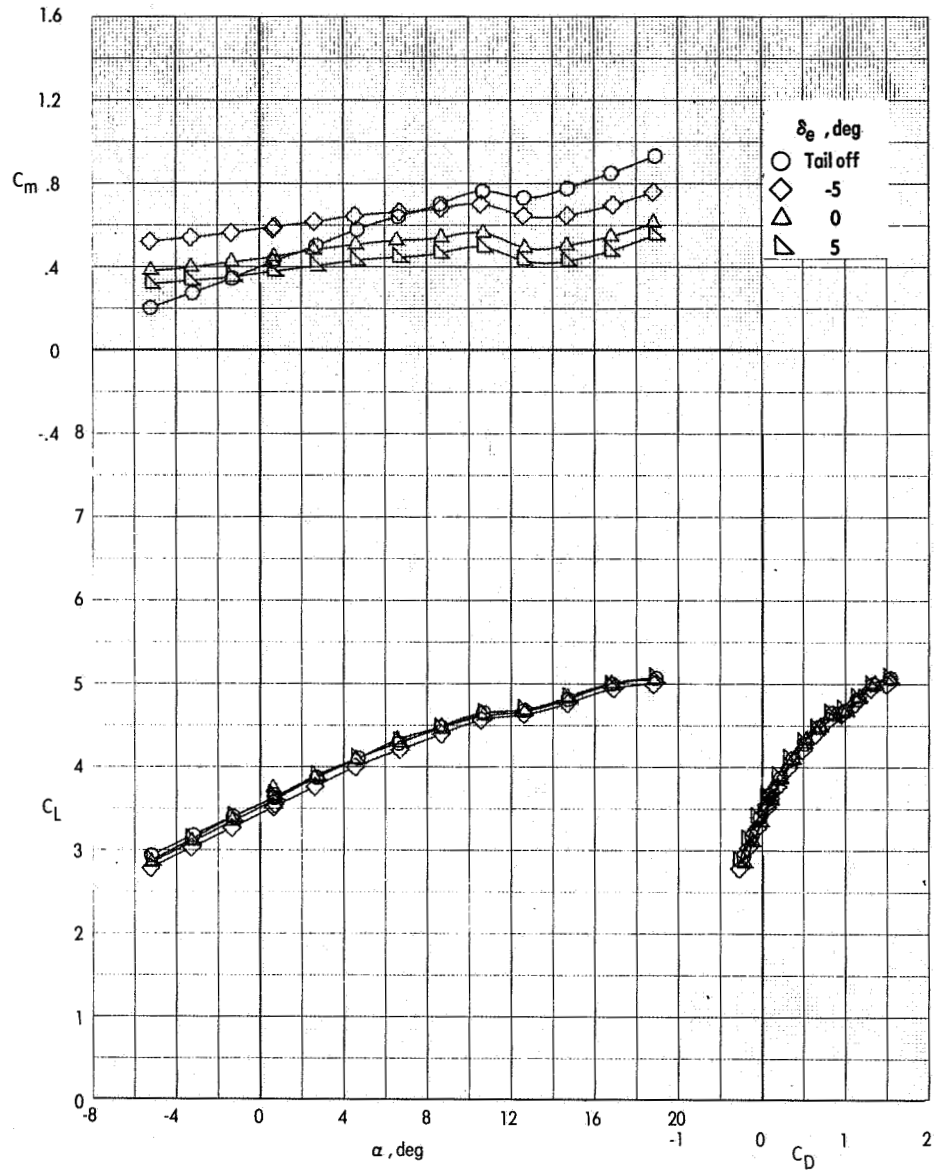
(a) $C_\mu = 2.0$.

Figure 46.- Effect of elevator deflection on longitudinal aerodynamic characteristics of the VTOL transition configuration ($\delta_L = 40^\circ$; $\delta_{LC} = 70^\circ$; $\delta_f = 40^\circ$; $i_t = 7.5^\circ$) with power on. $q_\infty = 1230$ Pa; $M_\infty = 0.133$.



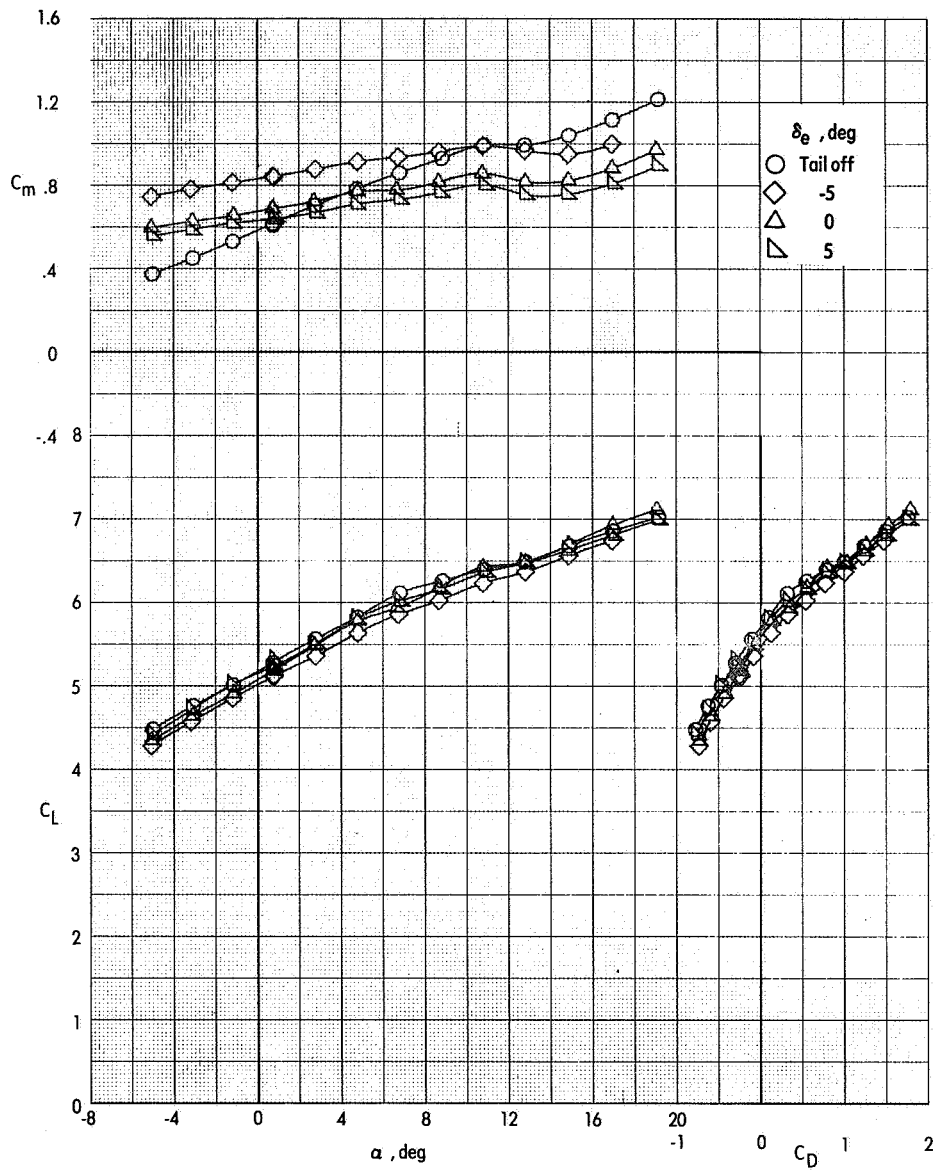
(b) $C_{\mu} = 2.9$.

Figure 46.- Concluded.



(a) $C_{\mu} = 3.4$.

Figure 47.- Effect of elevator deflection on longitudinal aerodynamic characteristics of the VTOL transition configuration ($\delta_L = 40^\circ$; $\delta_{LC} = 70^\circ$; $\delta_f = 40^\circ$; $i_t = 7.5^\circ$) with power on. $q_\infty = 709$ Pa; $M_\infty = 0.100$.



(b) $C_{\mu} = 5.1$.

Figure 47.- Concluded.

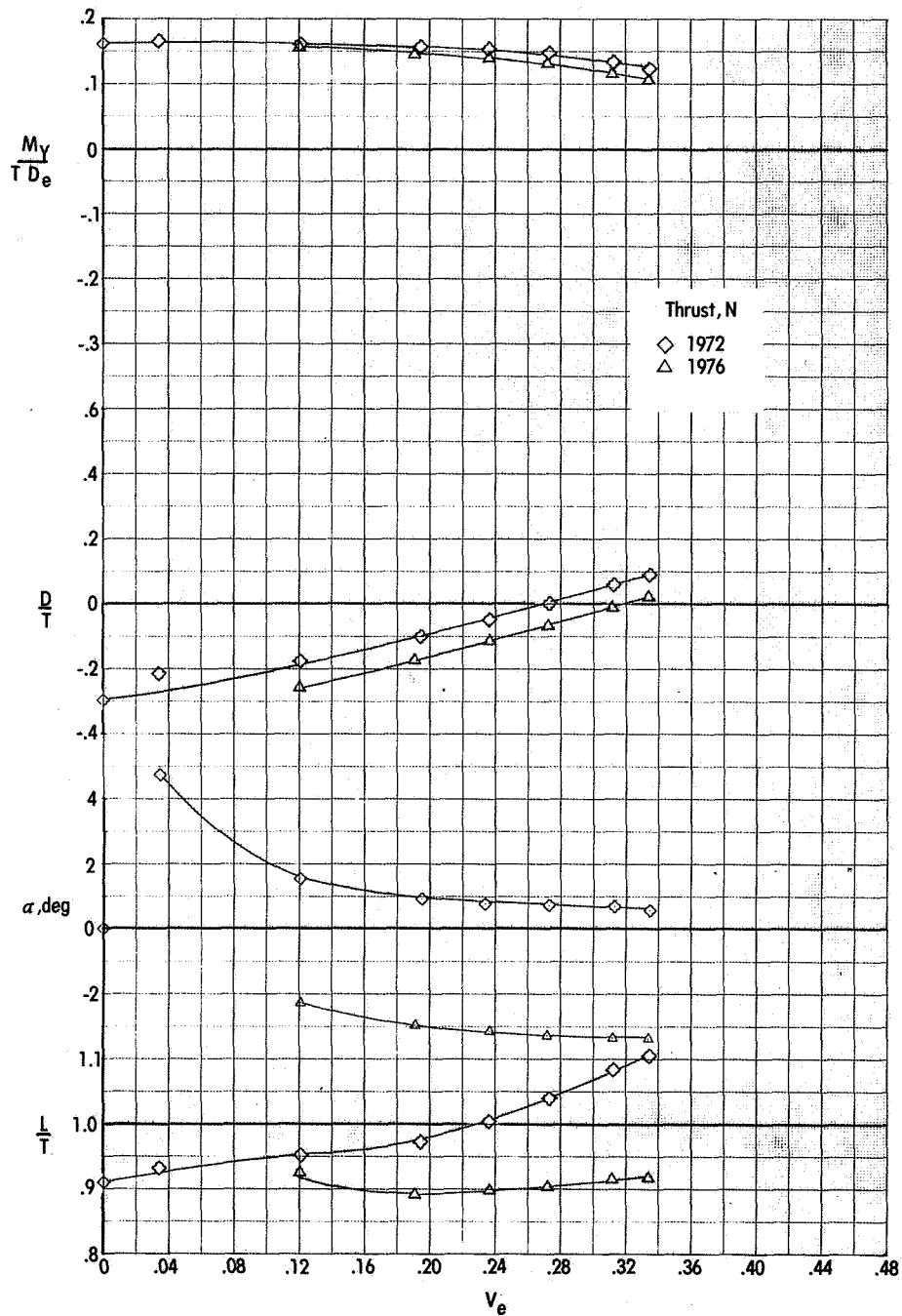
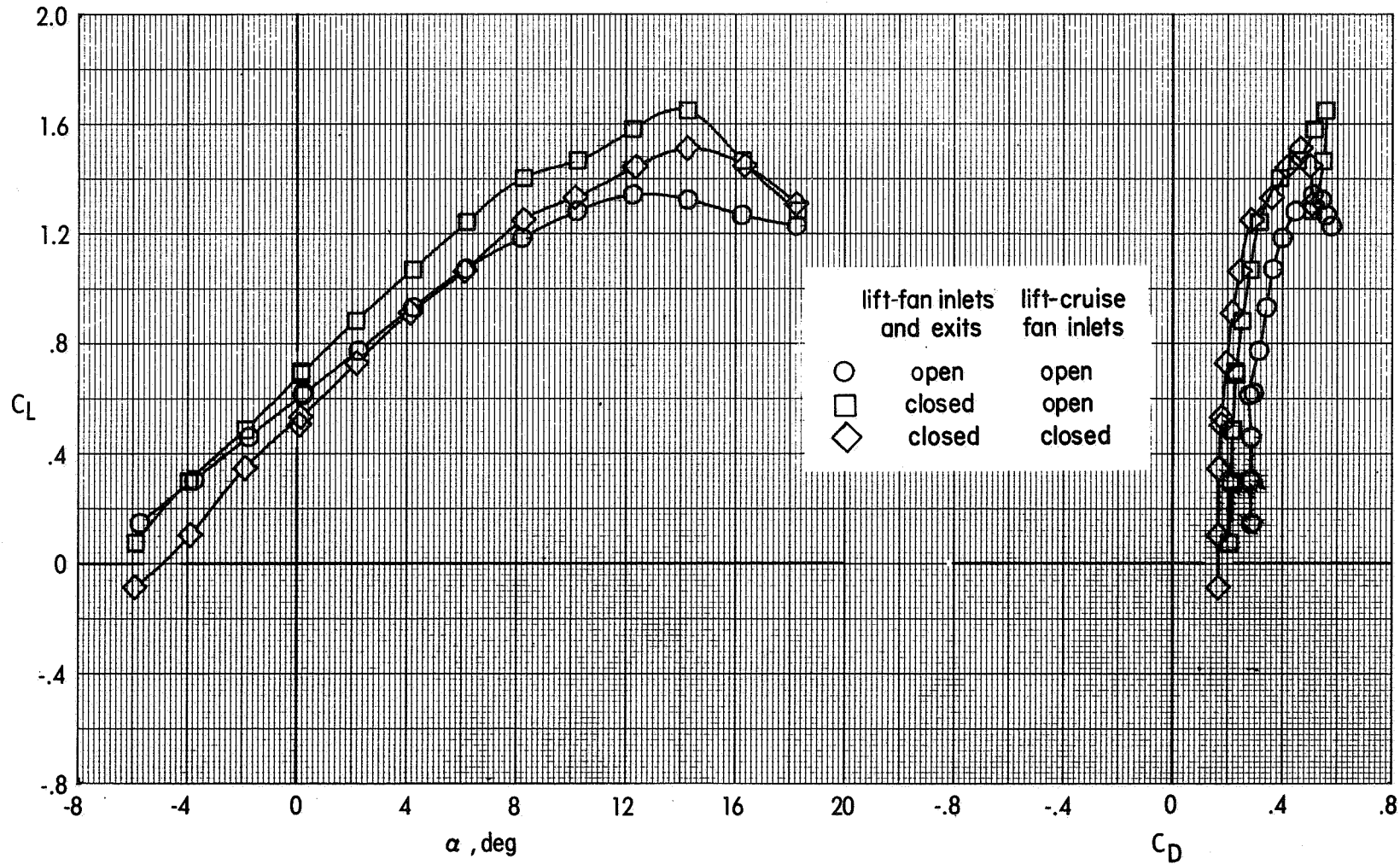
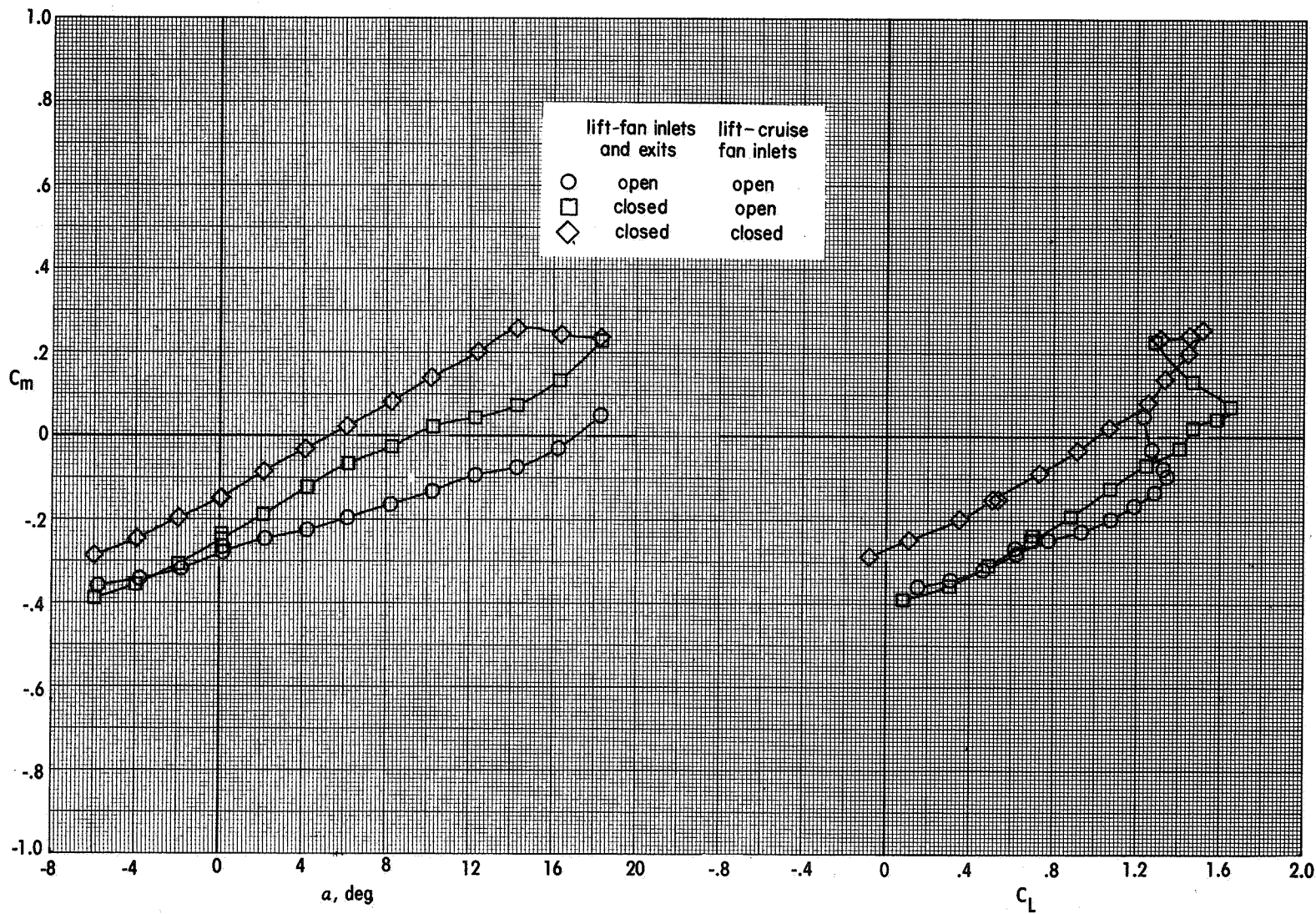


Figure 48.- Effect of effective velocity ratio on longitudinal aerodynamic characteristics of the VTOL transition configuration ($\delta_L = 40^\circ$; $\delta_{LC} = 70^\circ$; $\delta_f = 40^\circ$; $i_t = 7.5^\circ$; $\delta_e = 0^\circ$).



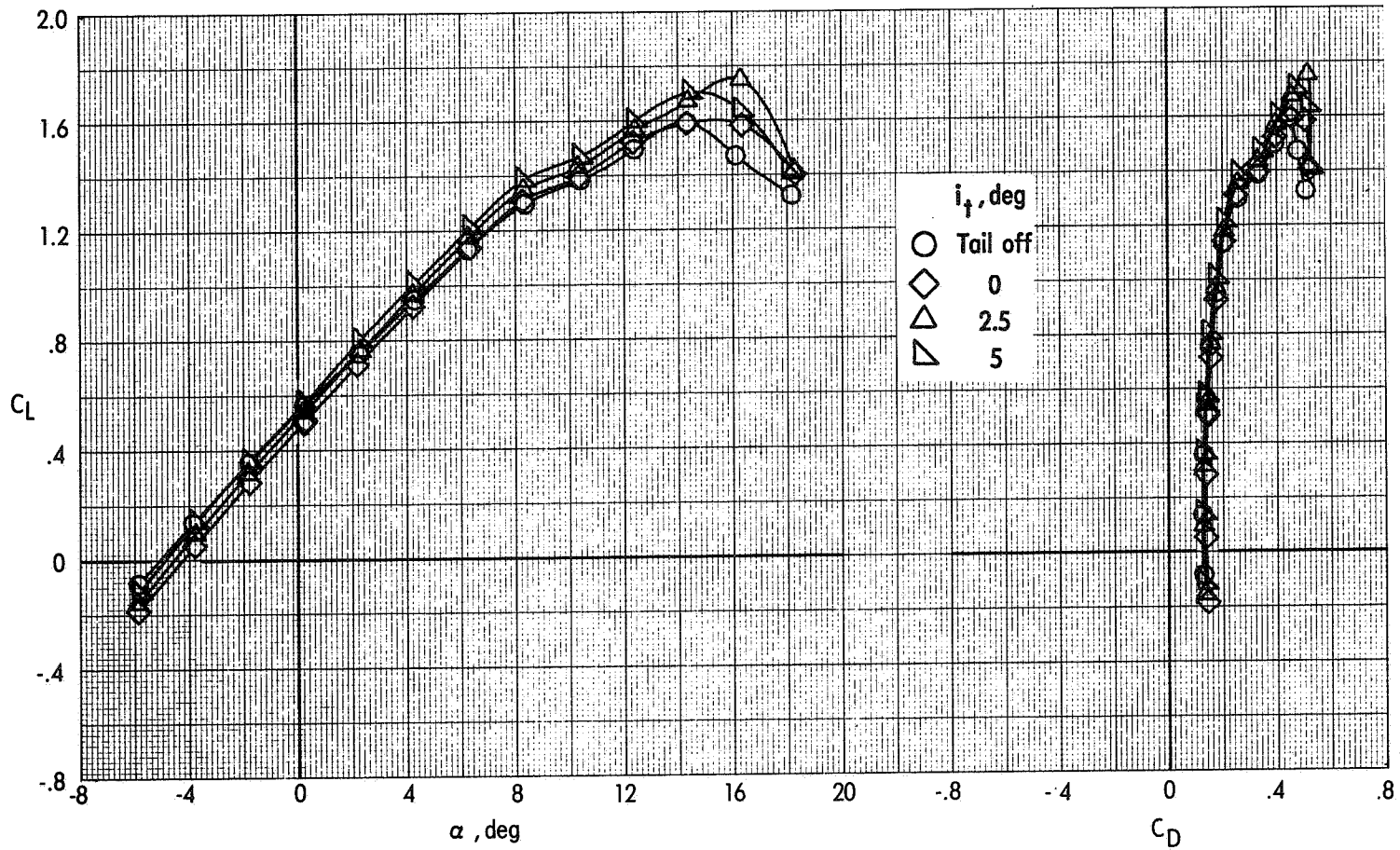
(a) Lift characteristics.

Figure 49.- Effect of closed lift-fan inlets and exits on longitudinal aerodynamics of the VTOL transition configuration ($\delta_L = 40^\circ$; $\delta_{LC} = 70^\circ$; $\delta_f = 40^\circ$; tail off) with power off. $q_\infty = 1245$ Pa; $M_\infty = 0.134$.



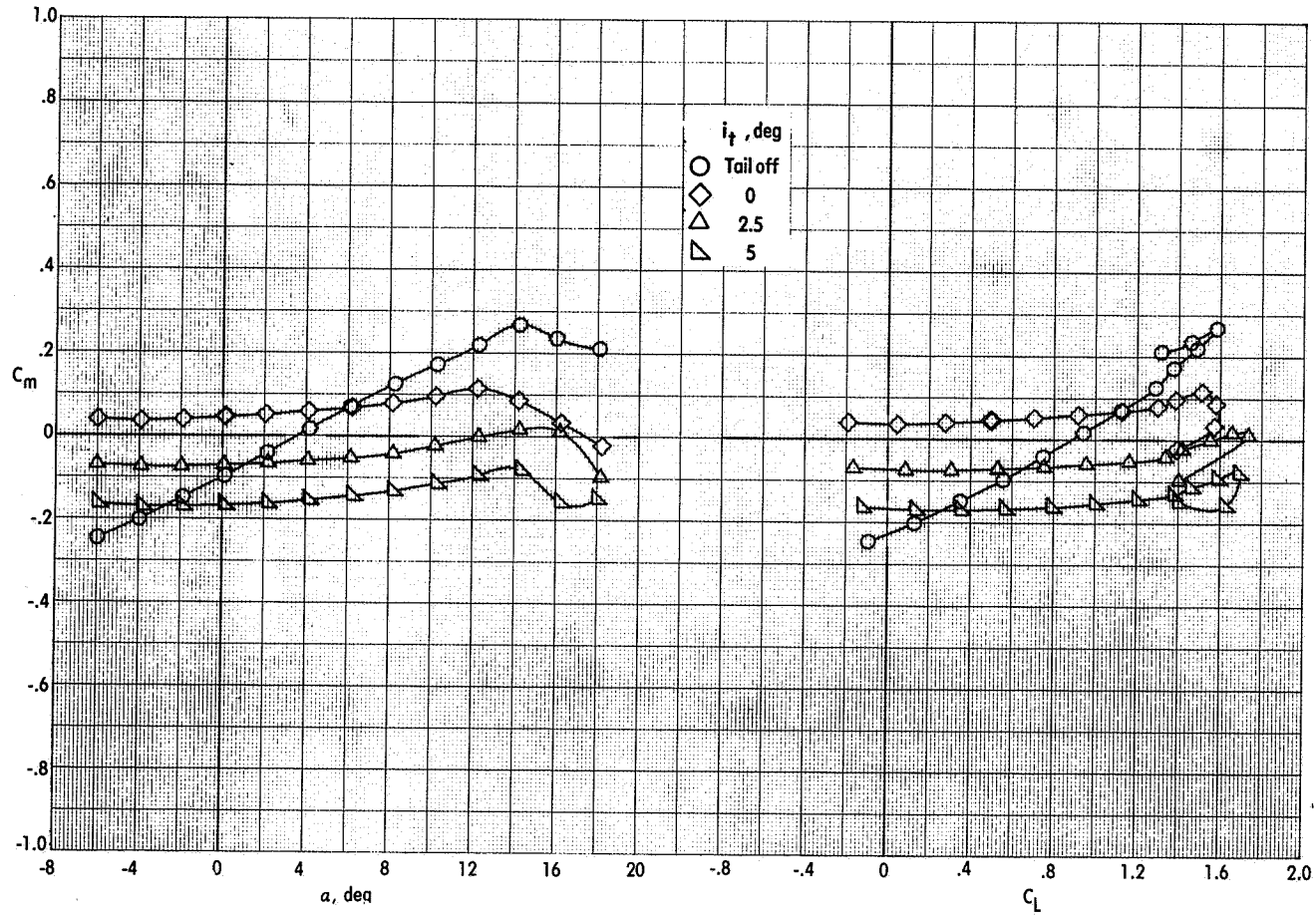
(b) Pitching-moment characteristics.

Figure 49.- Concluded.



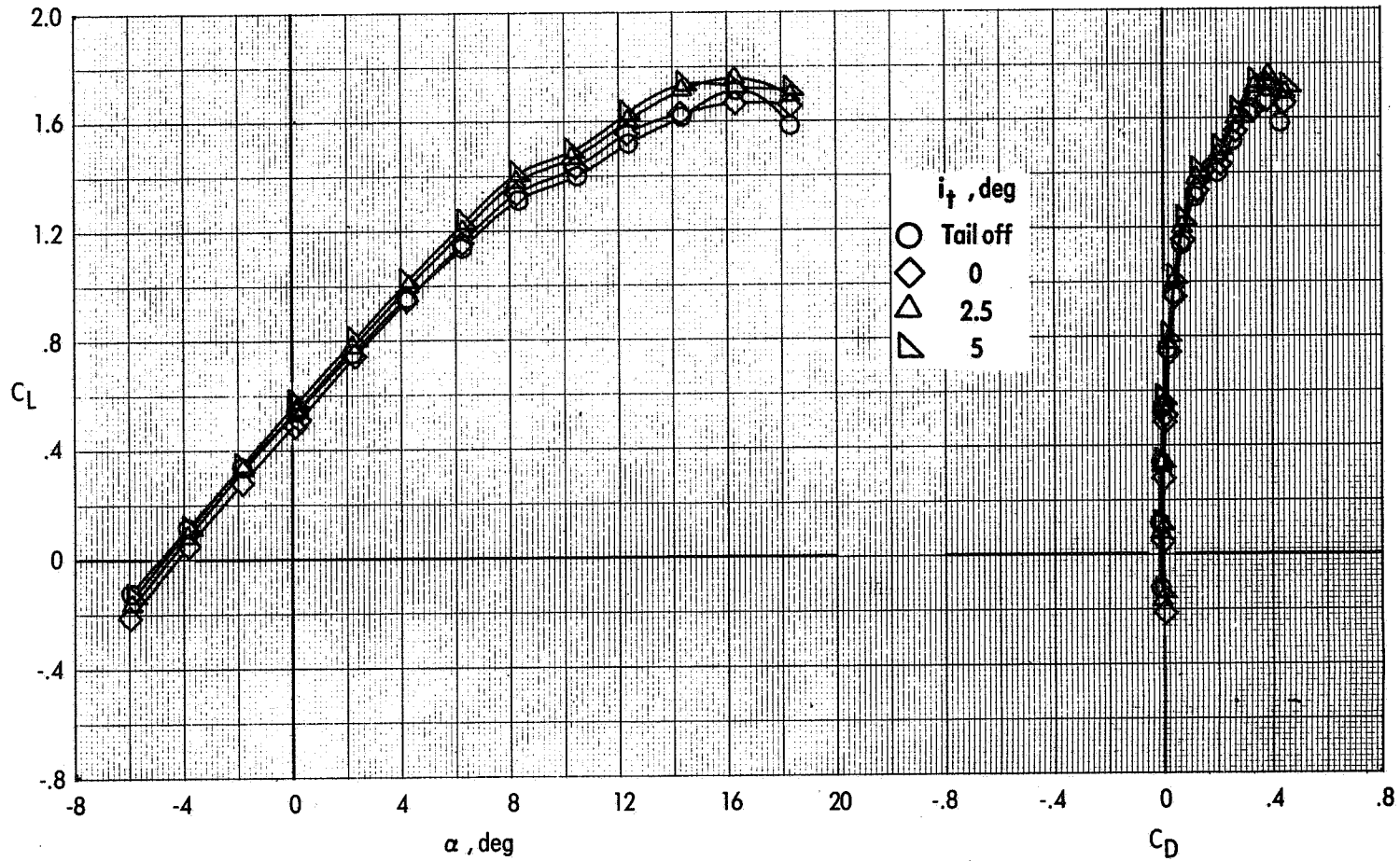
(a) Lift characteristics.

Figure 50.- Effect of tail incidence on longitudinal aerodynamic characteristics of the wingborne-flight configuration ($\delta_L = \text{closed}$; $\delta_{LC} = 0^\circ$; $\delta_f = 40^\circ$; $\delta_e = 0^\circ$) with power off. $q_\infty = 2672 \text{ Pa}$; $M_\infty = 0.236$.



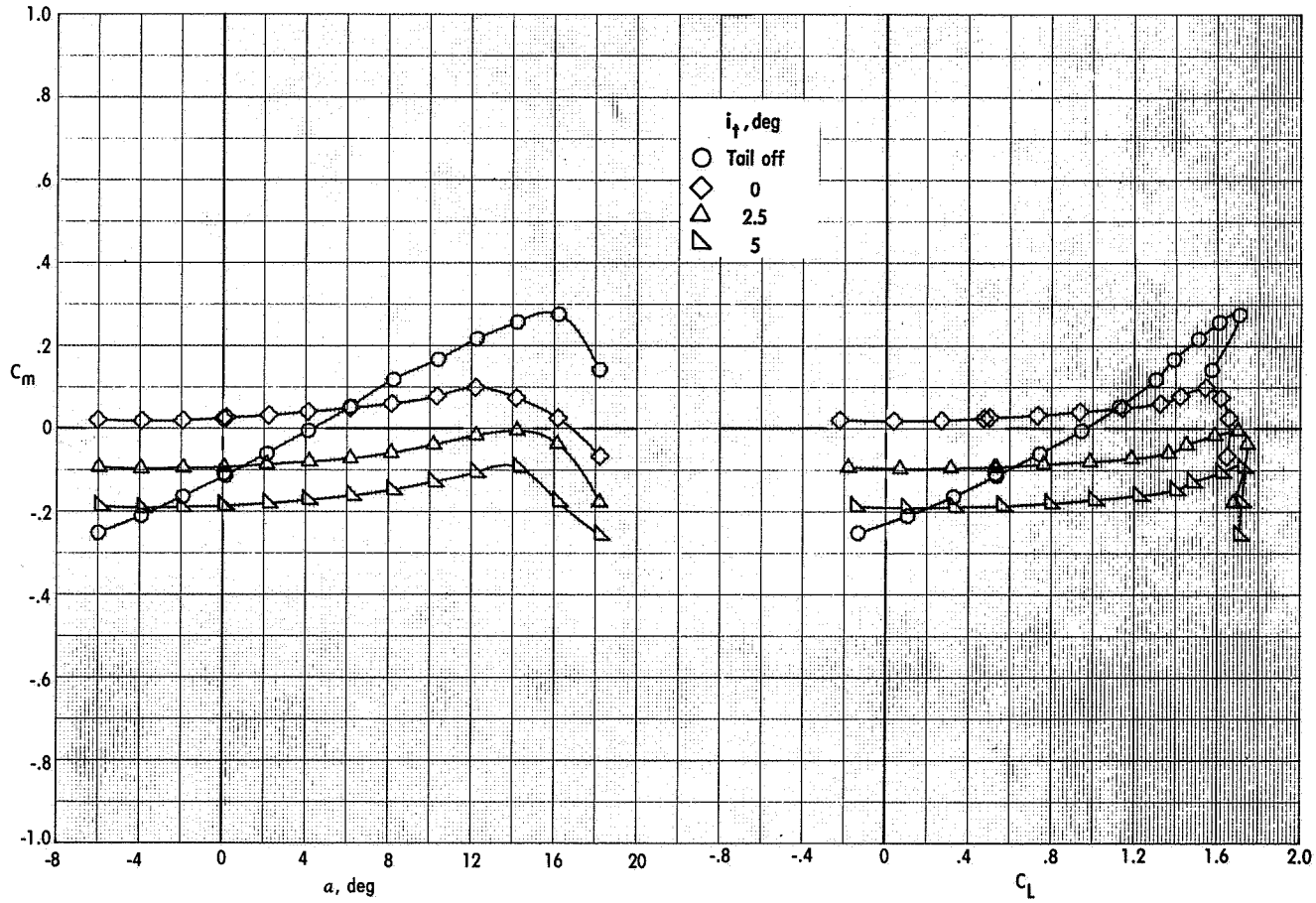
(b) Pitching-moment characteristics.

Figure 50.- Concluded.



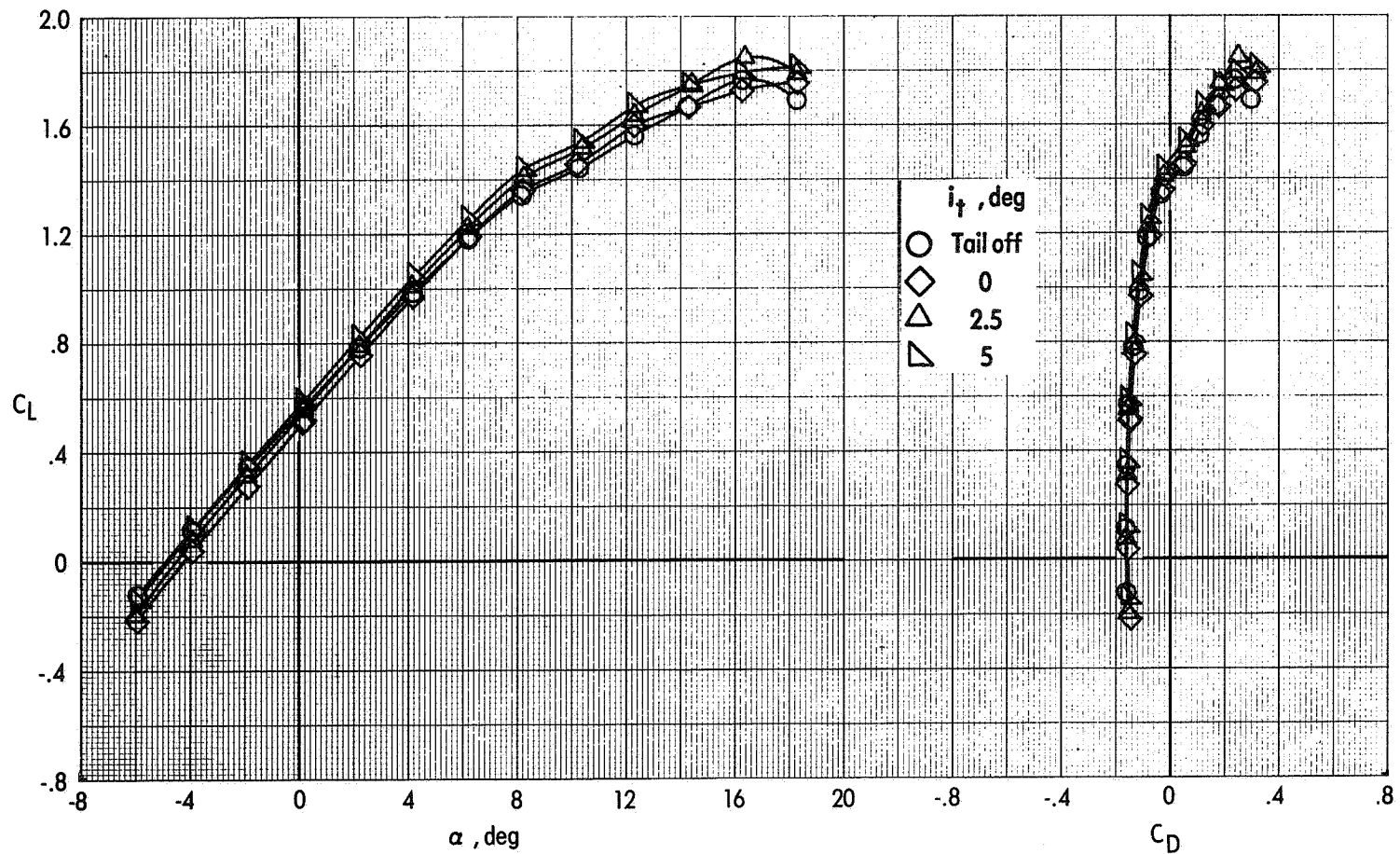
(a) Lift characteristics.

Figure 51.- Effect of tail incidence on longitudinal aerodynamic characteristics of the wingborne-flight configuration ($\delta_L = \text{closed}$; $\delta_{LC} = 0^\circ$; $\delta_f = 40^\circ$; $\delta_e = 0^\circ$) with power on ($C_\mu = 0.19$). $q_\infty = 2672$ Pa; $M_\infty = 0.236$.



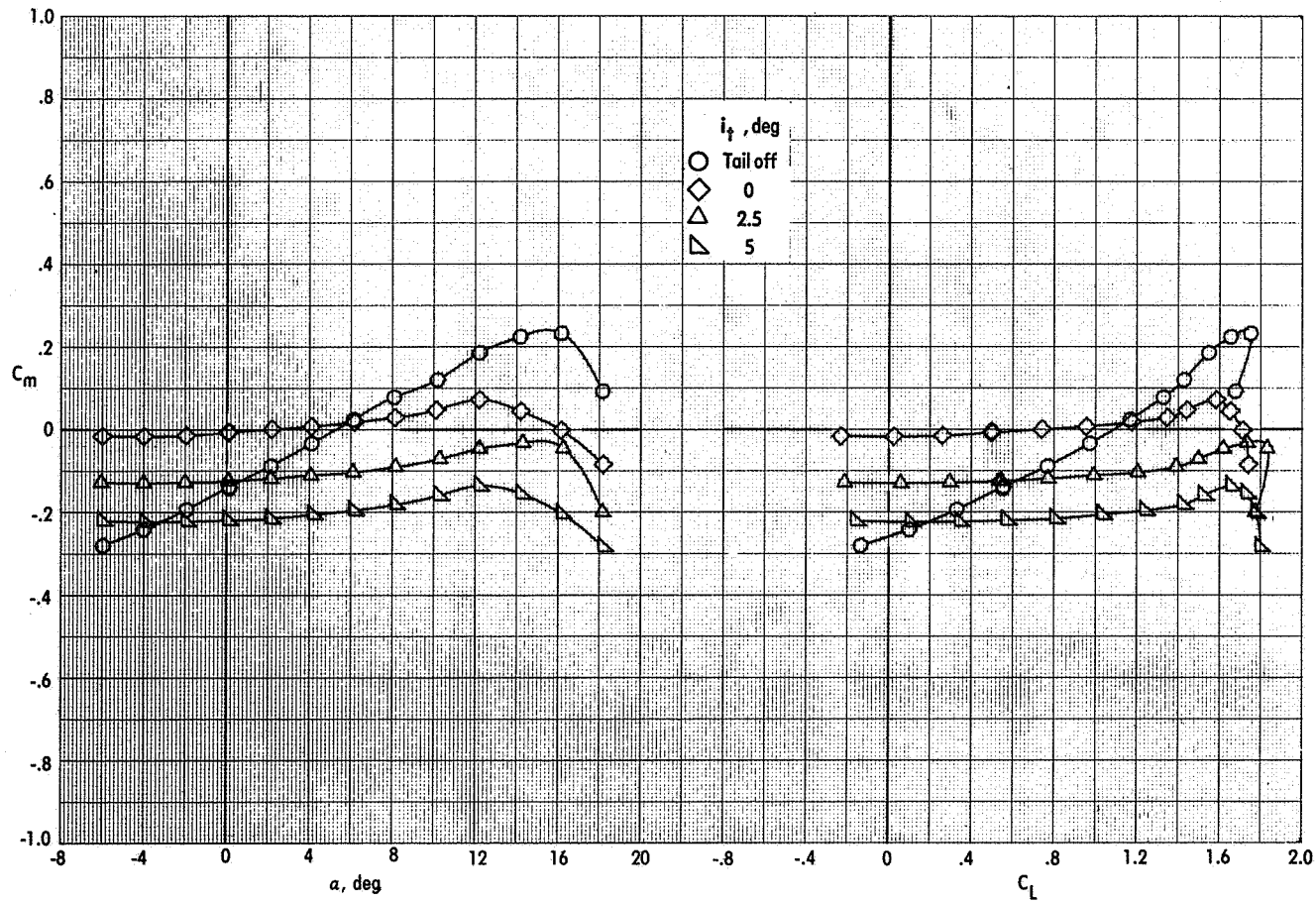
(b) Pitching-moment characteristics.

Figure 51.- Concluded.



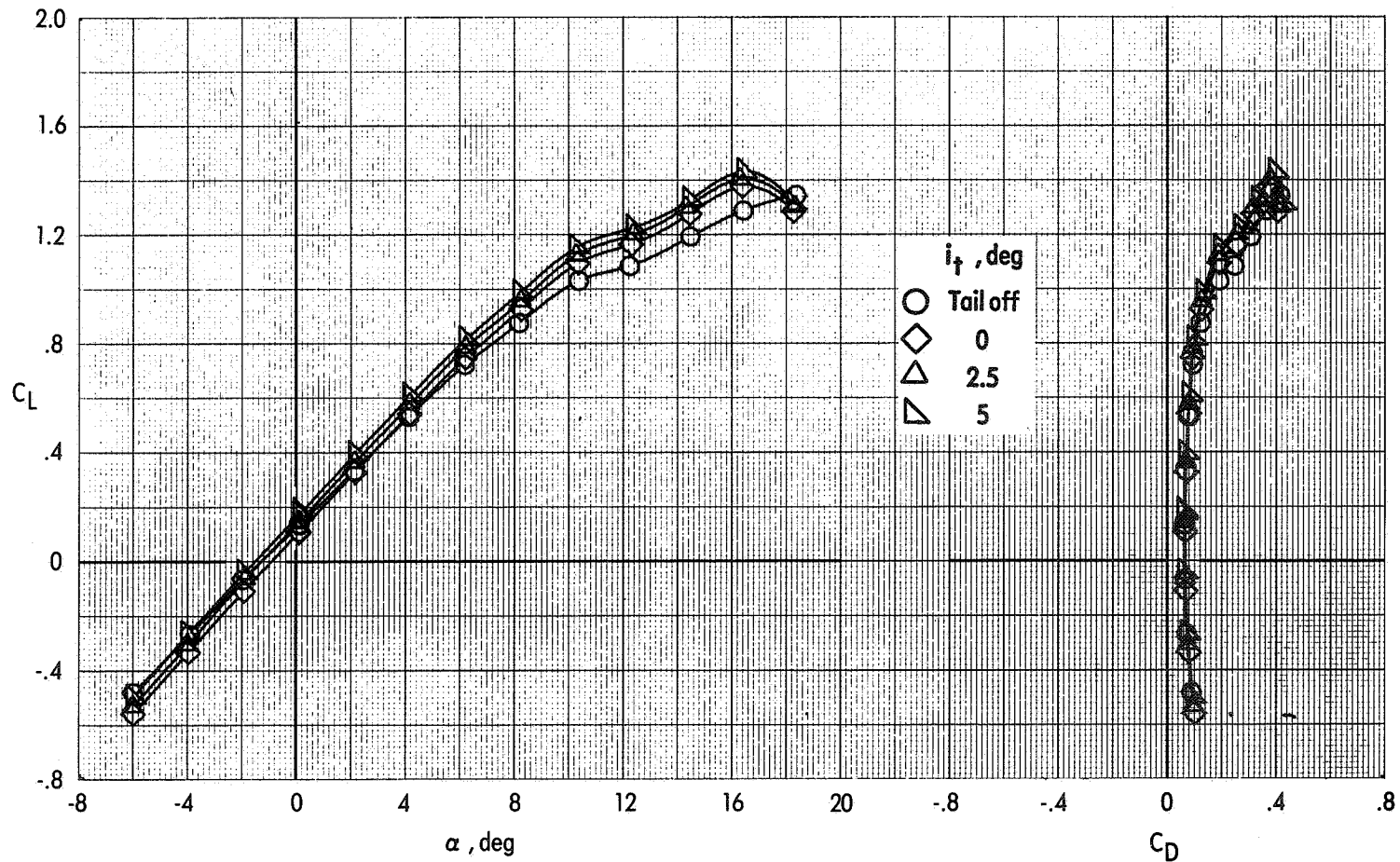
(a) Lift characteristics.

Figure 52.- Effect of tail incidence on longitudinal aerodynamic characteristics of the wingborne-flight configuration ($\delta_L = \text{closed}$; $\delta_{LC} = 0^\circ$; $\delta_f = 40^\circ$; $\delta_e = 0^\circ$) with power on ($C_\mu = 0.37$). $q_\infty = 2672 \text{ Pa}$; $M_\infty = 0.236$.



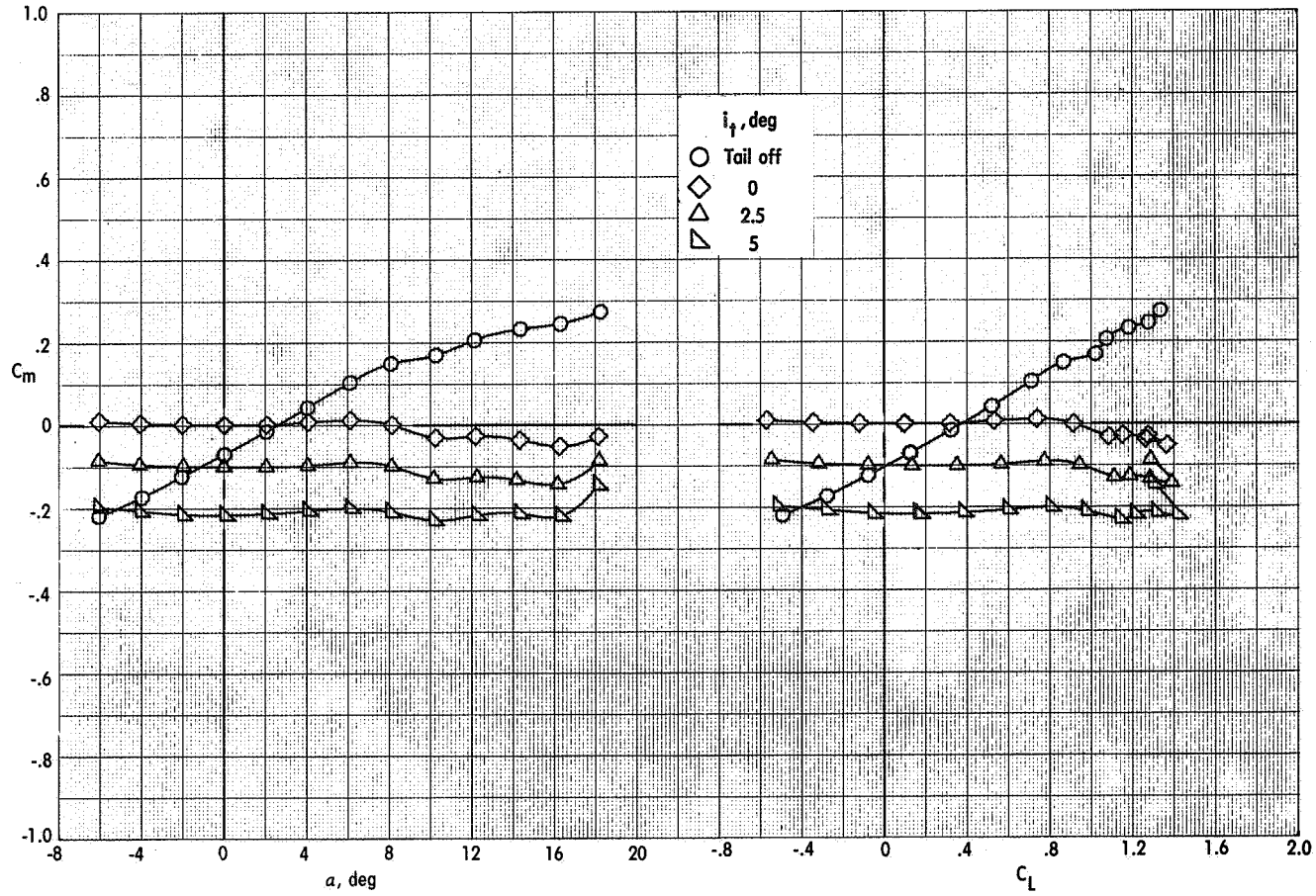
(b) Pitching-moment characteristics.

Figure 52.- Concluded.



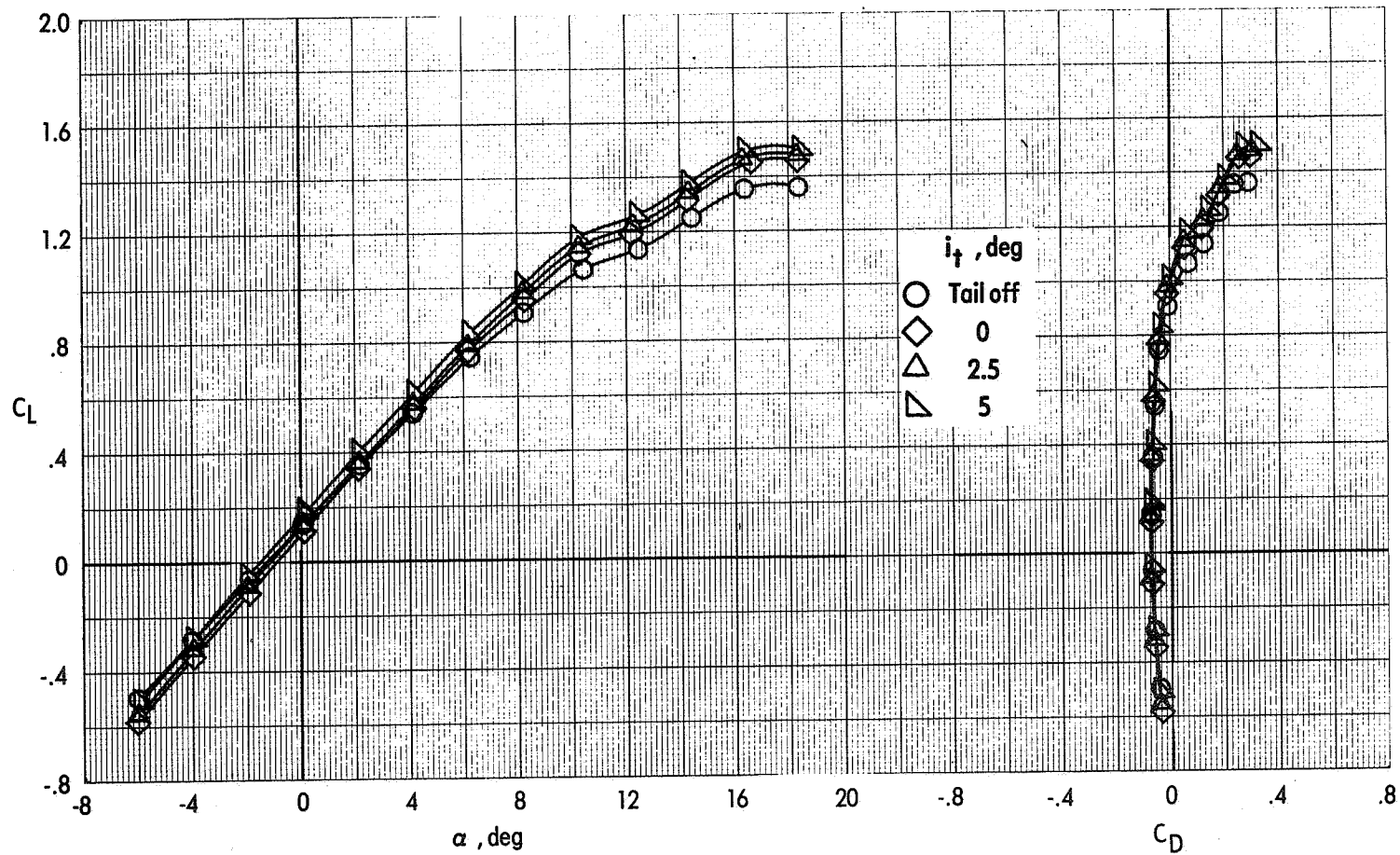
(a) Lift characteristics.

Figure 53.- Effect of tail incidence on longitudinal aerodynamic characteristics of the cruise configuration ($\delta_L = \text{closed}$; $\delta_{LC} = 0^\circ$; $\delta_f = 0^\circ$; $\delta_e = 0^\circ$) with power off. $q_\infty = 2672$ Pa; $M_\infty = 0.236$.



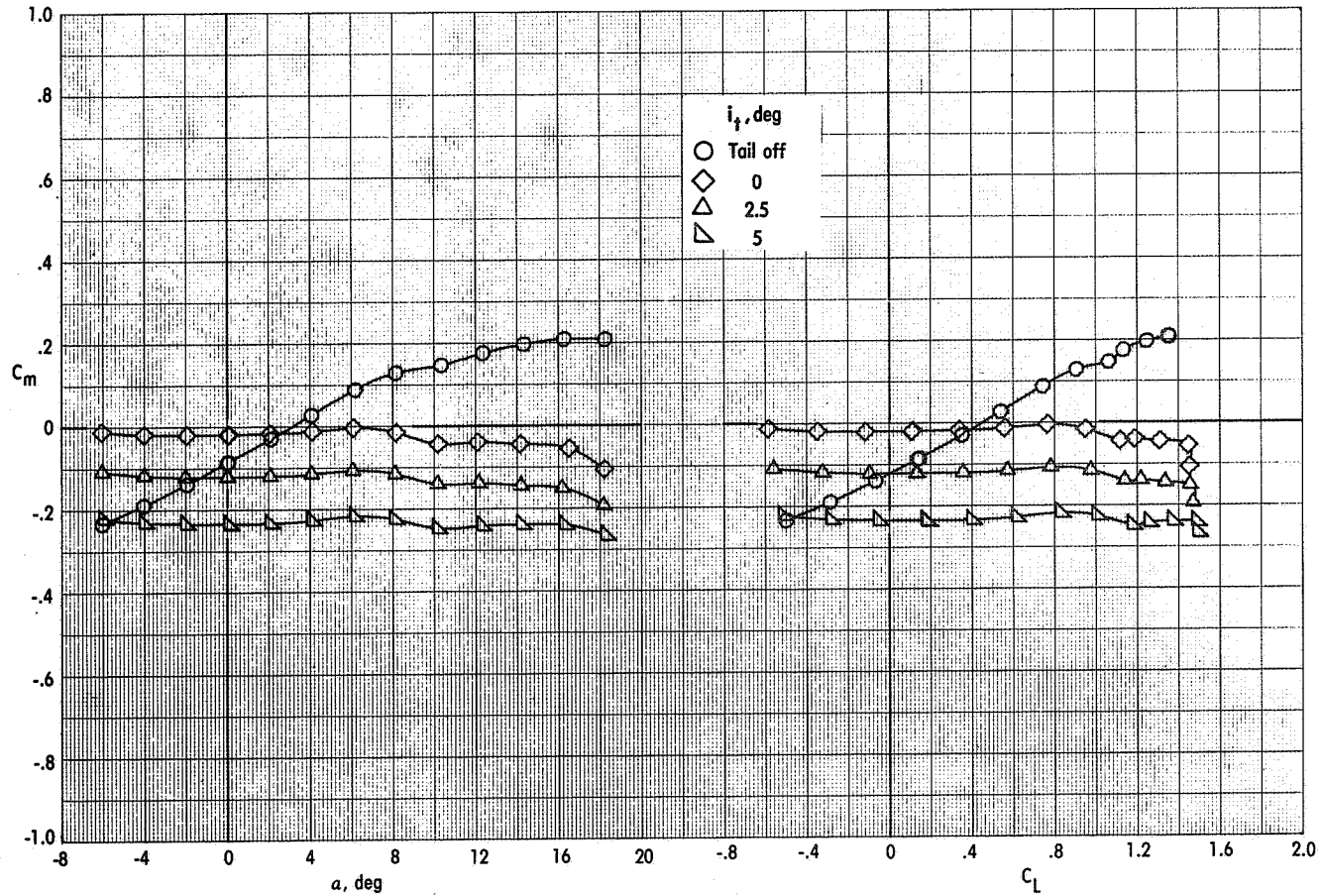
(b) Pitching-moment characteristics.

Figure 53.- Concluded.



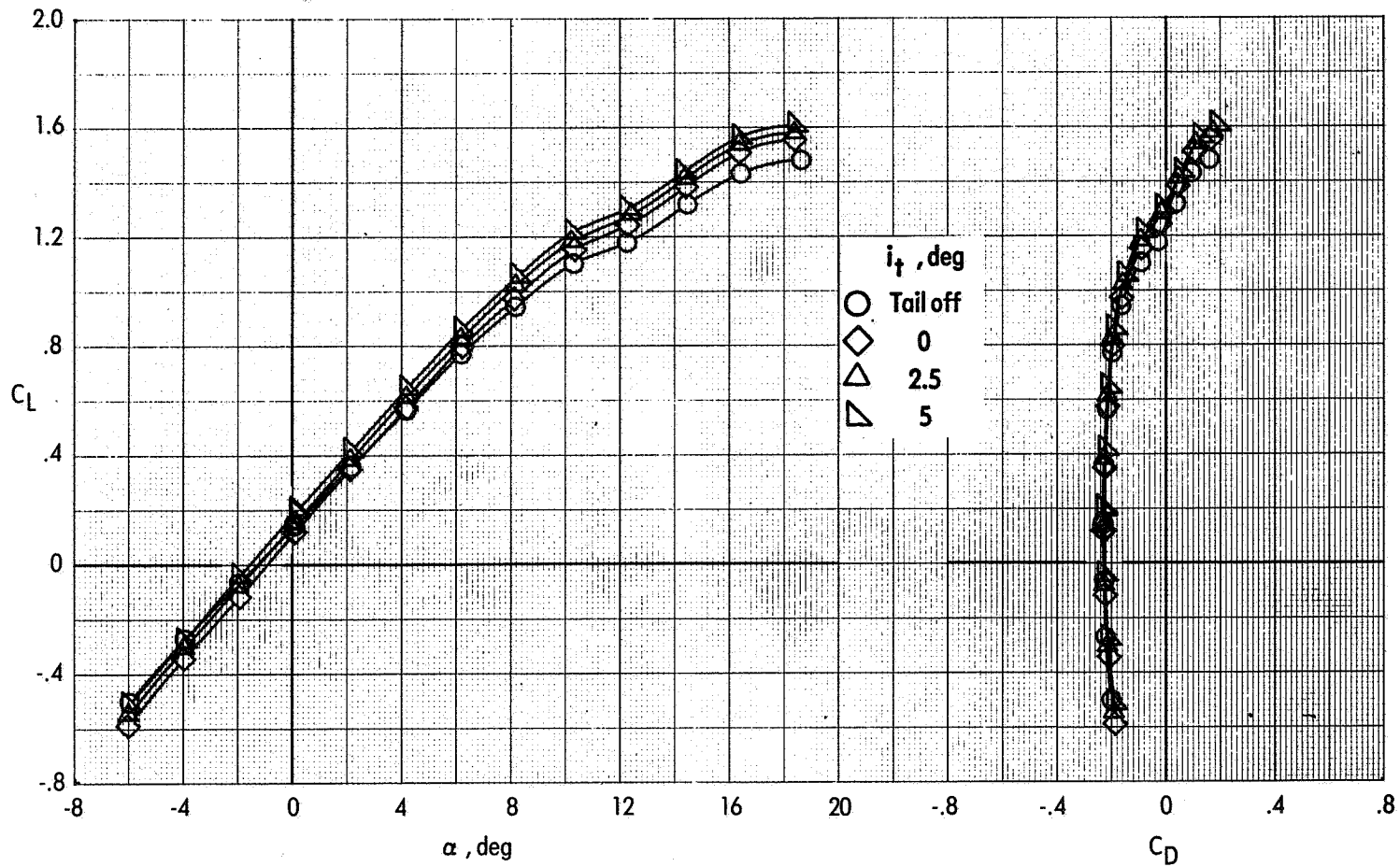
(a) Lift characteristics.

Figure 54.- Effect of tail incidence on longitudinal aerodynamic characteristics of the cruise configuration ($\delta_L = \text{closed}$; $\delta_{LC} = 0^\circ$; $\delta_f = 0^\circ$; $\delta_e = 0^\circ$) with power on ($C_\mu = 0.19$). $q_\infty = 2672$ Pa; $M_\infty = 0.236$.



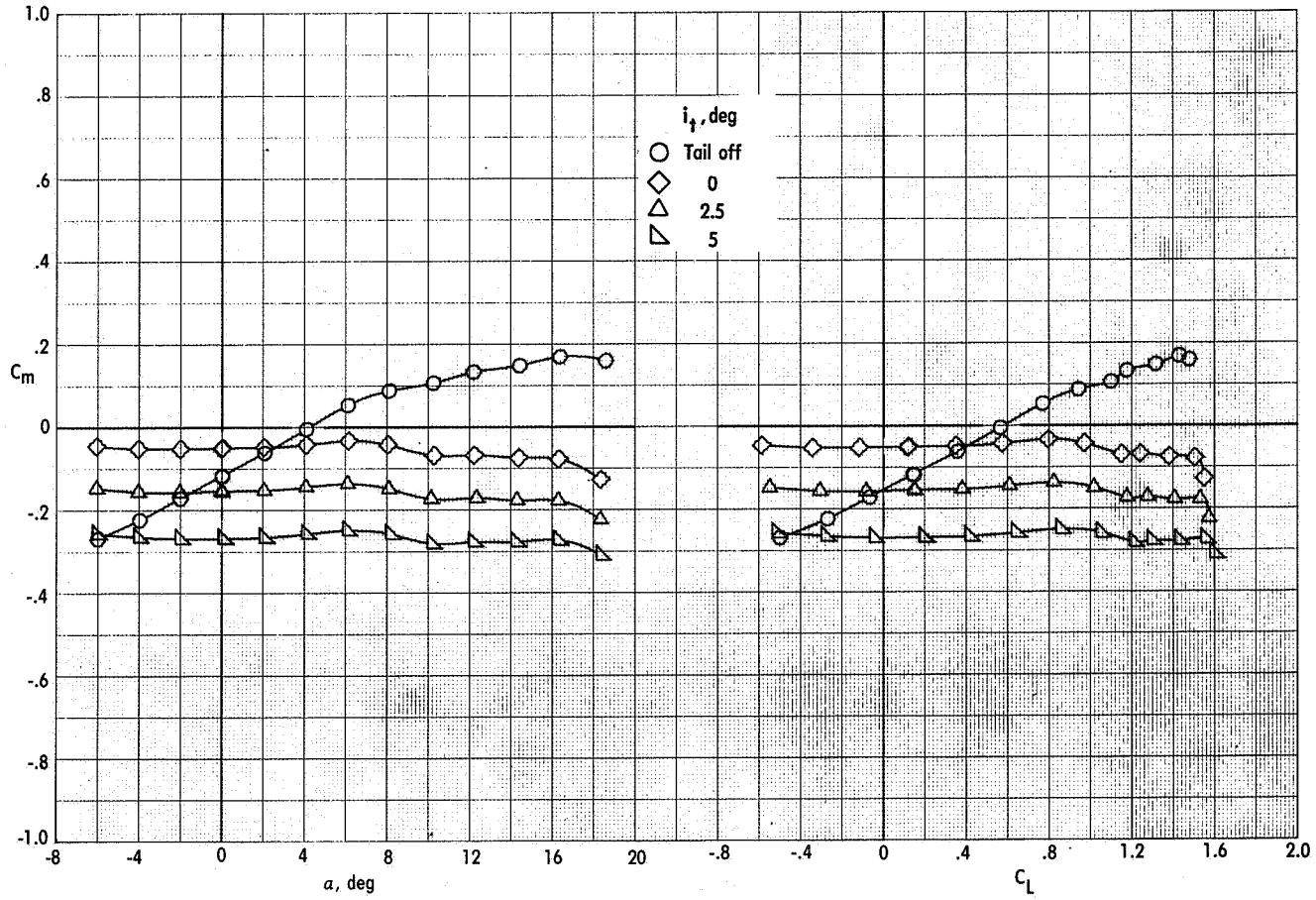
(b) Pitching-moment characteristics.

Figure 54.- Concluded.



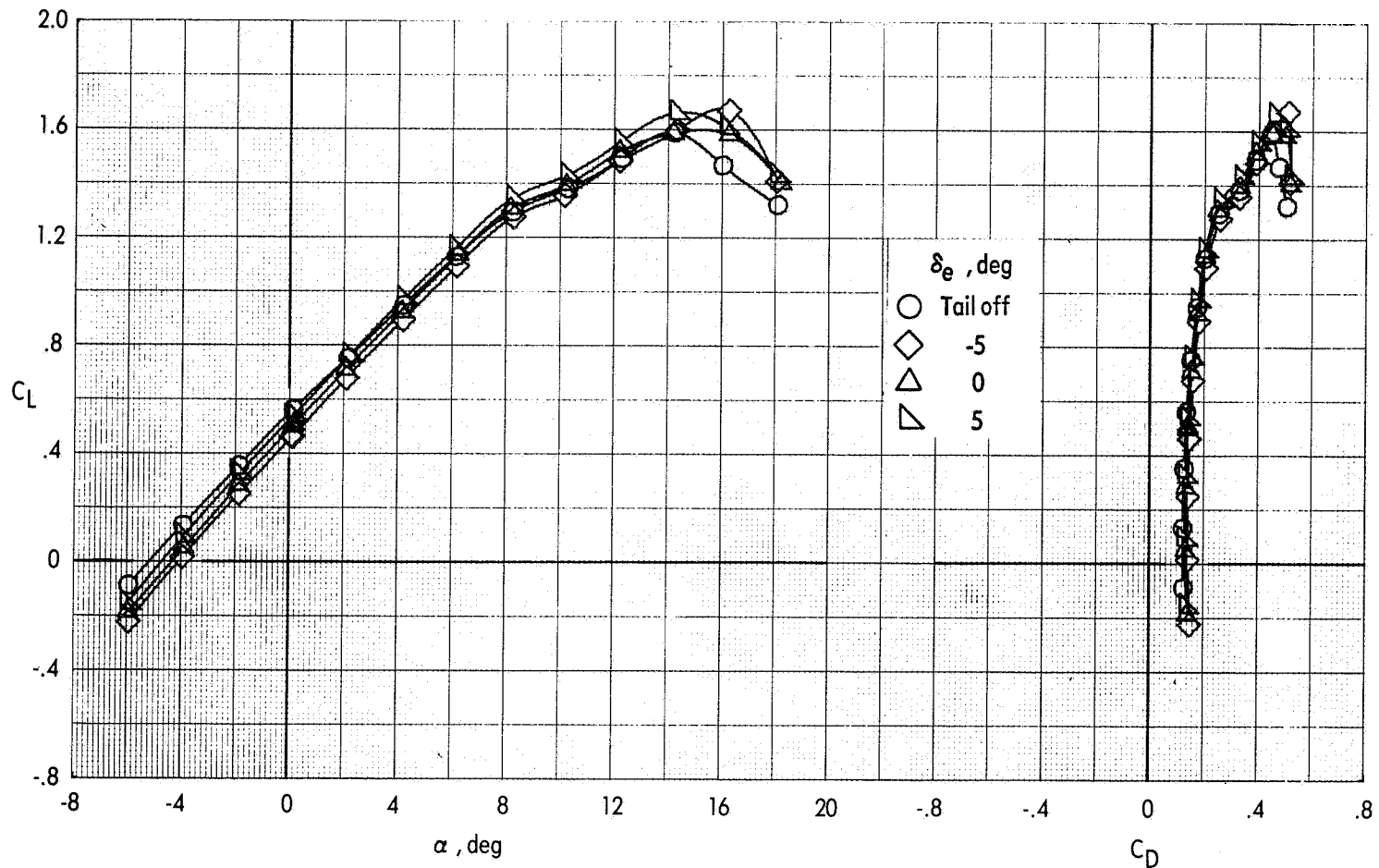
(a) Lift characteristics.

Figure 55.- Effect of tail incidence on longitudinal aerodynamic characteristics of the cruise configuration ($\delta_L = \text{closed}$; $\delta_{LC} = 0^\circ$; $\delta_f = 0^\circ$; $\delta_e = 0^\circ$) with power on ($C_\mu = 0.37$). $q_\infty = 2672 \text{ Pa}$; $M_\infty = 0.236$.



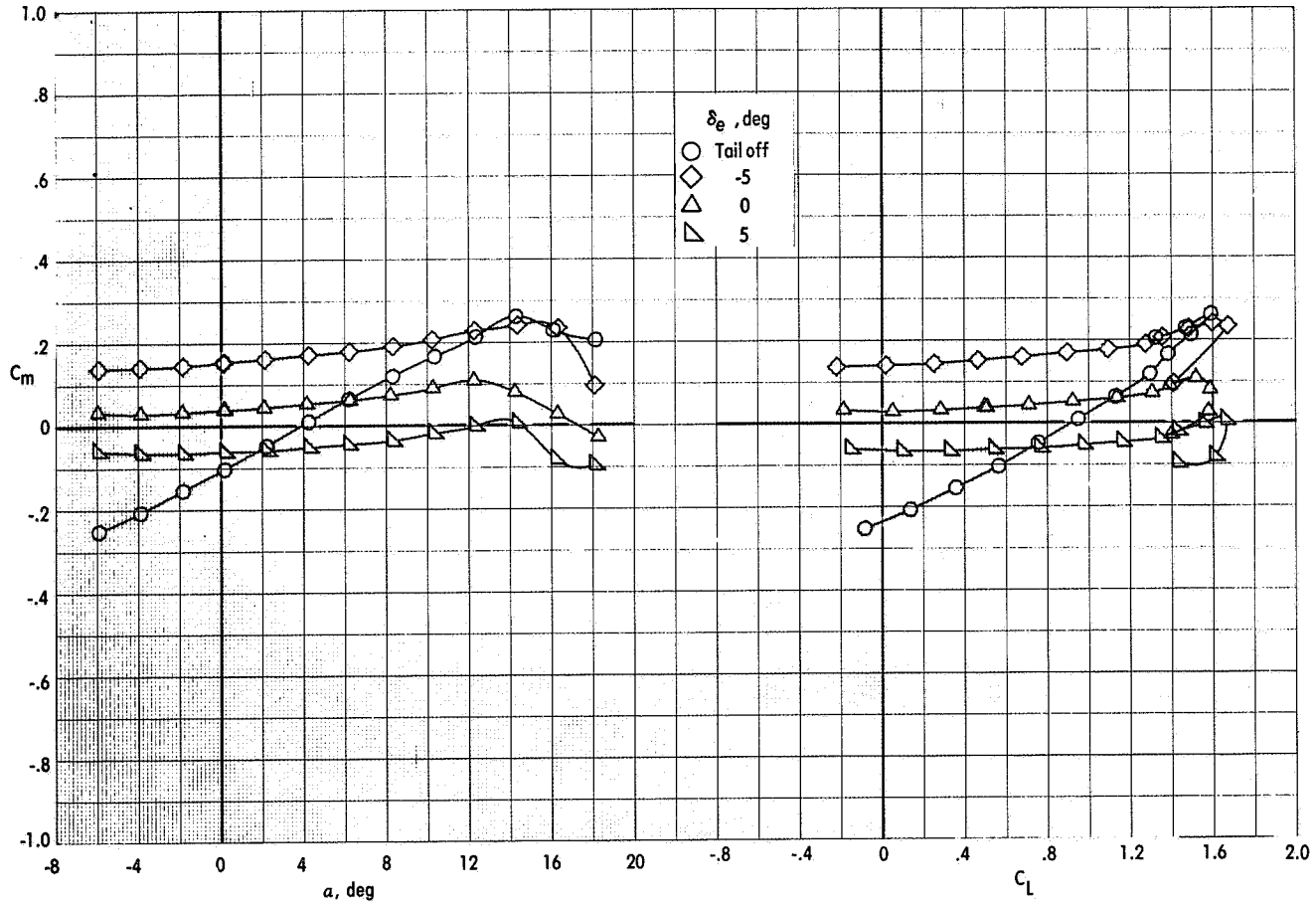
(b) Pitching-moment characteristics.

Figure 55.- Concluded.



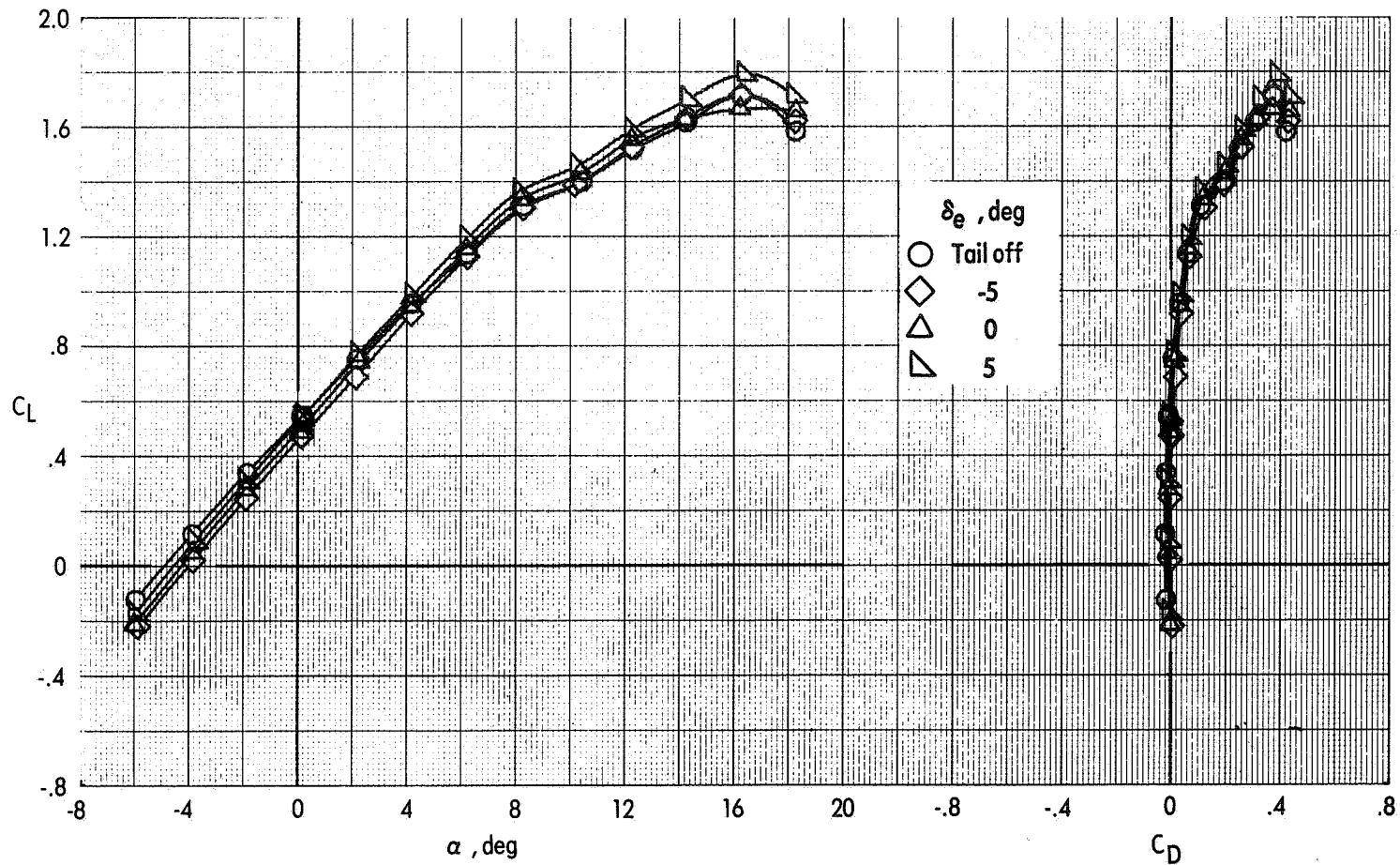
(a) Lift characteristics.

Figure 56.- Effect of elevator deflection on longitudinal aerodynamic characteristics of the wingborne-flight configuration ($\delta_L = \text{closed}$; $\delta_{LC} = 0^\circ$; $\delta_f = 40^\circ$; $i_t = 0^\circ$) with power off. $q_\infty = 2672 \text{ Pa}$; $M_\infty = 0.236$.



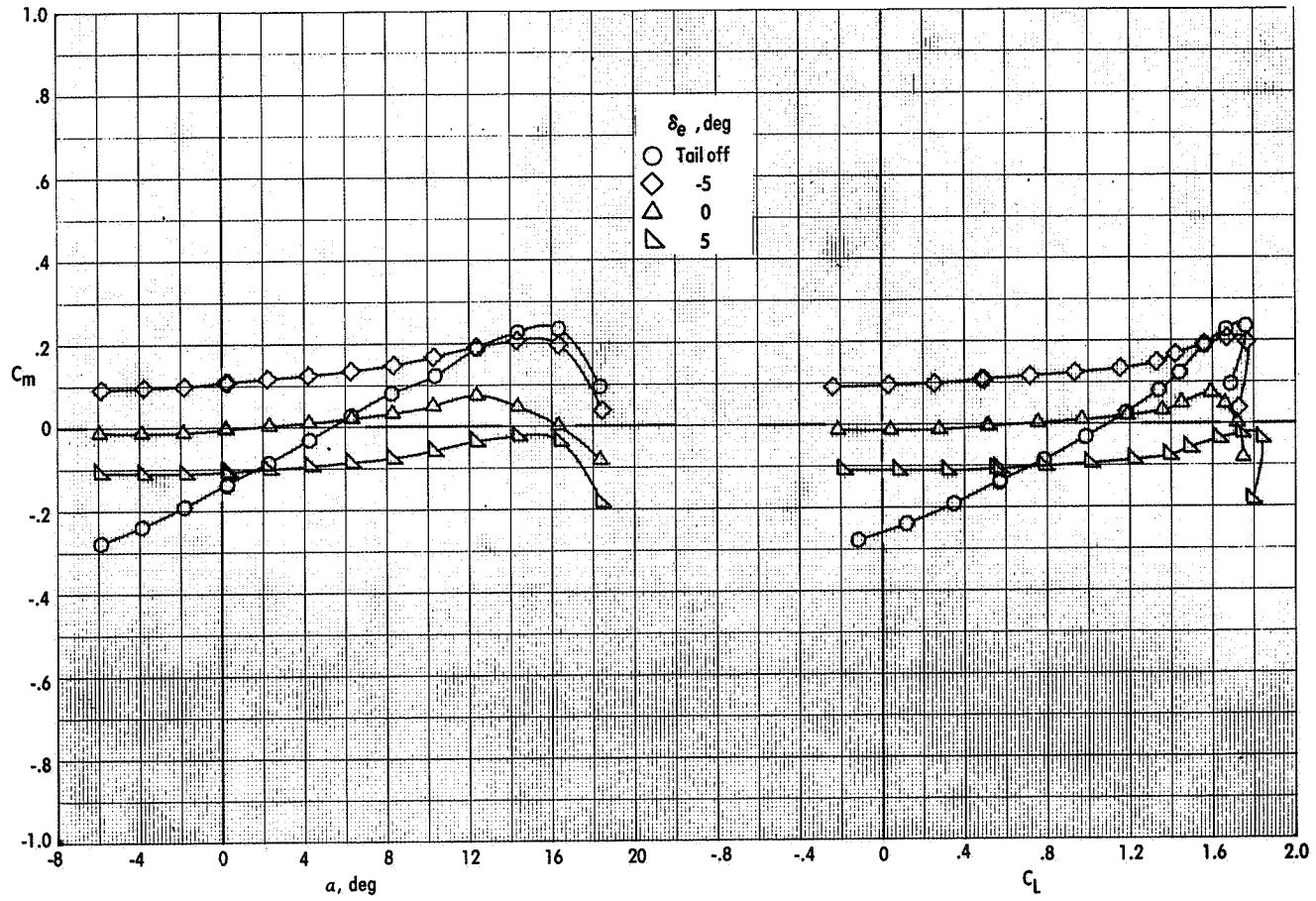
(b) Pitching-moment characteristics.

Figure 56. - Concluded.



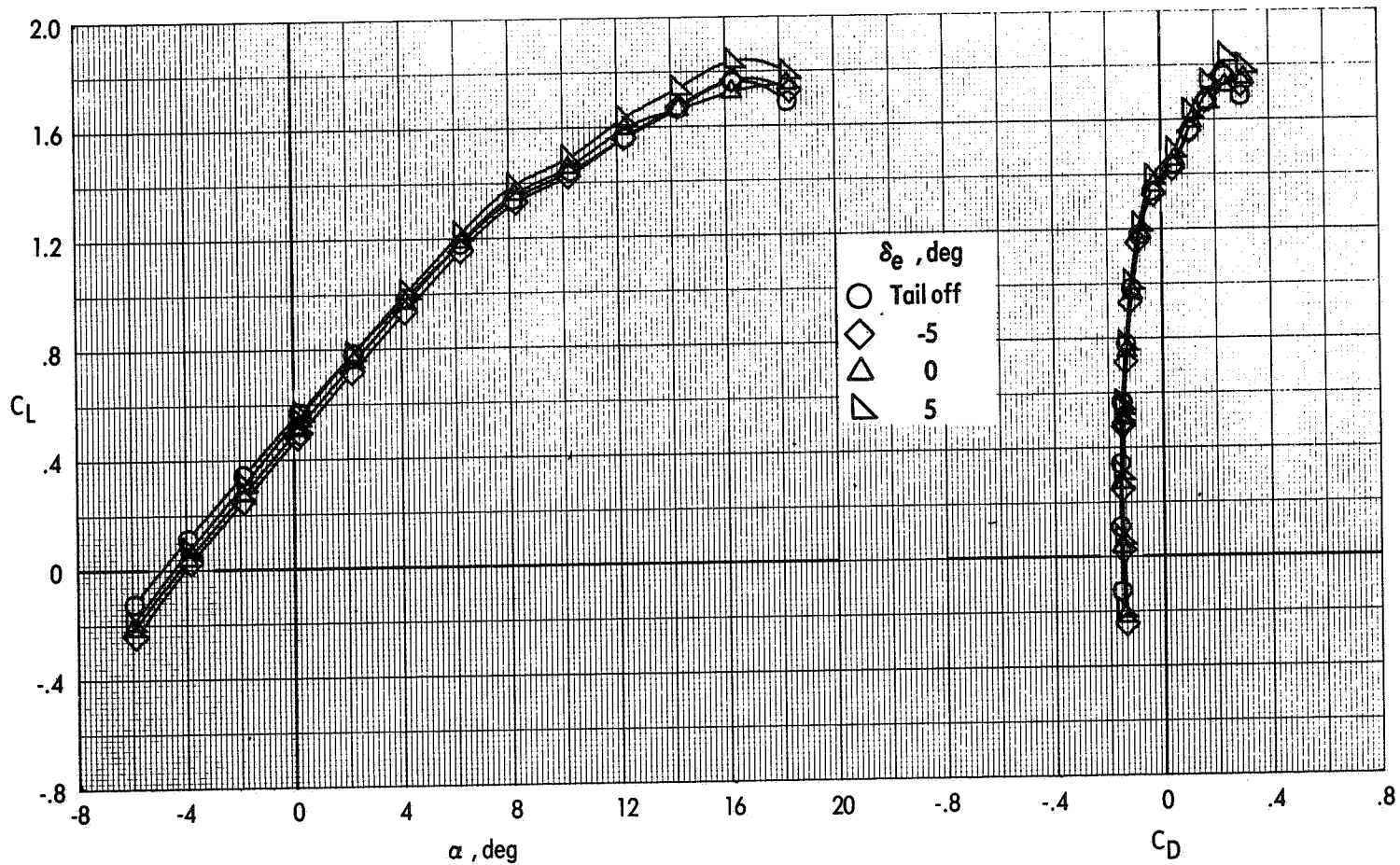
(a) Lift characteristics.

Figure 57.- Effect of elevator deflection on longitudinal aerodynamic characteristics of the wingborne-flight configuration ($\delta_L = \text{closed}$; $\delta_{LC} = 0^\circ$; $\delta_f = 40^\circ$; $i_t = 0^\circ$) with power on ($C_\mu = 0.19$). $q_\infty = 2672 \text{ Pa}$; $M_\infty = 0.236$.



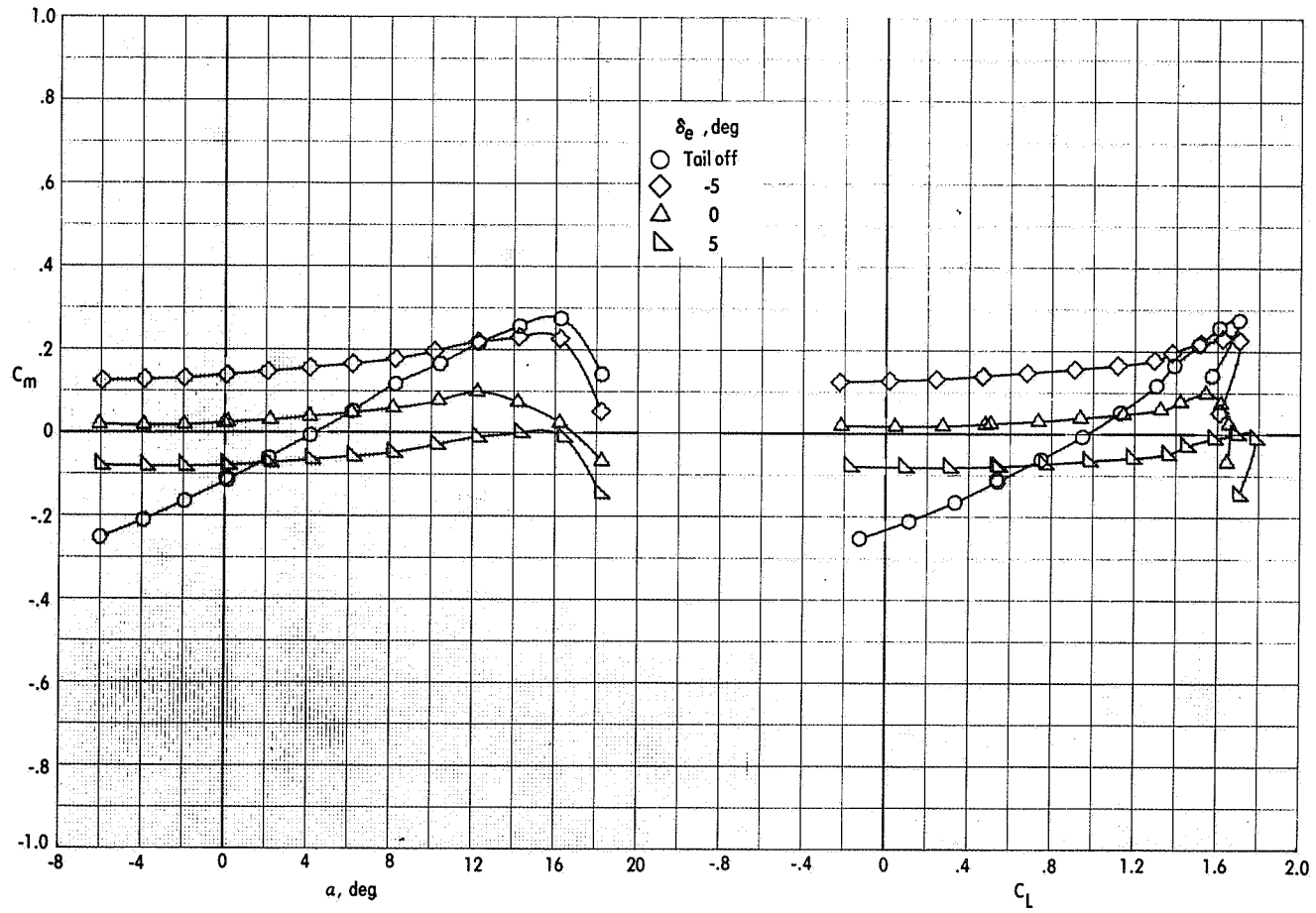
(b) Pitching-moment characteristics.

Figure 57.- Concluded.



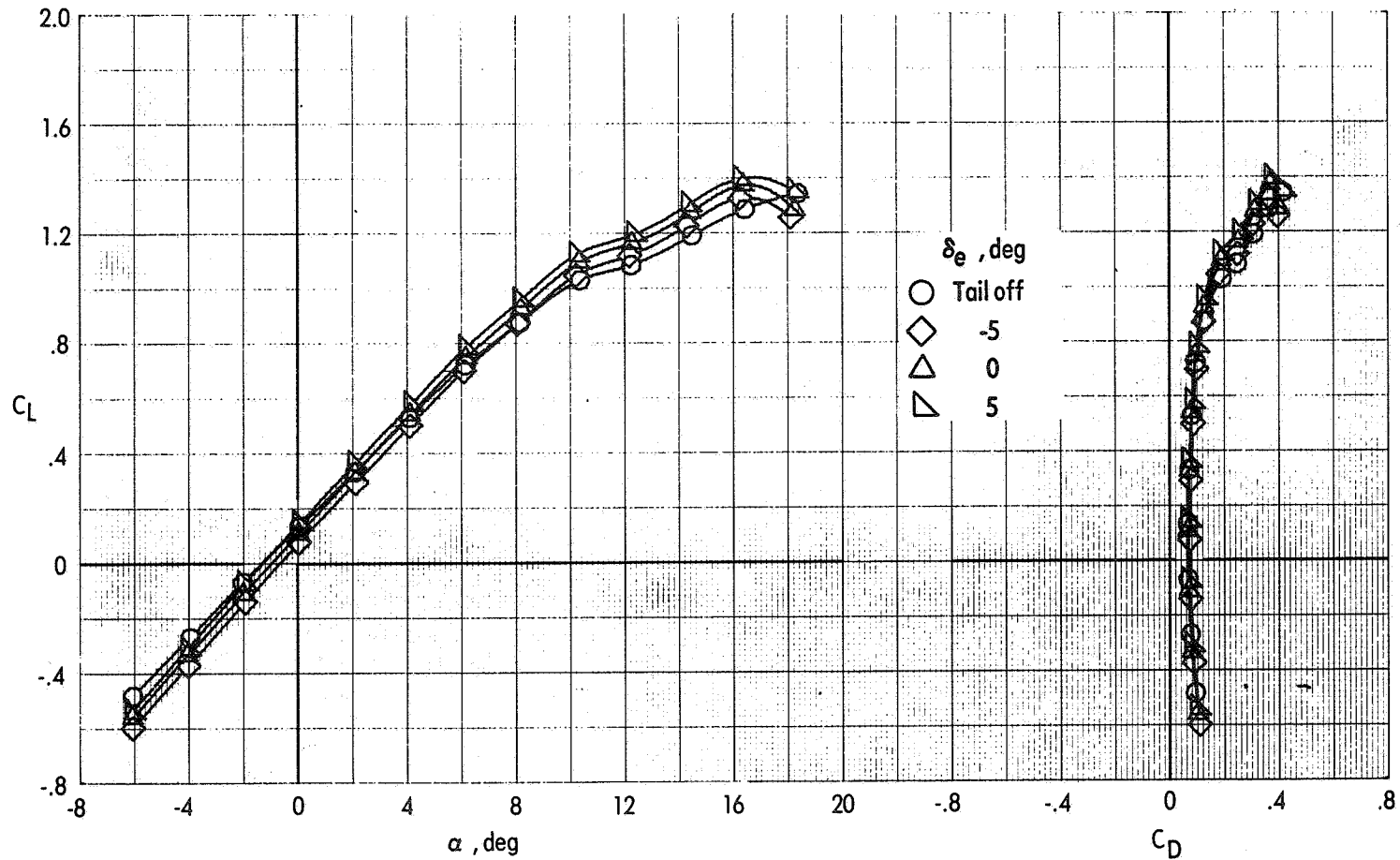
(a) Lift characteristics.

Figure 58.- Effect of elevator deflection on longitudinal aerodynamic characteristics of the wingborne-flight configuration ($\delta_L = \text{closed}$; $\delta_{LC} = 0^\circ$; $\delta_f = 40^\circ$; $i_t = 0^\circ$) with power on ($C_\mu = 0.37$). $q_\infty = 2672 \text{ Pa}$; $M_\infty = 0.236$.



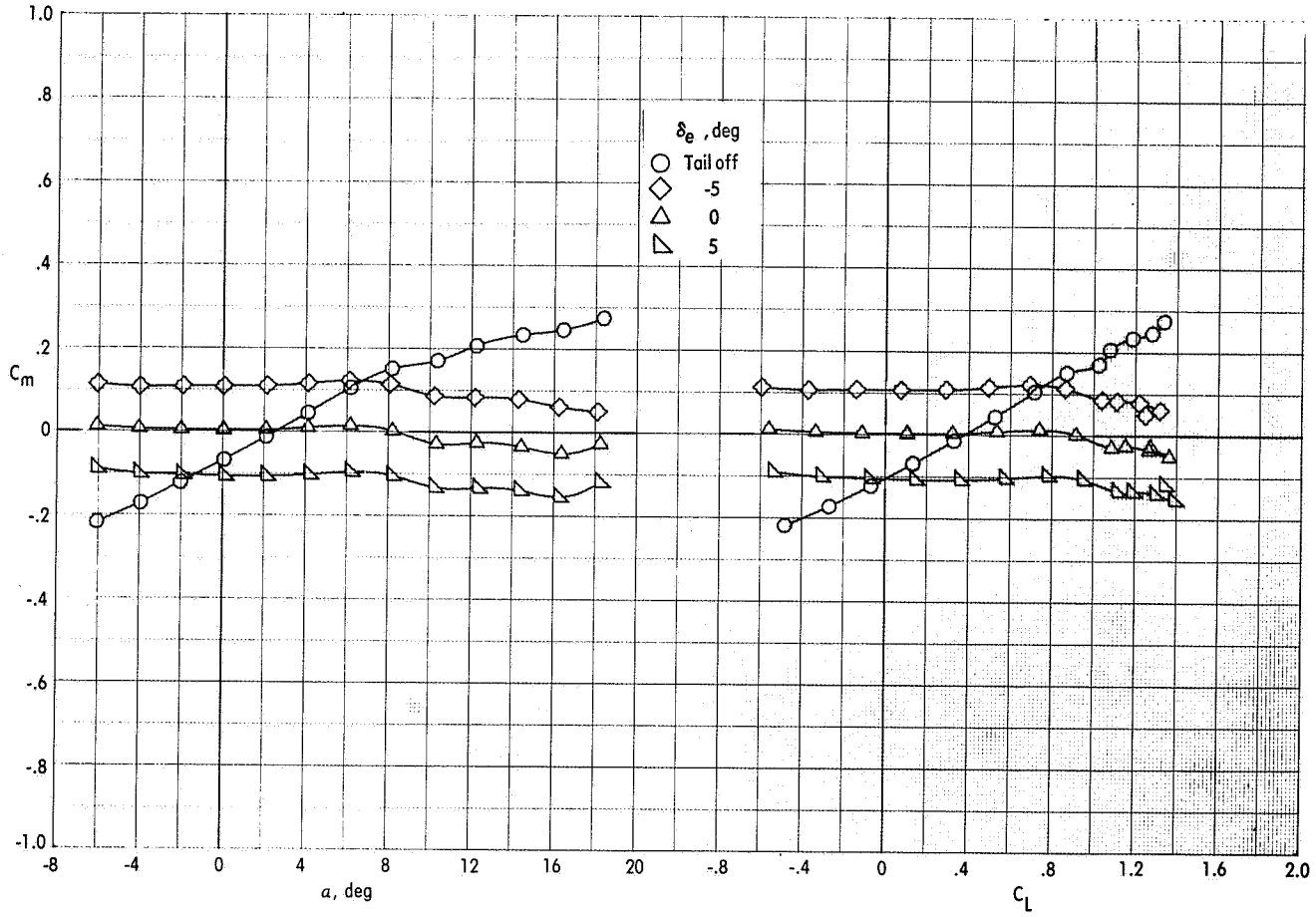
(b) Pitching-moment characteristics.

Figure 58.- Concluded.



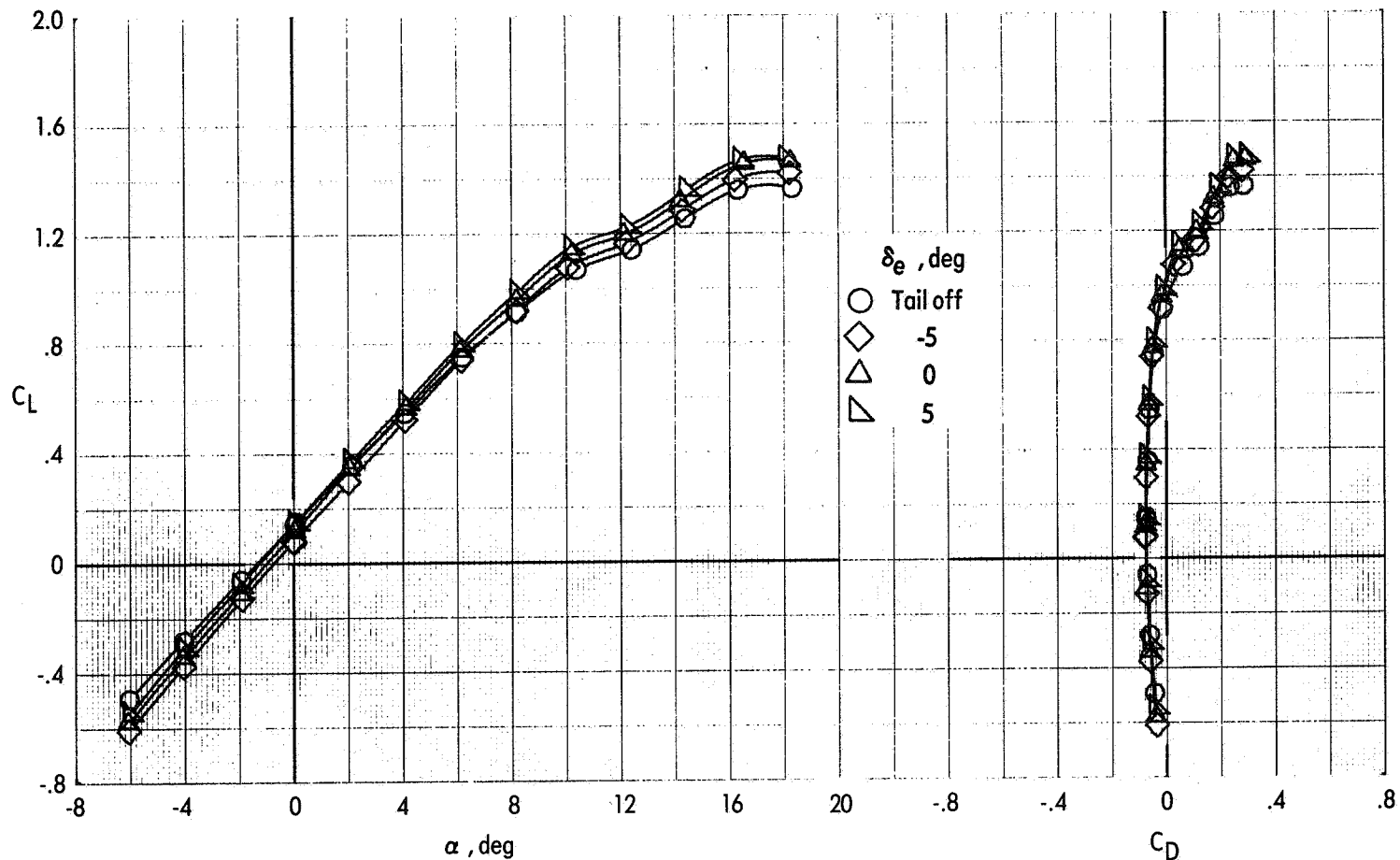
(a) Lift characteristics.

Figure 59.- Effect of elevator deflection on longitudinal aerodynamic characteristics of the cruise configuration ($\delta_L = \text{closed}$; $\delta_{LC} = 0^\circ$; $\delta_f = 0^\circ$; $i_t = 0^\circ$) with power off. $q_\infty = 2672 \text{ Pa}$; $M_\infty = 0.236$.



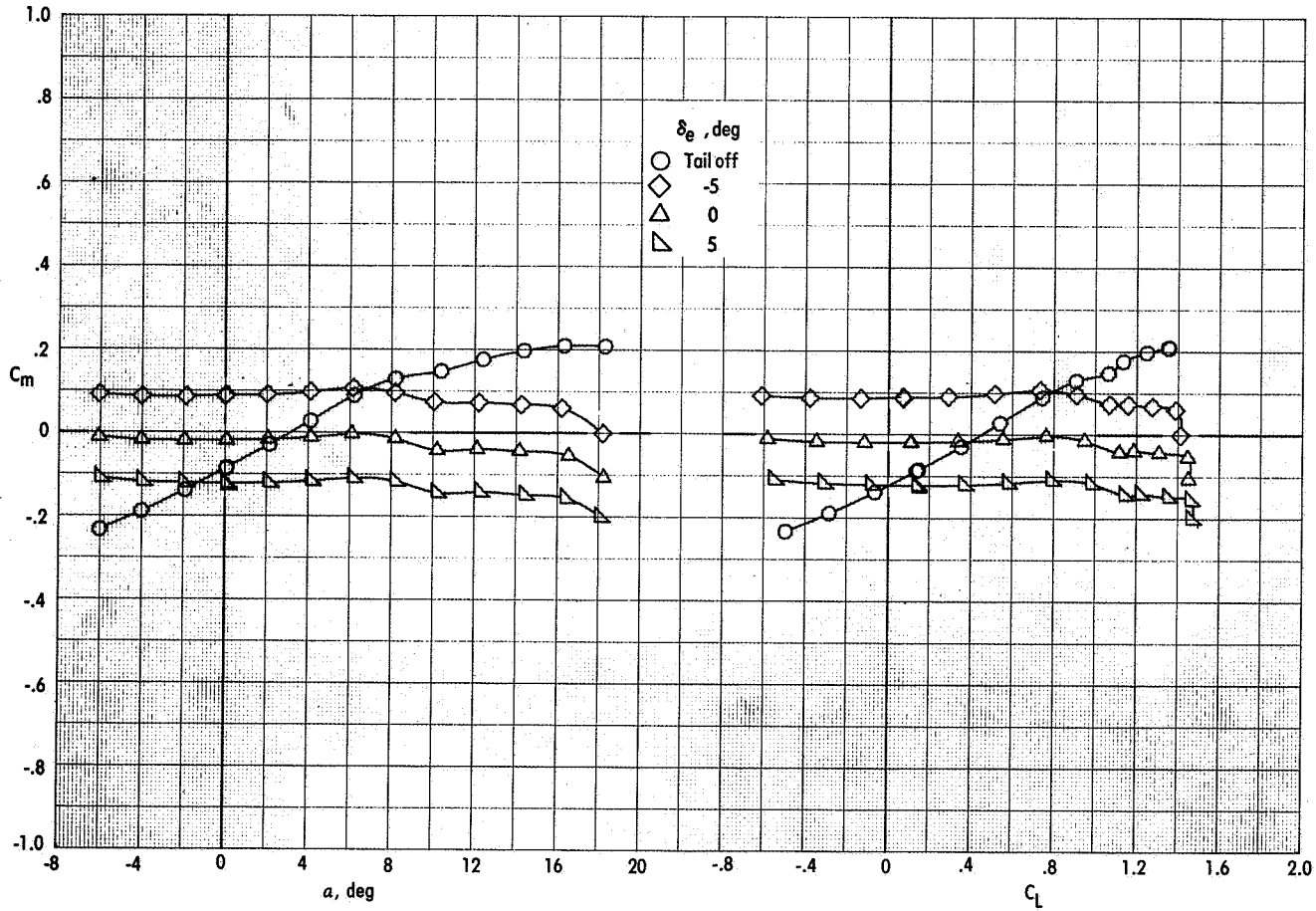
(b) Pitching-moment characteristics.

Figure 59.- Concluded.



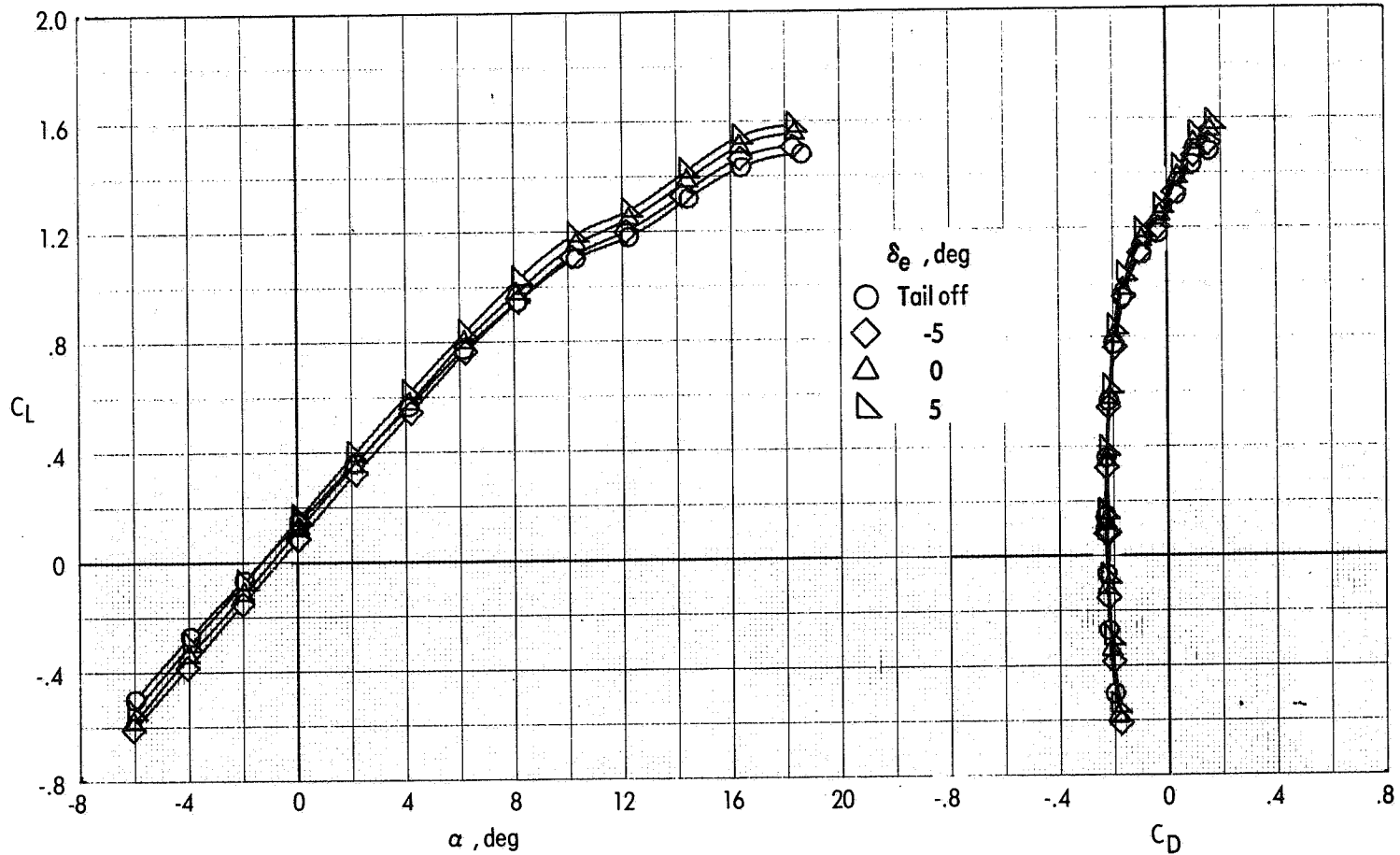
(a) Lift characteristics.

Figure 60.- Effect of elevator deflection on longitudinal aerodynamic characteristics of the cruise configuration ($\delta_L = \text{closed}$; $\delta_{LC} = 0^0$; $\delta_f = 0^0$; $i_t = 0^0$) with power on ($C_\mu = 0.19$). $q_\infty = 2672 \text{ Pa}$; $M_\infty = 0.236$.



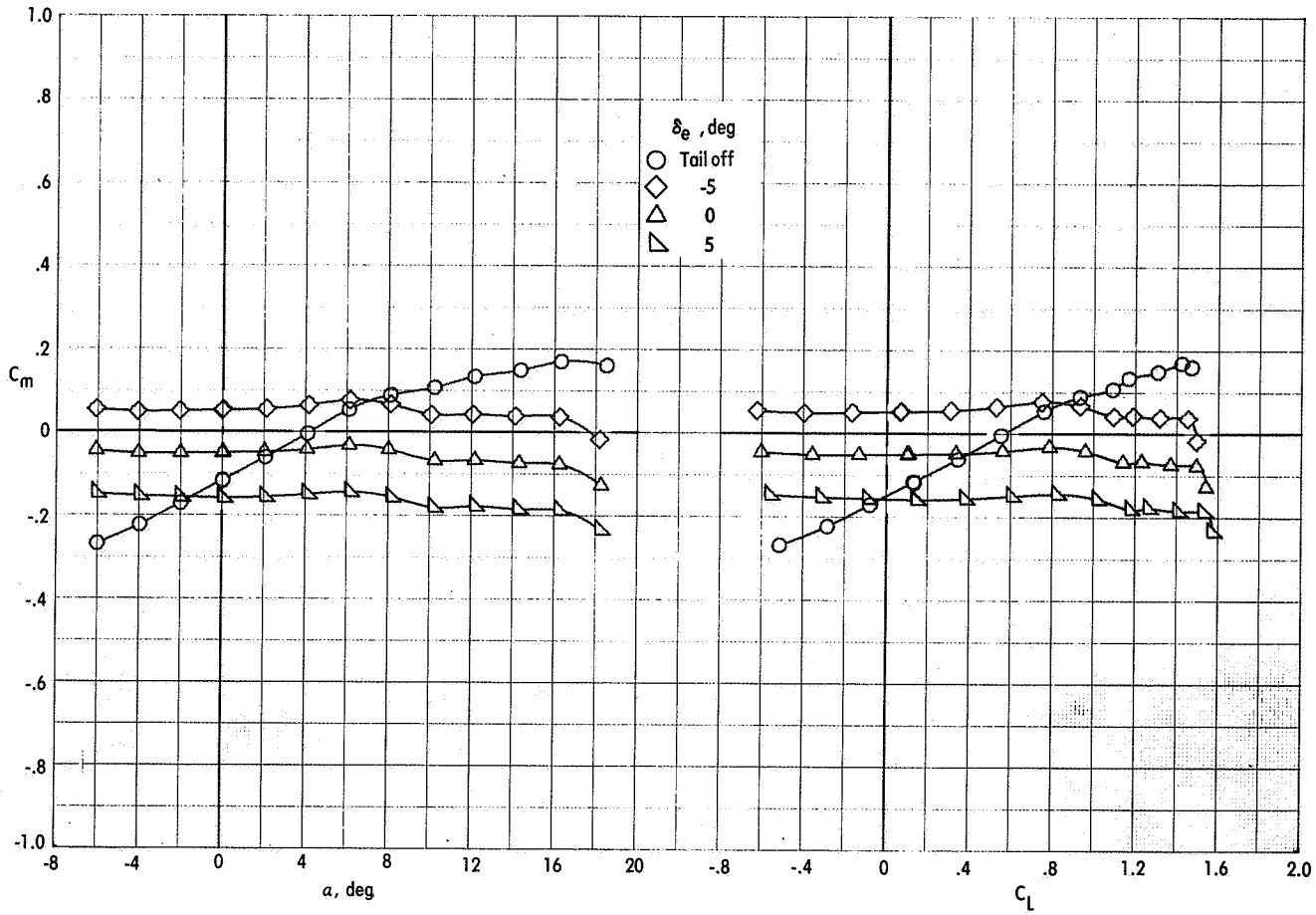
(b) Pitching-moment characteristics.

Figure 60.- Concluded.



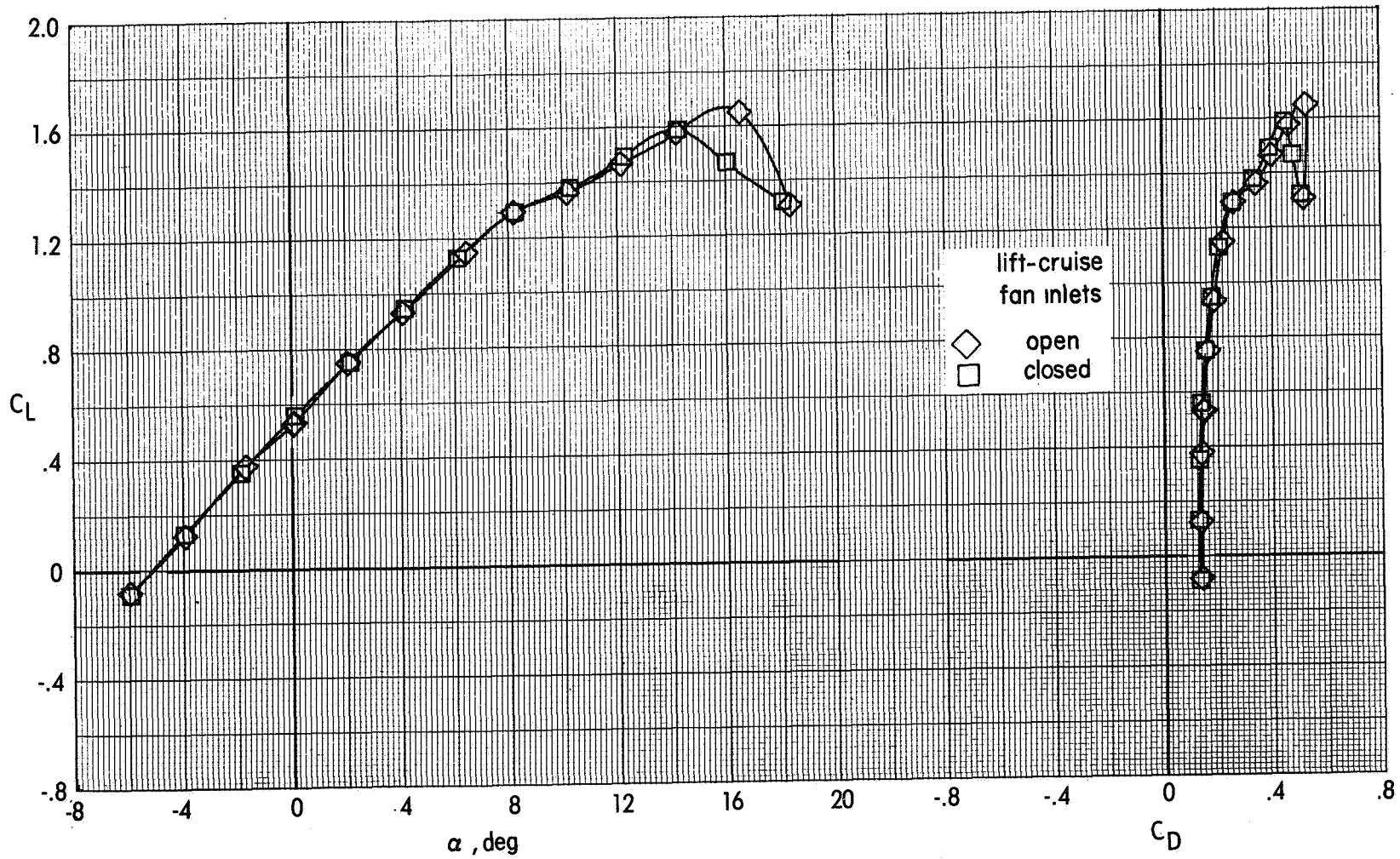
(a) Lift characteristics.

Figure 61.- Effect of elevator deflection on longitudinal aerodynamic characteristics of the cruise configuration ($\delta_L = \text{closed}$; $\delta_{LC} = 0^\circ$; $\delta_f = 0^\circ$; $i_t = 0^\circ$) with power on ($C_\mu = 0.37$). $q_\infty = 2672$ Pa; $M_\infty = 0.236$.



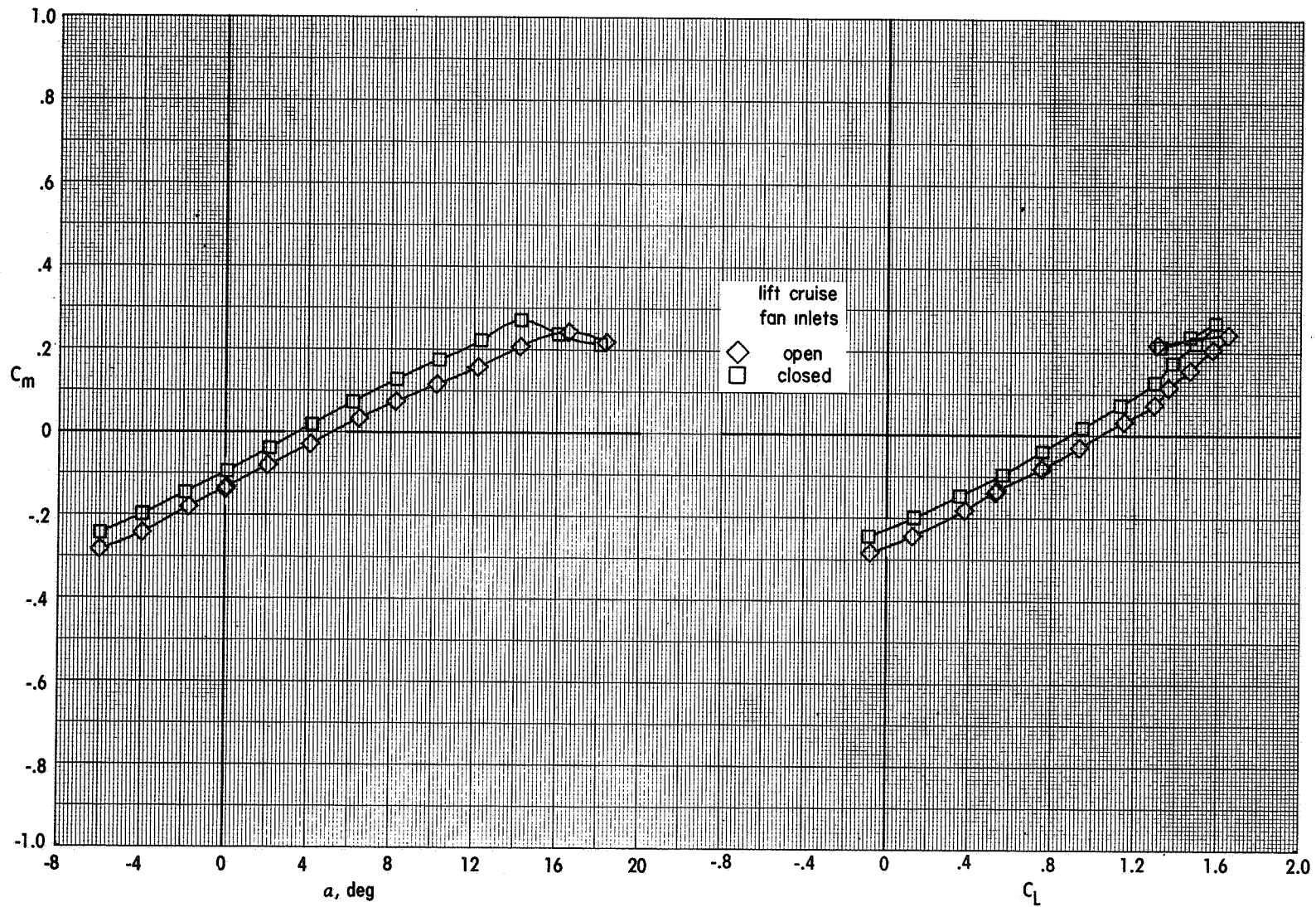
(b) Pitching-moment characteristics.

Figure 61.- Concluded.



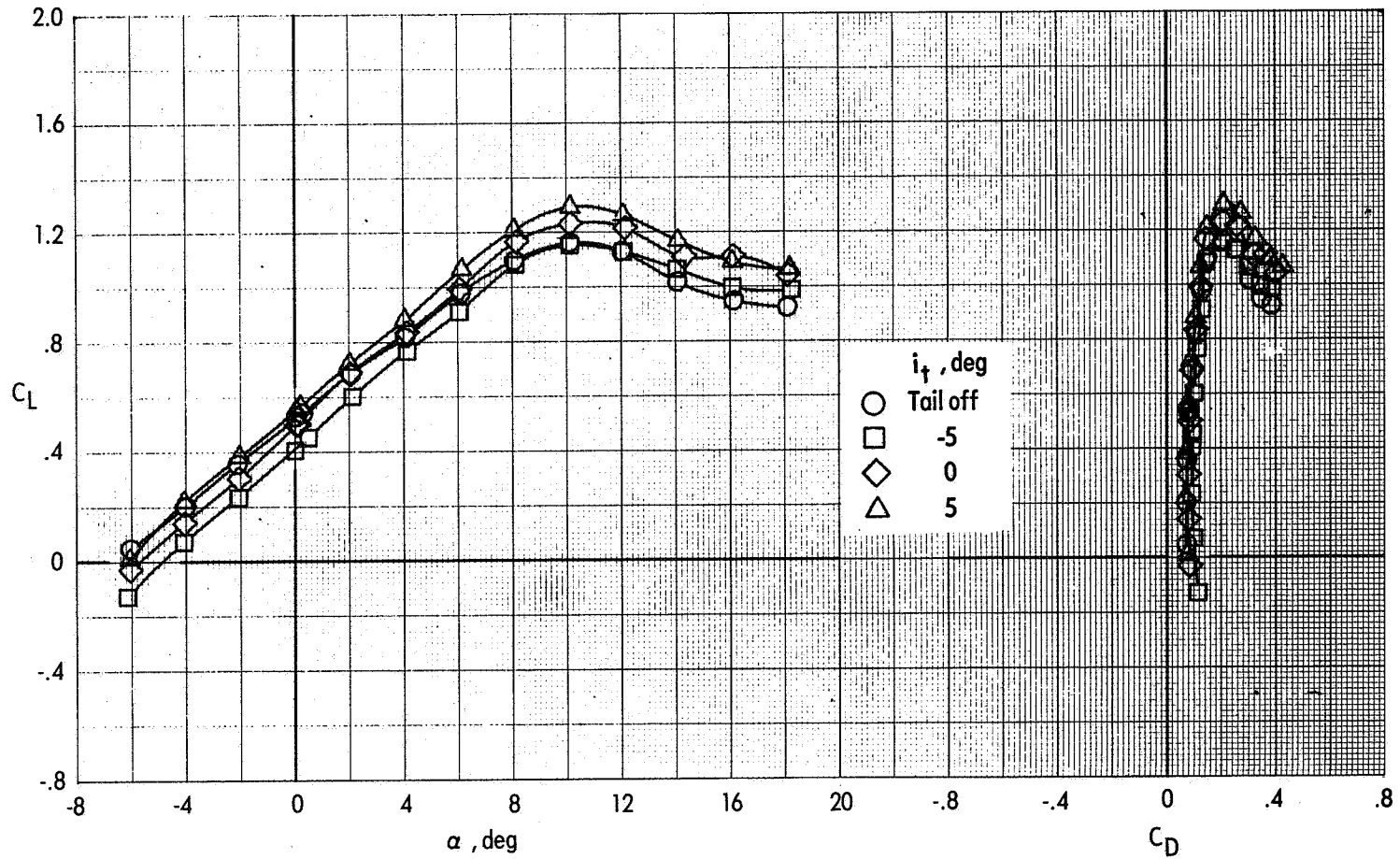
(a) Lift characteristics.

Figure 62.- Effect of closed lift-cruise fan inlets on longitudinal aerodynamic characteristics of the wingborne-flight configuration ($\delta_L = \text{closed}$; $\delta_{LC} = 0^\circ$; $\delta_f = 40^\circ$; tail off) with power off. $q_\infty = 2672 \text{ Pa}$; $M_\infty = 0.236$.



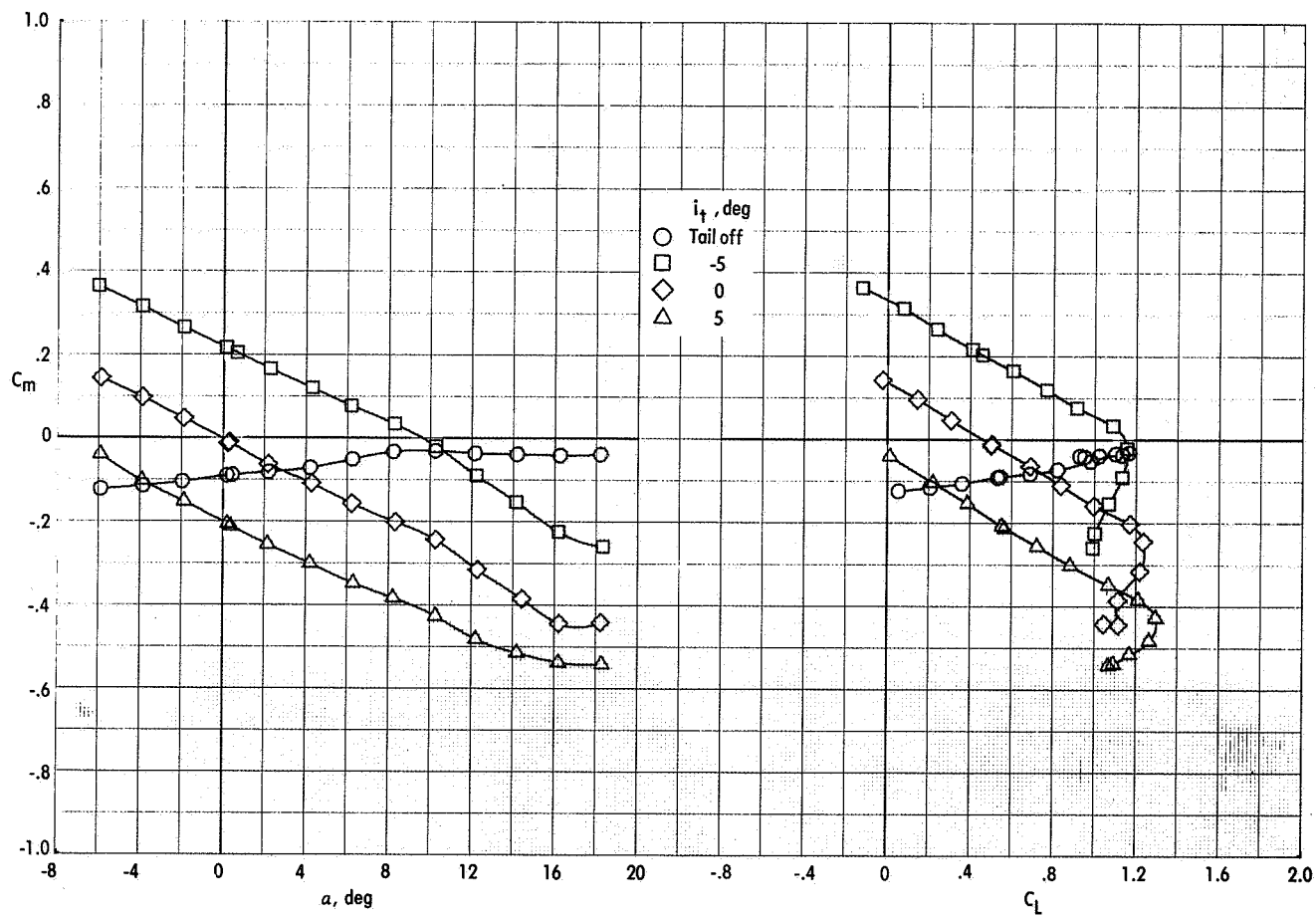
(b) Pitching-moment characteristics.

Figure 62.- Concluded.



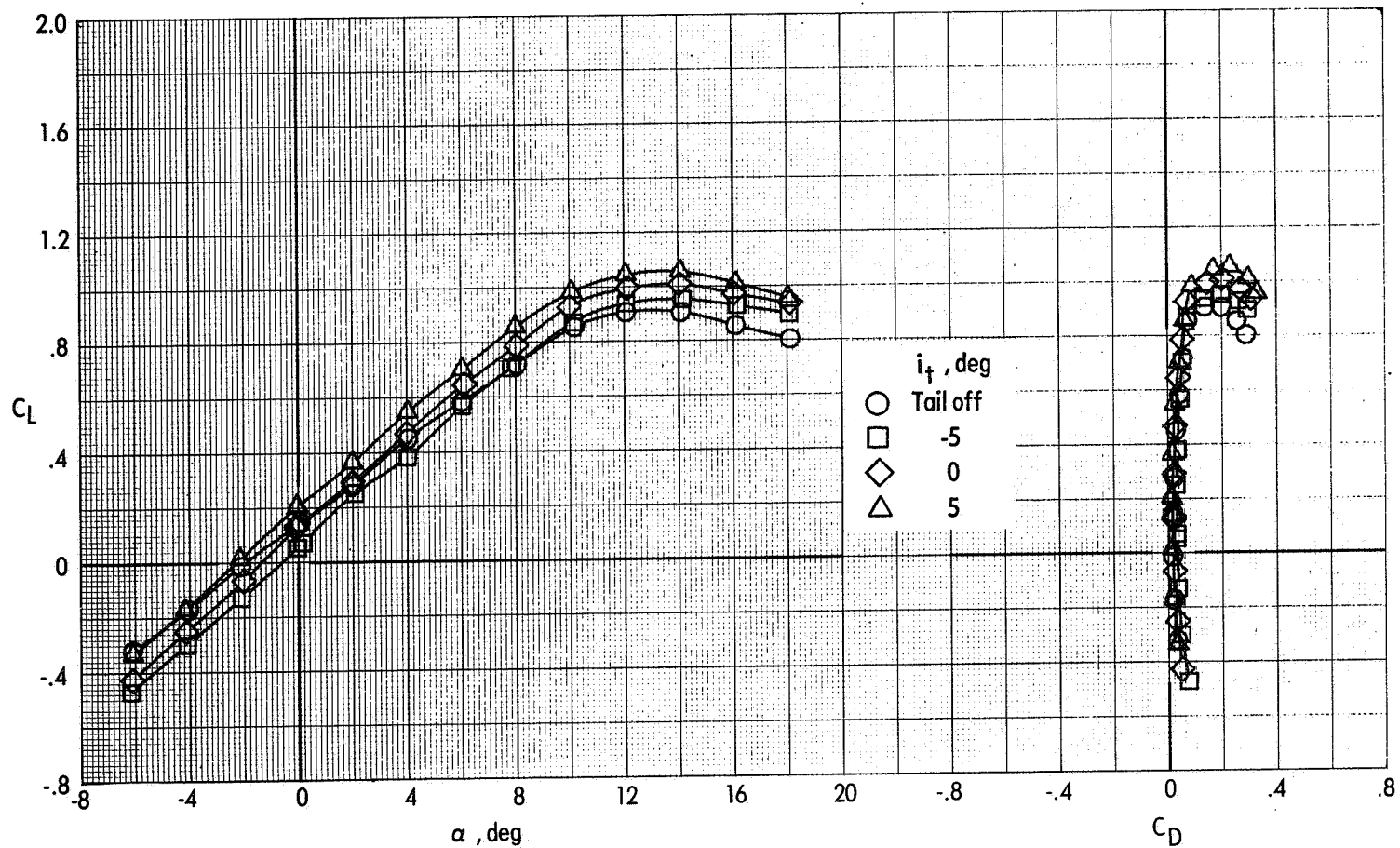
(a) Lift characteristics.

Figure 63.- Effect of tail incidence on the longitudinal aerodynamic characteristics of the VTOL configuration with the lift-fan pods and lift-cruise fans removed ($\delta_f = 40^\circ$; $\delta_e = 0^\circ$). $q_\infty = 2672$ Pa; $M_\infty = 0.236$.



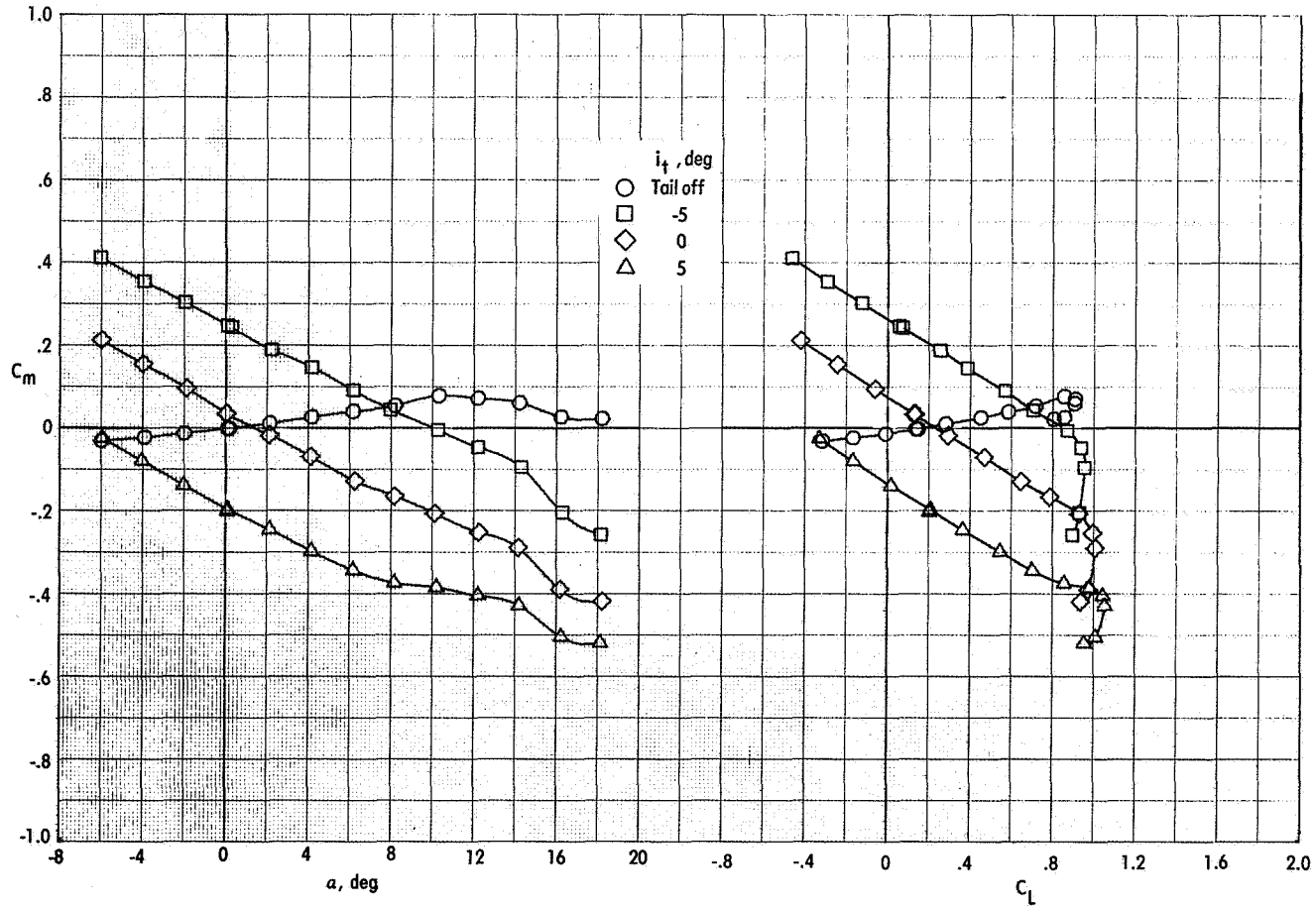
(b) Pitching-moment characteristics.

Figure 63.- Concluded.



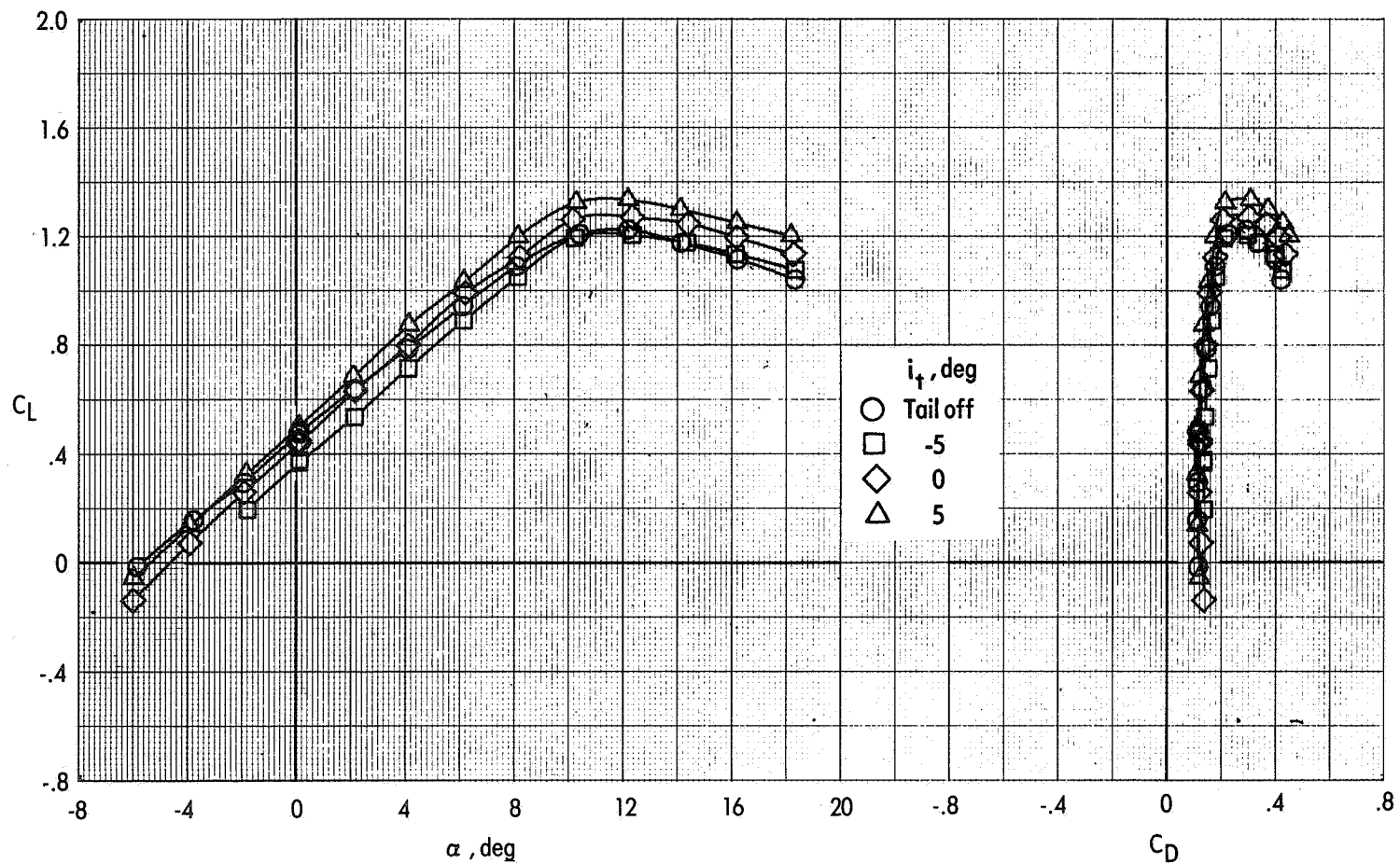
(a) Lift characteristics.

Figure 64.- Effect of tail incidence on the longitudinal aerodynamic characteristics of the cruise configuration with the lift-fan pods and lift-cruise fans removed ($\delta_f = 0^\circ$; $\delta_e = 0^\circ$). $q_\infty = 2672$ Pa; $M_\infty = 0.236$.



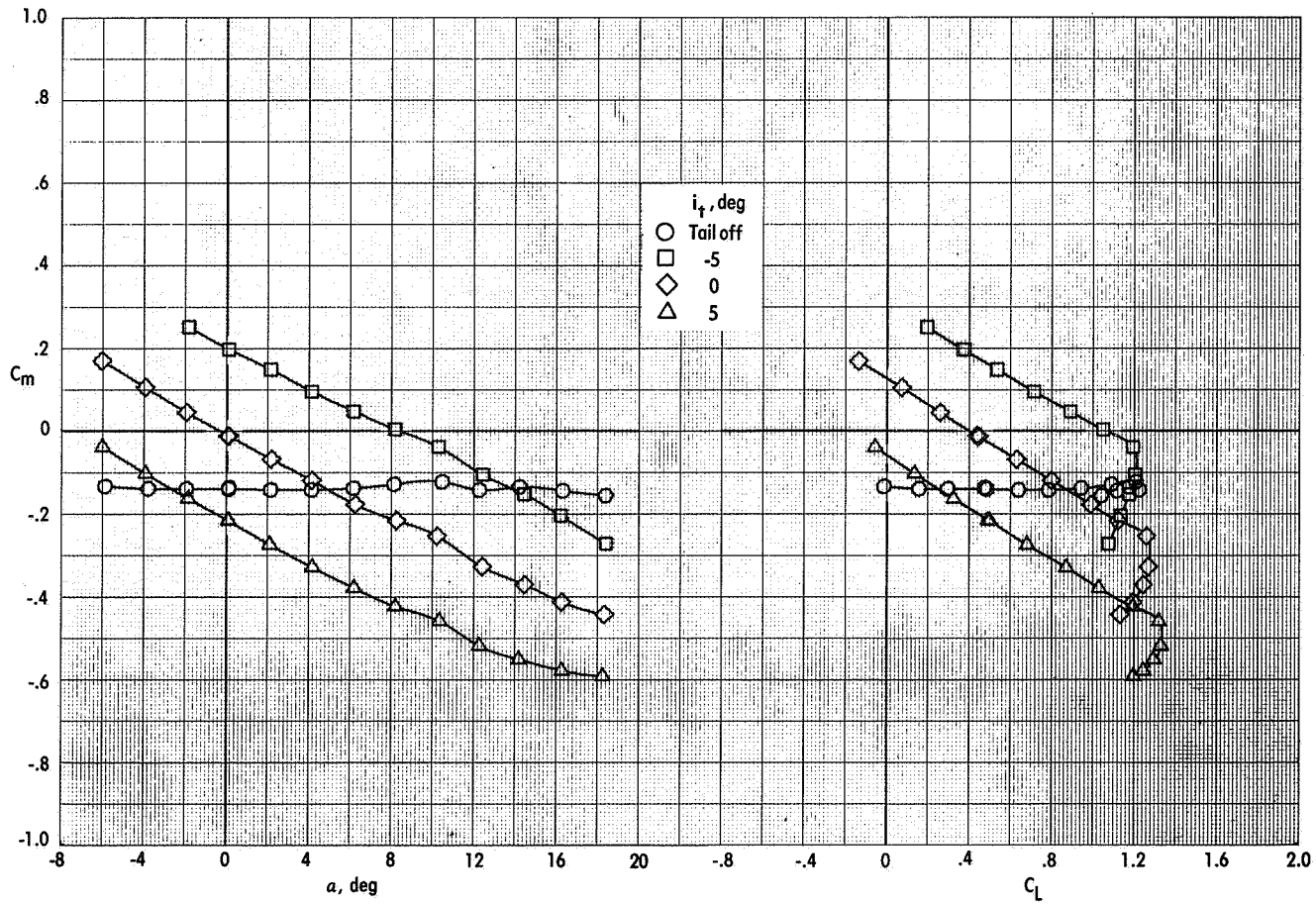
(b) Pitching-moment characteristics.

Figure 64. - Concluded.



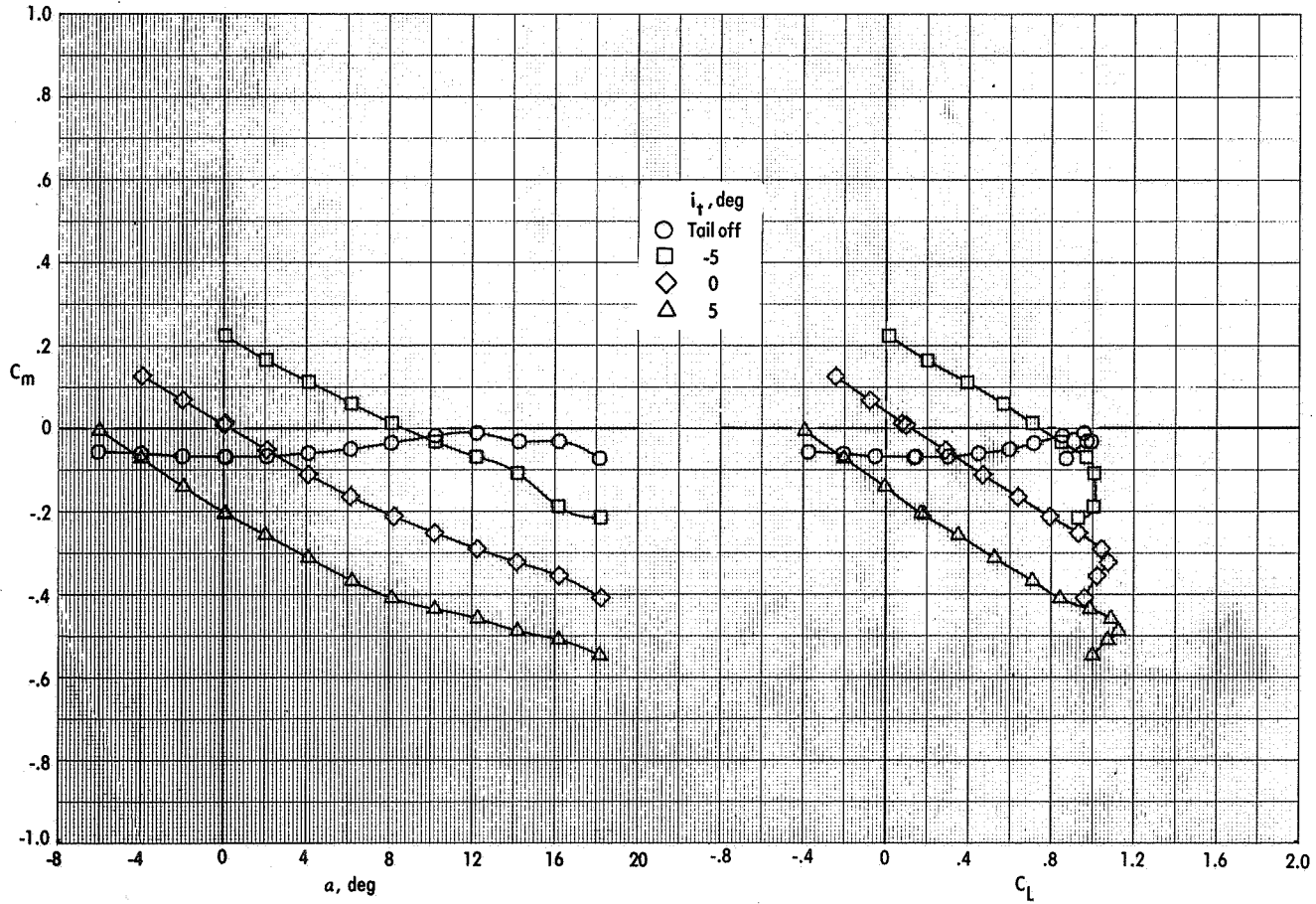
(a) Lift characteristics.

Figure 65.- Effect of tail incidence on the longitudinal aerodynamic characteristics of the VTOL configuration with the lift-fan pods removed ($\delta_{LC} = 0^\circ$; $\delta_f = 40^\circ$; $\delta_e = 0^\circ$). $q_\infty = 2672$ Pa; $M_\infty = 0.236$.



(b) Pitching-moment characteristics.

Figure 65.- Concluded.



(b) Pitching-moment characteristics.

Figure 66.- Concluded.

NATIONAL AERONAUTICS AND SPACE ADMINISTRATION
WASHINGTON, D.C. 20546

OFFICIAL BUSINESS
PENALTY FOR PRIVATE USE \$300

SPECIAL FOURTH-CLASS RATE
BOOK

POSTAGE AND FEES PAID
NATIONAL AERONAUTICS AND
SPACE ADMINISTRATION
451



POSTMASTER: If Undeliverable (Section 158
Postal Manual) Do Not Return

"The aeronautical and space activities of the United States shall be conducted so as to contribute . . . to the expansion of human knowledge of phenomena in the atmosphere and space. The Administration shall provide for the widest practicable and appropriate dissemination of information concerning its activities and the results thereof."

—NATIONAL AERONAUTICS AND SPACE ACT OF 1958

NASA SCIENTIFIC AND TECHNICAL PUBLICATIONS

TECHNICAL REPORTS: Scientific and technical information considered important, complete, and a lasting contribution to existing knowledge.

TECHNICAL NOTES: Information less broad in scope but nevertheless of importance as a contribution to existing knowledge.

TECHNICAL MEMORANDUMS: Information receiving limited distribution because of preliminary data, security classification, or other reasons. Also includes conference proceedings with either limited or unlimited distribution.

CONTRACTOR REPORTS: Scientific and technical information generated under a NASA contract or grant and considered an important contribution to existing knowledge.

TECHNICAL TRANSLATIONS: Information published in a foreign language considered to merit NASA distribution in English.

SPECIAL PUBLICATIONS: Information derived from or of value to NASA activities. Publications include final reports of major projects, monographs, data compilations, handbooks, sourcebooks, and special bibliographies.

TECHNOLOGY UTILIZATION PUBLICATIONS: Information on technology used by NASA that may be of particular interest in commercial and other non-aerospace applications. Publications include Tech Briefs, Technology Utilization Reports and Technology Surveys.

Details on the availability of these publications may be obtained from:

SCIENTIFIC AND TECHNICAL INFORMATION OFFICE

NATIONAL AERONAUTICS AND SPACE ADMINISTRATION
Washington, D.C. 20546